

**SYNTHESIS OF NEAR-IR INFRARED CYANINE DYE LIBRARY
WITH INCREASED PHOTOSTABILITY AND ITS
APPLICATION IN FLUORESCENCE AND SERS IMAGING**

ANIMESH SAMANTA

(M. Sc., Indian Institute of Technology Madras, Chennai, India)

**A THESIS SUBMITTED
FOR THE DEGREE OF DOCTOR OF PHILOSOPHY
DEPARTMENT OF CHEMISTRY
NATIONAL UNIVERSITY OF SINGAPORE**

2012

ACKNOWLEDGEMENTS

I would like to express my most sincere gratitude to my supervisor, Associate Professor Young-Tae Chang for his most valuable guidance, great support, lots of patience and endless encouragement during the last four years. His motivation always helped me to learn new things in the scientific field and to overcome difficult challenges.

I would also like to express my sincere gratitude to Dr. Marc Vendrell for his great support, guidance and continuous help for each and every moment. There are no sufficient words to express my gratitude to him. He did not only teach me research guidance but also to be a man. My sincere appreciation also goes to Dr. Kaustabh Kumar Maiti for his kind support, valuable guidance and continuous encouragement.

My sincere appreciation goes to all past and present members of our lab whose contribution made this journey really enjoyable in each and every step of my research life.

Words are insufficient to express my sincere thanks for being such helpful and cooperative lab-mates to Dr. Yun Seong Wook and others, specially Dr. Kang Nam-Young, Dr. Sung Chan Lee, Dr. Ha Hyung-Ho, Dr. Jun-Seok Lee, Dr. Yun-Kyung Kim, Dr. Kim Hanjo, Feng Suihan, Kelly, Dr. Sung Jin Park, Dr. Junyoung Kim, Dr. Woo Sirl Lee, Dr. Satoshi Arai, Dr. Li Xin, Dr. Yoo Jung Sun, Dr. Jiyeon Ock, Dr. Kim Jinmi, Dr. Taslima Khanam, Dr. Teoh Chai Lean, Chang Liang, Dr. Kale, Duanting, Dongdong, Xu Wang, Samira, MyungWon, Yoges, Emmiline, Jow Zhi Yen, Chee Geng, Physilia, Jimmy, Pamela, Fronia, Tang Mui Kee and Xiaojun Liao.

My special thanks go to Raj Kumar, Krishna Kanta, Bikram and Sanjay to make me so happy in my lab during my benchwork. These memorable days will remain as a sweet memory forever.

I would like to thank Dr. Malini Olivo and Dr. Qing-Hua Xu for allowing me to use their instrument facilities. I also thank the supportive hands to complete my project works to Dr. U.S. Dinish, Dr. Junho Chung, Zhenping Guan, Kiat-Seng Soh, Dr. Ramaswamy Bhuvaneswari, Dr. Hyori Kim, Dr. Shashi Rautela.

I take this opportunity to thank all of my friends and juniors who helped my dreams come true. I am thankful to Tanay, Mainakda, Pasarida, Gautam, Pradipta, Kausik, Sadanandada, Amarenduda, Subhankar, Srimanta, Asim, Hriday, Sudiptada, Sabyasachi, Nimai, Bijay and Jhinukdi who made my stay at NUS so pleasant.

Financial and technical support from the Department of Chemistry of the National University of Singapore (NUS) is greatly acknowledged. I would like to thank all the staffs in chemistry administrative office, Lab-supplies for their immense support.

Finally, I would like to express my deepest gratitude towards my parents, my brother, sister, brother in-law, all my relatives and soma. I think that without their continuous support and constant inspiration this thesis would not have been completed. At last I would like to heartily thank God for giving me the patience, faith and strength to complete my thesis.

Thesis Declaration


The work in this thesis is the original work of Animesh Samanta, performed independently under the supervision of Associate Professor Young Tae Chang, (in the laboratory LuminoGenomics, S9-03-03), Chemistry Department, National University of Singapore, between 09/01/2008 and 08/01/2012.

The content of the thesis has been partly published in:

- 1) Development of photostable near-IR cyanine dyes, Samanta, A.; Vendrell, M.; Das, R.; Chang, Y. T.* *Chem. Commun.*, **2010**, 46, 7406-7408.
- 2) A Photostable Near-Infrared Protein Labeling Dye for in vivo Imaging, Samanta, A.; Vendrell, M.; Yun, S. W.; Guan, Z.; Xu, Q. H.; Chang, Y. T.* *Chem. Asian J.* **2011**, 6, 1353-1356.
- 3) Synthesis and Characterization of a Cell-permeable Near-Infrared Fluorescent Deoxyglucose Analogue for Cancer Cell Imaging, Vendrell, M.; Samanta, A.; Yun, S. W.; Chang, Y. T.* *Org. Biomol. Chem.* **2011**, 9, 4760-4762.
- 4) Ultrasensitive Near-Infrared Raman Reporters for SERS-based in vivo Cancer Detection, Samanta, A.; Maiti, K. K.; Soh, K. S.; Liao, X.; Vendrell, M.; Dinish, U. S.; Yun, S. W.; Bhuvanewari, R.; Kim, H.; Rautela, S.; Chung, J.; Olivo, M.; Chang, Y. T.* *Angew. Chem. Int. Ed. Engl.*, **2011**, 50, 6089–6092.
- 5) Multiplex cancer cell detection by SERS nanotags with cyanine and triphenylmethine Raman reporters, Maiti K. K.; Samanta, A.; Vendrell, M.; Soh, K. S.; Olivo, M.; Chang, Y. T.* *Chem. Commun.*, **2011**, 47, 3514-3516.
- 6) SERS-based Multiplex Targeted Detection and Imaging in living mice by sensitive Near Infrared Raman reporter nanotags, Maiti, K. K.; Dinish, U. S.;

Samanta, A.; Soh, K. S.; Vendrell, M.; Yun, S. W.; Olivo, M.; Chang, Y. T.*
submitted to *Biosensor Bioelectron*.

Animesh Samanta



2012-06-01

Name

Signature

Date

Table of Contents

Acknowledgments	II
Thesis Declaration	IV
Table of contents	VI
Summary	XIII
List of Tables	XV
List of Figures	XVI
List of Charts	XXI
List of Schemes	XXII
Abbreviations and symbols	XXIII
List of publications	XXVI

Chapter 1

Introduction	1
1.1 Overview of fluorophores	1
1.2 Synthetic strategies for novel fluorescent probes	3
1.2.1 Diversity oriented synthesis	3
1.2.2 Target-Oriented Synthesis	5
1.3 Near-infrared fluorophores	6
1.3.1 Cyanine dyes	7
1.3.2 Tricarbocyanine dyes	7
1.4 Properties of cyanine dyes	10
1.4.1 Photophysical properties of cyanine dyes	10
1.4.2 Stability of Cyanine dyes	14
1.4.3. Surface enhanced Raman scattering (SERS) properties	15
1.5 Applications of cyanine dyes	16
1.5.1 <i>In vivo</i> fluorescence imaging	17
1.5.2 SERS imaging	19
1.6 Scope and outline of the thesis	20
1.7 References	22

Chapter 2 Development of photostable near-infrared (NIR) cyanine dyes

2.1 Introduction	30
2.2 Objectives	31
2.3 Results and discussion	31
2.3.1 Decomposition study of tricarbocyanine dye	31
2.3.2 Design and synthesis	34

2.3.3	Characterization of tricarboyanine	35
2.3.4	Photostability measurement	36
2.3.5	Library design, characterization and photostability studies	38
2.3.6	Secondary screening and comparative study with ICG	44
2.4	Conclusion	47
2.5	Experimental details	48
2.5.1	Synthesis of CyN and characterization	49
2.5.2	Synthesis of CyNA library and characterization	52
2.5.3	Photostability measurement	55
2.6	References	57
Chapter 3 A Photostable NIR Protein Labeling Dye for <i>In Vivo</i> Imaging		
3.1	Introduction	61
3.2	Objectives	61
3.3	Results and discussion	62
3.3.1	Design and synthesis	62
3.3.2	Photophysical properties study	64
3.3.3	Photostability measurement	67
3.3.4	Antibody conjugation and characterization	68
3.3.5	<i>In vitro</i> and <i>in vivo</i> Imaging	70
3.4	Conclusions	72
3.5	Experimental details	73
3.5.1	Synthesis and characterization of CyNE 790	73
3.5.2	Antibody conjugation and characterization	75
3.5.3	Cell Culture and cellular imaging of CyNE790 -anti-EGFR in	

SCC-15 and MCF-7 cells	75
3.5.4 <i>In vivo</i> imaging	76
3.6 References	78

Chapter 4. Synthesis and Characterization of a Cell-permeable NIR Fluorescent Deoxyglucose Analogue for Cancer Cell Imaging

4.1 Introduction	81
4.2 Objectives	82
4.3 Results and discussion	82
4.3.1 Design and Synthesis of CyNE 2-DG	82
4.3.2 Cellular uptake and competition assay	83
4.3.3 Comparative cell permeability study with IRDye 800CW 2-DG	88
4.4 Conclusions	90
4.5 Experimental details	91
4.5.1 Synthesis of CyNE 2DG and IRDye 800 2-DG	91
4.5.2 Cell culture and cellular imaging	93
4.6 References	95

Chapter 5. Ultrasensitive NIR Raman Reporters for SERS-Based *in vivo* Cancer Detection

5.1 Introduction	98
5.2 Objectives	99
5.3 Results and discussion	100
5.3.1 Design and Synthesis of CyNAMLA library	100
5.3.2 Characterization of CyNAMLA library	103

5.3.3	Measurement of SERS	106
5.3.4	Encapsulation of AuNPs and TEM characterization	109
5.3.5	Stability measurement of SERS nanotags	111
5.3.6	Antibody conjugation and SERS study	114
5.3.7	Cell SERS mapping	117
5.3.8	<i>In vivo</i> cancer detection in xenograft mice	119
5.3.10	<i>In vivo</i> SERS imaging	121
5.4	Conclusions	122
5.5	Experimental details	123
5.5.1	Synthesis and Characterization of 4 and CyNAB	123
5.5.2	Synthesis and Characterization of CyNAMLA library	126
5.5.3	Procedures for SERS measurements	129
5.5.4	BSA encapsulation of CyNAMLA -AuNPs and stability studies	129
5.5.5	Procedures for antibody conjugation and TEM Characterization	130
5.5.6	SERS Experiments in cells	131
5.5.7	SERS Mapping in SKBR-3 and MDA-MB231 cells	131
5.5.8	Dark Field microscopy experiments	132
5.5.9	SERS experiments in xenograft mice	132
5.5.10	SERS mapping in xenograft mice	133
5.6	References	134

Chapter 6. Multiplex Cancer Cell Detection by SERS nanotags with Cyanine and Triphenylmethine Raman Reporters

6.1	Introduction	138
6.2	Objectives	139
6.3	Results and discussion	139
6.3.1	Design and synthesis	139
6.3.2	Preparation of SERS nanotags and encapsulation	141
6.3.3	Measurement of SERS	143
6.3.4	Antibody conjugation and Characterization	144
6.3.5	Cell SERS study	145
6.3.6	Cell SERS mapping	148
6.4	Conclusions	149
6.5	Experimental details	151
6.5.1	Synthesis and characterization of Cy3LA and Cy5LA	151
6.5.2	Nanotags labeling and Antibody conjugation	153
6.5.3	Thiolated PEG encapsulation	154
6.5.4	SERS measurement of B2LA , Cy3LA , Cy5LA -Au colloid	154
6.5.5	Measurement of SERS spectra and SERS mapping in OSCC, SKBR-3 cells and co-cultured cells	155
6.6	References	157

Chapter 7 Multiplex Targeted Detection and Imaging in Living Mice Using SERS Nanotags with Sensitive Near-Infrared Raman Reporters

7.1	Introduction	160
7.2	Objectives	161

7.3	Results and discussion	161
7.3.1	Design and synthesis	161
7.3.2	Measurement of SERS	163
7.3.3	Signal stability of SERS nanotags	165
7.3.4	SERS multiplex detection in liver and tumor site	167
7.3.5	<i>In vivo</i> SERS mapping experiment	170
7.3.6	Determination of detection limit	171
7.3.7	Time-course distribution of SERS nanotags	172
7.4	Conclusions	173
7.5	Experimental details	174
7.5.1	Synthesis of Cy7LA and Cy7.5LA	174
7.5.2	<i>In vivo</i> SERS multiplexing	178
7.5.3	SERS mapping	179
7.5.4	Limit of detection (LOD) study	179
7.6	References	180

Chapter 8 Conclusions and Future perspectives

8.1	Conclusions	183
8.2	Future perspectives	186
8.2.1	Design of Cell tracker NIR fluorescence imaging agent	186
8.2.2	SERRS for ultrasensitive detection of multiple targets	187
8.3	References	190

Summary

Near-infrared (NIR) fluorescence (λ_{max} : 700-1000 nm) has recently received considerable attention in bioimaging studies due to its deep penetrating ability through animal tissue and its significant reduction of autofluorescence. Therefore, we designed and synthesized a set of photostable NIR cyanine dyes (named as CyNA library) composed of 80 molecules with structurally different amines. We later screened them and identified CyNA-414 as the most photostable dye. We compared CyNA-414 dye to the standard dye Indocyanine Green (ICG) and proved the superiority of our dye for NIR imaging. Next, we synthesized a succinimidyl ester derivative of CyNA-414 for bioconjugation (CyNE790) and compared its photophysical properties with the commercial standard ICG-sulpho-OSu which is the only NIR labeling dye clinically approved to date. A detailed evaluation of their photobleaching in buffer indicated a 15-fold higher photostability of CyNE790 when compared to ICG. Furthermore, the injection of CyNE790-anti-EGFR treated SCC-15 and MCF-7 cells allowed the visualization of the labeled cells in mice and confirmed that the conjugation of CyNE790 did not affect the recognition properties of the monoclonal anti-EGFR antibody. Furthermore, we synthesized a novel NIR fluorescent deoxyglucose analogue (CyNE 2-DG). We examined the staining of CyNE 2-DG in cancer cells and proved its superior cell permeability over the NIR standard IRDye 800CW 2-DG, altogether validating its application for cancer cell imaging in the NIR region.

The applicability of fluorescent imaging is sometimes limited due to photobleaching, peak overlapping or low signal-to-noise ratios in complex biological systems. Therefore, we studied the application of cyanine dyes in an alternative imaging technique (i.e. Surface-enhanced Raman Scattering (SERS)) that can minimize the

limitations of fluorescence imaging. We designed the first combinatorial approach to discover novel and highly sensitive NIR SERS reporters. The synthesis of a NIR-SERS active tricyanin library (CyNAMLA) and its screening led to the identification of CyNAMLA-381 as the most sensitive SERS reporter. scFv-conjugated CyNAMLA-381-SERS nanotags recognizing HER-2 receptors were prepared and SERS mapping analysis confirmed that the nanotags were mainly localized at the cell surface of HER-2 expressing cancer cells. We also administrated the nanotags to nude mice bearing xenografts generated from SKBR-3 cells, and observed that the signal of the tumor site perfectly resembled the SERS spectra while no signal was detected from other anatomical locations. These results clearly indicated that CyNAMLA-381-SERS nanotags were able to specifically detect tumors *in vivo*. In addition, we designed a derivative of cyanine dye (i.e. Cy3LA) as a multiplexing partner of triphenylmethine derivatives (i.e. B2LA). In order to examine the multiplex differential recognition of B2LA anti-EGFR and Cy3LA anti-HER2 nanotags in cells, we incubated an equal amount of both nanotags in OSCC cells (EGFR-positive) and SKBR-3 cells (HER2-positive). The SERS measurements in OSCC and SKBR-3 cells fully resembled the SERS spectra of B2LA and Cy3LA and demonstrated the multiplex properties of B2LA and Cy3LA SERS nanotags. At last, we demonstrated the multiplexing capability of three different NIR Raman reporters (i.e. CyNAMLA-381 and the newly synthesized Cy7 LA and Cy 7.5 LA). The high sensitivity and tumor specificity of antibody-conjugated SERS nanotags proves their excellent potential as non-invasive diagnostic tools and opens up a new window for the development of SERS probes for cancer bioimaging.

List of Tables

Table 1.1	Summary of the spectral properties of cyanine dyes.	11
Table 2.1	Characterization of CyN compounds.	36
Table 2.2	Photophysical properties of CyN and CyNA derivatives.	37
Table 2.3	Absorbance (λ_{abs}) and emission wavelengths (λ_{em}), quantum yields of CyNA library.	41
Table 3.1	Photophysical properties of CyNE790 and ICG-sulfo-OSu .	66
Table 3.2	Characterization of dye conjugated antibody.	70
Table 5.1	Characterization data of the CyNAMLA library.	103

List of Figures

Chapter 1

Figure 1.1	Visible spectral of different well-known fluorophores.	2
Figure 1.2	Representative different fluorophore analogues.	3
Figure 1.3	Diversity-Oriented Fluorescence library (DOFL) synthesis	5
Figure 1.4	Diversity at different position of cyanine dye cassettes.	5
Figure 1.5	General structure of cyanine dyes.	7
Figure 1.6	General structures of tricyanobenzene cyanine dyes.	8
Figure 1.7	Examples of cyanine dye cassettes.	10
Figure 1.8	Screening by high throughput manner.	17
Figure 1.9	Fluorescent imaging of <i>in vivo</i> mice model.	18
Figure 1.10	Various tricyanobenzene cassettes for fluorescent probes.	19

Chapter 2

Figure 2.1	HPLC monitoring of CyN-111 decomposition in aqueous media.	31
Figure 2.2	Mass spectrometry data for the decomposition of CyN-111 .	33
Figure 2.3	IR spectra of the reaction mixture of CyN-111 .	34
Figure 2.4	Absorbance and emission spectra of CyN(A)-111 in DMSO.	36
Figure 2.5	Photostability evaluations of 1 , CyN and CyNA derivatives.	37
Figure 2.6	Primary photostability evaluation of CyNA library.	40
Figure 2.7	Secondary photostability evaluation of selected CyNA in HEPES	44
Figure 2.8	Secondary photostability evaluation of selected CyNA in PBS.	45
Figure 2.9	Comparative photostability analysis of CyNA-414 , ICG .	46
Figure 2.10	Absorbance spectra of ICG , CyNA-414 in PBS.	47
Figure 2.11	Emission spectra of ICG , CyNA-414 in PBS.	47

Chapter 3

Figure 3.1	Absorbance, emission spectra of CyNA-414 and CyNE790 .	64
Figure 3.2	Comparative photostability of CyNA-414 and CyNE790 .	65
Figure 3.3	Absorbance spectra of CyNE790 and ICG-sulfo-OSu .	66
Figure 3.4	Emission spectra of CyNE790 and ICG-sulfo-OSu .	67
Figure 3.5	Photostability of CyNE790 and ICG-sulfo-OSu .	68
Figure 3.6	Characterization of CyNE790 and ICG -labelled antibodies.	69
Figure 3.7	Absorbance of CyNE790 and ICG -labelled anti-EGFR-IgG _{2a} .	69
Figure 3.8	Microscope images of cells with CyNE790 -anti-EGFR.	70
Figure 3.9	In vivo fluorescence images of mouse with dye-labelled antibody.	71
Figure 3.10	Comparison of <i>in vivo</i> imaging with 3 and CyNE -EGFR-Ab.	72

Chapter 4

Figure 4.1	Absorbance and emission spectra of 3 and CyNE 2-DG .	83
Figure 4.2	Mean fluorescence intensity of CyNE 2-DG in different cells.	84
Figure 4.3	Competition of CyNE 2-DG uptake with D-glucose.	85
Figure 4.4	Competition of CyNE 2-DG uptake with L-glucose.	85
Figure 4.5	Fluorescence images of MCF7 cells with CyNE 2-DG .	86
Figure 4.6	Cell viability in presence of CyNE 2-DG in MCF7 cells.	86
Figure 4.7	Fluorescence images of different cells with CyNE 2-DG or 3 .	87
Figure 4.8	Fluorescence images upon incubation with CyNE 2-DG and IRDye 800CW 2-DG .	89
Figure 4.9	Retention analysis of CyNE 2-DG in MCF7 cells.	90
Figure 4.10	¹ H-NMR spectrum of 2-D-deoxyglucosamine•HCl in D ₂ O.	92
Figure 4.11	¹ H-NMR spectrum of CyNE 2-DG in MeOD.	93

Chapter 5

Figure 5.1	Absorbance spectra of the 6 selected CyNAMLA compounds.	106
Figure 5.2	Comparative SERS intensities of CyNAMLA library.	107
Figure 5.3	SERS intensities of the selected CyNAMLA -AuNPs.	108
Figure 5.4	SERS spectra of BSA-encapsulated six nanotags.	109
Figure 5.5	Surface plasmon spectra of Au-colloids with CyNAMLA .	111
Figure 5.6	TEM images of BSA-encapsulated and antibody labeled nanotags.	111
Figure 5.7	Time-course SERS measurements of CyNAMLA-80 nanotags.	112
Figure 5.8	Time-course SERS measurements of CyNAMLA-92 nanotags.	112
Figure 5.9	Time-course SERS measurements of CyNAMLA-221 nanotags.	113
Figure 5.10	Time-course SERS measurements of CyNAMLA-262 nanotags.	113
Figure 5.11	Time-course SERS measurements of CyNAMLA-381 nanotags.	113
Figure 5.12	Time-course SERS measurements of CyNAMLA-478 nanotags.	114
Figure 5.13	Time-course SERS measurements of DTTC nanotag.	114
Figure 5.14	SDS-PAGE of scFv-anti-HER2 conjugated to SERS nanotags.	115
Figure 5.15	SERS spectra of scFv-conjugated nanotags.	116
Figure 5.16	Competition of scFv-conjugated and free nanotags-anti-HER2.	117
Figure 5.17	SERS mapping of cells treated with CyNAMLA-381 -nanotags.	118
Figure 5.18	Dark-field reflective microscopy images of nanotags.	119
Figure 5.19	<i>In vivo</i> detection of HER2-positive tumors with scFv-conjugated CyNAMLA-381 SERS nanotags.	120
Figure 5.20	<i>In vivo</i> imaging of HER2-negative tumors with scFv-conjugated CyNAMLA-381 -SERS nanotags.	120
Figure 5.21	SERS mapping on tumor and non-tumor regions upon injection of CyNAMLA381 -anti-HER2 nanotags.	121

Chapter 6

Figure 6.1	Absorption spectra of Au-colloid and B2LA , Cy3/5LA nanotags.	142
Figure 6.2	Evaluation of the SERS stability for B2LA and Cy3LA .	143
Figure 6.3	Normalized SERS spectra of B2LA , Cy3LA and Cy5LA .	144
Figure 6.4	TEM images of B2LA and Cy3LA nanotags.	145
Figure 6.5	SERS spectra of different cells with antibody-free nanotags or anti-EGFR/HER2 nanotags.	146
Figure 6.6	Multiplex SERS spectra of both B2LA anti-EGFR and Cy3LA anti-HER2-nanotags.	147
Figure 6.7	SERS mapping of B2LA anti-EGFR, Cy3LA anti-HER2 nanotags.	148
Figure 6.8	SERS mapping of non-treated OSCC / SKBR-3 cells.	149

Chapter 7

Figure 7.1	Absorption spectra of three Raman reporters.	163
Figure 7.2	Surface plasmon absorption spectra of three Raman reporters.	163
Figure 7.3	Normalized SERS spectra of CyNAMLA 381 .	164
Figure 7.4	Normalized SERS spectra of Cy7 LA and Cy7.5LA .	164
Figure 7.5	Identification of multiplex peak of three nanotags.	165
Figure 7.6	Time course SERS measurement of three nanotags.	166
Figure 7.7	TEM images of three nanotags after BSA-encapsulated.	167
Figure 7.8	Multiplex SERS detection from liver site of three nanotags.	168
Figure 7.9	<i>In vivo</i> multiplex detection in xenograft tumor containing two EGFR positive nanotags, Cy7LA and Cy7.5LA .	169
Figure 7.10	<i>In vivo</i> multiplex detection of xenograft tumor containing two EGFR positive nanotag Cy7LA and CyNAMLA-381 .	170

Figure 7.11	Multiplex SERS mapping images with three Raman reporters.	171
Figure 7.12	Normalized SERS spectra of EFGR-labeled Cy7LA-nanotag at different concentrations.	172
Figure 7.13	Kinetics studies of three nanotags in tumor and liver site.	173

Chapter 8

Figure 8.1	Design of fluorescence dye for the labeling of targeting ligand.	186
Figure 8.2	Schematic diagrams for the preparation of Au/Ag nanoshells from Ag nanospheres.	189

List of Charts

Chapter 2

Chart 2.1	Iminium intermediate of amine derivative tricyanocyanine dyes.	37
Chart 2.2	80-different amine structures with different numbers.	42
Chart 2.3	Chemical structures of CyNA-414 and ICG .	48
Chart 2.4	Chemical structures of CyN-111, 165, 272 and 295 .	55
Chart 2.5	Chemical structures of CyNA-111, 165, 272 and 295 .	58
Chart 3.1	Chemical structures of CyNE790 and ICG-sulfo-OSu .	72
Chart 5.1	Amine building blocks of the CyNAMLA library.	108

List of Schemes

Scheme 2.1	Synthesis of amine tricyanocyanine derivatives.	35
Scheme 2.2	Synthesis of 1a .	49
Scheme 2.3	Synthesis of 1b .	49
Scheme 2.4	Synthesis of 1 .	50
Scheme 2.5	Synthesis of CyNA from CyN	52
Scheme 3.1	Synthesis of CyNE790 .	63
Scheme 4.1	Synthesis of CyNE 2-DG .	83
Scheme 5.1	Synthesis of cyanine derivative (CyNAMLA).	100
Scheme 5.2	Preparation of BSA-stabilized SERS nanotags.	110
Scheme 5.3	Synthesis of 4b .	124
Scheme 5.4	Synthesis of 4 .	124
Scheme 6.1	Synthesis of Cy5LA and Cy3 LA .	141
Scheme 6.2	Synthesis of PEG-SH stabilized SERS nanotags.	142
Scheme 7.1	Synthesis of Cy7LA and Cy7.5LA .	162
Scheme 7.2	Synthesis of 8a .	174
Scheme 7.3	Synthesis of 8b .	174
Scheme 7.4	Synthesis of 8c .	175
Scheme 7.4	Synthesis of 9 .	176
Scheme 7.5	Synthesis of 10 .	176
Scheme 8.1	Synthesis of NIR cell tracker dye	187

Abbreviation of symbols

AcOH	Acetic acid
Ac ₂ O	Acetic anhydride
ACN	Acetonitrile
Au	Gold
Au-NPs	Gold Nanoparticles
BSA	Bovine serum albumin
BuOH	Butanol
CDCl ₃	Deuterated chloroform
CHCl ₃	Chloroform
CO ₂	Carbondioxide
D ₂ O	Deuterated oxide
DAD	Diode array detector
DCC	N,N'-Dicyclohexylcarbodiimide
DCM	Dichloromethane
DIC	N,N'-Diisopropylcarbodiimide
DIEA	Diisopropyl ethylamine
DMAP	Dimethylaminopyridine
DMF	N, N-Dimethylformamide
DMSO	Dimethyl sulfoxide
DMSO-d ₆	Deuterated dimethyl sulfoxide
DOS	Diversity oriented synthesis
DOFLA	Diversity oriented fluorescence library approach
DTTC	3,3'-diethylthiatricarbocyanine
EA	Ethyl acetate

EGFR	Epidermal growth factor receptor
ESI	Electrospray ionization
Et ₂ O	Diethyl ether
EtOH	Ethanol
Ex	Excitation
Em	Emission
HATU	2-(1H-7-Azabenzotriazol-1-yl) 1,1,3,3-tetramethyl uronium hexafluorophosphate methanaminium
HCl	Hydrochloric acid
HEPES	4-(2-Hydroxyethyl)-1-piperazineethanesulfonic acid
HER2	Herceptin
HPLC	High-performance liquid chromatography
HPLC-MS	High-performance liquid chromatography mass spectrometry
HTS	High throughput screening
LA	Lipoic acid
MeOH	Methanol
MeOD	Deuterated methanol
MeCN	Acetonitrile
MS	Mass spectrometry
NIR	Near infrared
NMR	Nuclear magnetic resonance
NPs	Nanoparticles
PEG-SH	Polyethyleneglycol
QY	Quantum yield

RES	Reticuloendothelial system
RM	Reporter molecule
RT	Room temperature
SERS	Surface enhanced Raman scattering
SERRS	Surface enhanced resonance Raman scattering
TEM	Transmission electron microscopy
TFA	Trifluoroacetic acid
THF	Tetrahydrofuran
TLC	Thin layer chromatography
TOS	Target oriented synthesis
TRITC	Tetramethylrhodamine-5-isothiocyanate
UV	Ultraviolet
XRITC	X-rhodamine-5-(and-6)-isothiocyanate

List of publications

1. Ultrasensitive Near-Infrared Raman Reporters for SERS-based in vivo Cancer Detection, **Samanta, A.**; Maiti, K. K.; Soh, K. S.; Liao, X.; Vendrell, M.; Dinish, U. S.; Yun, S. W.; Bhuvanewari, R.; Kim, H.; Rautela, S.; Chung, J.; Olivo, M.; Chang, Y. T.* *Angew. Chem. Int. Ed. Engl.*, **2011**, *50*, 6089–6092.
2. Development of photostable near-IR cyanine dyes, **Samanta, A.**; Vendrell, M.; Das, R.; Chang, Y. T.* *Chem. Commun.*, **2010**, *46*, 7406-7408.
3. A Photostable Near-Infrared Protein Labeling Dye for in vivo Imaging, **Samanta, A.**; Vendrell, M.; Yun, S. W.; Guan, Z.; Xu, Q. H.; Chang, Y. T.* *Chem. Asian J.* **2011**, *6*, 1353-1356.
4. Multiplex cancer cell detection by SERS nanotags with cyanine and triphenylmethine Raman reporters, Maiti K. K.; **Samanta, A.**; Vendrell, M.; Soh, K. S.; Olivo, M.; Chang, Y. T.* *Chem. Commun.*, **2011**, *47*, 3514-3516.
5. Synthesis and Characterization of a Cell-permeable Near-Infrared Fluorescent Deoxyglucose Analogue for Cancer Cell Imaging, Vendrell, M.; **Samanta, A.**; Yun, S. W.; Chang, Y. T.* *Org. Biomol. Chem.* **2011**, *9*, 4760-4762.
6. Target Identification: A Challenging Step in Forward Chemical Genetics, Das, R. K.; **Samanta, A.**; Ghosh, K.; Zhai, D.; Xu, W.; Su, D.; Leong, C.; Chang, Y. T.* *Interdiscip. Bio Central* **2011**, *3*, 1-16.
7. Solid Phase Synthesis of Ultra-Photostable Cyanine NIR dye library, Das, R. K.; **Samanta, A.**; Ha, H. H.; Chang, Y. T.* *RSC Advances*, **2011**, *1*, 573-575.
8. Synthesis of a BODIPY Library and Its Application to the Development of Live Cell Glucagon Imaging Probe, Lee, J. S.; Kang, N. Y.; Kim, Y. K.; **Samanta, A.**; Feng, S.; Kim, H. K.; Vendrell, M.; Park, J. H.; Chang, Y. T.* *J. Am. Chem. Soc.* **2009**, *131*,

10077-10082. Highlighted in JACS.

9. Novel orthogonal synthesis of tagged combinatorial triazine library via Grignard reaction, Lee, J. W.; Bork, J. T. Ha, H. H.; **Samanta, A.**; Chang, Y. T.* *Aust. J. Chem.* **2009**, *62*, 1000-1006.
10. Multiplex targeted in vivo cancer detection using sensitive near-infrared SERS nanotags, Maiti, K. K.; Dinis, U. S.; **Samanta, A.**; Soh, K. S.; Vendrell, M.; Yun, S. W.; Olivo, M.; Chang, Y. T.* *Nano Today*, **2012**, *7*, 85-93.
11. *ChemInform Abstract*: Development of Photostable Near-Infrared Cyanine Dye, **Samanta, A.**; Vendrell, M.; Das, R.; Chang, Y. T.* *ChemInform*, **2011**, *42*, 204.

Patent file

1. "Development of Photostable Near-IR Cyanine Dyes for In Vivo Imaging" Y. -T. Chang; **Samanta, A.**; Vendrell, M.; Kang, N. -Y.; Maiti, K. K.; Soh, K. S.; Dinis, U. S.; Olivo, M.; International Patent Application No: PCT/SG2011/000117.; Ref: 09227N-PCT.; Docket No. 4459.1016-000.

Symposia/Conference attended

1. Poster presentation at "NUS-Chemistry/Seoul National University/ Chemistry MOU and Joint Symposium" Organized by Seoul national University, Korea, 2009
2. Poster presentation at "RSC International conference; Challenges in Chemical Biology" Organized by Manchester University, U.K, 2011.

Award obtained

1. The first prize for the "Johnson & Johnson Asia Outstanding Graduate Thesis Award in Bio-tech".

CHAPTER 1

Introduction

Technological advances have enabled the finding of small molecular probes with high selectivity to specific targets. However, the most challenging step in the identification of small molecule probes turns to be easy process using fluorescent small molecules. In this conventional strategy, targeted ligands of specific organelles in complex biological systems can be fluorescently labeled and hence imaged using fluorescence microscopy. Selective and specific images can be obtained by applying these small molecules as bioimaging probes in which a probe is labeled with a fluorescent dye. The design of fluorescent probes was initially proposed by target-oriented synthesis (TOS) where fluorophores are simply used as signal amplifiers.

When a fluorescent molecule itself undergoes a change of emission intensity or emission color upon recognition of targeted ligands is defined as a fluorescent sensor. The development of fluorescence sensors is limited in the TOS approach. Recently diversity-oriented synthesis (DOS) approaches have been employed to discover novel probes or sensors.

1.1 Overview of fluorophores

A fluorophore is a molecule with different functional groups absorbing light of a specific wavelength (most commonly in the UV-visible range) to reach an electronically excited singlet state and later emit a photon at a longer wavelength. Molecules that absorb energy cannot always emit fluorescence due to their loss of energy through non-fluorescent mechanisms (e.g. vibrational, rotational and change of molecular bonds) and a very limited number of scaffolds are found to be fluorophores. Interestingly, these few fluorescent scaffolds cover almost all colors in the spectra, from UV-visible to near-infrared (NIR) (Figure 1.1). Well known fluorophores with different wavelengths are: DAPI (4',6-diamidino-2-phenylindole

dihydrochloride),¹ FITC (Fluorescein isothiocyanate),² TRITC (tetramethylrhodamine isothiocyanate), Texas Red (sulforhodamine 101 acid chloride)³ BODIPY (boron dipyrromethene),⁴ rosamine,⁵ styryl,⁶ xanthone,⁷ oxazine⁸ and cyanine⁹ (Figure 1.2) have been employed for a range of applications in the bioorganic field.

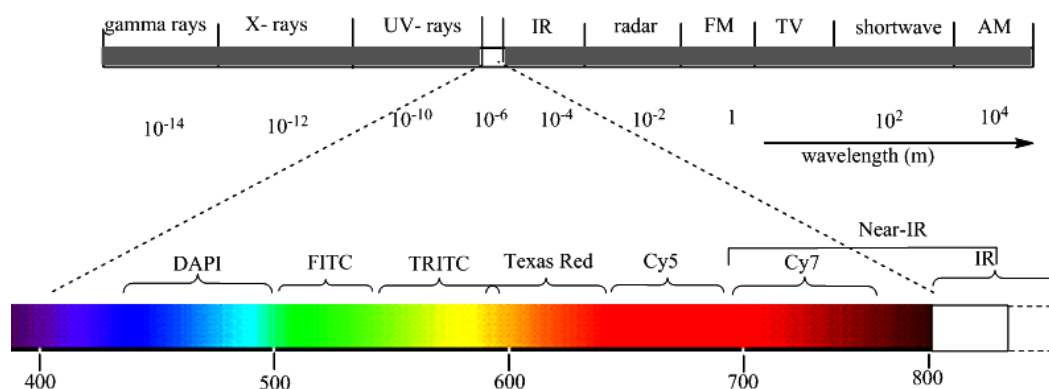


Figure 1.1. Visible spectral range of different well known fluorophores.

Recently, fluorescent small molecules have received a substantial attention in optical bioimaging studies¹⁰ due to their high detection sensitivity and minimal technical limitations. In addition, fluorescent small molecules can be applied to the development of chemosensors¹¹ for live cell imaging¹² due to their good solubility, cell permeability and low cost.

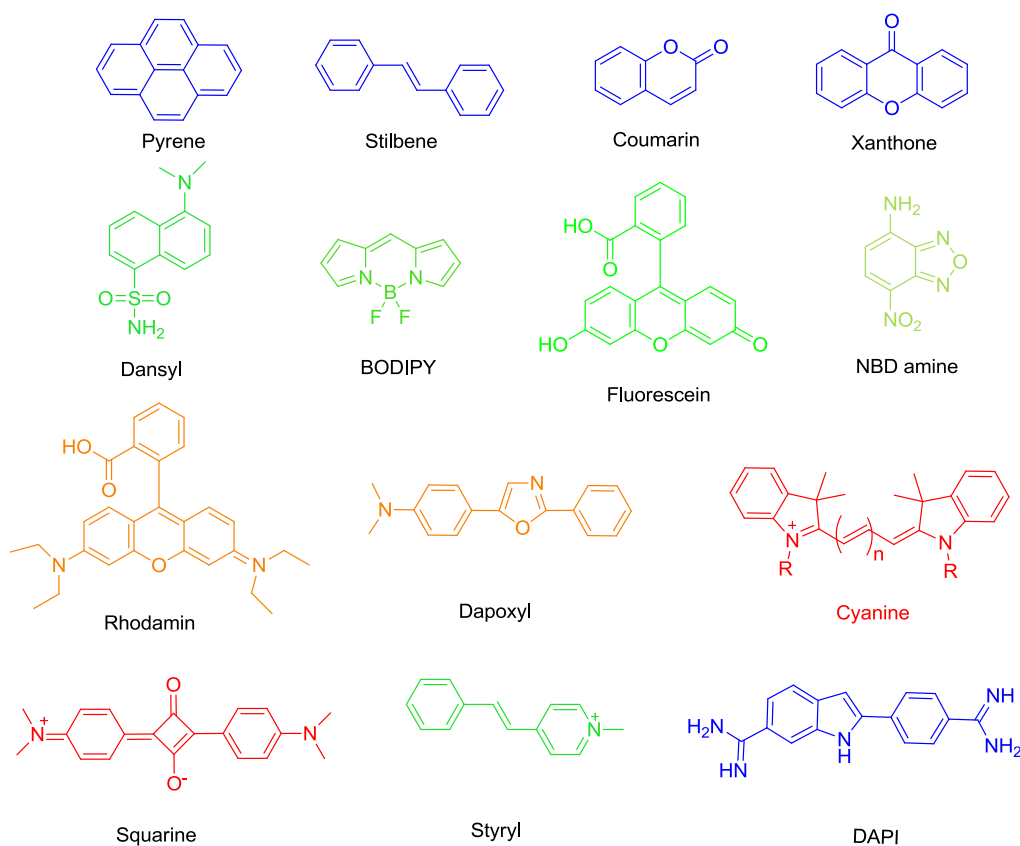


Figure 1.2. Representative fluorophores with emission ranging from blue to NIR.

1.2 Synthetic strategies for novel fluorescent probes

1.2.1 Diversity-oriented synthesis

Diversity Oriented Synthesis (DOS) has recently appeared as a powerful tool for the preparation of molecular probes to study different biological functions. In this strategy, the skeleton of a small molecule is explored in a combinatorial way to obtain a library of molecules (Figure 1.3). Based on this approach, the field of chemical genomics has rapidly expanded and facilitated the discovery of new mechanisms for a number of biological processes. Inspired by many successful attempts, research groups have been racing to invent effective functional networks at a cellular level by applying diverse chemical libraries. In the context of bioimaging, small molecules that undergo changes in fluorescence upon recognition of the specific target analytes have drawn considerable attention to recognize different biomolecules. For example, Hoechst and DAPI are well known DNA dyes that localize in the nucleus and

rhodamine dyes are widely used as mitochondria probes.¹³ However, the design of fluorescent sensors for specific organelle largely relies on empirical discovery, and one of the most convenient ways to develop specific organelle probes bases on high-throughput screenings: large numbers of molecules from different sources are screened in different organelles in order to identify the most suitable probes. The synthesis of a large number of molecules in high purities is challenging due to the difficulties in the purification steps. This limitation is particularly relevant in the development of novel bioimaging probes, with limited fluorophore scaffolds and several synthetic difficulties, and novel imaging probes are reported in a relatively low speed. To accelerate the development of imaging probes, Chang and co-workers proposed the concept of a diversity-oriented fluorescence library approach (DOFLA).¹⁴ As shown in Figure 1.3, one single molecular cassette can be modified in a combinatorial manner so that thousands of fluorescent small molecules covering UV-Vis to NIR colors can be synthesized. To date, several research groups have developed imaging probes for various targets (e.g. glucagon,¹⁵ DNA,¹⁶ GTP,¹⁷ RNA,¹⁸ β -amyloid,¹⁹ chymotrypsin,²⁰ heparin,²¹ ,glutathione,²² human serum albumin (HSA),²³ bovine serum albumin (BSA),²⁴ site-specific labeling of proteins inside live cells,²⁵ embryonic stem cell probe,²⁶ quantitative sugar analysis,²⁷ and an immunoglobulins²⁸). These examples validate the power of DOFLA, in which the synthesis of fluorescent libraries and their screening towards specific analytes can render active fluorescent probes.

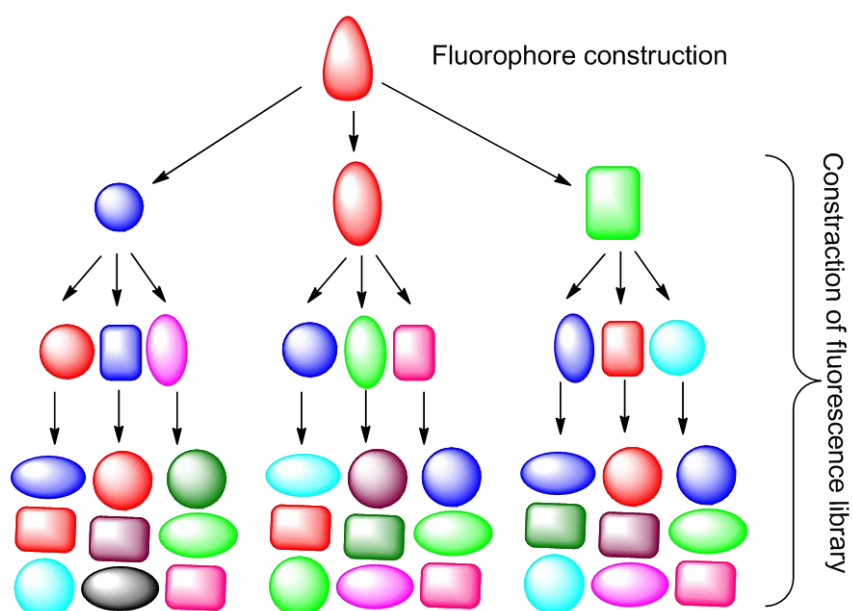


Figure 1.3. Diversity oriented fluorescence library approach.

The applicability of DOS can also be extended to optimize the photophysical properties of fluorescent dyes. As illustrated in Figure 1.4, the construction of a library of cyanine molecules to optimize their photostability properties was possible by modification of different “R_{1,9}” without changing the core cassette of tricarbocyanine dyes. Furthermore, highly sensitive SERS active Raman reporter molecules have been also found by applying this approach.

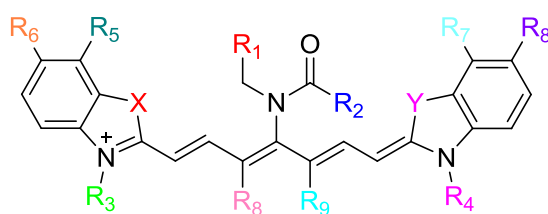


Figure 1.4. Diversity at different position depending on the requirement of cyanine dye cassette.

1.2.2 Target-Oriented Synthesis

Target oriented fluorescent probes have been designed by tagging fluorophores to recognition moieties. The recognition moieties are designed based on experienced knowledge. The experimental results may not reflect all the time as it is

expected. Hence the target oriented synthesis has some limitations to develop large number of molecular probes. Despite the limitations several advantages make it more suitable for the design of fluorescence probe. To do that, different approaches are available. The most common and powerful approach is fluorescent tag approach²⁹ and affinity approach³⁰.

1.3 Near-infrared fluorophores

Among the different fluorophores, NIR dyes (i.e. molecules absorbing light in the range of 700 to 1000 nm) are more suitable for the optical imaging *in vivo*³¹ while the shorter wavelength dyes ranging from blue to green are mainly used for *in vitro* cell imaging studies. Therefore, NIR light absorbing dyes have attracted much attention for the development of the *in vivo* optical imaging probes. NIR light has been employed in a wide range of biomedical applications due to its deep tissue penetration. UV-visible light often suffers from high autofluorescence and background limitations. On the contrary, NIR light minimizes the background problems and opens up a new window for the NIR light absorbing dyes. The advantages of imaging in the NIR region are numerous: (a) the low absorbance from tissue enables a deeper tissue penetration; (b) low auto-fluorescence reduces the fluorescence background and (c) low Raman scattering produces very high signal to noise ratio. Recently, the attention on tissue imaging or *in vivo* imaging has attracted the development of different NIR fluorophores. To date a very few number of scaffolds are available to develop NIR fluorophores (e.g. squaraine,³² quinone,³³ triphenylmethane,³⁴ cyanine³⁵). Among them, cyanine structures³⁶ have been one of the most popular scaffolds amongst the various fluorescent NIR dyes for the development of imaging probes due to their synthetic accessibility, large molar extinction coefficient and broad wavelength tenability. In addition, photo-switchable cyanine dyes are useful for high resolution microscopy (e.g. STORM and PALM³⁷) and fluorescent small molecules are useful for flow cytometry, sequencing assays,

optical sensing membranes³⁸ and high-throughput screening (HTS).³⁹ In view of these advantages over other fluorophores, cyanine dyes have been considered for the development of new NIR libraries for bioimaging purposes in this thesis.

1.3.1 Cyanine dyes

Cyanine dyes are a class of polymethine dyes which consist of an odd number of methine groups (CH). König et al. experimentally showed in 1925 that polymethine cyanine dyes shifted 100 nm absorbance wavelengths⁴⁰ due to the presence of vinylene functional groups (Figure 1.5). This broad range of wavelengths covered by the cyanine dyes has been employed for a wide range of applications in different fields. The applicability of cyanine dyes widely ranges from photographic sensitizers, nonlinear optical materials,⁴¹ and more recently, fluorescent probes for biomolecular labeling.⁴² Specially, one class of polymethine cyanine dyes for the generation of NIR compounds are tricarbocyanine and heptamethine cyanine dyes.

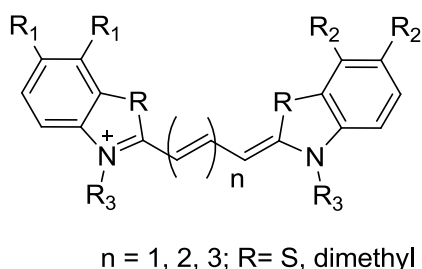


Figure 1.5. General structure of cyanine dyes.

1.3.2 Tricarbocyanine dyes

Carbocyanine dyes are a type of cyanine dyes whose structure has two heterocyclic rings connected by a carbon chain alternating single and double bonds (e.g. =CH-CH=CH-). These dyes are also known as polymethine cyanine dyes. Polymethine cyanine dyes are defined as pentamethine or heptamethine depending on the number of carbon atoms between the two heterocycle rings. In a similar way,

tricyanocyanine dyes are defined in the number of chain carbons between the two heterocyclic rings (Figure 1.6).

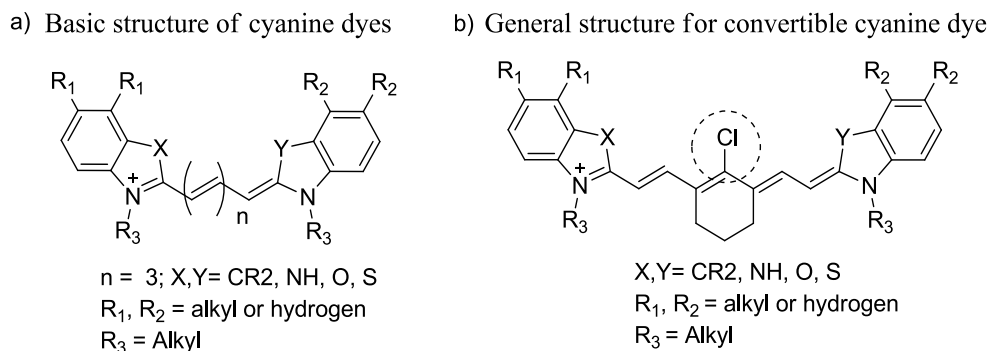


Figure 1.6. a) General structure of heptamethine and b) tricyanocyanine dyes.

A variety of tricyanocyanine cyanine dyes can be developed by modification of the side chain of the heterocyclic rings. The resulting derivatives show very similar spectroscopic properties due to the unaffected of π - π conjugation. In 1977, Reynolds et al. first reported a stable heptamethine pyrylium dyes bearing a reactive chloro functional group at the central position of the polymethine chain and two heterocyclic rings at the side chains.⁴³ These cyanine dyes mainly absorbed light at infra-red (IR) regions from 1000 to 1300 nm. At the same year, Makin et al. reported a different heterocyclic ring at the side chain of the dyes which absorbed light in the NIR region. In this synthetic procedure, a condensation reaction between a heterocyclic ring containing an activated methyl group and an unsaturated bisaldehyde or its derivative was performed in the presence of a catalyst such as a sodium acetate.⁴⁴ These cyanine dyes particularly offered a new functional group for further modification and the resulting compounds were more versatile in terms of spectroscopic properties, with absorbances ranging from 700 to 1100 nm.

To date, the central chlorine atom in the convertible tricyanocyanine structure (Figure 1.7) has been modified by different nucleophiles such as thiols, alcohols, phenols, amines and anilines. The substitution of the chlorine at the central position

was first derivatized by Streckowski et al.⁴⁵ in 1992. The authors reported the nucleophilic substitution with sodium methoxide, Methylamine, Sodium phenoxide, Sodium thiophenoxide, Thiophenol and 4-Aminothiophenol which yielded a diverse set of NIR dyes. This straightforward and highly efficient strategy opened up a new window for a broad range of chemical structures in the NIR region. To improve the synthetic procedure, Narayanan et al.⁴⁶ designed a new uncatalyzed synthetic route for heptamethine cyanine and tricarbocyanine dyes in 1995. Though the diverse range of chemistry was well explored, the detailed photophysical properties (especially fluorescence) were not well characterized. Next in 1997, Flanagan et al. reported a novel NIR absorbing tricarbocyanine dye with a reactive isothiocyanate functional group that could be easily conjugated to primary amines.⁴⁷ Until 2005, most of the NIR tricarbocyanine dyes based on the phenol and thiophenol derivatives were chemically unstable and displayed short Stokes shifts (~25 nm). Bearing this in mind, Peng et al. reported heptamethine cyanine dyes with the formation of a C-N bond at the central position, which helped the intramolecular charge transfer (ICT). The resulting derivatives showed a hypsochromic shift of the absorbance wavelengths as well as longer Stokes shifts (~150 nm). These NIR fluorescent probes have better properties than common cyanine dyes due to their minimum overlapping⁴⁸ of absorbance and emission wavelengths. Next in 2006, Lee et al. synthesized water-soluble heptamethine cyanine dyes by Suzuki-Miyaura reaction to introduce a robust C-C bond at the central position of the NIR tricarbocyanine scaffold.⁴⁹ The resulting dyes were more photostable when compared to aryl ether, aryl thioether, aryl amine, alkyl ether, and alkyl thioether fluorophores, which were found to have a poor stability.

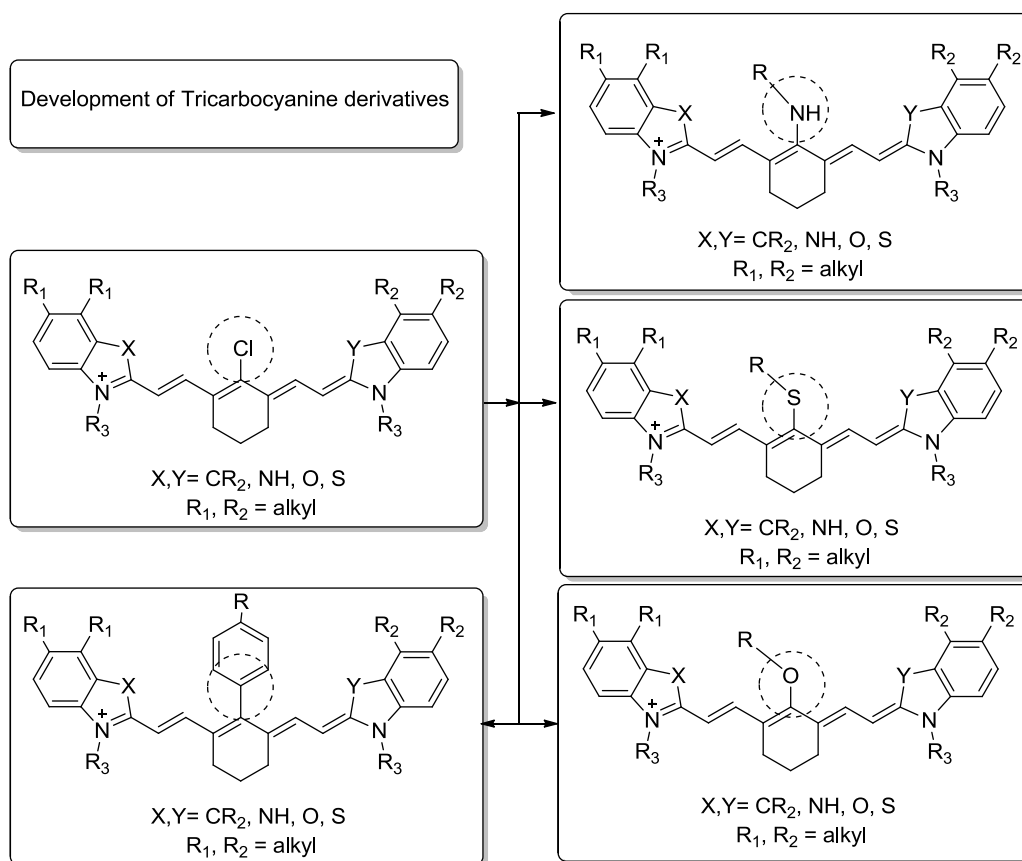


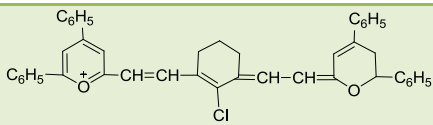
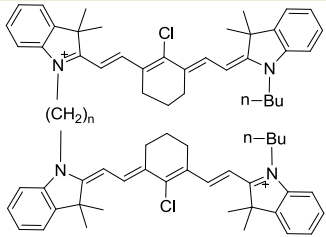
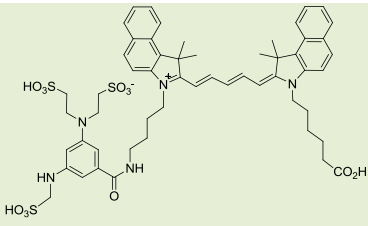
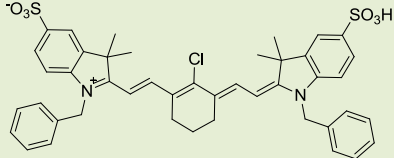
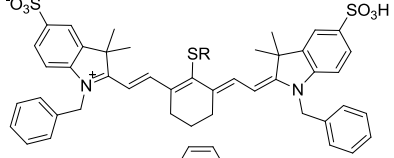
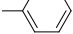
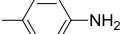
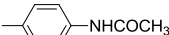
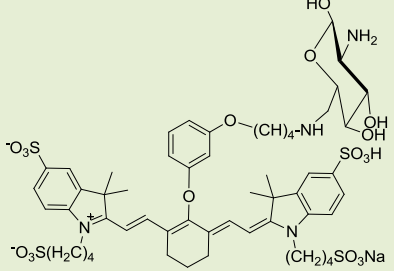
Figure 1.7. Examples of different tricarbocyanine dyes.

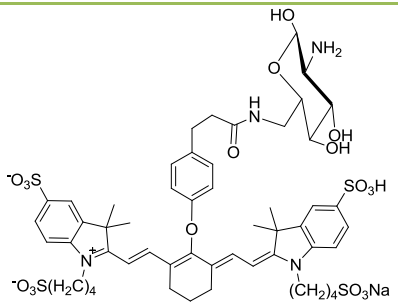
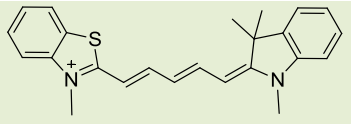
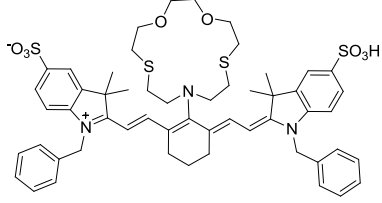
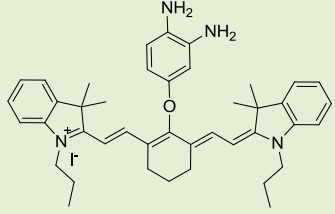
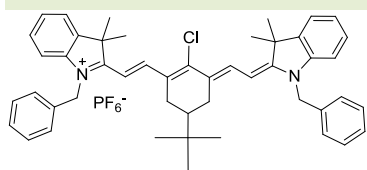
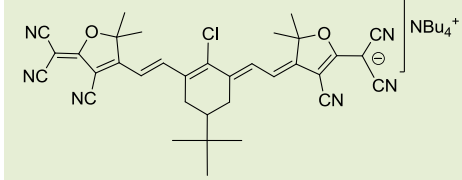
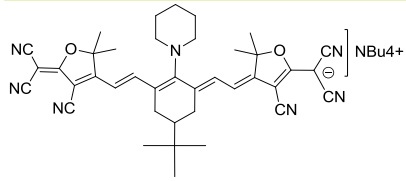
1.4 Properties of cyanine dyes

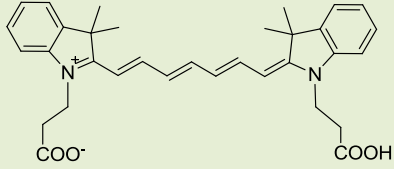
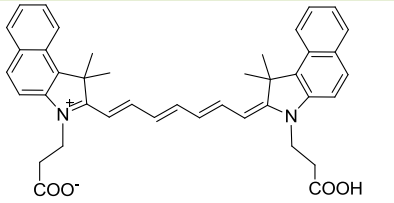
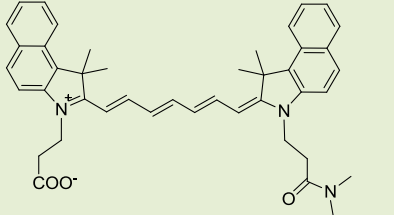
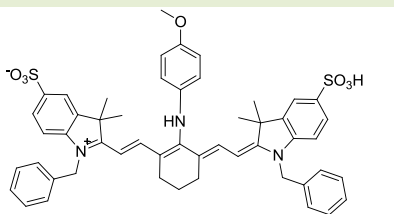
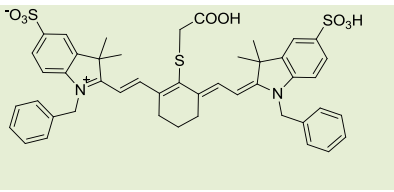
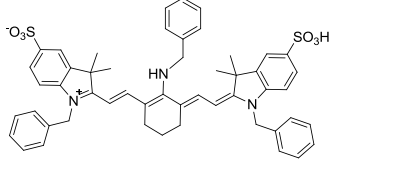
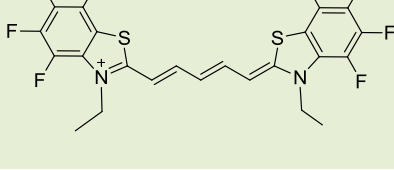
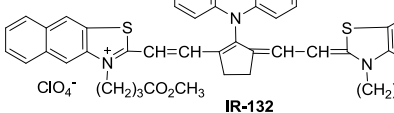
1.4.1 Photophysical properties of cyanine dyes

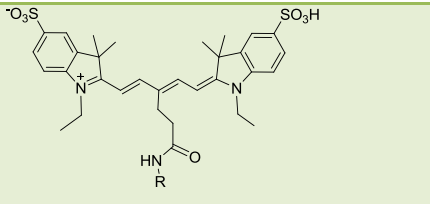
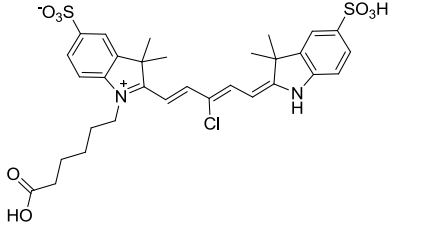
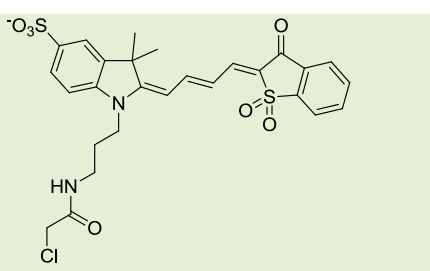
Cyanine dyes can absorb light in the range from UV-Visible to IR and emit at comparatively longer wavelengths. As they are positively charged species, their solubility is quite good in polar solvents. Generally, cyanine dyes show low to moderate quantum yields, and their extinction coefficients are high with respect to most common dyes. The intensity (molar absorption, extinction coefficients, and oscillator strength) of polymethine dyes generally increases as the vinylene chain length is extended, and the fluorescence efficiency of NIR cyanine dyes is generally enhanced if dye molecules are bound to macromolecules⁵⁰ (e.g. proteins) or coordinated to metal ions. Table 1.1 summarizes different cyanine dyes and their most representative photophysical properties.

Table 1.1. Spectral properties of cyanine dyes.

Compounds	Absorbance	Emission	Ref
	1072 nm (H ₂ O)	n.a	43
	780 nm (DMSO)	n.a	51
	680 nm (PBS buffer)	710 nm (PBS buffer)	52
	783 nm (H ₂ O)	803 nm (H ₂ O)	53
 <p> 1a R =  1b R =  1c R =  </p>	794 nm (H ₂ O) 795 nm (H ₂ O) 798 nm (H ₂ O)	817 nm (H ₂ O) 820 nm (H ₂ O) 823 nm (H ₂ O)	53
	766 nm (DMSO)	782 nm (DMSO)	54

 <p> HO NH_2 OH O_3S SO_3H $\text{O}_3\text{S}(\text{H}_2\text{C})_4$ $(\text{CH}_2)_4\text{SO}_3\text{Na}$ </p>	768 nm (DMSO)	784 nm (DMSO)	54
	648 nm (DMSO)	674 nm (DMSO)	55
 <p> O_3S SO_3H </p>	695 nm (MeOH)	775 nm (MeOH)	56
 <p> NH_2 NH_2 </p>	755 nm (sodium phosphate buffer)	790 nm (sodium phosphate buffer)	57
 <p> Cl PF_6^- </p>	802 nm (DCM)	818 nm (DCM)	58
 <p> NC NC Cl NC NC NBu_4^+ </p>	900 nm (DCM)	936 nm (DCM)	58
 <p> NC NC CN CN NBu_4^+ </p>	715 nm (DCM)	900 nm (DCM)	58

	748 nm (DMSO)	768 nm (DMSO)	59
	783 nm (DMSO)	808 nm (DMSO)	59, 60, 61
	783 nm (DMSO)	807 nm (DMSO)	59
	686 nm (H ₂ O)	783 nm (H ₂ O)	62
	786 nm (H ₂ O)	808 nm (H ₂ O)	62
	617 nm (H ₂ O)	757 nm (H ₂ O)	48
	648 nm (DMSO)	n.a	63
	814 nm (EtOH)	n.a	64

	642 nm (H ₂ O)	656 nm (H ₂ O)	65
	646 nm (H ₂ O)	670 nm (H ₂ O)	66
	594 nm (H ₂ O)	616 nm (H ₂ O)	67

1.4.2 Stability of cyanine dyes

Cyanine dyes are generally prepared by alternating the conjugation of double bonds between two heterocyclic rings, one of which contains a heterocyclic ring with a positive charge on the nitrogen atom. Thus these cationic dyes are highly affected by nucleophilic solvents, and aqueous or methanolic solvents can react as nucleophiles under basic conditions.⁶⁸ This low chemical stability of cyanine (e.g. Cy3, Cy5 and Cy7) dyes has been considered their most significant drawbacks. Furthermore, most of the tricarbocyanine derivatives (e.g. aryl ether, aryl thioether, aryl amine, alkyl ether, and alkyl thioether) are unstable even in physiological conditions for long time. In addition to chemical stability, a major limitation of cyanine dyes is photobleaching or photodestruction. Upon irradiation of light to aqueous solutions of cyanine dyes, reactive oxygen species such as singlet oxygen (¹O₂), peroxide, superoxide and redox active metabolites can react with the fluorophores⁶⁹ and lead to their degradation. Specially, tricarbocyanine dyes are known to be relatively low photostable due to their long π - π conjugation. Very few

reports about the photostability of cyanine dyes are available in the literature. For example, Song et al. reported in 1997 a comparative photobleaching study between aryl thioether and aryl amine derivatives of tricarbocyanine dyes and proved the superiority of amine derivatives.⁶² Though there are several examples of NIR probes based on aryl ether, aryl thioether and aryl amines of tricarbocyanines, there is a need for more photostable NIR cyanine dyes for long-term *in vivo* experiments. To date, few examples of photostable cyanine dyes have been described. In 1997, Guther et al. first introduced cyclodextrins to enhance the chemical stability by protecting dyes from the collisions with reactive species. In 2004 Renikuntala et al. first reported the chemical modification by introducing electron-withdrawing fluorine atoms to the phenyl rings of cyanine dyes in order to improve the photostability of pentamethine cyanine dyes.⁶³ In 2006 Chen et al. reported that the decomposition of tricarbocyanine dyes due to the incorporation of singlet oxygen ($^1\text{O}_2$) and introduced an electron-withdrawing group on the nitrogen atom of the indole rings in side chain of the heterocycle.⁷⁰ Touthkine et al. introduced a small cyano group in merocyanine dyes and demonstrated their improved photostability of cyanine dyes.⁷¹ Tricarbocyanine dyes have not been extensively explored in terms of improving their photostability. Even though their applicability as NIR dyes for *in vivo* imaging is highly demanded.

1.4.3 Surface enhanced Raman scattering (SERS) properties

Raman active molecules can be highly sensitive when they are in close proximity to the roughened surface of noble metal nanoparticles or when they are adsorbed on metallic nanostructures. This phenomenon is known as surface-enhanced Raman scattering (SERS). In 1974, Fleischmann et al. described the surface effect on Raman active molecules, in which the Raman scattering of pyridine and its derivatives was significantly enhanced when adsorbed on the surface of silver nanoparticles.⁷² After that, the first report of SERS on silver and gold colloids was published in 1979 by Creighton et al.⁷³ Since then, noble metal colloids have become

the most common material for the development of nanostructures of SERS active nanoparticles (NPs). SERS spectroscopy has several advantages over conventional fluorescence spectroscopy. For examples, SERS has a lower susceptibility to photobleaching and an enhanced multiplex capability due to the non-overlapping narrow bandwidths of the peaks. However, the reproducibility of the signal intensities of SERS nanotags, which are prone to aggregate formation, has been identified as the major drawback of SERS spectroscopy. This phenomenon is generally observed due to the interaction of nanotags with the environment.⁷⁴ For example, SERS nanotags suspended in aqueous buffers containing chloride ions can lead to aggregation due to the ionic exchange on the surface of the NPs. This limitation has been recently solved with encapsulation strategies and incorporation of linkers. To improve the stability and biocompatibility of NPs, a protective layer of polyethylene glycol (PEG) has been used to encapsulate the noble metal nanoparticles. PEG-SH encapsulation is now a very well-known method to prevent gold nanoparticles from aggregation in buffer solutions and organic solvents.^{75,76} Encapsulation strategies have been extended to DNA or proteins like bovine serum albumin (BSA).⁷⁷⁻⁸⁴ PEG-SH protected gold NPs show negligible cytotoxicity and better biocompatibility when compared to free NPs.⁸⁵ Moreover, this protecting layer not only enhances the stability of NPs but also opens up the possibility of incorporating new functional groups which can be conjugated to a variety of biologically relevant ligands or antibodies for targeted approaches.

1.5 Applications of cyanine dyes

I have discussed earlier the diversity oriented synthesis (DOS) of fluorescent libraries by combinatorial methods. These libraries of fluorescent small molecules are excellent toolboxes for the discovery of fluorescent probes. High- throughput screening is a key strategy in the finding of active molecules towards selected analytes. Inglese et al.⁸⁶ demonstrated the efficiency of high-throughput screenings of

libraries in microtiter plate assays to discover active small molecule probes. Based on this concept, I aim to perform high-throughput screenings to discover photostable and Raman-active cyanine dyes from our libraries (Figure 1.8).

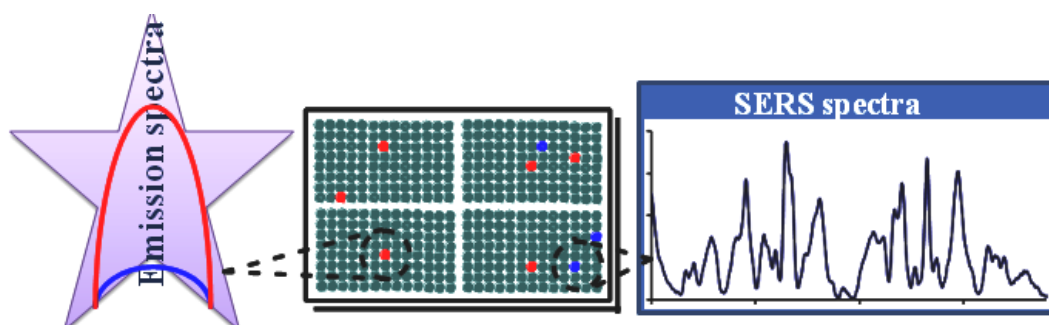


Figure 1.8. Representing high-throughput screening strategy in microplate readers.

1.5.1 *In vivo* fluorescence imaging

In vivo fluorescence imaging using NIR light has a great prospective for molecular diagnostics and therapeutic studies. Furthermore, as NIR *in vivo* imaging is non-invasive, there is significant concern for the translation of novel optical NIR imaging into the clinic. The applicability of exogenous NIR-emissive contrast agents is highly demanded for deep-tissue fluorescence imaging, and a large number of NIR cyanine probes have been reported to date. In 1999, Weissleder et al.⁸⁷ applied a NIR fluorescent cyanine dye for *in vivo* imaging of tumors and successfully demonstrated their applicability to detect tumors of submillimeter size. Hence, these NIR fluorescence probes did show a very high potential to identify early stage tumors *in vivo*. The applicability of NIR tricyanobocyanine probes regarding *in vivo* tumor imaging was later described for the early detection of stomach, colon, and breast cancer as reported by Becker et al.⁸⁸ In 2006, Leevy et al. demonstrated the applicability of fluorescent molecular probes containing zinc (II) dipicolylamine (Zn-DPA) which is able to selectively stain the surfaces of apoptotic animal cells and obtained a tumor imaging in living mice system (Figure 1.9).⁸⁹

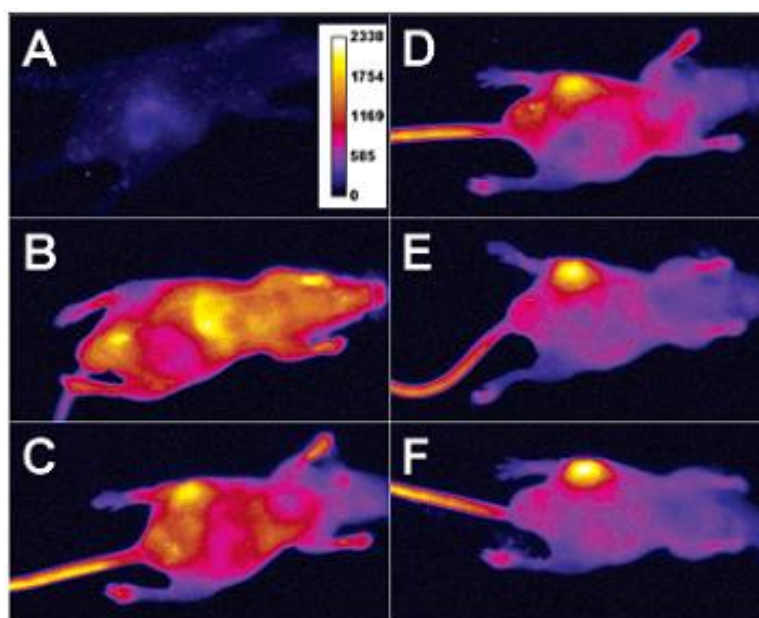


Figure 1.9. Optical images of a mouse with a *S. aureus* infection in the left rear thigh muscle. Images were acquired before (A), and immediately following (B), intravenous injection of probe 1 and at 6 h (C), 12 h (D), 18 h (E), and 21 h (F). *This picture has been copied from *J. Am. Chem. Soc.* **2006**, *128*, 16476-16477 under copyright permission.

In 2002 Ntziachistos et al. reported *in vivo* imaging by Cy5.5 as NIR labeling dye,⁹⁰ and recent approaches have pursued their use to study protein-DNA interactions.⁹¹ Sasaki et al. also demonstrated the applicability of NIR fluorophores as turn-on fluorescent sensors for the detection of nitric oxide (NO). The authors proved the detection of NO in cells, indicating that this NIR probe could be applicable for the detection of *in vivo* NO imaging.⁵⁷ Kiyose et al. developed a ratiometric fluorescent Zn(II) probe based on tricyanocyanine structure composed of a tricyanocyanine dye and a Zn(II) ion chelating ligand.⁸⁹ NIR tricyanocyanine dyes have been also applied to imaging bacterial infection in mice,⁹² the detection of heavy metals (e.g. Hg(II)⁵⁶) or to monitor the pH (Figure 1.10).⁹³

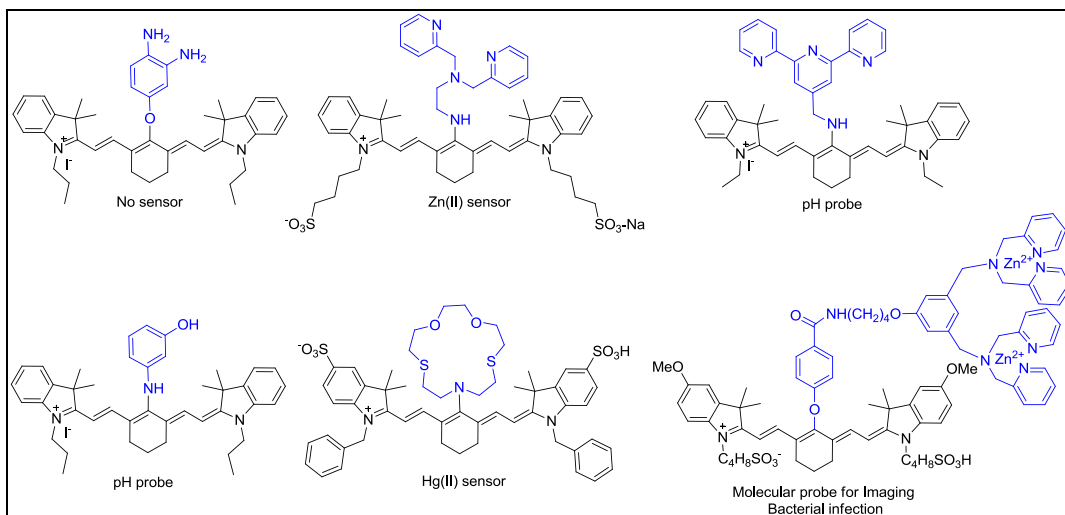


Figure 1.10. Representative examples of tricyanocyanine fluorescent probes.

1.5.2 SERS imaging

There has been a substantial interest during the last decade to apply SERS to the sensitive detection of biomolecules inside living cells,⁹⁴ glucose sensing,⁹⁵ protein analysis,⁹⁶ or the investigation of sensitive biological samples.⁹⁷ For these purposes, reporter molecules (i.e. Raman-active dyes) with thiol functional groups have been attached on the surface of silver or gold NPs with variable sizes (10–80 nm) to obtain SERS nanotags. As discussed earlier, the reproducibility and spectral intensity of these nanotags can be controlled by encapsulation and shielding from the environment. In the recent years, stable and biocompatible nanoparticles (NPs) have been used for SERS cellular imaging. Antibody-conjugated gold nanoparticles (AuNPs) and nanorods have been employed for the targeted imaging of specific cancer markers that are highly expressed on the surface of cancer cells. Hence, antibody-conjugated AuNPs are selectively attached to the target cancers cells and the higher SERS intensity from the target cancer cells enables their imaging and detection. In this context, antibodies that recognize the epidermal growth factor receptor (EGFR)⁹⁸ over-expressed in human tumors have been conjugated to SERS nanotags and applied to the detection of tumors *in vivo*.⁹⁸ NIR dyes (e.g.

diethylthiatricarbocyanine (DTTC)) have been also employed as specific Raman reporters for *in vivo* surface-enhanced resonance Raman scattering (SERRS).⁹⁹ With the demonstration by Tang et al. that 60-nm AuNPs could enter human osteosarcoma cells (G292 line) and reside in the cytoplasm and surrounding of the nucleus,¹⁰⁰ I was encouraged to develop novel SERS AuNPs as diagnostic tools for the detection of tumors *in vivo* or multiple cancer cells *in vitro*.

1.6 Scope and outline of the thesis

I have discussed earlier the synthesis of polymethine cyanine dyes and the different synthetic strategies for tricarbocyanine dyes. I have also highlighted the photophysical properties of cyanine dyes. The promising spectral properties of NIR dyes have attracted our interest due to their potential application for *in vivo* imaging and I have introduced the concept of DOFL for the development of new bioimaging probes. Hence, we aim at designing new libraries of NIR dyes with a diverse range of spectral properties. To date, the most common approach to synthesize a large set of molecules based on the tricarbocyanine structure considers the use of amines as nucleophiles since thioether and ether derivatives are chemically unstable.

The aims for this thesis project are:

- 1) To develop a novel strategy to improve the photostability of tricarbocyanine dyes.

In this strategy, we introduced an electron-withdrawing group at the central nitrogen atom of amine tricarbocyanine dyes. The higher stability of this new set of molecules (**CyNA**) led to the design of a diversity-oriented library to identify the most photostable cyanine dyes.

- 2) To modify the most photostable cyanine dye from our library so that it included a functional group for further conjugation to small molecules or macromolecules.

We introduced a glutaric acid linker and the functionalized dye (**CyNE790**) was applied to the conjugation of an antibody to target specific cancer cells. Furthermore, we proved the applicability of this protein labeling dye for *in vivo*

- imaging and showed its better photophysical properties compared to the commercial ICG-sulpho-OSu.
- 3) To apply **CyNE790** to the conjugation of small metabolites, such as glucose, and prove its applicability in cancer cell imaging. This dye-conjugated glucose derivative behaved similar to glucose and the cell permeability of our new tricyanocyanine dye was better when compared to the reported IR800CW-2DG derivative.
 - 4) To develop the new detection tool for the identification of cancer *in vivo* based on the surface-enhanced Raman scattering (SERS) of cyanine dyes. I have applied the **CyNA** structure to design novel Raman active signature molecules and introduced a thiol linker motif (lipoic acid) to chemisorb an 80-member **CyNAMLA** library on gold nanoparticles (AuNPs). I have screened the full library and selected the most responsive compounds and compared their performance with the only commercially available NIR Raman reporter (i.e. DTTC).
 - 5) To design multiplex partners of Raman active dyes based on a different set of cyanine dyes, specifically **Cy3LA** and **Cy5LA** derivatives. These cyanine dyes are highly Raman active at 633 nm laser source, and we selected a triphenylmethene multiplex partner (**B2LA**) for the multiplex detection of cancer cells *in vitro*.
 - 6) To demonstrate the applicability of SERS multiplicity *in vivo*. I have designed a novel pair of NIR-active tricyanocyanine Raman reporters (**Cy7LA** and **Cy7.5LA**) to partner with our previously synthesized **CyNAMLA381**. We demonstrated that anti-EGFR antibody conjugated nanotags displayed excellent selectivity towards EGFR+ tumors in xenograft models and it could be applied for multiplexed detection *in vivo*.

1.7 References

1. B. I. Tarnowski, F. G. Spinale, J. H. Nicholson, *Biotech. Histochem.* **1991**, *66*, 296.
2. W. Pham, J. Xie, J. C. Gore, *Neoplasia* **2007**, *9*, 1130.
3. G. MacBeath, S. L. Schreiber, *Science* **2000**, *289*, 1760.
4. (a) P. J. Emmerson, S. Archer, W. El-Hamouly, A. Mansour, H. Akil, F. Medzihradsky, *Biochem. Pharmacol.* **1997**, *54*, 1315.; (b) L. J. Jones, R. H. Upson, R. P. Haugland, N. Panchuk-Voloshina, M. Zhou, *Anal. Biochem.* **1997**, *251*, 144.; (c) J. Bai, R. E. Pagano, *Biochemistry* **1997**, *36*, 8840.
5. (a) Y. H. Ahn, J. S. Lee, Y. T. Chang, *J. Am. Chem. Soc.* **2007**, *129*, 4510.; (b) T. Tokimoto, S. Tsukahara, H. Watarai, *Langmuir* **2005**, *21*, 1299.
6. G. R. Rosania, J. W. Lee, L. Ding, H. S. Yoon, Y. T. Chang, *J. Am. Chem. Soc.* **2003**, *125*, 1130.
7. L. Hu, H. Hu, W. Wu, X. Chai, J. Luo, Q. Wu, *Bioorg. Med. Chem. Lett.* **2011**, *21*, 4013.
8. (a) B. J. McAuley, M. Nieuwenhuyzen, G. N. Sheldrake, *Org. Lett.* **2000**, *2*, 1457.; (b) P. Gizecki, R. Dhal, L. Toupet, G. Dujardin, *Org. Lett.* **2000**, *2*, 585.
9. (a) N. Yamamoto, S. Homma, Y. Nakagawa, M. Hayami, H. Imanaga, M. Kurimoto, M. Mitsunashi, T. Kimoto, *J. Photochem. Photobiol. B* **1992**, *13*, 295.; (b) R. B. Mujumdar, L. A. Ernst, S. R. Mujumdar, C. J. Lewis, A. S. Waggoner, *Bioconjugate Chem.* **1993**, *4*, 105.; (c) A. Mishra, R. K. Behera, P. K. Behera, B. K. Mishra, G. B. Behera, *Chem. Rev.* **2000**, *100*, 1973.
10. (a) K. Giewekemeyer, P. Thibault, S. Kalbfleisch, A. Beerlink, C. M. Kewish, M. Dierolf, F. Pfeiffer, T. Salditt, *Proc. Natl. Acad. Sci. U. S. A.* **2010**, *107*, 529.; (b) M. Cui, M. Ono, H. Kimura, B. L. Liu, H. Saji, *Bioorg. Med. Chem. Lett.* **2011**, *21*, 980.; (c) B. E. Cohen, *Nature* **2010**, *467*, 407.; (d) K. Kikuchi, *Chem. Soc. Rev.* **2010**, *39*, 2048. d) M. Y. Berezin, S. Achilefu, *Chem. Rev.* **2010**, *110*, 2641.
11. Z. Xu, J. Yoon, D. R. Spring, *Chem. Soc. Rev.* **2010**, *39*, 1996.

12. S. Cutler, D. Ehrhardt, *Curr. Opin. Plant. Biol.* **2000**, *3*, 532.
13. a) G. J. Spangrude, M. J. Kim, D. D. Cooper, S. F. Hayes, *Blood* **1998**, *91*, 4106.;
(b) S. Zhang, V. Metelev, D. Tabatadze, P. C. Zamecnik, A. Bogdanov, Jr., *Proc. Natl. Acad. Sci. U. S. A.* **2008**, *105*, 4156.; (c) B. C. Dickinson, D. Srikun, C. J. Chang, *Curr. Opin. Chem. Biol.* **2010**, *14*, 50.
14. J. S. Lee, Y. K. Kim, M. Vendrell, Y. T. Chang, *Mol. Biosyst.* **2009**, *5*, 411.
15. J. S. Lee, N. Y. Kang, Y. K. Kim, A. Samanta, S. Feng, H. K. Kim, M. Vendrell, J. H. Park, Y. T. Chang, *J. Am. Chem. Soc.* **2009**, *131*, 10077.
16. J. W. Lee, M. Jung, G. R. Rosania, Y. T. Chang, *Chem. Commun.* **2003**, *18*, 52.
17. Q. Li, Y. T. Chang, *Nat. Protoc.* **2006**, *1*, 2922.
18. S. Wang, Y. T. Chang, *J. Am. Chem. Soc.* **2006**, *128*, 10380.
19. Q. Li, J. S. Lee, C. Ha, C. B. Park, G. Yang, W. B. Gan, Y. T. Chang, *Angew. Chem. Int. Ed. Engl.* **2004**, *43*, 6331.
20. S. Wang, Y. K. Kim, Y. T. Chang, *J. Comb. Chem.* **2008**, *10*, 460.
21. S. Wang, Y. T. Chang, *Chem. Commun.* **2008**, *10*, 1173.
22. Y. H. Ahn, J. S. Lee, Y. T. Chang, *J. Am. Chem. Soc.* **2007**, *129*, 4510.
23. Y. H. Ahn, J. S. Lee, Y. T. Chang, *J. Comb. Chem.* **2008**, *10*, 376.
24. J. S. Lee, H. K. Kim, S. Feng, M. Vendrell, Y. T. Chang, *Chem. Commun.* **2011**, *47*, 2339.
25. J. J. Lee, S. C. Lee, D. Zhai, Y. H. Ahn, H. Y. Yeo, Y. L. Tan, Y. T. Chang, *Chem. Commun.* **2011**, *47*, 4508.
26. K. K. Ghosh, H. H. Ha, N. Y. Kang, Y. Chandran, Y. T. Chang, *Chem. Commun.* **2011**, *47*, 7488.
27. K. K. Ghosh, E. Yap, H. Kim, J. S. Lee, Y. T. Chang, *Chem. Commun.* **2011**, *47*, 4001.
28. M. Vendrell, G. G. Krishna, K. K. Ghosh, D. Zhai, J. S. Lee, Q. Zhu, Y. H. Yau, S. G. Shochat, H. Kim, J. Chung, Y. T. Chang, *Chem. Commun.* **2011**, *47*, 8424.

29. M. J. Evans, A. Saghatelian, E. J. Sorensen, B. F. Cravatt, *Nat. Biotechnol.* **2005**, *23*, 1303.
30. Y. Webb, X. Zhou, L. Ngo, V. Cornish, J. Stahl, H. Erdjument-Bromage, P. Tempst, R. A. Rifkind, P. A. Marks, R. Breslow, V. M. Richon, *J. Biol. Chem.* **1999**, *274*, 14280.
31. K. A. Kelly, J. Carson, J. R. McCarthy, R. Weissleder, *PLoS One* **2007**, *2*, e665.
32. K. Jyothish, K. T. Arun and D. Ramaiah, *Org. Lett.* **2004**, *6*, 3965–3968.
33. K. Takagi, M. Kawabe, M. Matsuoka and T. Kitao, *Dyes Pigm.* **1985**, *6*, 177-188.
34. W. B. Tuemmler and B. S. Wildi, *J. Am. Chem. Soc.* **1958**, *80*, 3772.
35. (a) J. Chen, I. R. Corbin, H. Li, W. Cao, J. D. Glickson and G. Zheng, *J. Am. Chem. Soc.* **2007**, *129*, 5798.; (b) S. A. Hilderbrand and R. Weissleder, *Curr. Opin. Chem. Biol.* **2010**, *14*, 71.
36. (a) J. Panda, P. R. Virkler and M. R. Detty, *J. Org. Chem.* **2003**, *68*, 1804.; (b) P. J. Sims, A. S. Waggoner, C. H. Wang and J. F. Hoffman, *Biochemistry* **1974**, *13*, 3315.; (c) S. J. Mason and S. Balasubramanian, *Org. Lett.* **2002**, *4*, 4261.; (d) S. J. Mason, J. L. Hake, J. Nairne, W. J. Cummins and S. Balasubramanian, *J. Org. Chem.* **2005**, *70*, 2939.; (e) M. Lopalco, E. N. Koini, J. K. Cho and M. Bradley, *Org. Biomol. Chem.* **2009**, *7*, 856.
37. a) M. Bates, B. Huang, G. T. Dempsey, X. Zhuang, *Science* **2007**, *317*, 1749.; b) M. Bates, B. Huang, X. Zhuang, *Curr. Opin. Chem. Biol.* **2008**, *12*, 505.
38. D. Citterio, S. Rasonyi, U. E. Spichiger, *Anal. Bioanal. Chem.* **1996**, *354*, 836.
39. B. K. Wagner, H. A. Carrinski, Y. H. Ahn, Y. K. Kim, T. J. Gilbert, D. A. Fomina, S. L. Schreiber, Y. T. Chang, P. A. Clemons, *J. Am. Chem. Soc.* **2008**, *130*, 4208.
40. W. Z. Konigm, *Angew. Chem.* **1925**, *38*, 743.
41. J. Fabian, H. Nakazumi, M. Matsuoka, *Chem. Rev.* **1992**, *92*, 1197.
42. N. Karton-Lifshin, E. Segal, L. Omer, M. Portnoy, R. Satchi-Fainaro, D. Shabat, *J. Am. Chem. Soc.* **2011**, *133*, 10960.

43. G. A. Reynolds, K. H. Drexhage, *J. Org. Chem.* **1977**, *42*, 885.
44. S. M. Makin, L. I. Boiko, O. A. Shavrygina, *Zh. Org. Khim.* **1977**, *13*, 2440.
45. L. Strekowski, M. Lipowska, G. Patonay, *J. Org. Chem.* **1992**, *57*, 4578.
46. N. Narayanan, G. Patonay, *J. Org. Chem.* **1995**, *60*, 2391.
47. J. H. Flanagan, S. H. Khan, S. Menchen, S. A. Soper, R. P. Hammer, *Bioconjugate Chem.* **1997**, *8*, 751.
48. X. Peng, F. Song, E. Lu, Y. Wang, W. Zhou, J. Fan, Y. Gao, *J. Am. Chem. Soc.* **2005**, *127*, 4170.
49. H. Lee, J. C. Mason, S. Achilefu, *J. Org. Chem.* **2006**, *71*, 7862.
50. K. Sauda, T. Imasaka, N. Ishibashi, *Anal. Chem.* **1986**, *58*, 2649.
51. J. S. Kim, R. Kodagahally, L. Strekowski, G. Patonay, *Talanta* **2005**, *67*, 947.
52. B. Chipon, G. Clave, C. Bouteiller, M. Massonneau, P. Y. Renard, A. Romieu, *Tetrahedron Lett.* **2006**, *47*, 8279.
53. F. L. Song, X. J. Peng, E. H. Lu, Y. N. Wang, W. Zhou, J. L. Fan, *Tetrahedron Lett.* **2005**, *46*, 4817.
54. C. Li, T. R. Greenwood, Z. M. Bhujwalla, K. Glunde, *Org. Lett.* **2006**, *8*, 3623.
55. K. Meguellati, M. Spichy, S. Ladame, *Org. Lett.* **2009**, *11*, 1123.
56. M. Zhu, M. Yuan, X. Liu, J. Xu, J. Lv, C. Huang, H. Liu, Y. Li, S. Wang, D. Zhu, *Org. Lett.* **2008**, *10*, 1481.
57. E. Sasaki, H. Kojima, H. Nishimatsu, Y. Urano, K. Kikuchi, Y. Hirata, T. Nagano, *J. Am. Chem. Soc.* **2005**, *127*, 3684.
58. P. A. Bouit, E. Di Piazza, S. Rigaut, B. Le Guennic, C. Aronica, L. Toupet, C. Andraud, O. Maury, *Org. Lett.* **2008**, *10*, 4159.
59. Z. Zhang, J. Fan, P. P. Cheney, M. Y. Berezin, W. B. Edwards, W. J. Akers, D. Shen, K. Liang, J. P. Culver, S. Achilefu, *Mol. Pharmaceutics* **2009**, *6*, 416.
60. W. B. Edwards, B. Xu, W. Akers, P. P. Cheney, K. Liang, B. E. Rogers, C. J. Anderson, S. Achilefu, *Bioconjugate Chem.* **2008**, *19*, 192.

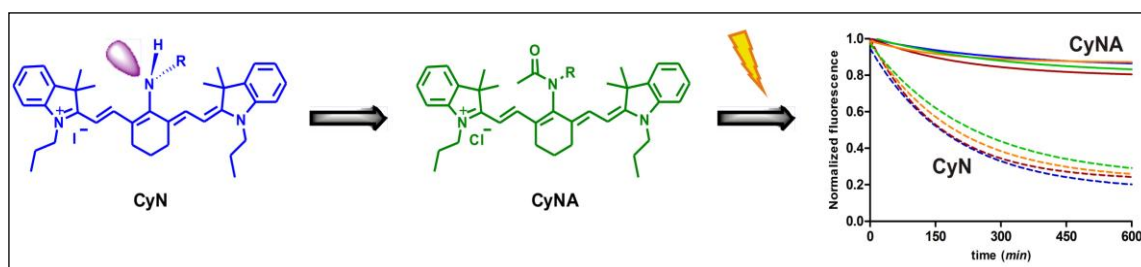
61. C. Bouteiller, G. Clave, A. Bernardin, B. Chipon, M. Massonneau, P. Y. Renard, A. Romieu, *Bioconjugate Chem.* **2007**, *18*, 1303.
62. F. Song, X. Peng, E. Lu, R. Zhang, X. Chen, B. Song, *J. Photochem. Photobiol. A: Chem.* **2004**, *168*, 53.
63. B. R. Renikuntla, H. C. Rose, J. Eldo, A. S. Waggoner, B. A. Armitage, *Org. Lett.* **2004**, *6*, 909.
64. Q. L. Mattingly, S. A. Soper, *J. Am. Chem. Soc.* **1994**, *116*, 3744.
65. F. Shao, R. Weissleder, S. A. Hilderbrand, *Bioconjugate Chem.* **2008**, *19*, 2487.
66. S. A. Hilderbrand, K. A. Kelly, M. Niedre, R. Weissleder, *Bioconjugate Chem.* **2008**, *19*, 1635.
67. A. Toutchkine, D. V. Nguyen, K. M. Hahn, *Bioconjugate Chem.* **2007**, *18*, 1344.
68. C. Encinas, S. Miltsov, E. Otazo, L. Rivera, M. Puyol, J. Alonso, *Dyes Pigm.* **2006**, *71*, 28.
69. C. S. Foote, *Science* **1968**, *162*, 963.
70. X. Chen, X. Peng, A. Cui, B. Wang, L. Wang and R. Zhang, *J. Photochem. Photobiol. A* **2006**, *181*, 79.
71. A. Toutchkine, D. V. Nguyen, K. M. Hahn, *Org. Lett.* **2007**, *9*, 2775.
72. M. Fleischmann, I. R. Hill, *J. Electroanal. Chem.* **1983**, *146*, 367.
73. J. A. Creighton, C. G. Blatchford and M. G. Albretch, *J. Chem. Soc. Faraday Trans. 2*, **1979**, *75*, 790.
74. X. M. Qian, S. M. Nie, *Chem. Soc. Rev.* **2008**, *37*, 912.
75. W. P. Wuelfing, S. M. Gross, D. T. Miles, R. W. Murray, *J. Am. Chem. Soc.* **1998**, *120*, 12696.
76. M. C. Daniel, D. Astruc, *Chem. Rev.* **2004**, *104*, 293.
77. D. Graham, K. Faulds, *Chem. Soc. Rev.* **2008**, *37*, 1042.
78. A. F. McCabe, C. Eliasson, R. A. Prasath, A. Hernandez-Santana, L. Stevenson, I. Apple, P. A. G. Cormack, D. Graham, W. E. Smith, P. Corish, S. J. Lipscomb, E. R. Holland and P. D. Prince, *Faraday Discuss.* **2006**, *132*, 303.

79. L. Sun, C. X. Yu, J. Irudayaraj, *Anal. Chem.* **2007**, *79*, 3981.
80. W. E. Doering and S. M. Nie, *Anal. Chem.* **2003**, *75*, 6171.
81. S. P. Mulvaney, M. D. Musick, C. D. Keating and M. J. Natan, *Langmuir* **2003**, *19*, 4784.
82. S. Kaufmann and M. Tanaka, *Chem. Phys. Chem.* **2003**, *4*, 699.
83. X. M. Qian, X. H. Peng, D. O. Ansari, Q. Yin-Goen, G. Z. Chen, D. M. Shin, L. Yang, A. N. Young, M. D. Wang and S. M. Nie, *Nat. Biotechnol.* **2008**, *26*, 83.
84. D. K. Lim, K. S. Jeon, J. H. Hwang, H. Kim, S. Kwon, Y. D. Suh, J. M. Nam, *Nat. Nanotechnol.* **2011**, *6*, 452.
85. D. Shenoy, W. Fu, J. Li, C. Crasto, G. Jones, C. Dimarzio, S. Sridhar and M. Amiji, *Int. J. Nanomed.* **2006**, *1*, 51.
86. J. Inglese, C. E. Shamu, R. K. Guy, *Nat. Chem. Bio.* **2007**, *3*, 438.
87. R. Weissleder, C. H. Tung, U. Mahmood, A. Bogdanov, Jr., *Nat. Biotechnol.* **1999**, *17*, 375.
88. A. Becker, C. Hessenius, K. Licha, B. Ebert, U. Sukowski, W. Semmler, B. Wiedenmann, C. Grotzinger, *Nat. Biotechnol.* **2001**, *19*, 327.
89. (a) W. M. Leevy, S. T. Gammon, H. Jiang, J. R. Johnson, D. J. Maxwell, E. N. Jackson, M. Marquez, D. Piwnica-Worms, B. D. Smith, *J. Am. Chem. Soc.* **2006**, *128*, 16476.; (b) W. M. Leevy, S. T. Gammon, J. R. Johnson, A. J. Lampkins, H. Jiang, M. Marquez, D. Piwnica-Worms, M. A. Suckow, B. D. Smith, *Bioconjugate Chem.* **2008**, *19*, 686.
90. V. Ntziachristos, C. H. Tung, C. Bremer, R. Weissleder, *Nat. Med.* **2002**, *8*, 757.
91. S. Zhang, V. Metelev, D. Tabatadze, P. C. Zamecnik, A. Bogdanov, Jr., *Proc. Natl. Acad. Sci. U. S. A.* **2008**, *105*, 4156.
92. K. Kiyose, H. Kojima, Y. Urano, T. Nagano, *J. Am. Chem. Soc.* **2006**, *128*, 6548.
93. Y. Kim, S. A. Hilderbrand, R. Weissleder, C. H. Tung, *Chem. Commun.* **2007**, *22*, 2299.

94. S. Boca, D. Rugina, A. Pintea, L. Barbu-Tudoran, S. Astilean, *Nanotechnology* **2011**, 22, 055702.
95. U. S. Dinish, F. C. Yaw, A. Agarwal, M. Olivo, *Biosens. Bioelectron.* **2011**, 26, 1987.
96. G. Das, F. Mearini, F. Gentile, F. De Angelis, H. Mohan Kumar, P. Candeloro, C. Liberale, G. Cuda, E. Di Fabrizio, *Biosens. Bioelectron.* **2009**, 24, 1693.
97. R. Gessner, P. Rosch, R. Petry, M. Schmitt, M. A. Strehle, W. Kiefer, J. Popp, *Analyst* **2004**, 129, 1193.
98. L. Sun, B-K. Sung, C. Dentinger, B. Lutz, L. Nguyen, J. Zhang, H. Qin, M. Yamakawa, M. Cao, Y. Lu, A. Chmura, J. Zhu, X. Su, A. A. Berlin, S. Chan, B. Knudsen, *Nano Lett.* **2007**, 7, 351.
99. X. M. Qian, X. H. Peng, D. O. Ansari, Q. Yin-Goen, G. Z. Chen, D. M. Shin, L. Yang, A. N. Young, M. D. Wang, S. M. Nie, *Nat. Biotechnol.* **2008**, 26, 83.
100. H. W. Tang, X. B. Yang, J. Kirkham, D. A. Smith, *Anal. Chem.* **2007**, 79, 3646.

CHAPTER 2

DEVELOPMENT OF PHOTOSTABLE NEAR-INFRARED CYANINE DYES



2.1 Introduction

The field of bioimaging research has recently focused considerable attention on NIR dyes. Amongst several advantages, NIR light can deeply penetrate into tissues with lower light scattering and auto-fluorescence than visible light. NIR dyes have been used in a broad range of biological applications such as DNA sequencing¹ and proteins labeling.² To date, limited scaffolds such as squaraine,³ triphenylmethane,⁴ quinone,⁵ and cyanine⁶ have been employed for organic NIR fluorophores. Among them, cyanine dyes⁷ are the most popular due to their synthetic accessibility, broad wavelength tunability, and large molar extinction coefficient with moderate fluorescence quantum yields. Although a few number of NIR dyes, mainly based on the cyanine structure, have been reported as effective fluorescent probes for *in vivo* imaging studies,⁸ most of them are described as individual examples. The synthetic limitations to incorporate broad chemical diversity into NIR scaffolds have hindered their derivatization in a combinatorial manner, and thus restricted their range of applications. A rigid cyclohexenyl ring in heptamethine chain and a reactive vinylic chlorine atom that can be replaced by a diverse range of nucleophiles have been familiar for the synthesis of NIR dyes. The resulting derivatives show maximum absorbance wavelengths above 600 nm, which is essential to develop in NIR dyes.

The incorporation of phenols and thiophenols⁹ has rendered tricarbocyanine derivatives with low chemical stability in aqueous media. In addition, the photodegradation of NIR cyanine dyes is significant for dyes with absorbance λ_{\max} longer than 700 nm.¹⁰ The photostability of the dyes diminishes significantly along with the increase of the π -conjugation system. To overcome such limitation, amine and aniline building blocks have been employed, yet the low photostability of the resulting compounds remains as a major drawback.¹¹ Therefore, libraries of NIR fluorophores with increased photostability would enormously expand the scope of cyanine-based dyes for biomedical research.

2.2 Objectives

To overcome the photostability and chemical diversity limitations of NIR dyes, first I modified the tricarbocyanine scaffold and improved its photostability and secondly I expanded its chemical diversity by applying a diversity-oriented fluorescence library approach (DOFLA). As a result, I created the first NIR library based on a tricarbocyanine structure (CyNA) with improved photostability. The CyNA scaffold was derivatized in a combinatorial manner and screened to identify CyNA-414 as a highly photostable NIR dye with superior fluorescent properties than the NIR standard Indocyanine green (ICG).

2.3 Results and discussion

2.3.1 Decomposition study of tricarbocyanine dye

A rigid cyclohexenyl ring within the heptamethine chain increases photostability compared to cyanine dyes with an open polymethine chain¹² and a reactive vinylic chlorine atom that can be replaced by different amine derivatives opens a new window for the synthesis of a relatively better photostable cyanine dyes than aryl thioethers or aryl ethers. While amine derivatives of the tricarbocyanine structure (CyN) have been described as promising NIR cyanine dyes for broad chemical derivatization,¹³ the low photostability in aqueous media has hampered their biological application. Although the decomposition mechanism of some cyanine dyes has been studied,¹⁴ no systematic study regarding the photostability of tricarbocyanine analogues in aqueous media has been reported to date. In order to examine such mechanism and surmount the stability limitations of tricarbocyanine dyes, I analyzed the decomposition products of one amine tricarbocyanine derivative (CyN-111). Upon light irradiation, CyN-111 quickly underwent the incorporation of a reactive singlet oxygen species to render CyN-111a, which subsequently generated the non-fluorescent CyN-111b and CyN-111c. In presence of light, the formation of singlet

oxygen ($^1\text{O}_2$) results in the reaction with the double bonds of cyanine dyes to form an unstable intermediate peroxo compound (CyN-111a).

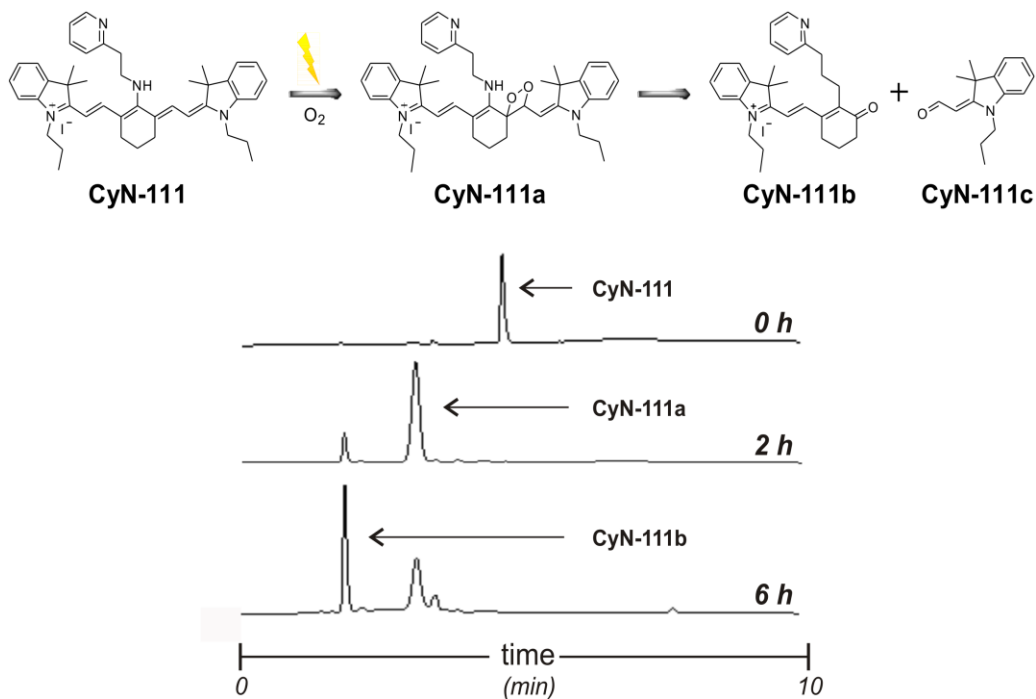


Figure 2.1. Reverse-phase HPLC monitoring of CyN-111 decomposition in aqueous media (UV detection: 500 nm).

The HPLC analysis in Figure 2.1 clearly shows that a distinct retention time at 500 nm is shifted from the mother compound (CyN-111). As CyN-111a compound is highly active at 500 nm instead of 640 nm (λ_{max} of CyN-111, see Table 2.1, Figure 2.4) I selected 500 nm wavelengths for HPLC analysis. Absorbance differences clearly supports that π conjugation in polymethine chain is highly affected due to the loss of π - π conjugation. In addition, mass analysis data (Figure 2.2.) supports the incorporation of singlet oxygen into the main tricarbocyanine scaffold. Eventually, the unstable intermediate led to the more stable CyN-111b and CyN-111c compounds. CyN-111c was fully characterized after isolation from the reaction mixture by $^1\text{H-NMR}$, $^{13}\text{C-NMR}$ and mass analysis. Moreover, I compared the IR spectra (Figure 2.3) of CyN-111 compound with a reaction mixture which was obtained after 6 h light irradiation in aqueous solution. Two new bands at 1707 cm^{-1}

and 1606 cm^{-1} corresponding to the ketone and aldehyde bands also confirmed the formation of CyN-111b and CyN-111c.

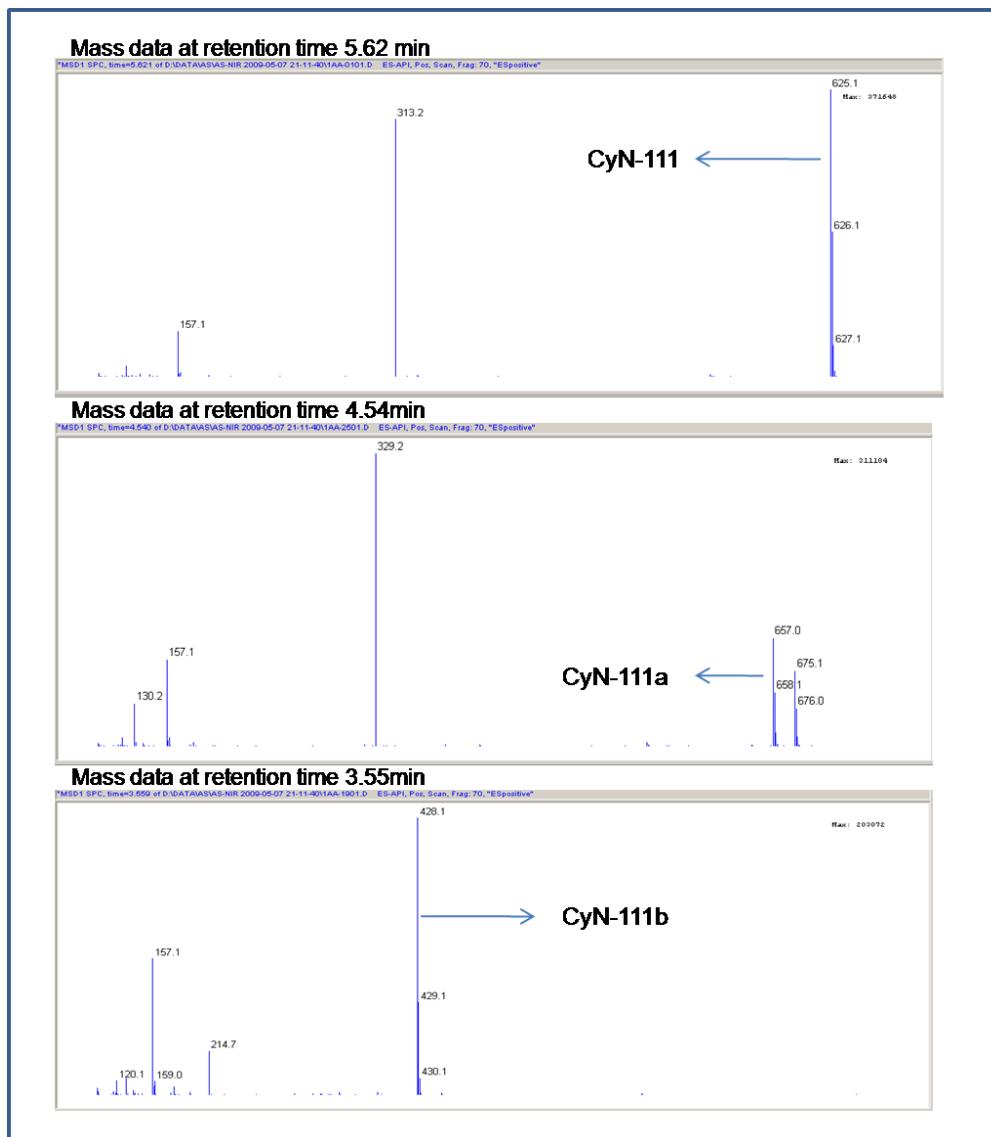


Figure 2.2. Mass spectrometry data for the decomposition of CyN-111.

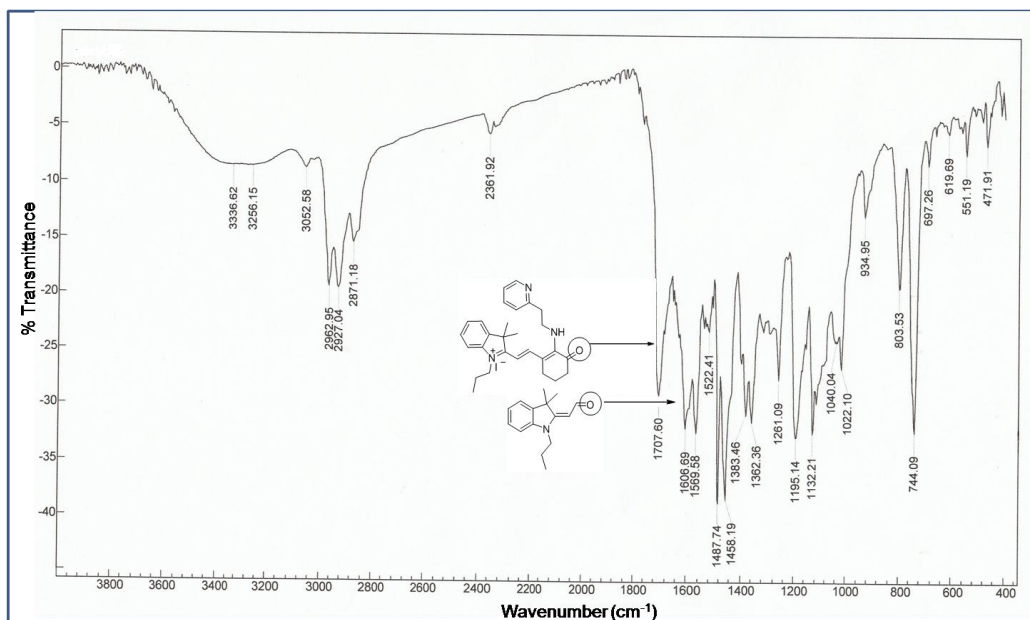
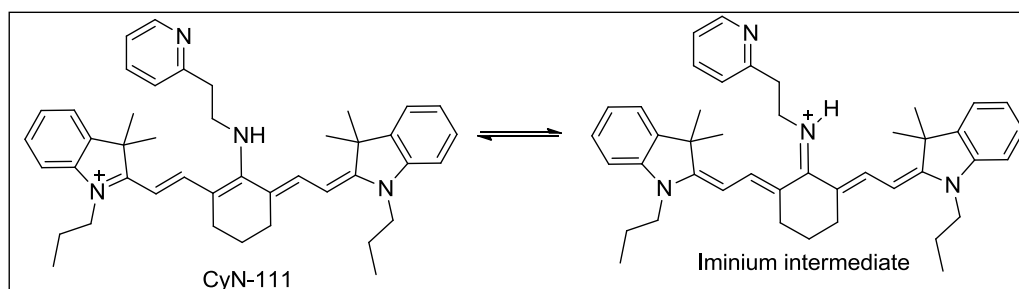


Figure 2.3. IR spectra of the reaction mixture after 6 h of light irradiation. The carbonyl bands corresponding to **CyN-111b** (ketone) and **CyN-111c** (aldehyde) are easily distinguishable.

2.3.2 Design and synthesis

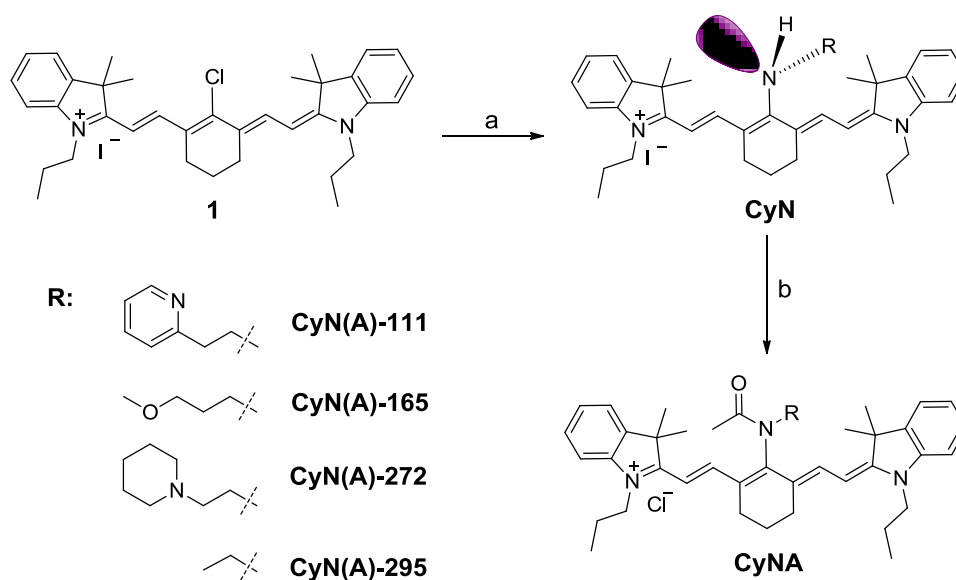
In view of these results, I hypothesized that the modification of the central nitrogen atom with an electron-withdrawing group would suppress the stabilization of the iminium intermediate (Chart 2.1) that facilitates the incorporation of the reactive oxygen species. The removal of electron density from the amine tricarbo-cyanine structure may minimize the photoinduced decomposition and improve its photostability.

Chart 2.1. Formation of iminium intermediate of amine derivative tricarbo-cyanine dyes.



To investigate this hypothesis, I modified 4 structurally diverse (including different-length aliphatic, aromatic, and heterocycle-containing amines) CyN compounds with an electron withdrawing acetyl group to afford the corresponding acetylated compounds (CyNA) (Scheme 2.1).

Scheme 2.1. Synthesis of amine tricyanocyanine derivatives.



Reagents and conditions: (a) RNH_2 , DIEA, CH_3CN , 80°C , 10–60 min; (b) CH_3COCl , DIEA, CH_2Cl_2 , 0°C , 15 min.

2.3.3 Characterization of tricyanocyanine dyes

Absorbance (λ_{abs}) and fluorescence maximum wavelengths (λ_{em}), quantum yields (ϕ), and extinction coefficients (ϵ) of **CyN-111**, **CyN-165**, **CyN-272**, and **CyN-295** were measured in DMSO (Table 2.1). After acetylation on the central nitrogen atom of CyN compounds, the absorbance band was shifted approximately 160 nm towards the NIR region (Figure 2.4). This effect may be due to the intramolecular charge transfer (ICT), which is restricted in the presence of the strong electron withdrawing acetyl group.

Table 2.1. Characterization of CyN compounds.

compound	$\lambda_{\text{abs}}(\text{nm})$	$\lambda_{\text{em}}(\text{nm})$	ϕ^*	$\epsilon(\text{cm}^{-1}\text{M}^{-1})$
CyN-111	640	760	0.42	0.538×10^5
CyN-165	640	762	0.37	0.352×10^5
CyN-272	635	765	0.41	0.516×10^5
CyN-295	640	760	0.35	0.519×10^5

* Quantum yields were measured in DMSO, using IndoCyanine Green as a standard (ϕ : 0.13, in DMSO).¹

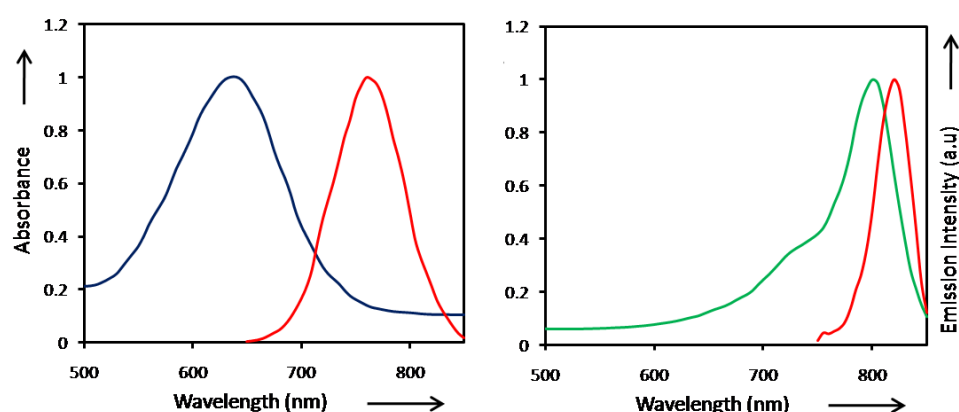


Figure 2.4. (a) Absorbance (blue) and emission (red) spectra of CyN-111 in DMSO (1 μM); (b) absorbance (green) and emission (red) spectra of CyNA-111 in DMSO.

2.3.4 Photostability measurements

The photostability properties of CyN and CyNA structures (CyN-111, CyN-165, CyN-272, CyN-295, and their CyNA counterparts) were evaluated by time-course fluorescence measurements in HEPES buffer, and compared to the starting material **1** (Figure 2.5). Interestingly, the *pseudo* first order rate constants (k) of the CyN compounds were 8 to 13-fold faster than those of the corresponding CyNA derivatives, indicating the significantly ameliorated photostability of the CyNA scaffold. The improved photostability of the CyNA scaffold validated our initial

hypothesis that the incorporation of an electron withdrawing group could increase the photostability of the amine tricarbocyanine structure.

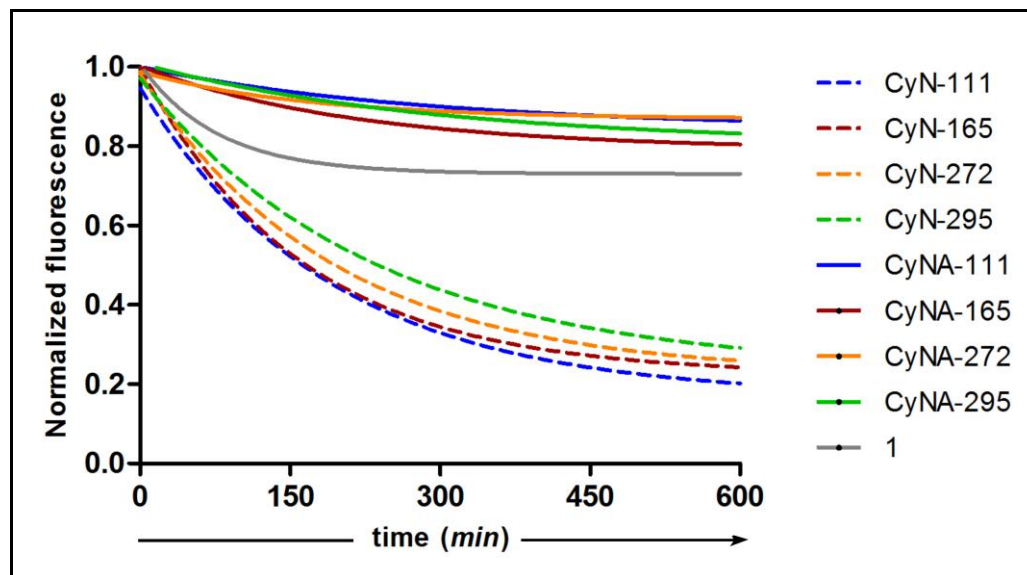


Figure 2.5. Photostability evaluation of 1, CyN and CyNA derivatives under a xenon flash lamp. Compounds were dissolved in HEPES buffer (10 mM, pH 7.4) containing 1% DMSO to a 10 mM final concentration, and fluorescence measurements were recorded for 10 h at r.t. Values are represented as means for sequential measurements every 10 min and fitted to a non-linear regression, one-phase exponential decay.

Table 2.2. Fluorescence and photostability properties of CyN and CyNA derivatives.

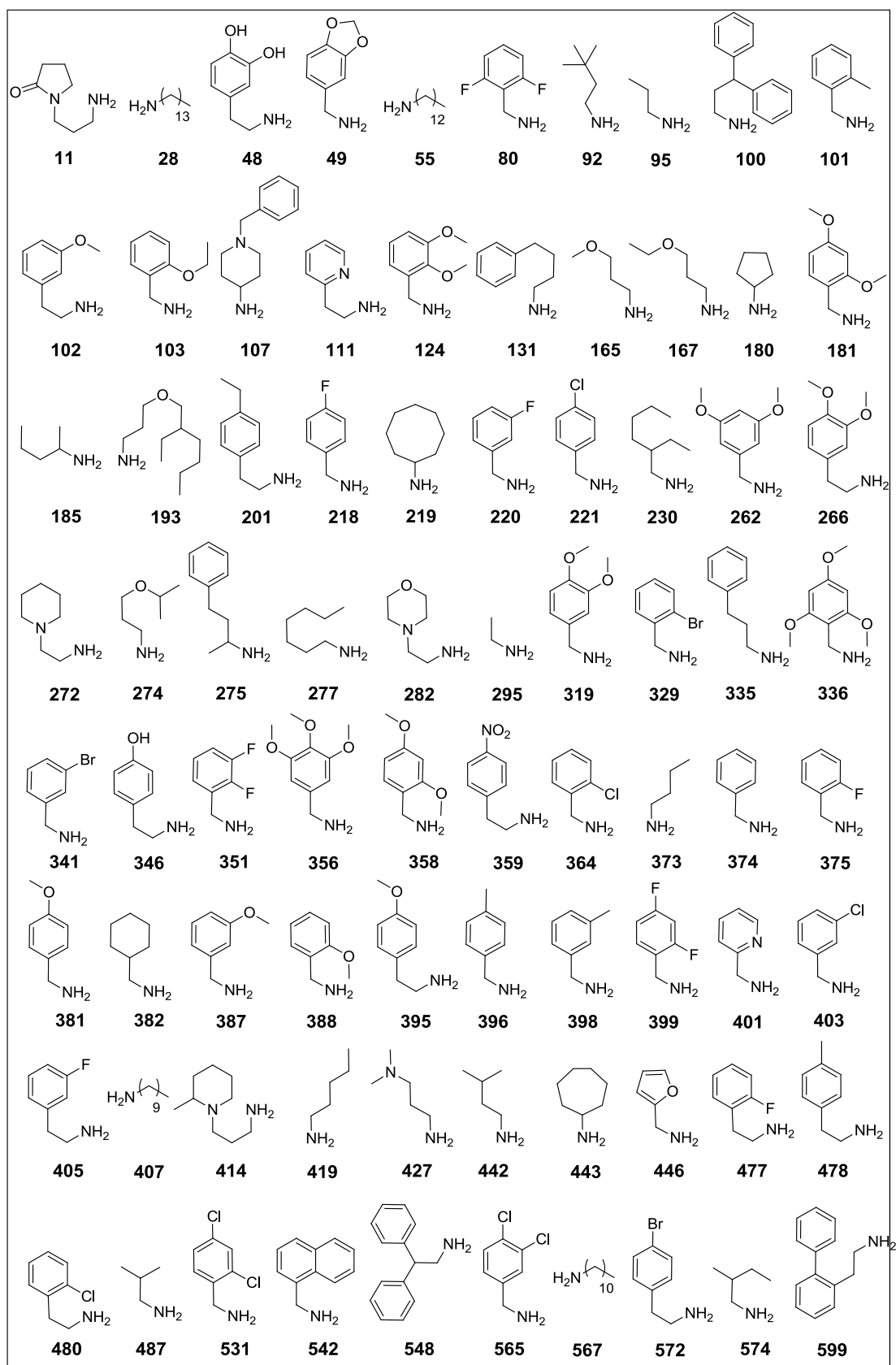
compound	$\lambda_{\text{abs}}(\text{nm})/\epsilon(\text{cm}^{-1}\text{M}^{-1})$	$\lambda_{\text{em}}(\text{nm})/\phi^{[\text{a}]}$	$k(\text{s}^{-1})^{[\text{b}]}$	$k_{\text{CyN}}/k_{\text{CyNA}}$
CyN-111	640 / 0.538×10^5	760 / 0.42	40.4×10^{-6}	n.a.
CyN-165	640 / 0.352×10^5	762 / 0.37	34.9×10^{-6}	n.a.
CyN-272	635 / 0.516×10^5	765 / 0.41	35.2×10^{-6}	n.a.
CyN-295	640 / 0.519×10^5	760 / 0.35	31.3×10^{-6}	n.a.
CyNA-111	802 / 1.162×10^5	820 / 0.11	3.41×10^{-6}	12
CyNA-165	801 / 1.062×10^5	821 / 0.09	4.53×10^{-6}	8
CyNA-272	804 / 2.004×10^5	820 / 0.10	2.67×10^{-6}	13
CyNA-295	801 / 1.578×10^5	821 / 0.11	3.81×10^{-6}	8

^[a] Quantum yields 10 μM DMSO solutions, standard ICG (ϕ : 0.13, in DMSO). ^[b] k in 10 μM (1% DMSO in HEPES buffer; 10 mM, pH 7.4). n.a.: not applicable.

2.3.5 Library design, characterization and photostability studies

Since the *pseudo* first order rate constant (k) values of the different CyNA compounds indicated some dependency on the amine chemical structure (Table 2.2), I expanded the derivatization of the CyNA scaffold to a broad range of 80 primary amines (Chart 2.2) so that I could identify the compounds with the best photostability properties. Compound **1** was derivatized with 80 different amines in solution phase chemistry, and subsequently these compounds were further modified with an acetyl group onto the central nitrogen atom to render 80 CyNA compounds.

Chart 2.2. 80-different amine structures with different numbers according to our chemical inventory list.



The fluorescence properties of the 80-membered CyNA library were measured. The absorption maximum wavelengths ranged from 802 nm to 806 nm, emission maximum wavelength from 817 nm to 823 nm, and average quantum yields were around 0.10 (Table 2.3). As a primary photostability evaluation, I analyzed the fluorescence decrease of the 80 CyNA compounds under a xenon lamp. Figure 2.6 clearly shows that the 80 CyNA molecules show different photostability under identical experimental conditions. Table 2.3 clearly indicates that the discrepancy of the fluorescence intensity ratio at 8 h mainly depends on different amine structures.

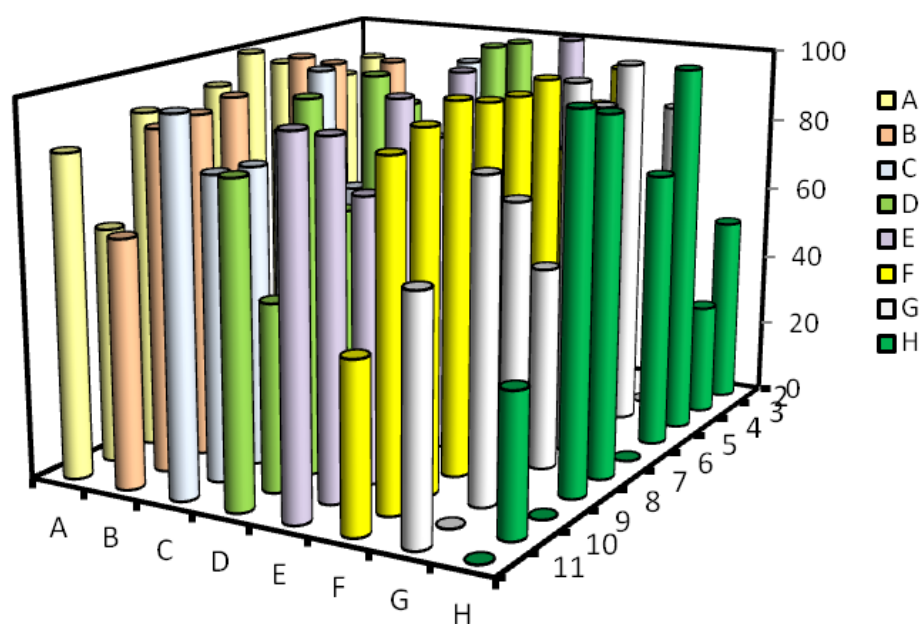


Figure 2.6. Primary photostability evaluation: Quotients of fluorescent intensities (8h) vs. fluorescent intensities (0h), in a time-course fluorescence measurement using 10 μ M (2% DMSO) solutions in HEPES buffer (100 mM, pH 7.4).

Table 2.3. Absorbance (λ_{abs}) and fluorescence maximum wavelengths (λ_{em}), quantum yields (ϕ), LC-MS data, condensation reaction times, and photostability primary evaluation (F/F_0) for the whole **CyNA** library.

compound	M^+ (exp.)	λ_{abs} (nm)	λ_{em} (nm)	ϕ^{*1}	purity ^{*2}	F/F_0^{*3}
CyNA-11	687.1	802	820	0.11	95.3	90
CyNA-28	758.2	804	818	0.05	93.2	87
CyNA-48*⁴	783.0	804	819	0.06	94.6	45
CyNA-49	696.1	804	818	0.10	95.3	95
CyNA-55	744.2	804	819	0.13	97.1	100
CyNA-80	688.2	804	817	0.08	96.1	93
CyNA-92	646.1	805	821	0.09	96.3	64
CyNA-95	604.2	806	818	0.09	95.6	91
CyNA-100	756.1	804	819	0.08	94.4	63
CyNA-101	666.1	806	822	0.08	94.6	86
CyNA-102	696.1	805	822	0.14	97.1	63
CyNA-103	696.2	804	821	0.14	96.9	92
CyNA-107	735.1	803	820	0.07	93.4	50
CyNA-111	667.1	804	818	0.11	98.2	96
CyNA-124	712.1	803	820	0.15	98.1	100
CyNA-131	694.1	804	819	0.13	97.3	n.d
CyNA-165	634.1	806	821	0.09	98.1	94
CyNA-167	648.1	804	818	0.10	94.8	92
CyNA-180	630.1	805	821	0.14	97.5	91
CyNA-181	712.1	805	821	0.14	96.5	66
CyNA-185	632.1	804	820	0.15	97.4	91
CyNA-193	732.2	806	822	0.12	96.2	n.d
CyNA-201	694.1	803	820	0.08	93.2	33
CyNA-218	670.1	802	823	0.08	94.2	85

CyNA-219	672.1	804	822	0.14	96.4	65
CyNA-220	686.1	804	823	0.12	95.3	100
CyNA-221	687.1	803	820	0.07	93.2	86
CyNA-230	674.2	805	822	0.09	94.3	80
CyNA-262	712.1	803	822	0.10	95.1	81
CyNA-266	726.1	804	823	0.08	93.5	99
CyNA-272	673.1	804	820	0.10	93.8	98
CyNA-274	662.1	805	820	0.12	95.6	99
CyNA-275	694.1	804	817	0.14	96.8	62
CyNA-277	660.1	804	817	0.11	93.7	n.d
CyNA-282	675.1	805	819	0.09	93.5	90
CyNA-295	590.1	806	820	0.11	96.4	100
CyNA-319	712.1	805	820	0.06	92.1	67
CyNA-329	731.9	806	821	0.10	94.5	99
CyNA-335	680.1	804	821	0.06	93.2	50
CyNA-336	742.1	804	820	0.11	94.5	85
CyNA-341	732.1	805	822	0.10	93.7	100
CyNA-346*⁵	724.1	804	822	0.07	92.7	69
CyNA-351	688.1	805	818	0.10	95.8	52
CyNA-356	742.1	804	820	0.12	96.9	83
CyNA-358	712.0	805	819	0.14	98.2	100
CyNA-359	711.1	805	821	0.11	95.6	85
CyNA-364	686.0	804	821	0.05	92.1	98
CyNA-373	618.1	805	820	0.07	93.6	76
CyNA-374	652.1	806	821	0.14	97.3	94
CyNA-375	670.1	804	821	0.07	93.3	98
CyNA-381	668.0	805	821	0.14	96.5	93
CyNA-382	658.1	804	820	0.08	93.4	85

CyNA-387	682.1	804	820	0.07	92.9	75
CyNA-388	682.0	803	819	0.14	97.8	97
CyNA-395	696.1	804	820	0.07	95.1	95
CyNA-396	666.1	804	820	0.09	94.7	96
CyNA-398	666.1	804	819	0.07	93.4	99
CyNA-399	688.1	804	819	0.10	95.8	95
CyNA-401	653.1	805	820	0.10	94.9	91
CyNA-403	686.0	805	819	0.05	93.5	45
CyNA-405	684.0	806	820	0.06	94.5	83
CyNA-407	702.1	805	820	0.08	96.1	n.d.
CyNA-414	701.2	804	819	0.13	95.9	100
CyNA-419	632.0	804	820	0.13	97.4	91
CyNA-427	647.0	805	821	0.14	96.7	100
CyNA-442	632.1	806	822	0.07	94.3	54
CyNA-443	630.0	806	821	0.09	95.6	75
CyNA-446	642.1	804	821	0.08	94.2	85
CyNA-477	684.1	805	819	0.09	93.7	n.d.
CyNA-478	680.1	805	821	0.09	95.4	64
CyNA-480	700.1	803	817	0.06	92.1	51
CyNA-487	618.1	806	823	0.04	91.6	30
CyNA-531	720.1	804	820	0.08	97.3	100
CyNA-542	702.1	805	821	0.08	94.5	74
CyNA-548	742.1	804	820	0.04	92.9	n.d.
CyNA-565	720.1	805	821	0.09	95.3	96
CyNA-567	716.2	805	820	0.14	98.3	100
CyNA-572	684.1	805	818	0.05	93.2	n.d.
CyNA-574	632.1	803	818	0.06	93.8	38
CyNA-599	742.1	805	819	0.07	97.6	n.d.

*¹ Quantum yields were measured in DMSO, using Cardiogreen as a standard (ϕ : 0.13, in DMSO).

*² Purities were determined according to UV absorption at 365 nm.

*³ Quotients of fluorescent intensities (8h) vs. fluorescent intensities (0h), in a time-course fluorescence measurement using 10 μ M (2% DMSO) solutions in HEPES buffer (100 mM, pH 7.4).

*⁴ Triacetylated derivative was isolated as the main product.

*⁵ Diacetylated derivative was isolated as the main product.

n.d.: non-determined value due to fluctuation of the experimental data.

2.3.6 Secondary screening and comparative study with ICG

The average intensity decrease after 8 h due to decomposition was around 18%, and a subset with the most photostable 15 CyNA compounds were selected for the secondary screening under strong light irradiation for periods of 15 min (for 2 h) with a high intensity UV lamp (100 W, 365 nm) at 2-cm distance. Two different buffer conditions HEPES (4-(2-hydroxyethyl)-1-piperazineethanesulfonic acid)) and PBS (Phosphate buffered saline) were applied to evaluate the photostability. The stability in PBS buffer condition was better than in HEPES under identical pH and 1% DMSO as co-solvent (Figures 2.7 and 2.8). From the secondary screening, **CyNA-414** and **CyNA-111** showed almost similar photostability after 2 h.

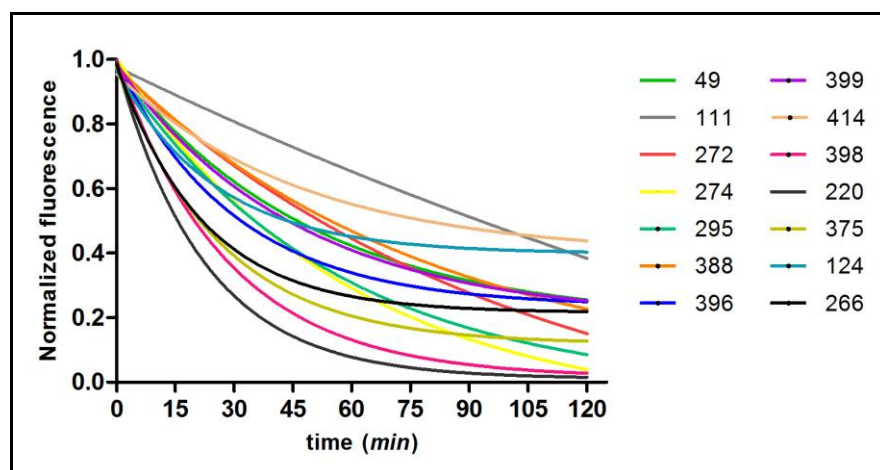


Figure 2.7. Photostability secondary screening of the CyNA library in HEPES buffer (10mM, pH 7.4).

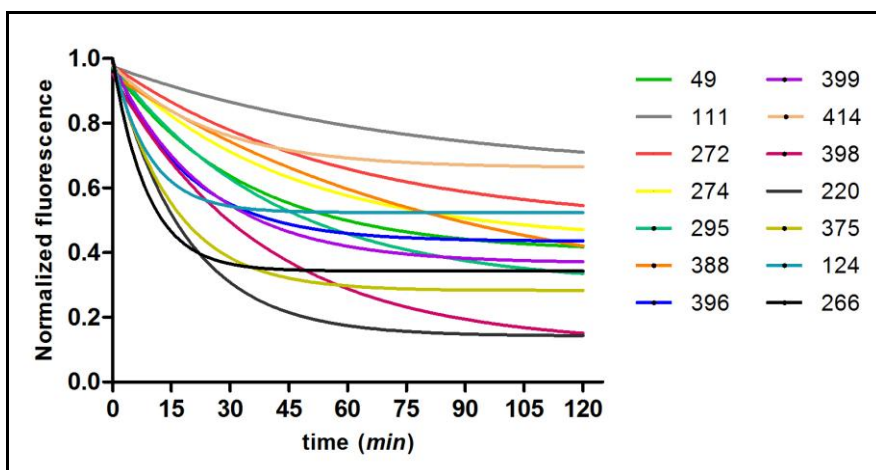
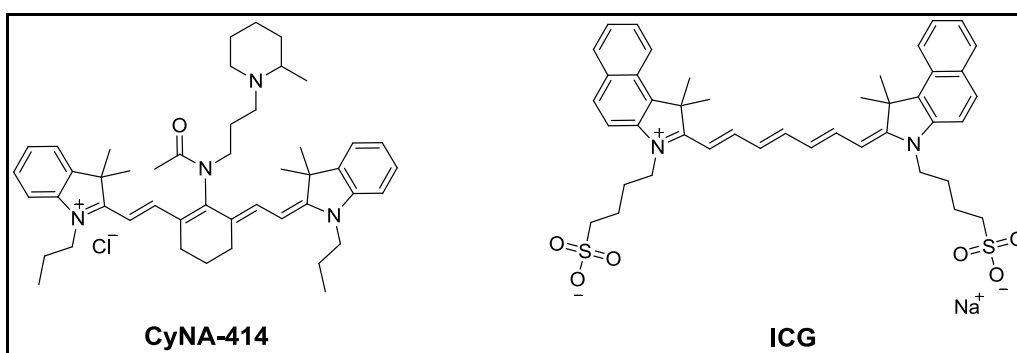


Figure 2.8. Photostability secondary screening of the **CyNA** library in PBS buffer (10mM, pH 7.4).

Among all **CyNA** compounds, **CyNA-414** displayed the best photostability and fluorescence quantum yield (Table 2.2, Figure 2.7 & 2.8) and the lowest photobleaching rate ($2.5 \times 10^{-6} \text{ s}^{-1}$) hence it was selected for further examination.

CyNA-414 exhibited outstanding properties as NIR dye and I compared it to the NIR standard ICG (Chart 2.3). ICG is the only NIR dye clinically approved to date,¹⁵ and has a very similar spectral profile (absorption–emission: 790–810 nm) to **CyNA-414**. However, ICG shows a low quantum yield and a poor stability in aqueous media that have hampered its use for many bioimaging applications.¹⁶

Chart 2.3. Chemical structure of **CyNA-414** and **ICG**.



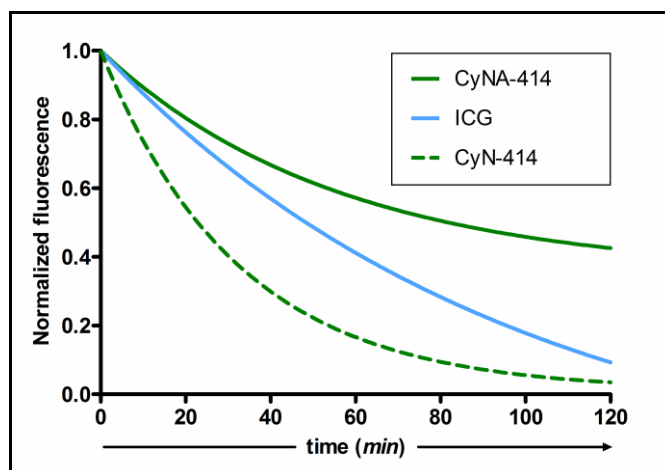


Figure 2.9. Photostability analysis of CyNA-414, ICG and CyN-414 under a high-intensity ultraviolet lamp in PBS buffer (pH 7.3) containing 1% DMSO to a 10 μ M final concentration. Values are represented as means ($n = 6$) for sequential measurements every 10 min and fitted to a non-linear regression, one-phase exponential decay.

The comparative analysis of the fluorescence properties of **CyNA-414** and ICG indicated that **CyNA-414** emitted stronger NIR fluorescence intensity in aqueous media (Figure 2.11) and exhibited a remarkably higher photostability than ICG (Figure 2.9). In addition, ICG has low fluorescence intensities in aqueous solution and low fluorescence quantum yields due to the extensive aggregation.¹⁷ I compared the spectral properties of **CyNA-414** with ICG in buffer solution, and observed that **CyNA-414** showed exactly similar absorbance spectral profile in DMSO and HEPES buffer solution except intensity whereas ICG showed remarkable different spectra profile (Figure 2.10). The ICG band at 660 nm may be due to its aggregation in aqueous media.

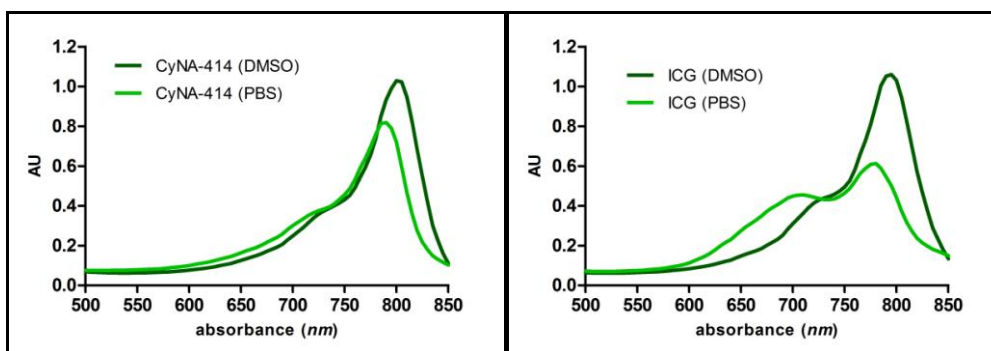


Figure 2.10. Absorbance spectra: 5 μ M solutions in PBS (pH 7.3) containing 1% DMSO or in pure DMSO.

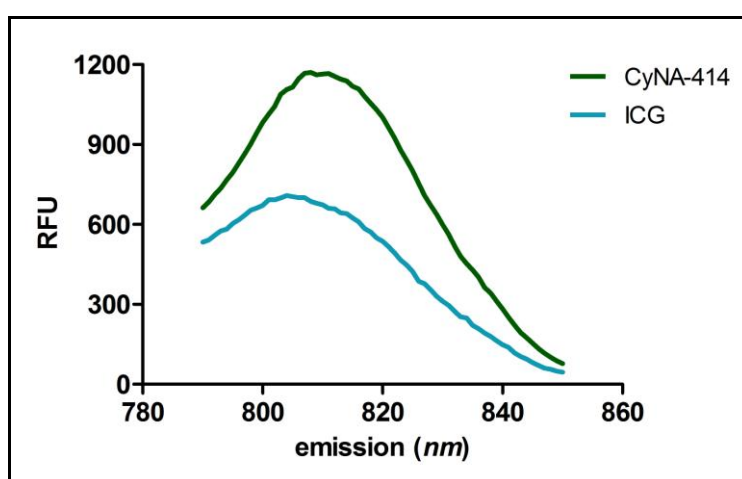


Figure 2.11. Emission spectra: 10 μ M solutions in PBS (pH 7.3) containing 1% DMSO.

2.4 Conclusion

In summary, I designed a NIR fluorescent scaffold (CyNA) with excellent photostability properties. **CyNA** was designed after examining the decomposition mechanism of amine tricarbocyanine derivatives, whose poor photostability was largely improved upon incorporation of an electron withdrawing acetyl group. The combinatorial derivatization of **CyNA** enabled the identification of **CyNA-414** as a highly fluorescent NIR dye with significantly better photostability than the NIR standard ICG. **CyNA-414** encloses a practical prospective for NIR *in vivo* imaging, Furthermore, this set of fluorophores exhibits a significant photostability in

physiological conditions, and thus encloses a remarkable prospective for the discovery of new fluorescent bioimaging probes.

2.5 Experimental details

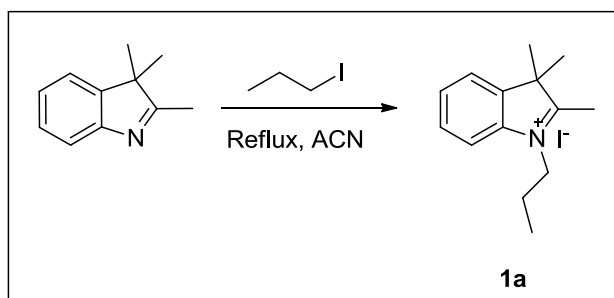
Materials and Methods:

All the chemicals (building block amines plus others) and solvents were purchased from Sigma Aldrich, Alfa Aesar, Fluka, MERCK or Acros, and used without further purification. Normal phase purifications were carried out using Merck Silica Gel 60 (particle size: 0.040- 0.063mm, 230-400 mesh). Analytical characterization was performed on a HPLC-MS (Agilent-1200 series) with a DAD detector and a single quadruple mass spectrometer (6130 series) with an ESI probe. Analytical method, unless indicated: eluents: A: H₂O (0.1% HCOOH), B: ACN (0.1% HCOOH), gradient from 5 to 95% B in 6 min; C18 (2) Luna column (4.6 x 50mm², 5µm particle size). Normal phase purifications of **CyN** and **CyNA** compounds were performed using column chromatography, and eluting with DCM-MeOH (ranging from 100:0 to 97:3). ¹H-NMR and ¹³C-NMR spectra were recorded on Bruker Avance 300 NMR and 500 NMR spectrometers, and chemical shifts are expressed in parts per million (ppm). High resolution mass spectrometry (HRMS) data was recorded on a Micromass VG 7035 (Mass Spectrometry Laboratory at National University of Singapore (NUS)). Photobleaching irradiation experiments were performed using a UVP Blak-Ray® B-100AP high intensity UV lamp (100W, 365 nm) in Singapore Bioimaging Consortium, Agency for Science, Technology and Research (A*STAR), Singapore. Spectroscopic and quantum yield data were measured on a SpectraMax M2 spectrophotometer (Molecular Devices), and the data analysis was performed using GraphPrism 5.0, Origin 6.0 and Microsoft Excel 2007.

2.5.1 Synthesis of CyN and characterization

Synthesis of 1a:

Scheme 2.2. Synthesis of intermediate 1a.



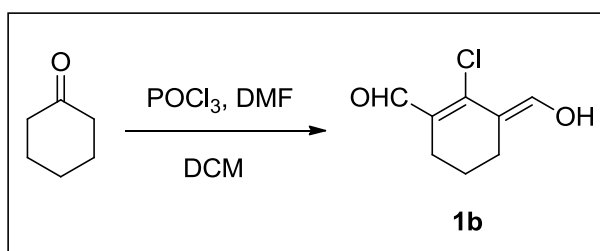
Reagents and conditions: 1-Iodopropane, CH₃CN, Reflux at 80 °C, 15h.

To a solution of 2,3,3-trimethyl-3H-indole (2 g, 12.5 mmol, 1 eq.) in ACN, 1-Iodopropane (10.6 mL, 62 mmol, 5 eq.) was added, and refluxed with continuous stirring for 15 h. The mixture was dried in high vacuum and washed by Et₂O. The resulting solid was recrystallized in acetone to obtain **1a** as a white solid (3.9 g, 95%).

¹HNMR (300 MHz, DMSO-d₆): δ = 1.04 (t, 3H, J=7.2), 1.64 (s, 6H), 2.67 (s, 3H), 1.34 (m, 2H), 4.17 (t, 2H, J=7.8 Hz), 7.63 (d, 2H), 7.82 (m, 2H). tR: 2.46 min, ESI m/z (C₁₄H₂₀N⁺) calc: 202.4; found: 202.1.

Synthesis of 1b:

Scheme 2.3. Synthesis of intermediate 1b



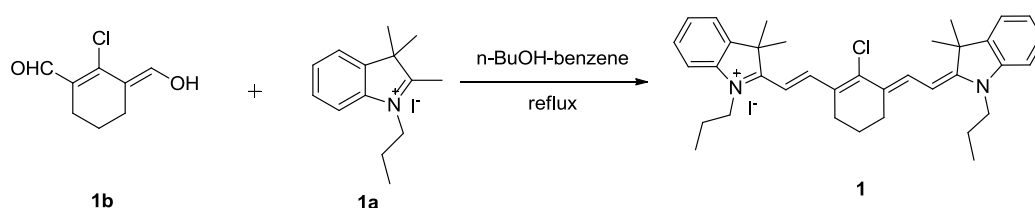
Reagents and conditions: Cyclohexanone, DMF, POCl₃, addition at 0 °C then refluxed for 3 h.

To a chilled solution of dimethylformamide (20 mL, 273 mmol, 5.4 eq.) in 20 mL CH₂Cl₂ under N₂ atmosphere, 20 mL of POCl₃ (17.5 ml, 115 mmol, 2.3 eq.) in DCM were added dropwise under an ice bath. After 30 min, cyclohexanone was added (5 g, 50mmol, 1 eq.), and the resulting mixture was refluxed with vigorous stirring for 3 h at 80 °C, poured into ice-cold water, and kept it overnight to obtain **1b** as a yellow solid (8.0 g, 92%).

¹H-NMR (300 MHz, CDCl₃): δ = 1.57 (m, 2H), 2.35 (t, 4H, *J*=6.3 Hz), 2.5 (s, 1H), 10.10 (s, 1H). tR: 4.30 min, ESI *m/z* (C₈H₉ClO₂): calc: 172.0; found: 173.1.

Synthesis of 1:

Scheme 2.4. Synthesis of 1.



Reagents and conditions: 1a (2 eq.) and 1b (1eq.) in 7:3 (butanol:benzene) refluxed for 12 hrs at 110 °C.

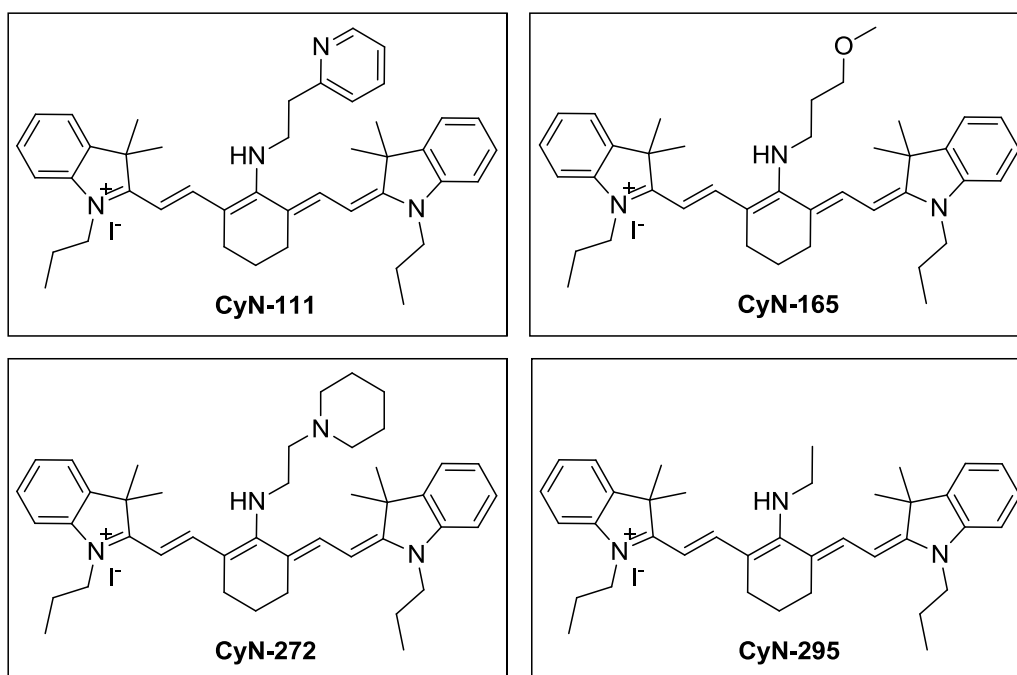
1b (500 mg, 2.9 mmol, 1eq.) and **1a** (1.91g, 5.81 mmol, 2 eq.) were dissolved in BuOH-benzene (7:3) under N₂ atmosphere, and refluxed at 120 °C for 10 h with a Dean-Stark condenser. Afterwards, the solvent was evaporated, and the resulting green solid mixture was washed with Et₂O and purified by flash chromatography (DCM-MeOH, 50:1) to obtain **1** as a green solid (1.8 g, 96%).

¹H-NMR (300 MHz, CDCl₃) δ=1.06 (t, 6H, *J*=7.5 Hz), 1.31 (m, 4H), 1.64 (s, 12H), 1.95 (m, 2H), 2.73 (m, 4H), 4.15 (t, 4H, *J*=6.9Hz), 6.23 (d, 2H, *J*=14.2 Hz), 7.15-7.72 (m, 8H), 8.19 (d, 2H, *J*=13.8 Hz). tR: 5.64 min, ESI *m/z* (C₃₆H₄₄ClN₂⁺), calc: 539.4; found: 539.1.

General procedure for the synthesis of CyN-111, 165, 272, 295

1 (100 mg, 149.5 μmol) was mixed with the corresponding amine building blocks (Chart 2.1, 598 μmol , 4 eq.), DIEA (38.6 μL , 299 μmol , 2 eq.), and dissolved in ACN. The reaction mixture was heated at 80 $^{\circ}\text{C}$ for 20 min, quenched with 0.1 N HCl, concentrated under vacuum, and purified by normal-phase chromatography (DCM-MeOH, 98:2) to render the corresponding CyN derivatives.

Chart 2.4. Chemical structures of CyN-111, 165, 272 and 295



CyN-111 (95 mg, 85%): $^1\text{H-NMR}$ (300 MHz, CDCl_3) δ =1.03 (t, 6H, J =7.5Hz), 1.31 (m, 2H), 1.62 (s, 12H), 1.83 (m, 4H), 2.47 (t, 4H, J =6.3Hz), 3.38 (t, 2H, J =5.7Hz), 3.80 (t, 2H, J =7.2Hz), 4.17 (t, 4H, J =6.2Hz), 5.63 (d, 2H, J = 12.9Hz), 6.85-7.72 (m, 12H), 8.52 (d, 2H, J =3.9Hz).

tR: 5.56 min, HRMS ($\text{C}_{43}\text{H}_{53}\text{N}_4^+$), calc: 625.4257; found: 625.4265.

CyN-165 (86 mg, 80%): $^1\text{H-NMR}$ (300 MHz, CDCl_3): δ =1.05 (t, 6H, J =7.5Hz), 1.24 (m, 2H), 1.32 (m, 2H), 1.68 (s, 12H), 1.85 (m, 4H), 2.16 (t, 2H, J =5.4 Hz), 2.47 (t,

4H, $J=6.3$ Hz), 3.44 (s, 3H), 3.71 (t, 2H, $J=5.4$ Hz), 3.95 (t, 4H, $J=6.3$ Hz), 5.61 (d, 2H, $J=12.9$ Hz), 6.50-7.72 (m, 8H), 7.64 (d, 2H, $J=12.9$ Hz), 7.92 (bs, 1H).

tR: 5.66 min, HRMS ($C_{40}H_{54}N_3O^+$), calc: 592.4255; found: 592.4261.

CyN-272 (93 mg, 83%): 1H -NMR (300 MHz, $CDCl_3$): $\delta=1.08$ (t, 6H, $J=7.5$ Hz), 1.31 (m, 2H), 1.45 (m, 4H), 1.54 (m, 2H), 1.68 (s, 12H), 1.85 (m, 4H), 2.51 (t, 4H, $J=6.3$ Hz), 3.44 (t, 6H, $J=7.7$ Hz), 3.81 (t, 4H, $J=6.9$ Hz), 4.21 (m, 2H), 5.65 (d, 2H, $J=12.9$ Hz), 6.80-7.70 (m, 8H), 7.72 (d, 2H, $J=12.9$ Hz).

tR: 5.62 min, HRMS ($C_{43}H_{59}N_4^+$), calc: 631.4740; found: 631.4734.

CyN-295 (88 mg, 87%): 1H -NMR (300 MHz, $CDCl_3$): $\delta=1.05$ (t, 6H, $J=7.5$ Hz), 1.56 (t, 3H, $J=7.0$ Hz), 1.68 (s, 12H), 1.85 (m, 4H), 1.83 (m, 2H), 2.47 (t, 4H, $J=6.3$ Hz), 3.79 (t, 4H, $J=6.9$ Hz), 3.96 (m, 2H), 5.62 (d, 2H, $J=12.9$ Hz), 6.80-7.28 (m, 8H), 7.72 (d, 2H, $J=12.5$ Hz).

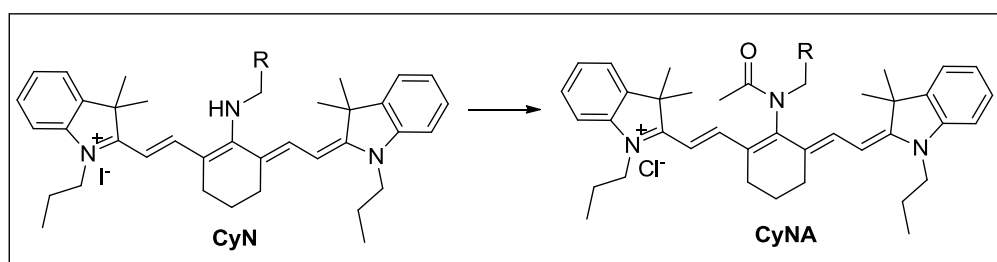
tR: 5.66 min, HRMS ($C_{38}H_{50}N_3^+$), calc: 548.3999; found: 548.3999.

CyN-414 (82 mg, 70%): 1H -NMR (300 MHz, $CDCl_3$): $\delta=1.03$ (t, 6H, $J=7.5$ Hz), 1.24 (d, 3H, $J=6.6$ Hz), 1.32 (m, 4H), 1.36 (t, 2H, $J=5.4$ Hz), 1.70 (s, 12H), 1.78-1.85 (m, 11H), 2.02-2.16 (m, 4H), 2.47 (t, 4H, $J=5.4$ Hz), 3.76 (t, 2H, $J=6.0$ Hz), 3.93 (t, 2H, $J=6.0$ Hz), 5.58 (d, 2H, $J=14.1$ Hz), 6.83 (d, 2H, $J=14.1$ Hz), 6.83-7.72 (m, 8H).

tR: 5.97 min, ESI-MS ($C_{45}H_{63}N_4^+$), calc: 659.5; found: 659.4.

2.5.2 Synthesis of the CyNA library and characterization

Scheme 2.5. Synthesis of CyNA from CyN

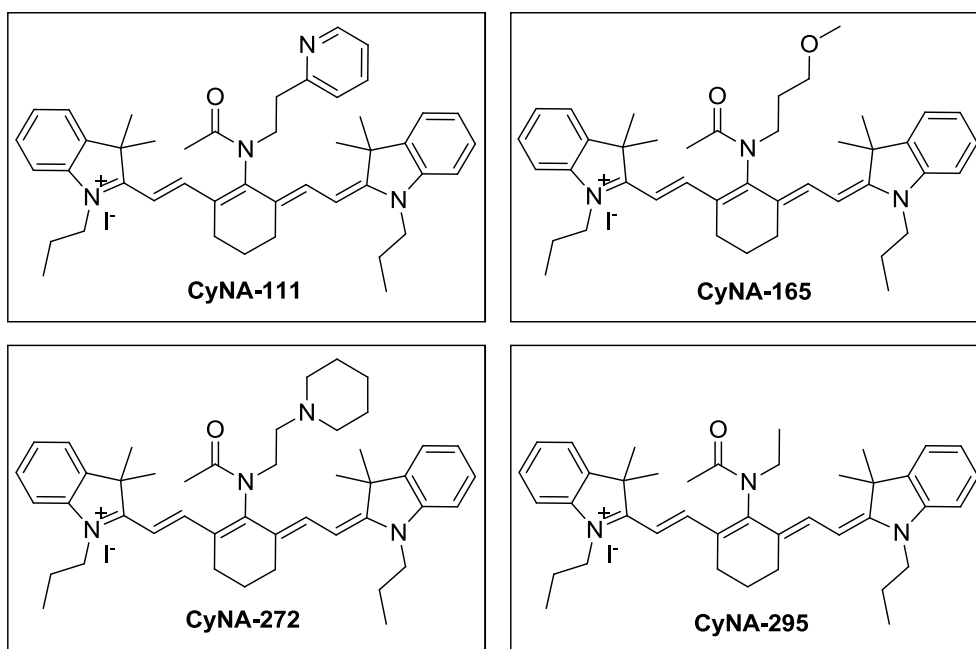


Reagents and conditions: a) CH_3COCl , DIEA in DCM at 0 °C.

For every reaction, **1** (20 mg, 30 μmol , 1 eq.) and the primary amine building block (Chart 2.2) (120 μmol , 4 eq.) were dissolved in ACN, and *N,N*-diisopropylethylamine (DIEA) (7.7 μL , 60 μmol , 2 eq.) was added. The reaction mixture was heated at 80 $^{\circ}\text{C}$ for 10-60 min, depending on the reactivity of the amine. The resulting blue color crude mixtures (**CyN**) were neutralized with 0.1 N HCl, and concentrated under vacuum. Resulting **CyN** crudes were dissolved in DCM under N_2 atmosphere, and treated with excess DIEA (96.2 μL , 750 μmol , 25 eq.) and acetyl chloride (11.7 μL , 150 μmol , 5 eq.) at 0 $^{\circ}\text{C}$ for 15 min. The final green products were washed with 0.1 N HCl to remove the excess of DIEA, concentrated under vacuum, and purified by a normal-phase silica short column using DCM-MeOH (ranging from 100:0 to 97:3) as the eluting solvent. The characterization of the whole library was performed by HPLC-MS (Table 2.3), and the compounds studied in detail were also characterized by $^1\text{H-NMR}$ and HRMS.

Characterization: CyNA-111, 165, 272, 295, 414

Chart 2.5. Chemical structures of **CyNA-111, 165, 272** and **295**.



CyNA-111 (12 mg, 45%): $^1\text{H-NMR}$ (300MHz, CDCl_3): $\delta=1.05$ (t, 6H, $J=7.5\text{Hz}$), 1.29 (m, 2H), 1.63 (s, 6H), 1.65 (s, 6H), 1.72 (m, 4H), 1.94 (t, 4H), 2.05 (s, 3H), 3.09 (m, 2H), 3.63 (m, 2H), 4.18 (t, 4H, $J=3.9\text{Hz}$), 6.07 (d, 0.3H, $J=13.5\text{Hz}$), 6.28 (d, 1.7H, $J=14.1\text{Hz}$), 7.02-7.72 (m, 12H), 8.43 (d, 0.4H, $J=14.1\text{Hz}$), 8.68 (d, 1.6 H, $J=3.3\text{Hz}$).

tR: 4.70 min, HRMS ($\text{C}_{45}\text{H}_{55}\text{ON}_4^+$), calc: 667.4370; found: 667.4350.

CyNA-165 (10 mg, 50%): $^1\text{H-NMR}$ (300 MHz, CDCl_3): $\delta=1.05$ (t, 6H, $J=7.5\text{Hz}$), 1.76 (s, 12H), 1.87-1.92 (m, 8H), 2.58 (t, 4H, $J=6.3$ Hz), 3.28 (s, 3H), 3.32 (t, 2H, $J=5.4\text{Hz}$), 3.45 (t, 2H, $J=6.3$ Hz), 3.92 (t, 4H, $J=7.5$ Hz), 4.16 (s, 3H), 6.02 (d, 2H, $J=13.1$ Hz), 6.90-7.30 (m, 8H), 7.35 (d, 2H, $J=4.5\text{Hz}$).

tR: 6.1 min, HRMS ($\text{C}_{42}\text{H}_{56}\text{N}_3\text{O}_2^+$), calc: 634.4367; found: 634.4352.

CyNA-272 (9 mg, 42%): $^1\text{H-NMR}$ (300 MHz, CDCl_3): $\delta=1.08$ (t, 6H, $J=7.5\text{Hz}$), 1.31 (m, 2H), 1.45 (m, 4H), 1.54 (m, 2H), 1.69 (s, 12H), 1.86 (m, 4H), 1.94 (s, 3H), 2.51 (t, 4H, $J=6.3$ Hz), 3.44 (t, 6H, $J=7.7\text{Hz}$), 3.81 (t, 4H, $J=6.9\text{Hz}$), 4.21 (m, 2H), 5.65 (d, 2H, $J=12.9\text{Hz}$), 6.80-7.70 (m, 8H), 7.72 (d, 2H, $J=12.9\text{Hz}$).

tR: 4.24min, HRMS ($\text{C}_{45}\text{H}_{61}\text{N}_4\text{O}^+$), calc: 673.4840; found: 673.4845.

CyNA-295 (9 mg, 48%): $^1\text{H-NMR}$ (300 MHz, CDCl_3): $\delta=1.05$ (t, 6H, $J=7.5\text{Hz}$), 1.56 (t, 3H, $J=7.0$ Hz), 1.68 (s, 12H), 1.83 (m, 2H), 1.85 (m, 4H), 1.94 (s, 3H), 2.59 (t, 4H, $J=6.3\text{Hz}$), 3.79 (t, 4H, $J=6.9\text{Hz}$), 3.96 (m, 2H), 6.04 (d, 2H, $J=14.0\text{Hz}$), 6.80-7.28 (m, 8H), 8.14 (d, 2H, $J=14.0\text{Hz}$).

tR: 4.87 min, HRMS ($\text{C}_{40}\text{H}_{52}\text{N}_3\text{O}^+$), calc: 590.4105; found: 590.4113.

CyNA-414 (9 mg, 41%): $^1\text{H-NMR}$ (300MHz, CDCl_3): $\delta=1.06$ (t, 6H, $J=7.5\text{Hz}$), 1.24 (d, 3H, $J=6.6$ Hz), 1.23 (m, 2H), 1.58 (s, 6H), 1.66 (s, 6H), 1.83-2.06 (m, 6H), 1.95 (s, 3H), 2.46-2.56 (m, 4H), 2.82 (t, 2H, $J=5.4$ Hz), 2.87 (t, 2H, $J=5.4$ Hz), 3.08

(t, 4H), 2.96-2.98 (m, 2H), 3.08-3.12 (m, 1H), 3.67 (t, 2H, $J=6.0\text{Hz}$), 4.12 (t, 4H, $J=7.2\text{Hz}$), 6.21 (d, 1H, $J=14.1\text{Hz}$), 6.26 (d, 1H, $J=14.1\text{Hz}$), 7.11 (d, 2H, $J=7.5\text{ Hz}$), 7.20 (d, 2H, $J=6.9\text{ Hz}$), 7.34 (m, 4H), 7.55 (d, 1H, $J=14.1\text{ Hz}$), 7.59 (d, 1H, $J=14.1\text{Hz}$).

^{13}C -NMR (75.5MHz, CDCl_3): 11.6, 11.7, 20.5, 20.6, 20.8, 20.9, 22.9, 23.7, 25.0, 28.1, 28.2, 28.3, 28.5, 28.6, 29.6, 30.8, 46.2, 46.2, 49.2, 49.3, 102.2, 110.7, 110.8, 122.3, 125.3, 125.4, 128.2, 128.4, 128.6, 140.9, 141.0, 142.2, 154.2, 170.4, 172.1.

tR: 4.32 min, HRMS ($\text{C}_{47}\text{H}_{65}\text{N}_4\text{O}^+$), calc: 701.5153; found: 701.5147.

2.5.3 Photostability measurements

Time-course fluorescence measurements of CyN-111, 165, 272, 295 vs. CyNA-111, 165, 272, 295 and 1

Procedure: 10 μM CyN(A) solutions in 10mM HEPES buffer (pH 7.4) containing 1% DMSO were placed in a 96-well black plate, and fluorescence intensity measurements were recorded every 10 min for a total period of 10 h (excitation-emission: 640-750 nm for CyN derivatives, and 790-820 nm for 1 and CyNA derivatives). Values are fitted to a non-linear regression one-phase exponential decay (GraphPad Prism 5.0).

CyNA library (primary and secondary screening)

Primary screening: 10 μM CyN(A) solutions in 100 mM HEPES buffer (pH 7.4) containing 2% DMSO were placed in a 96-well black plate, and fluorescence intensity measurements were recorded every 10 min for a total period of 8 h (excitation emission: 790-820 nm). A subset of 14 compounds selected according to their quotients F_{8h}/F_0 , quantum yields and maximum RFU values (Table 2.3) was further evaluated on the secondary screening.

Secondary screening: 10 μ M solutions in 10 mM HEPES buffer (pH 7.4) or PBS (pH 7.3) containing 1% DMSO were placed in a 96-well black plate, and irradiated for periods of 15 min (up to 2h) with a high intensity UV lamp (100W, 365 nm) at 2-cm distance. Values are represented as means (n=2), and fitted to a non-linear regression one-phase exponential decay (GraphPad Prism 5.0).

2.6 References

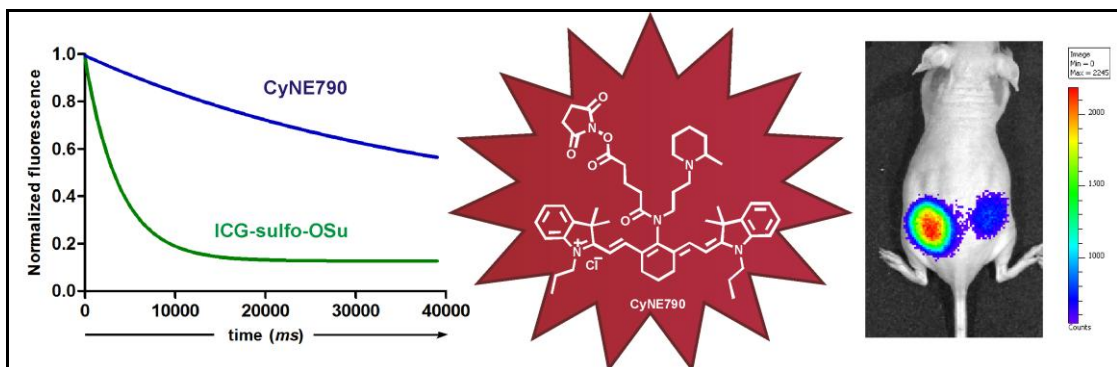
1. D. B. Shealy, M. Lipowska, J. Lipowski, N. Narayanan, S. Sutter, L. Strekowski, G. Patonay, *Anal. Chem.* **1995**, *67*, 247.
2. W. Pham, W. F. Lai, R. Weissleder, C. H. Tung, *Bioconjugate Chem.* **2003**, *14*, 1048.
3. (a) K. Jyothish, R. R. Avirah, D. Ramaiah, *Org. Lett.* **2006**, *8*, 111.; (b) S. Sreejith, K. P. Divya, A. Ajayaghosh, *Angew. Chem. Int. Ed. Engl.* **2008**, *47*, 7883.; (c) Y. Xu, M. J. Panzner, X. Li, W. J. Youngs, Y. Pang, *Chem. Commun.* **2010**, *46*, 4073.; (d) S. Y. Hsueh, C. C. Lai, Y. H. Liu, Y. Wang, S. M. Peng, S. H. Chiu, *Org. Lett.* **2007**, *9*, 4523.
4. W. B. Tuemmler, B. S. Wildi, *J. Am. Chem. Soc.* **1958**, *80*, 3772.
5. K. Takagi, M. Kawabe, M. Matsuoka, T. Kitao, *Dyes Pigm.* **1985**, *6*, 177.
6. (a) S. A. Hilderbrand, R. Weissleder, *Curr. Opin. Chem. Biol.* **2010**, *14*, 71.; (b) L. Xiao, Y. Zhang, Z. Liu, M. Yang, L. Pu, D. Pan, *Bioorg. Med. Chem. Lett.* **2010**, *20*, 3515. (c) J. Fabian, H. Kakazumi, M. Matsuoka, *Chem. Rev.* 1992, *92*, 1197.
7. (a) G. A. Reynolds, K. H. Drexhage, *J. Org. Chem.* **1977**, *42*, 885.; (b) N. Narayanan, G. Patonay, *J. Org. Chem.* **1995**, *60*, 2391.; (c) P. J. Sims, A. S. Waggoner, C. H. Wang, J. F. Hoffman, *Biochemistry* **1974**, *13*, 3315.; (d) S. J. Mason, S. Balasubramanian, *Org. Lett.* **2002**, *4*, 4261.; (e) M. Lopalco, E. N. Koini, J. K. Cho, M. Bradley, *Org. Biomol. Chem.* **2009**, *7*, 856.
8. (a) J. V. Frangioni, *Curr. Opin. Chem. Biol.* **2003**, *7*, 626.; (b) W. M. Leevy, S. T. Gammon, J. R. Johnson, A. J. Lampkins, H. Jiang, M. Marquez, D. Piwnicka-Worms, M. A. Suckow, B. D. Smith, *Bioconjugate Chem.* **2008**, *19*, 686.; (c) E. M. Sevick-Muraca, J. P. Houston, M. Gurfinkel, *Curr. Opin. Chem. Biol.* **2002**, *6*, 642.; (d) K. Kiyose, H. Kojima, Y. Urano, T. Nagano, *J. Am. Chem. Soc.* **2006**, *128*, 6548.; (e) A. Becker, C. Hessenius, K. Licha, B. Ebert, U. Sukowski, W. Semmler, B. Wiedenmann, C. Grotzinger, *Nat. Biotechnol.* **2001**, *19*, 327.; (f) W.

- M. Leevy, S. T. Gammon, H. Jiang, J. R. Johnson, D. J. Maxwell, E. N. Jackson, M. Marquez, D. P. Worms, B. D. Smith, *J. Am. Chem. Soc.* **2006**, *128*, 16476.; (g) E. Sasaki, H. Kojima, H. Nishimatsu, Y. Urano, K. Kikuchi, Y. Hirata, T. Nagano, *J. Am. Chem. Soc.* **2005**, *127*, 3684.; (h) R. Weissleder, C. H. Tung, U. Mahmood, A. Bodganov Jr., *Nat. Biotechnol.* **1999**, *17*, 375.
9. J. H. Flangan Jr., S. H. Khan, S. Menchen, S. A. Soper, R. P. Hammer, *Bioconjugate Chem.* **1997**, *8*, 751.
10. M. Lipowska, G. Patonay, L. Strekowski, *Synthetic Commun.* **1993**, *23*, 3087.
11. (a) M. Bai, M. Sexton, N. Stella, D. J. Bornhop, *Bioconjugate Chem.* **2008**, *19*, 988.; (b) S. A. Hilderbrand, K. A. Kelly, R. Weissleder, C. H. Tung, *Bioconjugate Chem.* **2005**, *16*, 1275.
12. (a) Strekowski, L.; Lipowska, M.; Patonay, G. *J. Org. Chem.* **1992**, *57*, 4578.; (b) Tyutyulkov, N. F. J.; Mehlhorn, A.; Dietz, F.; Tadjer, A. Polymethine dyes: Structure and Properties; St. Kliment Ohridski University Press: Sofia, Bulgaria, **1991**. (c) G. A. Reynolds, K. H. Drexhage, *J. Org. Chem.* **1977**, *42*, 885. (d) N. Narayanan, G. Patonay, *J. Org. Chem.* **1995**, *60*, 2391.
13. F. Song, X. Peng, E. Lu, R. Zhang, X. Chen, B. Song, *J. Photochem. Photobiol. A: Chem.* **2004**, *168*, 53.
14. (a) A. Toutchkine, D. V. Nguyen, K. M. Hahn, *Org. Lett.*, **2007**, *9*, 2775.; (b) B. R. Renikuntla, H. C. Rose, J. Eldo, A. S. Waggoner, B. A. Armitage, *Org. Lett.* **2004**, *6*, 909.; (c) M. Wang, R. H. Davis, Z. Rafinski, B. Jedrzejewska, K. Y. Choi, M. Zwick, C. Bupp, A. Izmailov, J. Paczkowski, B. Warner, H. Koshinsky, *Anal. Chem.* **2009**, *81*, 2043.; (d) R. Schraml, T. Maisch, K. Kobuch, B. Konig, R. M. Szeimies, J. Hillenkamp, W. Baumler, R. Vasold, *Invest. Ophthalmol. Visual Sci.* **2008**, *49*, 1777.; (e) X. Chen, X. Peng, A. Cui, B. Wang, L. Wang, R. Zhang, *J. Photochem. Photobiol. A* **2006**, *181*, 79.

15. (a) S. G. Sakka, *Curr. Opin. Crit. Care* **2007**, *13*, 207.; (b) V. L. Dzurinko, A. S. Gurwood, J. R. Price, *J. Am. Optom. Assoc.* **2004**, *75*, 743.; (b) M. Ogawa, N. Kosaka, P. L. Choyke, H. Kobayashi, *Cancer Res.* **2009**, *69*, 1268.
16. J. O. Escobedo, O. Rusin, S. Lim, R. M. Strongin, *Curr. Opin. Chem. Biol.* **2010**, *14*, 64.
17. (a) F. Rotermund, R. Weigand, A. Penzkofer, *Chem. Phys.* **1997**, *220*, 385.; (b) R. Weigand, F. Rotermund, A. Penzkofer, *Chem. Phys.* **1997**, *220*, 373.; (c) J. Zweck, A. Penzkofer, *Chem. Phys.* **2001**, *269*, 399.; (d) R. Weigand, F. Rotermund, A. Penzkofer, *J. Phys. Chem. A* **1997**, *101*, 7729.

CHAPTER 3

A PHOTOSTABLE NIR PROTEIN LABELING DYE FOR *IN VIVO* IMAGING



3.1 Introduction

Fluorescence imaging techniques are widely used in biomedical research. A majority of these applications are based on the use of NIR labeling dyes for *in vivo* imaging. The suitability of the NIR region for *in vivo* imaging (e.g., deep tissue penetration, low auto-fluorescence background) has been extensively described.¹⁻³ *In vivo* imaging typically involves the administration of NIR probes either in the form of fluorescent small molecules⁴ or fluorescent proteins⁵ upon covalent attachment of the metabolite of protein of interest to NIR labeling reagent. NIR protein labeling dyes must ideally retain identical fluorescent properties and good photostability profiles after conjugation. In addition, they must maintain the specific recognition and functional abilities of the protein. The increasing importance of small animal optical *in vivo* imaging has underscored the need for NIR protein labelling compounds that fulfil such requirements. The most common organic NIR fluorophores are polymethine cyanine dyes. Among them, heptamethine and pentamethine cyanines comprising benzoxazole, benzothiazole and indolyl have been the most useful for fluorescent imaging as their physical properties, biodistribution, and pharmacokinetics have been well characterized. For example, while Indocyanine green (ICG) is the only NIR dye clinically approved to date, its poor photostability, low quantum yield in buffer solutions are major concerns for its applicability in biological systems. Hence, chemist have devoted lots of efforts to develop new NIR labeling dyes with improved fluorescence quantum yields, high chemical and photostability, low aggregation in buffer solution and low cytotoxicity.

3.2 Objectives

Herein, I report the synthesis of a novel NIR labeling dye (**CyNE790**) based on the structure of **CyNA-414**, which is the most photostable tricarbocyanine dye among the 80-member library discussed in Chapter 2. The application of **CyNE790** for protein labeling has been compared to the NIR standard **ICG-sulpho-OSu**. The

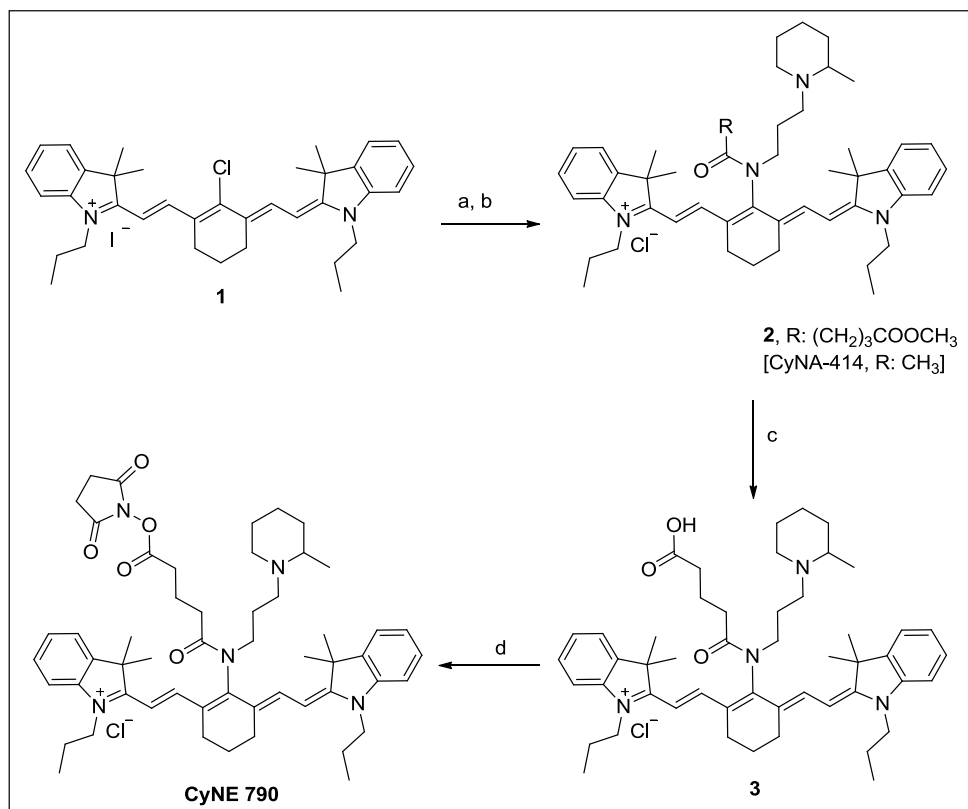
analysis of the photostability before and after bio-conjugation proved the superiority of **CyNE 790**, whose practical use as a NIR protein labeling dye was demonstrated with *in vivo* imaging studies.

3.3 Results and discussion

3.3.1 Design and synthesis

The tricyanocyanine scaffold (**1**) is a synthetically accessible NIR structure, and shows improved fluorescent properties when compared to other heptamethine cyanines.^{6,7} I have discussed earlier chapter about the superior photostability of the amine acetylated tricyanocyanine (**CyNA**) structure. The electron-withdrawing acetyl group incorporated into **CyNA** significantly increased the photostability properties of the amine tricyanocyanine core, and a combinatorial approach was applied to identify **CyNA-414** as a highly fluorescent and photostable NIR dye (Scheme 2.1).⁸ Whereas **CyNA-414** exhibits good properties as a NIR dye, it lacks a reactive functional group that enables protein labeling. I designed the synthesis of a reactive ester **CyNE790** by replacing the electron-withdrawing acetyl group with a glutaric acid moiety. Hence, I envisioned that the glutaric acid would not only provide a suitable spacer to incorporate a reactive succinidimyl ester group but also preserved the electron-withdrawing effect, which was critical to retain the good photostability profile.

Scheme 3.1. Synthesis of **CyNE790**.



Reagents and conditions: (a) 1-(3-aminopropyl)-2-pipecoline, DIEA, CH₃CN, 80 °C, 40 min.; (b) acetyl chloride (for **CyNA-414**) or methyl 4-(chloroformyl)butyrate (for **2**), DIEA, CH₂Cl₂, 0 °C to r.t., 15 min.; (c) from **2**, CHCl₃:THF:H₂O:HCl_{conc} (6:3:2:1), 80 °C, 12 h; (d) DCC, *N*-hydroxysuccinimide, anhydrous DMF.

CyNE790 was prepared in a three-step synthesis with overall reasonable yields. Notably, the hydrolysis of the methyl ester **2** to afford the corresponding carboxylic acid **3** required a rigorous evaluation of the reaction conditions, since tricyanopyrene compounds are inherently labile under strong acid and basic media.^{9,10} An optimized treatment of **2** with a solution of HCl in CHCl₃-THF-H₂O (6:3:2) rendered **3**, which could be isolated after normal-phase chromatography. **CyNE790** was readily prepared from **3** by derivatization with *N*-hydroxysuccinimide (Scheme 3.1).

3.3.2 Photophysical properties study

The spectral characterization of **CyNE790** demonstrated that the incorporation of the linker did not affect the maximum excitation and emission wavelengths or the fluorescence emission intensity of the original compound (Figure 3.1).

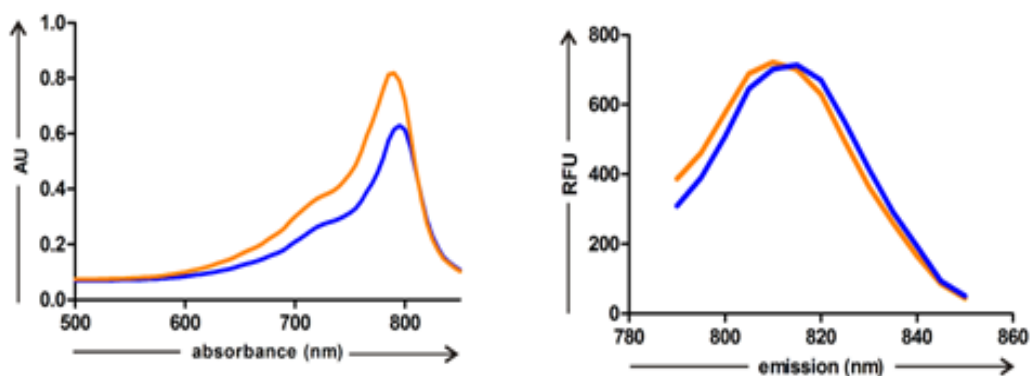


Figure 3.1. Absorbance and emission spectra of CyNA-414 (orange) and CyNE790 (blue). Absorbance spectra: 5 μM solutions in PBS (pH 7.3) containing 1% DMSO. Emission spectra: 10 μM solutions in PBS (pH 7.3) containing 1% DMSO, excitation wavelength: 760 nm.

CyNE790 showed an excellent photostability in aqueous media. 10 μM solutions in 10 mM HEPES buffer (pH 7.4) or PBS (pH 7.3) containing 1% DMSO were placed in a 96-well black plate, and irradiated for periods of 15 min (up to 1.5 h) with a high intensity UV lamp (100W, 365 nm) at 2-cm distance. Figure 3.2 clearly shows that the incorporation of the glutaric acid as the spacer moiety for bioconjugation does not change the photostability property also.

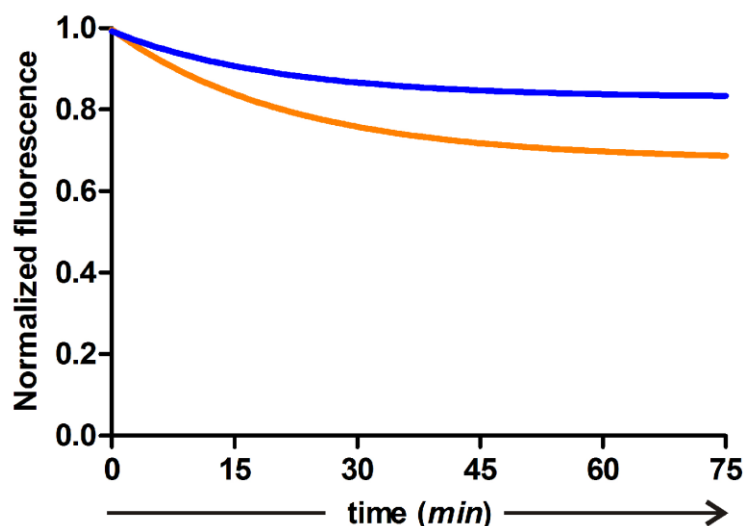


Figure 3.2. Comparative photostability of **CyNA-414** (orange) and **CyNE790** (blue) under a high intensity ultraviolet lamp. Briefly, 10 μM solutions in PBS (pH 7.3) containing 1% DMSO were irradiated for periods of 15 min (up to 75 min) with UVP Blak-Ray® B-100AP high intensity mercury lamp (100W, 365 nm) at 2 cm distance. Values are represented as means ($n=4$), and fitted to a non-linear regression one-phase exponential decay (right hand side).

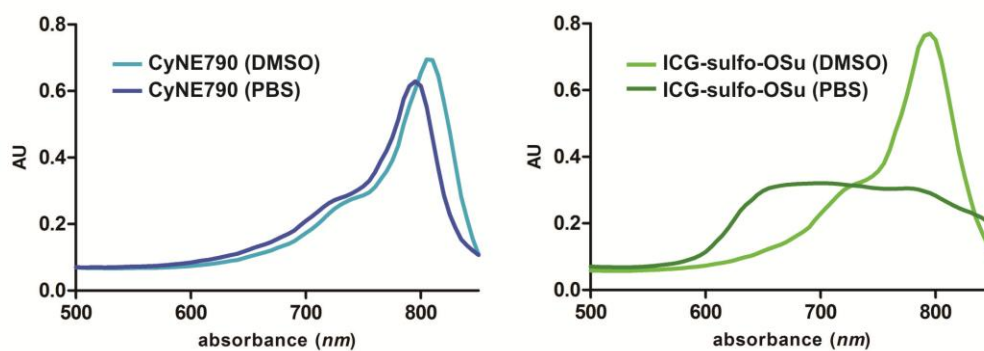
After confirming the spectral properties of **CyNE790** as a fluorescent NIR labeling dye, I compared its applicability for protein conjugation with **ICG-sulfo-OSu**, the commercially available succinidimyl ester of **ICG**.^{11,12} Whereas the structure of **ICG** has a similar spectral profile (absorption-emission: 790-810 nm) to **CyNE790**, the application of **ICG** in molecular imaging has been limited because its fluorescence is drastically quenched after protein conjugation.^{13,14} Moreover, **ICG** derivatives embody several disadvantages that hampered their use in bioimaging,¹⁵ such as low quantum yield, poor photostability and the formation of aggregates in aqueous media.^{16,17} **CyNE790** exhibited superior fluorescent properties to **ICG-sulfo-OSu**. In addition to its higher fluorescence quantum yield in aqueous media (Table 3.1), **CyNE790** showed little or no aggregates formation in buffer conditions.

Table 3.1. Photophysical properties of **CyNE790** and **ICG-sulfo-OSu**.

	Quantum yield (DMSO) ^[a]	Quantum yield (aqueous media) ^[b]	ϵ ($M^{-1} \cdot cm^{-1}$) (aqueous media) ^[b]
CyNE790	13%	3.3%	108,000
ICG-sulfo-OSu	12%	0.4%	42,000

[a] **ICG** was used as a standard in DMSO^{19a} and in aqueous media.^[19b] [b] Dyes were dissolved in phosphate buffered saline (PBS, pH 7.3) with 0.1% DMSO.

On the contrary, the aggregate formation of **ICG-sulfo-OSu** in aqueous media was evidenced by the shift of the absorbance maximum values from 780 nm to 695 nm¹⁸ (Figure 3.3). Interestingly, the data shows in Table 3.1 that the brightness ($\Theta \times \epsilon$) of **CyNE 790** is 21-fold higher than **ICG-sulfo-OSu**.

**Figure 3.3.** Absorbance spectra of **CyNE790** (blue) and **ICG-sulfo-OSu** (green), 5 μ M solutions in PBS (pH 7.3) containing 1% DMSO or 0.5 μ M solutions in DMSO.

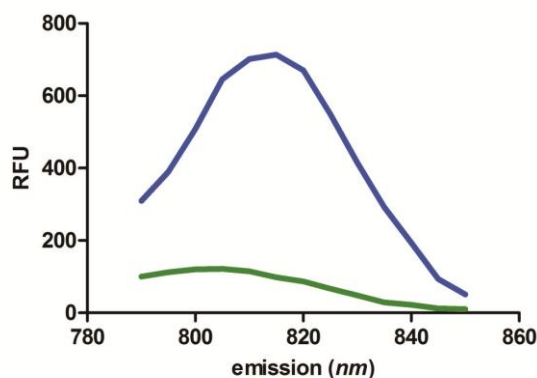


Figure 3.4. Emission spectra of **CyNE790** (blue) and **ICG-sulfo-OSu** (green), 10 μ M solutions in PBS (pH 7.3) containing 1% DMSO, excitation wavelength: 760 nm (left hand side).

3.3.3 Photostability measurements

Photostability evaluation of **CyNE790** and **ICG-sulfo-OSu**: 10 μ M solutions in phosphate buffered saline (PBS, pH 7.3) containing 1% DMSO were fixed in a glass cover slide, and irradiated with a diode laser (95 mW, 740 nm, time frame: 500 ms, no delay). Emission was recorded with a NIR-enhanced CCD camera (Andor Technology) adapted to an Eclipse Ti-U microscope (objective 40 \times , filter cube 750/800), and images were processed using the software NIS-Elements 3.10. The resulting values were represented as means ($n=3$), and fitted to a non-linear regression one-phase exponential decay (GraphPad Prism 5.0). A detailed evaluation of their photobleaching in buffer attested a 15-fold higher photostability of **CyNE790** when compared to **ICG-sulfo-OSu** (Chart 3.1, Figure 3.5).

Chart 3.1. Chemical structures of **CyNE790** and **ICG-sulfo-OSu**

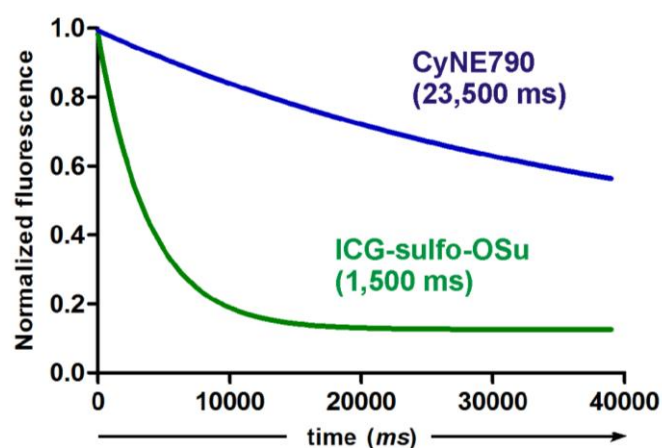
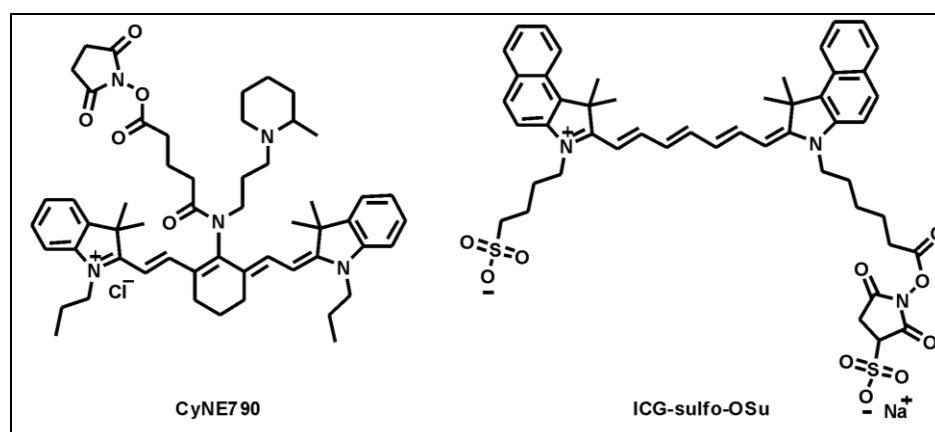


Figure 3.5. Photostability of **CyNE790** (black) and **ICG-sulfo-OSu** (grey) under laser irradiation (740 nm). Values are represented as means (n=3) for sequential measurements every 500 ms. Conditions: 10 μ M (1% DMSO) solutions in PBS buffer (pH 7.3). Time needed to bleach 35% of the maximum fluorescence intensity for every compound is indicated in brackets.

3.3.4 Antibody conjugation and characterization

With the aim of comparing both reactive esters (**CyNE790** and **ICG-sulfo-OSu**) for *in vivo* imaging studies, we conjugated them to a monoclonal anti-EGFR antibody. As shown in Figure 3.6, the **CyNE790**-labelled antibody showed stronger fluorescence intensity than the **ICG**-labelled antibody, according to both emission spectra and gel electrophoresis scanning.

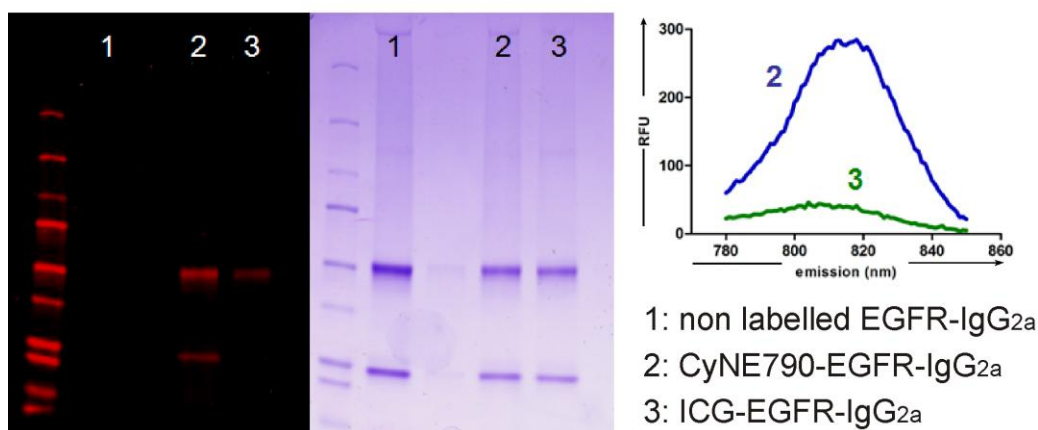


Figure 3.6. Characterization of CyNE790 and ICG-labelled antibodies: *left*) fluorescence SDS-PAGE image; *centre*) SDS-PAGE image after Coomassie Blue staining; *right*) emission spectra (exc: 750 nm).

Additional characterization of both antibodies indicated that the superior spectra properties of **CyNE790** were also maintained after protein conjugation (Figures 3.7). Dye/protein (D/P) ratios were determined using reported procedures and the labeling efficiencies were similar for both dyes (Table 3.2). The dye/protein ratio was calculated according to the following equation $D/P = (A_{790}/\epsilon_{790}) / \{(A_{280} - \Theta \times A_{790}) / 170,000\}$, whereas ϵ_{790} are the extinction coefficients in PBS (790 nm) and Θ the ratios $\epsilon_{280} / \epsilon_{790}$.

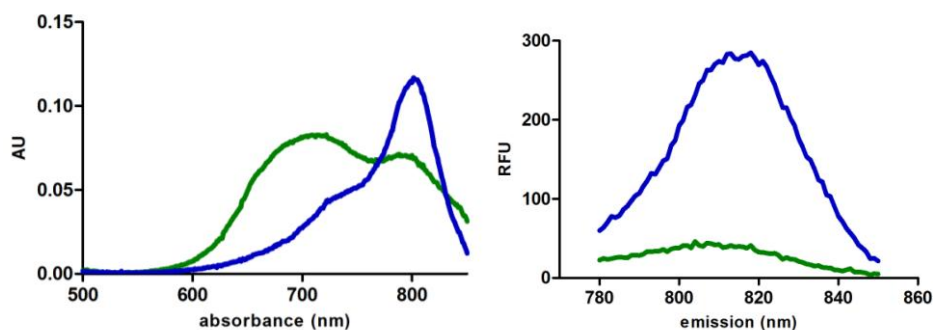


Figure 3.7. Absorbance and emission spectra of **CyNE790**-labelled (blue) and **ICG**-labelled anti-EGFR-IgG_{2a} (green). Excitation wavelength (for the emission spectra): 750 nm.

Table 3.2. Characterization of dye conjugated antibody in buffer solution.

Dye conjugated antibody	ϵ_{790}	Θ	D/P	labeling efficiency
ICG-labelled anti-EGFR	42,000	0.081	3.5	17.5%
CyNE790-labelled anti-EGFR	108,000	0.037	3.6	18.0%

3.3.5 *In vitro* and *in vivo* imaging

In addition, we (I and Dr. Marc Vendrell) proved the applicability of **CyNE790** by detecting EGFR-expressing cells with the **CyNE790**-labelled anti-EGFR. SCC-15 and MCF-7 are human cancer cell lines with respectively high and low expression levels of EGFR, a known target protein for tumor diagnosis and anticancer therapy.^{20,21} Cell imaging after incubating SCC-15 and MCF-7 cells with **CyNE790**-labelled anti-EGFR showed a brighter staining in SCC-15 cells, which corresponds to the higher expression level of EGFR in this cell line (Figure 3.8).

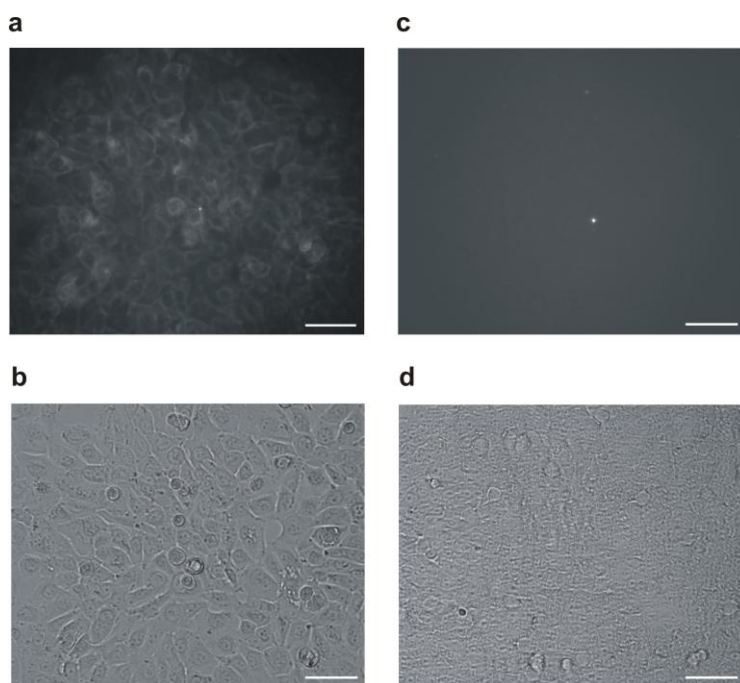


Figure 3.8. Microscope images of SCC-15 (a, b) and MCF-7 cells (c,d) after incubation with **CyNE790**-anti-EGFR: a) and c) correspond to NIR-fluorescence images, b) and d) are bright-field images. Scale bar: 80 μm .

The better fluorescence properties of the **CyNE790**-labelled antibody were further demonstrated by examining the NIR emission of both antibodies in mice (Figure 3.9a). The **CyNE790**-labelled antibody displayed a quantum yield of 3%, with a stronger fluorescence signal than the **ICG**-labelled antibody that enabled *in vivo* imaging with a significantly lower detection limit. Furthermore, the injection of **CyNE790**-anti-EGFR treated SCC-15 and MCF-7 cells allowed the visualization of SCC-15 cells in mice with much higher intensity compared to MCF-7 (Figure 3.9b), and confirmed that the conjugation of **CyNE790** did not affect the recognition properties of the monoclonal anti-EGFR antibody.

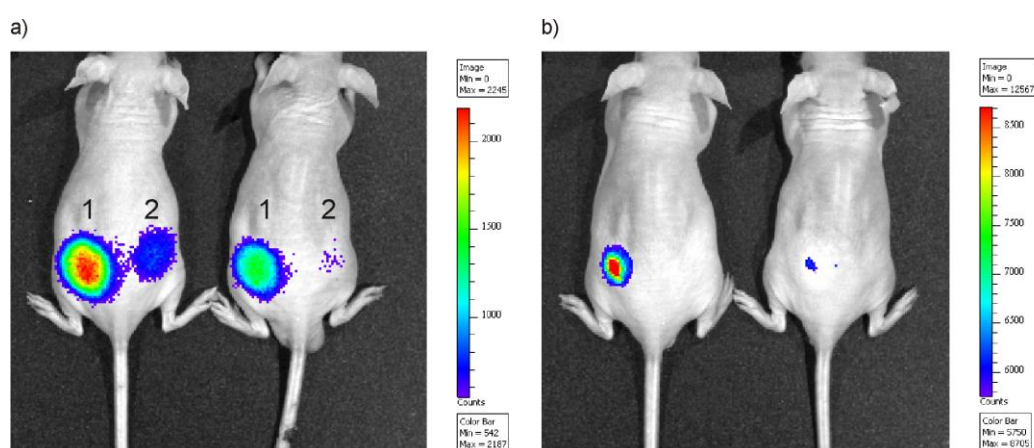


Figure 3.9. Fluorescence images after injection of: a) CyNE790-labelled antibody (left mouse), ICG-labelled antibody (right mouse) (protein amount per site: 1) 0.85 μg , 2) 0.15 μg); b) CyNE790-anti-EGFR treated SCC-15 cells (left flank, left mouse) and CyNE790-anti-EGFR treated MCF-7 cells (left flank, right mouse).

The application of CyNE790-anti-EGFR for *in vivo* imaging was further validated in xenografts prepared by injection of EGFR+ breast cancer cells MDA-MB-231 in nude mice. Upon tumor formation (approximate tumor size: 0.3-0.5 cm), CyNE790-anti-EGFR was injected via tail vein, and mice were imaged in a time-course manner. When the mice were examined 1 hr after injection the fluorescence was detected from whole body of all animals. The signal of compound 3 started to disappear earlier than antibody conjugated dye at 4 hr. The fluorescence signal from the tumor was clearly visible only in EGFR Ab-CyNE injected mice at 26 hr after

injection. The NIR fluorescence images proved that CyNE790-anti-EGFR selectively stained the tumor regions while no staining was observed for CyNE790, and the signal of CyNE790-anti-EGFR could be detected up to 50 h after injection (Figure 3.10).

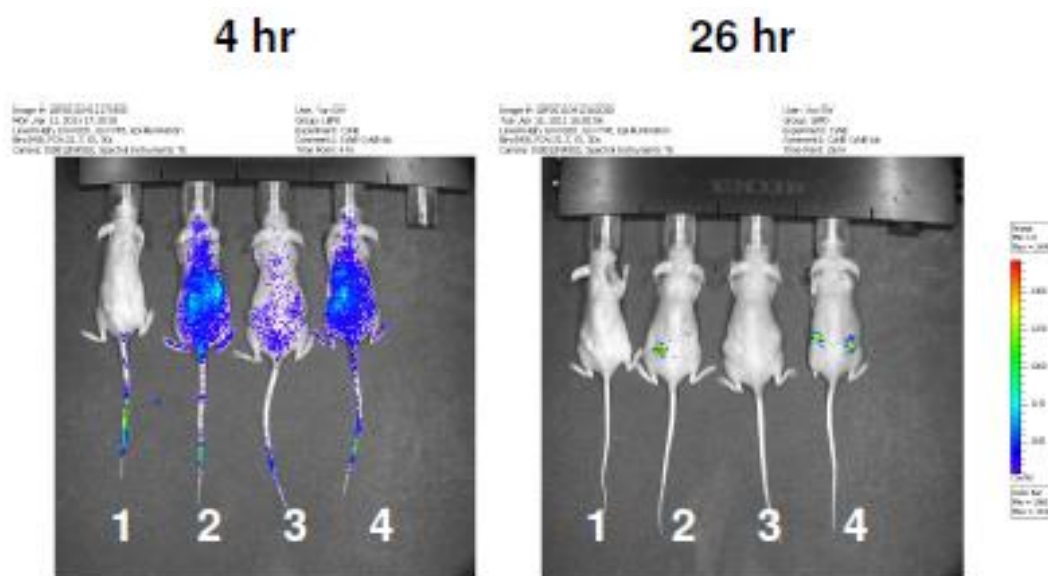


Figure 3.10. Compound 3 was injected number 1 and 3 mice which contain MDA-MB 231 cell and CRL-2095 tumor. CyNE-EGFR-Ab was injected in number 2 and 4 mice which contain MDA-MB 231 cell and CRL-2095 tumor.

3.4 Conclusions

In conclusion, I developed a highly fluorescent and photostable NIR protein labelling dye (**CyNE790**). **CyNE790** incorporates a glutaric acid linker that enables protein bioconjugation and preserves the excellent photostability and NIR fluorescence intensity of the amine acetylated tricyanocyanine scaffold. Upon protein conjugation, the fluorescent properties of **CyNE790** were maintained, and proved to be superior to the NIR standard **ICG-sulfo-OSu**. Furthermore, we (I, and Dr. Yun Seong Wook) demonstrated the adequacy of **CyNE790** for *in vivo* NIR imaging by labelling a monoclonal anti-EGFR antibody and confirming that its recognition properties remained unaffected.

3.5 Experimental details

Materials and Methods:

All materials and methods have been described in earlier section 2.5. **ICG-sulfo-OSu** was purchased from Dojindo Laboratories, and anti-EGFR-IgG_{2a} (sc-120) was supplied by Santa Cruz Biotechnology, Inc. Photobleaching measurements were performed using an Eclipse Ti-U Nikon microscope (filter cube: 750/800) attached to Ti:sapphire oscillator that operated in continuous wave mode in Singapore Bioimaging Consortium, Agency for Science, Technology and Research (A*STAR), Singapore, and the data was processed using the software NIS-Elements 3.10. *In vivo* images were taken in an IVIS spectrum imaging system (Caliper Life Sciences).

3.5.1 Synthesis and characterization of CyNE 790

Synthesis of 2:

1 (300 mg, 0.45 mmol) and 1-(3-aminopropyl)-2-pipecoline (170 mg, 0.9 mmol) were dissolved in ACN (2 mL), and *N,N*-diisopropylethylamine (DIEA) (87 μ L, 0.67 mmol) was added. The reaction mixture was heated at 80 °C for 40 min, and the resulting blue color crude was neutralized with 0.1 N HCl (aq) and concentrated under vacuum. The crude mixture was dissolved in DCM under N₂ atmosphere, and treated with excess DIEA (700 μ L, 5.39 mmol) and methyl 4-(chloroformyl) butyrate (110 μ L, 0.67 mmol) at 0 °C for 15 min. The resulting green product was washed with 0.1 N HCl (aq) and brine, concentrated under vacuum. **2** was isolated as a green solid (360 mg, yield 92%) and used without further purification.

Synthesis of 3:

2 (360 mg, 0.41 mmol) was dissolved in 40 mL of CHCl₃, and a mixture of THF:H₂O:HCl_{conc} (3:2:1, 40 mL) was slowly added with continuous stirring at 0 °C. After 5 min. the reaction mixture was refluxed at 80 °C for 12 h, and monitored by HPLC-MS. After complete hydrolysis of the methyl ester, CHCl₃ was added to the

reaction mixture, the organic layer was collected (3 × 20 mL), washed with H₂O and purified by normal-phase chromatography using DCM-MeOH (from 100:0 to 88:12) as the eluting solvent. **3** was obtained as a green solid (70 mg, yield 20%).

Characterization data for 3: ¹H-NMR (300 MHz, CDCl₃): 1.06 (t, 6H, *J*=7.5Hz), 1.24 (d, 3H, *J*=6.6 Hz), 1.39 (m, 2H), 1.61 (s, 6H), 1.62 (s, 6H), 1.79-1.95 (m, 6H), 2.22 (t, 2H, *J*=7.8 Hz), 2.33 (t, 2H, *J*=6.6 Hz), 2.52-2.56 (m, 4H), 2.82 (t, 2H, *J*=5.4 Hz), 2.87 (t, 2H, *J*=5.4 Hz), 2.96-2.98 (m, 2H), 3.09-3.12 (m, 1H), 3.36 (t, 4H), 3.53 (t, 2H, *J*=6.6 Hz), 3.67 (t, 2H, *J*=6.6 Hz), 4.06 (t, 2H, 4.2 Hz), 4.15 (t, 2H, *J*=4.8 Hz), 6.15 (d, 1H, *J*=14.1Hz), 6.20 (d, 1H, *J*=14.1Hz), 7.07-7.38 (m, 8H), 7.51 (d, 1H, *J*=14.1Hz), 7.60 (d, 1H, *J*=14.1Hz). ¹³C-NMR (75 MHz, CDCl₃): 11.6, 12.2, 19.5, 20.4, 20.6, 20.7, 22.2, 22.9, 24.8, 28.1, 28.2, 28.3, 31.3, 32.3, 41.9, 43.9, 48.3, 49.1, 49.3, 50.2, 51.8, 53.7, 60.4, 101.5, 101.9, 102.4, 106.2, 110.6, 110.8, 114.9, 118.8, 122.3, 125.5, 125.6, 127.7, 128.1, 128.6, 140.6, 140.9, 141.4, 142.1, 142.2, 144.6, 153.9, 160.9, 161.4, 171.7, 172.5, 173.6, 174.3.

tR: 4.13 min, ESI (HRMS) *m/z* (C₅₀H₆₉N₄O₃⁺), calc: 773.5364; found: 773.5351.

Synthesis of CyNE790:

N,N'-dicyclohexylcarbodiimide (11 mg, 56 μmol) and **3** (30 mg, 37 μmol) were dissolved in anhydrous THF (2 mL), stirred for 10 min at r.t, and mixed with *N*-hydroxysuccinimide (7 mg, 59 μmol). The reaction mixture was stirred at r.t. for 12 h, washed with Et₂O, concentrated under reduced pressure, and purified by normal-phase chromatography using DCM-MeOH (from 100:0 to 94:6) as the eluting solvent. **CyNE790** was isolated as a green solid (21 mg, yield 65%).

Characterization data for CyNE790: ¹H-NMR (300 MHz, CDCl₃): 1.06 (t, 6H, *J*=7.5Hz), 1.22 (d, 3H, *J*=6.6 Hz), 1.39 (m, 2H), 1.61 (s, 6H), 1.62 (s, 6H), 1.79-1.95 (m, 6H), 2.22 (t, 2H, *J*=7.8 Hz), 2.33 (t, 2H, *J*=6.6 Hz), 2.52-2.56 (m, 4H), 2.64 (s, 2H), 2.68 (s, 2H), 2.82 (t, 2H, *J*=5.4 Hz), 2.87 (t, 2H, *J*=5.4 Hz), 2.96-2.98 (m, 2H),

3.09-3.12 (m, 1H), 3.36 (m, 4H), 3.53 (t, 2H, $J=6.6$ Hz), 3.67 (t, 2H, $J=6.6$ Hz), 4.06 (t, 2H, 4.2 Hz), 4.15 (t, 2H, $J=4.8$ Hz), 6.15 (d, 1H, $J=14.1$ Hz), 6.20 (d, 1H, $J=14.1$ Hz), 7.07-7.38 (m, 8H), 7.51 (d, 1H, $J=14.1$ Hz), 7.60 (d, 1H, $J=14.1$ Hz).

^{13}C -NMR (75 MHz, CDCl_3): 11.6, 12.3, 20.1, 20.5, 20.8, 22.9, 24.8, 25.4, 25.5, 25.7, 28.1, 28.2, 28.3, 28.4, 29.6, 30.2, 31.6, 32.4, 33.9, 46.1, 46.2, 48.2, 49.1, 49.2, 49.3, 101.8, 102.2, 110.6, 110.8, 110.9, 122.3, 122.4, 125.3, 125.4, 125.6, 128.0, 128.3, 128.5, 128.7, 140.7, 140.9, 141.0, 141.1, 142.1, 142.2, 153.3, 153.9, 167.9, 168.9, 172.0, 172.2, 172.3, 172.7, 173.6.

tR: 4.20 min, ESI (HRMS) m/z ($\text{C}_{54}\text{H}_{72}\text{N}_5\text{O}_5^+$), calc: 870.5528; found: 870.5534.

3.5.2 Antibody conjugation and characterization

Antibody conjugation:

100 μg of anti-EGFR-IgG_{2a} were washed with PBS using a Microcon 3K filter (Millipore), and re-suspended in 100 μL of Na_2CO_3 - NaHCO_3 buffer (pH: 9.2). 20 eq. of **CyNE790** or **ICG-sulfo-OSu** (typically 1.0-1.2 μL of a 10 mM DMSO solution) were added and the whole mixture was shaken at dark for 2 h. The excess of dye was removed by washing with PBS (3 \times 500 μL) using a Microcon 3K filter (Millipore) (3 rounds at 14,000 rpm at 4 $^\circ\text{C}$ for 60 min).

3.5.3 Cell culture and cellular imaging of CyNE790-anti-EGFR in SCC-15 and MCF-7 cells

SCC-15 and MCF-7 cell lines were grown as above described. Both cell lines were cultured in 96-well plates at 85-90% confluence and incubated with **CyNE790-anti-EGFR** for 1 h at r.t (1:50 dilution of a 1 $\mu\text{g}/\mu\text{L}$ antibody solution in PBS). After incubation, cells were washed with media (\times 3) and images were taken (10 \times magnification) using an Eclipse Ti-U Nikon microscope (filter cube: 750/800)

attached to Ti: sapphire oscillator that operated in continuous wave mode (750 nm, 120 mW), and a NIR-enhanced CCD camera (Andor Technology).

3.5.4 *In vivo* imaging

CyNE790-labelled and ICG-labelled anti-EGFR-comparative visualization:

Balb/c nude mice obtained from the Biological Resource Centre (Biomedical Sciences Institutes) were anesthetized by intraperitoneal injection of ketamine (150 mg/kg)/xylazine (10 mg/kg) at the age of 8 weeks. **CyNE790**-labelled and **ICG**-labelled anti-EGFR antibodies (0.15 µg or 0.85 µg in PBS for both antibodies) were injected subcutaneously in the right and left rear flanks of the mice in a volume of 150 µL for each side. The animals were placed in an IVIS Spectrum imaging system (Caliper Life Sciences) immediately after antibody injection, and the fluorescence image was acquired using the 745 nm excitation and 820 nm emission filters.

***In vivo* detection of SCC-15 cells using CyNE790-anti-EGFR:**

SCC-15 and MCF-7 cell lines were grown using RPMI media supplemented with 10% fetal bovine serum (FBS), 2 mM L-glutamine, and antibiotics (100 U/mL penicillin/ 100 µg/mL streptomycin mixture) in a humidified atmosphere at 37 °C with 5% CO₂. Every cell line cultured in one 10-cm dish at 50% confluency was incubated with 15µg **CyNE790**-labelled anti-EGFR-IgG_{2a} for 1 h at r.t. After incubation, cells were washed with media and PBS (× 2), scrapped and resuspended in 150 µL PBS. **CyNE790**-anti-EGFR treated SCC-15 and MCF-7 cells were injected subcutaneously in the left rear flank of two separate mice (injection volume: 150 µL). The animals were placed in an IVIS Spectrum imaging system (Caliper Life Sciences), and the fluorescence images were acquired using 745 nm excitation and 820 nm emission filters after 15 min from the injection. All animal experiment procedures were performed in accordance with a protocol approved by the Institutional Animal Care and Use Committee.

Xenograft preparation:

The dye solutions were injected into the tail vein of the mice in a volume of 150 μ l. Immediately (1 hr) after the injection, the animals were placed in an IVIS Spectrum imaging system (Caliper Life Sciences), and the fluorescence image was acquired using the 745 nm excitation and 820 nm emission filters. More images were obtained after 4 hr, 24 hr and 48 hr post injection.

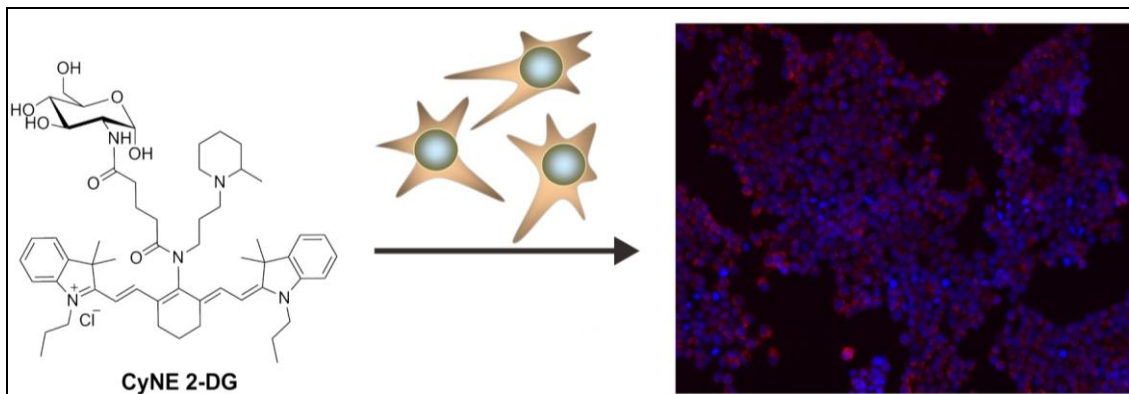
3.6 References

1. J. H. Flanagan Jr., S. H. Khan, S. Menchen, S. A. Soper, R. P. Hammer, *Bioconjugate Chem.* **1997**, *8*, 751.
2. J. V. Frangioni, *Curr. Opin. Chem. Biol.* **2003**, *7*, 626.
3. V. Ntziachristos, C. H. Tung, C. Bremer, R. Weissleder, *Nat. Med.* **2002**, *8*, 757.
4. B. Tang, L. J. Cui, K. H. Xu, L. L. Tong, G. W. Yang, L. G. An, *ChemBioChem* **2008**, *9*, 1159.
5. I. Hilger, Y. Leistner, A. Berndt, C. Fritsche, K. M. Haas, H. Kosmehl, W. A. Kaiser, *Eur. Radiol.* **2004**, *14*, 1124.
6. H. Lee, C. Mason, S. Achilefu, *J. Org. Chem.* **2006**, *71*, 7862.
7. H. Lee, C. Mason, S. Achilefu, *J. Org. Chem.* **2008**, *73*, 723.
8. A. Samanta, M. Vendrell, R. Das, Y. T. Chang, *Chem. Commun.* **2010**, *46*, 7406.
9. C. Encinas, S. Miltsov, E. Otazo, L. Rivera, M. Puyol, J. Alonso, *Dyes Pigm.* **2006**, *71*, 28.
10. L. Streckowski, J. C. Mason, J. E. Britton, H. Lee, K. V. Aken, G. Patonay, *Dyes Pigm.* **2000**, *46*, 163.
11. S. G. Sakka, *Curr. Opin. Crit. Care* **2007**, *13*, 207.
12. V. L. Dzurinko, A. S. Gurwood, J. R. Price, *Optometry* **2004**, *75*, 743.
13. M. Tadatsu, S. Ito, N. Muguruma, Y. Kakehashi, S. Hayashi, S. Okamura, H. Shibata, T. Okahisa, M. Kanamori, S. Shibamura, K. Takesako, M. Nozawa, K. Ishida, M. Shiga, *Bioorg. Med. Chem. Lett.* **1995**, *5*, 2689.
14. M. Ogawa, N. Kosaka, P. L. Choyke, H. Kobayashi, *Cancer Res.* **2009**, *69*, 1268.
15. J. O. Escobedo, O. Rusin, S. Lim, R. M. Strongin, *Curr. Opin. Chem. Biol.* **2010**, *14*, 64.
16. K. J. Baker, *Proc. Soc. Exptl. Biol. Med.* **1966**, *122*, 957.
17. I. J. Fox, E. H. Wood, *Mayo Clin. Proc.* **1960**, *35*, 732.
18. M. L. J. Landsman, G. Kwant, G. A. Mook, G. Zijlstra, *J. Appl. Phys.* **1976**, *40*, 575.

19. a) K. Licha, B. Riefke, V. Ntziachristos, A. Becker, B. Chance, W. Semmler, *Photochem. Photobiol.* **2000**, 72, 392.; b) S. A. Soper, Q. L. Mattingly, *J. Am. Chem. Soc.* **1994**, 116, 3744.
20. D. W. Rusnak, K. J. Alligood, R. J. Mullin, G. M. Spehar, C. Arenas-Elliott, A. M. Martin, Y. Degenhardt, S. K. Rudolph, T. F. Haws Jr., B. L. Hudson-Curtis, T. M. Gilmer, *Cell Prolif.* **2007**, 40, 580.
21. K. Wang, K. Wang, W. Li, T. Huang, R. Li, D. Wang, B. Shen, X. Chen, *Acta Radiol.* **2009**, 50, 1092.

CHAPTER 4

SYNTHESIS AND CHARACTERIZATION OF A CELL PERMEABLE NIR FLUORSCENT DEOXYGLUCOSE ANALOGUE FOR CANCER CELL IMAGING



4.1 Introduction

In biomedical applications, optical imaging has become a powerful diagnostic tool to monitor biological functions non-invasively, either in cell-based assays or in living systems. Several studies demonstrated that fluorescent imaging allows the identification of cancer cells and even the state of tumors *in vivo*.¹ Among all the fluorophores, NIR-absorbing molecules have some significant advantages, hence considerable efforts have been driven toward the synthesis of NIR probes to monitor the cellular mechanism at a molecular level.

To date, optical imaging has been highly focused on the basis of glucose analogues as glucose is one of the major metabolites in living systems. In 1983, Chiro et al. employed positron emission tomography (PET) using ¹⁸F-2-deoxyglucose to study the metabolic of the brain stem and spinal cord.² ¹⁸F-2-deoxyglucose has been also applied as a PET imaging probe for gynecologic cancers,³ and [¹⁴C] 2-deoxyglucose has been reported in the selective uptake by neurons and astrocytes by high-resolution micro auto radiographic imaging.⁴ Thus, the applicability of glucose analogues for different imaging modalities has been well reported. In recent years, the diagnosis of mammalian cancer cells has been highly focused on the basis of glucose analogues as cancer cells uptake more glucose to grow the cells than the normal cells. Malignant cancer cells can be discriminated rate when compared to normal cells due to their increased glycolysis, their over expression of glucose transporters (GLUTs), and the higher activity of hexokinases.^{5,6} These differences in metabolism have been applied to the identification of cancer cells by optical imaging methods that rely on the preparation of reporter-containing glucose analogues. A number of fluorescent glucose derivatives have been reported. 2-[*N*-(7-nitrobenz-2-oxa-1,3-dioxol-4-yl)amino]-2-deoxyglucose (2-NBDG),⁷ the first fluorescent probe to monitor glucose uptake through GLUTs, has been widely used in cancer imaging.⁸ Limitations on the photophysical properties of 2-NBDG (e.g. low brightness) led to the preparation of

glucose analogues with improved fluorescent properties by conjugation to Cy3, rhodamine or two-photon dyes.⁹⁻¹¹ NIR probes have recently applied to the preparation of fluorescent glucose analogues.¹²⁻¹⁶ NIR glucose derivatives have been prepared by conjugation of 2-deoxyglucose to penta- or heptamethine cyanine dyes (i.e. Cy5.5 and IRDye 800CW respectively). Cy5.5 2-DG proved to be trapped by tumor cells, but its uptake is not blocked by D-glucose, questioning its delivery through GLUTs.¹² On the other hand, IRDye 800CW 2-DG is uptaken in cancer cells and specifically blocked by excess of D-glucose,¹⁵ but the highly negatively charged chemical structure may hamper its application in cell imaging due to low cell membrane permeability.

4.2 Objectives

I prepared a NIR 2-deoxyglucose derivative (**CyNE 2-DG**) based on an amine acetylated tricarbocyanine structure. **CyNE 2-DG** showed preferential uptake in cancer cells and competition with excess D-glucose and its suitable cell permeability asserts the potential for cancer cell imaging in the NIR region.

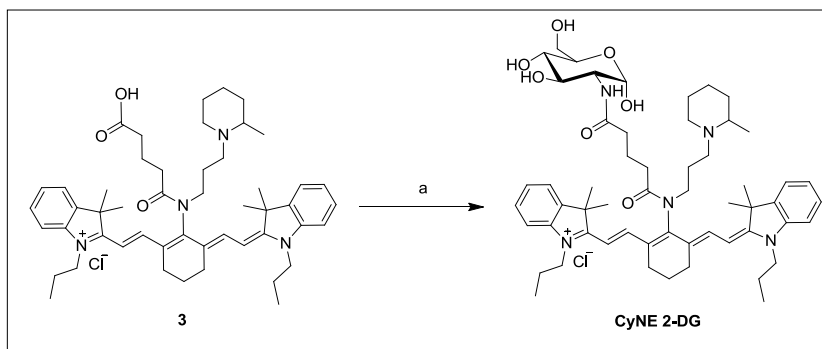
4.3 Results and discussion

4.3.1 Design and synthesis

I have discussed in Chapter 2 about the development of an amine acetylated tricarbocyanine scaffold (**CyNA**) with excellent photophysical properties, low aggregation in aqueous media and fluorescence emission in the NIR region.¹⁷ **CyNA** dyes have been also adapted for bioconjugation purposes after incorporation of a glutaric acid linker (**1**, Scheme 3.1 in Chapter 3) that maintains the spectral and photostability properties while enables the conjugation to macromolecules such as antibodies.¹⁸ The chemical structure of **3** is positively charged while many NIR fluorescent cyanine labeling dyes are highly negatively charged molecules. The minimization or absence of charges is particularly important when labeling small

molecules since neutral conjugates may exhibit greater permeability properties.¹⁹ Thus, **CyNE 2-DG** was prepared by coupling 2-deoxyglucosamine to the tricyanocyanine carboxylic acid **3** using HATU as the coupling reagent (Scheme 4.1).

Scheme 4.1. Synthesis of **CyNE 2-DG**.



Reagents and conditions: a) 2-D-deoxyglucosamine, HATU, DIEA, DMF_{anh}, r.t., 30 min.

I envisaged that the conjugation of 2-deoxyglucose, a fluorescent glucose analogue (**CyNE 2-DG**) exhibited similar spectral properties to **3** with absorption and emission maxima around 790 and 815 nm respectively (Figure 4.1).

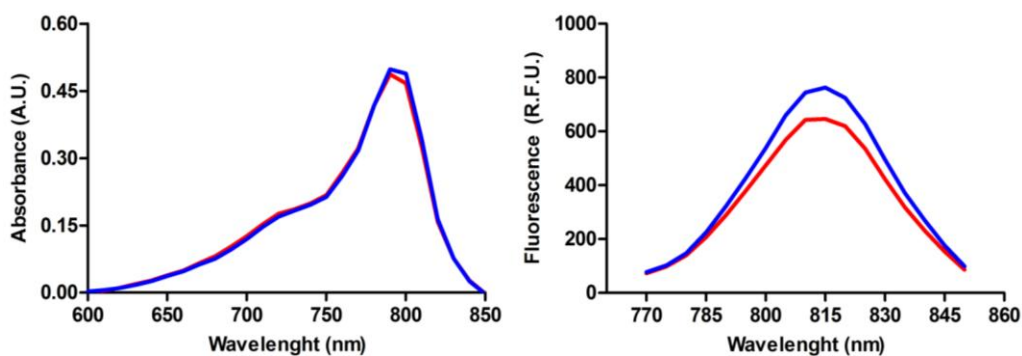


Figure 4.1. Absorbance and fluorescence spectra of **3** (blue) and **CyNE 2-DG** (red) in phosphate buffer saline (PBS, pH 7.3) containing 1% DMSO. Excitation wavelength: 740 nm.

4.3.2 Cellular uptake and competition assay

In order to compare the uptake of **CyNE 2-DG** in different cells, serum-starved cultures of breast cancer MCF7 and MDA-MB-231 cell lines and non-tumor human foreskin fibroblasts (HFF) were incubated at 37 °C for 20 min with 20 μ M

CyNE 2-DG, and analyzed by fluorescence microscopy. Mean NIR fluorescence intensity values of the different cell lines indicated that **CyNE 2-DG** was preferentially uptaken in tumor cells when compared to fibroblasts (Figure 4.2). This observation corresponds to the higher glycolysis rate of cancer cells than normal cells.¹⁴

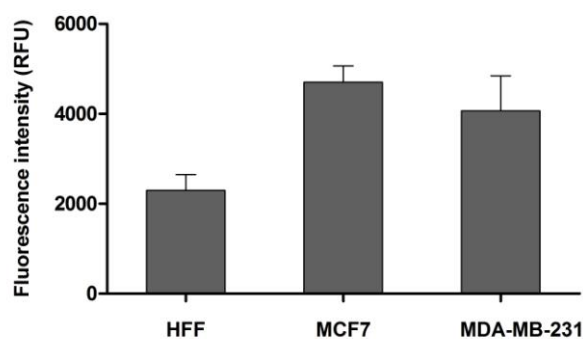


Figure 4.2. NIR fluorescence intensities in human tumor cell lines and fibroblasts upon incubation with 20 μ M **CyNE 2-DG**. Mean intensity values are plotted as average fluorescence intensities from 5 to 10 different regions and error bars as standard deviations.

Further experiments were aimed at determining whether the uptake of **CyNE 2-DG** was mediated by GLUTs. We (I and Dr. Marc Vendrell) performed competition experiments with increasing concentrations of D-glucose in MCF7 and MDA-MB-231 cells.^{20,21} As shown in Figure 4.3, the uptake of **CyNE 2-DG** was significantly reduced upon competition with D-glucose, indicating that **CyNE 2-DG** enters the cell through GLUTs. We (I and Dr. Marc Vendrell) confirmed that the uptake of **CyNE 2-DG** in MCF7 and MDA-MB-231 cells was not affected by competition with L-glucose (Figure 4.4) demonstrating the stereoselective interaction with GLUT transporters.

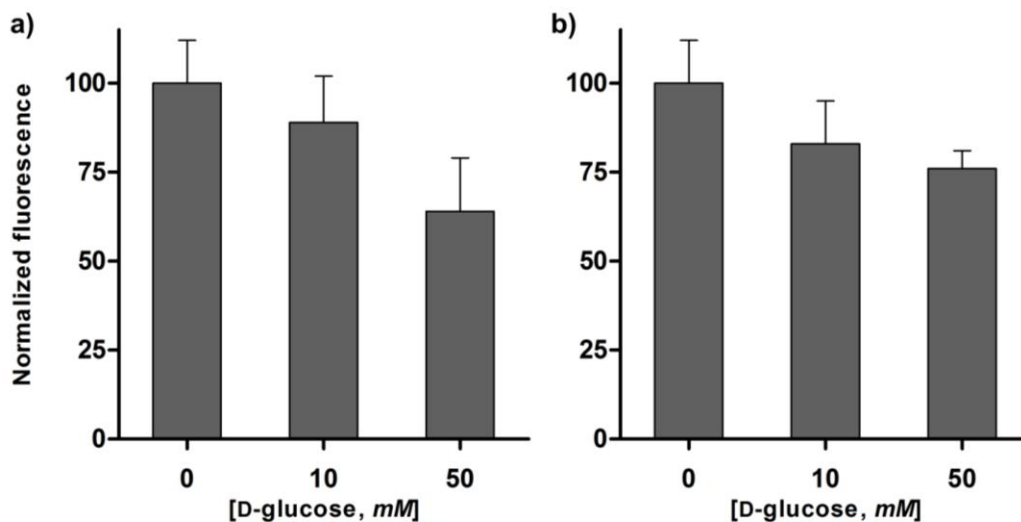


Figure 4.3. Dose-dependent inhibition of the CyNE 2-DG uptake after competition with D-glucose in: a) MCF7 and b) MDA-MB-231 cells. Fluorescence intensity values from 5 to 10 different regions were averaged and referred to the fluorescence intensity measured in cells with no glucose competition. Error bars correspond to standard deviations.

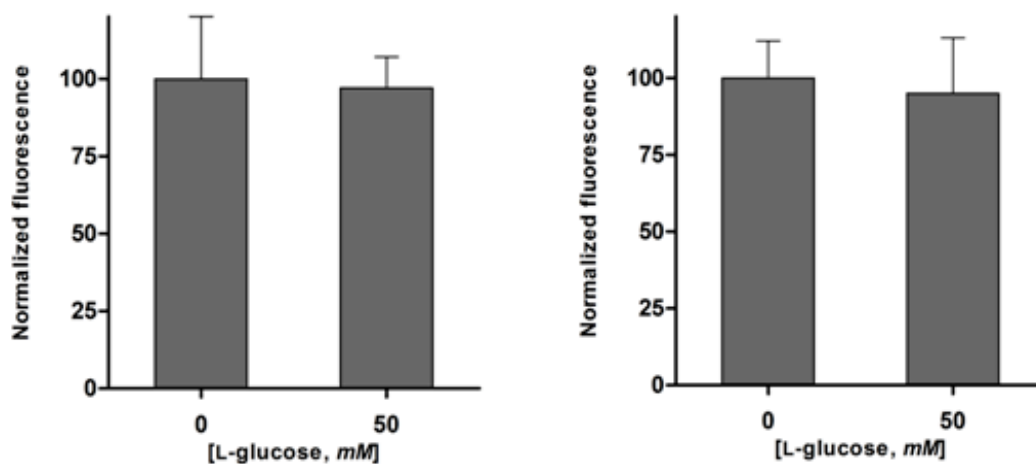


Figure 4.4. CyNE 2-DG uptake after competition with L-glucose in MCF7 (*left*) and MDA-MB-231 (*right*) cells. Fluorescence intensity values from 5 to 10 different regions were averaged and referred to the fluorescence intensity measured in cells with no glucose competition. Error bars correspond to standard deviations.

The uptake of CyNE 2-DG at different concentrations (10, 20 and 50 μM) was evaluated in MCF7 cells (Figures 4.5). We chose 20 μM as the optimum concentration since it showed a reasonable cell staining and a higher cell viability than 50 μM . I performed toxicity assays of CyNE 2-DG in MCF7 cells (Figure 4.6),

which indicated the incubation of **CyNE 2-DG** (20 μM) maintains a cell viability higher than 90% even after incubating the dye for 2 h.

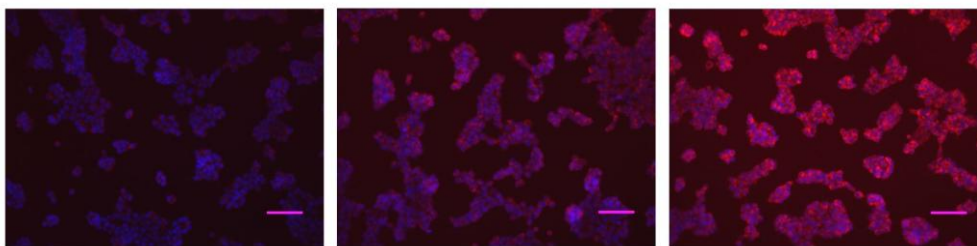


Figure 4.5. Fluorescence images of MCF7 cells upon incubation with **CyNE 2-DG** (*left*: 10 μM , *center*: 20 μM , *right*: 50 μM) at 37 $^{\circ}\text{C}$ for 20 min followed by nuclear staining with Hoechst. Fluorescence images were taken under the same acquisition conditions. NIR fluorescence is shown in red color and Hoechst staining in blue color. Scale bar: 100 μm .

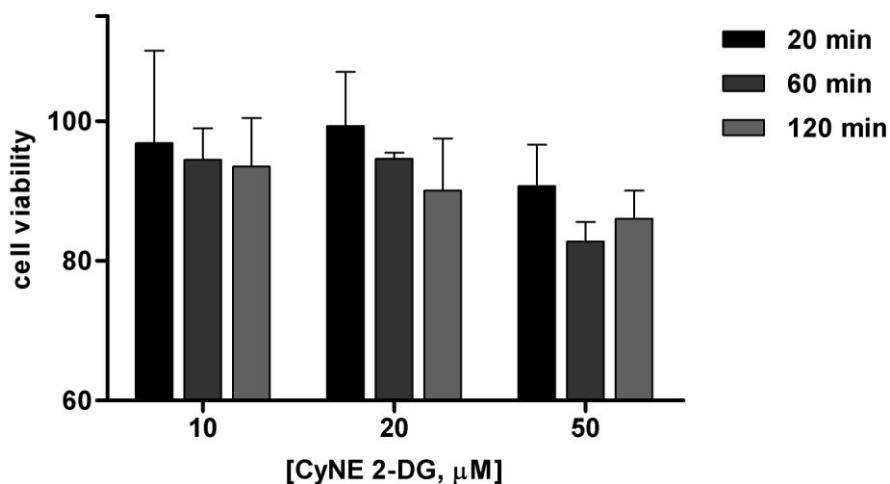


Figure 4.6. Cell viability of **CyNE 2-DG** at different concentrations and incubation times in MCF7 cells. Values are referred to untreated cells (100% viability) and plotted as average from 3 replicates with error bars as standard deviations.

Furthermore, I corroborated the role of 2-deoxyglucose in the cellular uptake by determining higher intracellular fluorescence intensities upon incubation with **CyNE 2-DG** when compared to the carboxylic acid **3** (Figure 4.7).

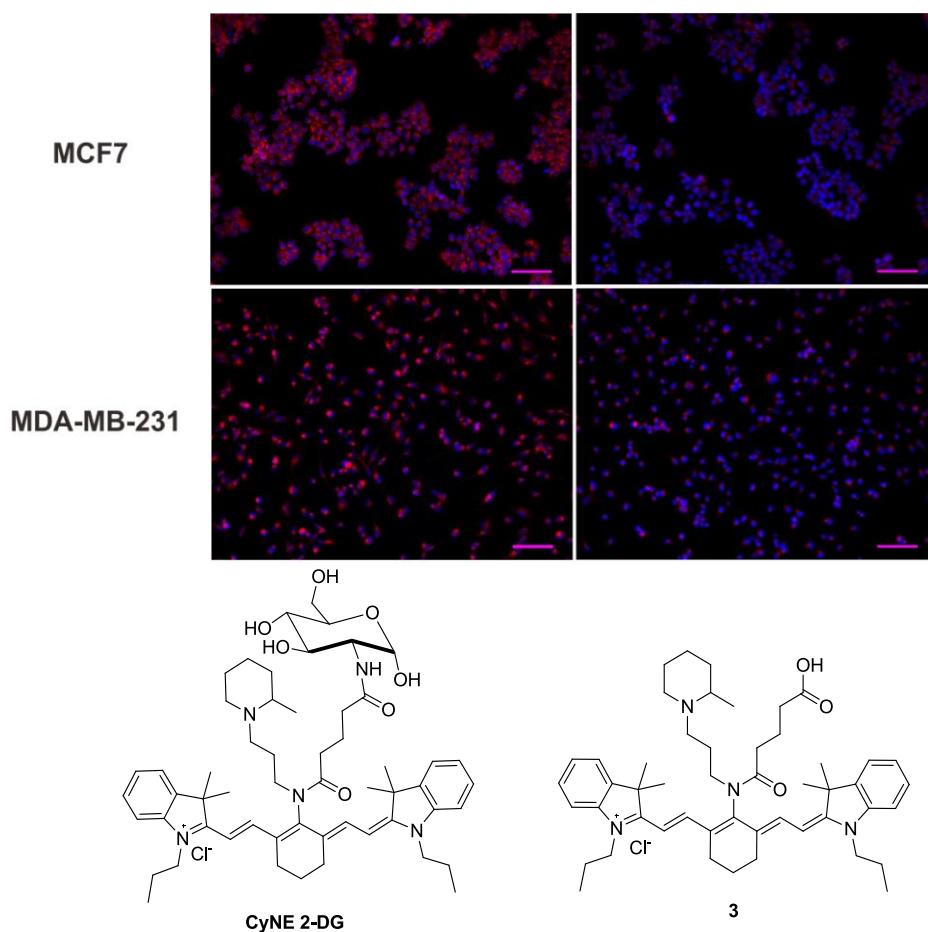


Figure 4.7. Fluorescence images of MCF7 and MDA-MB-231 cells upon incubation with **CyNE 2-DG** or **3**. Cells were incubated with 20 μM **CyNE 2-DG** or **1** at 37°C for 20 min followed by nuclear staining with Hoechst, and fluorescence images were taken under the same acquisition conditions. NIR fluorescence is shown in red color and Hoechst staining in blue color. Scale bar: 100 μm .

Altogether these results suggested that the uptake of **CyNE 2-DG** in tumor cell lines is specifically regulated by GLUTs rather than by passive penetration. I selected 20 min of incubation time as it has been previously reported with other fluorescent glucose probes.^{7,10} While **3** is slightly more fluorescent than **CyNE 2-DG**, both compounds showed a similar range of intensities in their fluorescence spectra, hence the differences observed in cell imaging (Figure 4.7) are basically due to their different uptake in MCF7 cells, proving that the glucose moiety enhances the cell uptake of the fluorophore through GLUTs in cancer cells.

4.3.3 Comparative cell permeability study with IRDye 800CW 2-DG

After validating **CyNE 2-DG** as a NIR fluorescent glucose analogue, I compared its application for cell imaging studies to **IRDye 800CW 2-DG**, a tumor targeting NIR fluorescent agent that is uptaken by cancer cells through GLUT family proteins.¹⁵ **CyNE 2-DG** and **IRDye 800CW 2-DG** have similar fluorescence emission maxima (around 794 nm for **IRDye 800CW 2-DG**, 815 nm for **CyNE 2-DG**), but the negatively charged structure of **IRDye 800CW 2-DG** entails a lower permeability that can hinder its application in cell imaging experiments. We (I and Dr. Marc Vendrell) compared the NIR fluorescence images of MCF7 cells upon incubation with **CyNE 2-DG** and **IRDye 800CW 2-DG** (both at 20 μ M) at 37°C for 20 min. Images taken under the same acquisition conditions proved that the cytoplasmatic fluorescence intensities of the cells incubated with **CyNE 2-DG** were significantly higher than those treated with **IRDye 800CW 2-DG** (Figure 4.8). These results demonstrated the superior uptake of **CyNE 2-DG** in cancer cells and validated the good cell permeability properties of **CyNE 2-DG**.

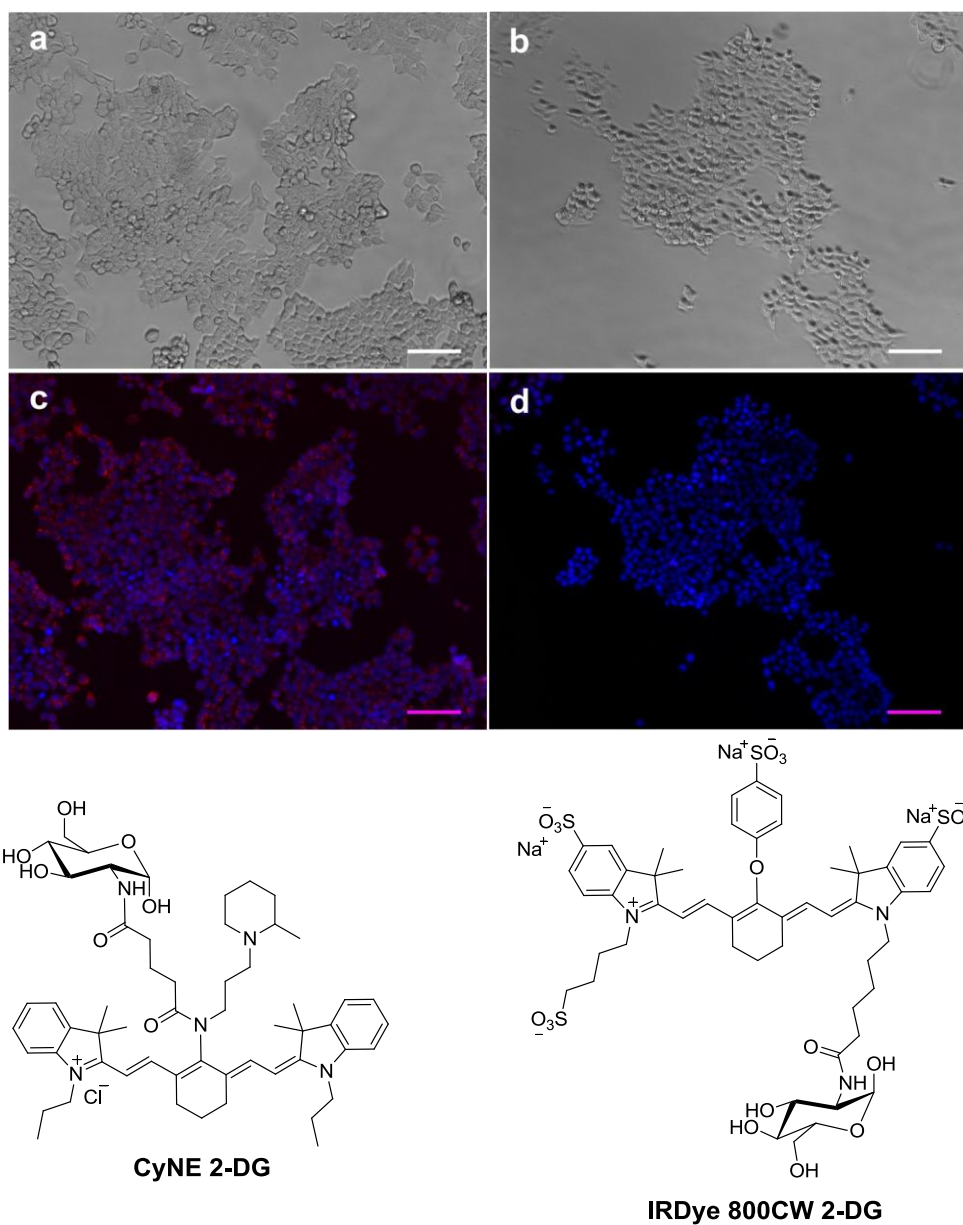


Figure 4.8. Brightfield and merged fluorescence images of MCF7 cells upon incubation with **CyNE 2-DG** (a and c) and **IRDye 800CW 2-DG** (b and d). Cells were incubated with 20 μM **CyNE 2-DG** or **IRDye 800CW 2-DG** at 37 $^{\circ}\text{C}$ for 20 min followed by nuclear staining with Hoechst, and fluorescence images were taken under the same acquisition conditions. NIR fluorescence is shown in red color and Hoechst staining in blue color. Scale bar: 100 μm .

In addition to that, we (I and Dr. Marc Vendrell) examined the cell retention of **CyNE 2-DG** in MCF7 cells. As shown in Figure 4.9, **CyNE 2-DG** was still detectable inside the cells after 3 h of the treatment. While these results are still

preliminary, they indicate that **CyNE 2-DG** may be phosphorylated by the hexokinases and retained inside the cells.

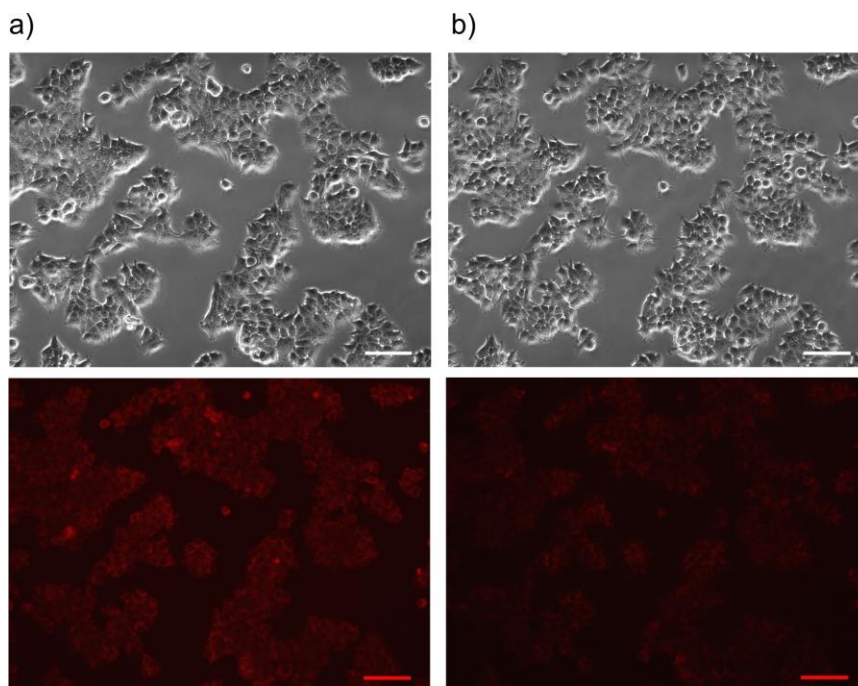


Figure 4.9. Retention analysis of **CyNE 2-DG** in MCF7 cells upon incubation with 20 μM **CyNE 2-DG** at 37°C for 20 min. Brightfield and fluorescence images were taken under the same acquisition conditions just after treatment (a) and 3 h after treatment with **CyNE 2-DG** (b). Scale bar: 100 μm .

4.4 Conclusions

In conclusion, I synthesized and characterized **CyNE 2-DG** as a novel NIR fluorescent glucose derivative. **CyNE 2-DG** showed a higher uptake in cancer cell lines than in human primary fibroblasts, and its competition with unlabeled D-glucose implied that its uptake into the cells may be mediated by GLUTs. **CyNE 2-DG** exhibited a brighter staining of cancer cells when compared to the commercially available **IRDye 800CW 2-DG**, which suggests its good cell permeability properties and its applicability to cancer cell imaging in the NIR region.

4.5 Experimental details

Materials and Methods:

IRDye 800CW-OSu was purchased from LI-COR Biosciences. Fluorescence microscopy experiments were performed in a Nikon Ti microscope attached to a Cool LED (740 nm) excitation source in Singapore Bioimaging Consortium, Agency for Science, Technology and Research (A*STAR), Singapore, and images were processed using the software NIS-Elements 3.10. Cell viability assays were performed using a CellTiter 96® Aqueous Non-Radioactive Cell Proliferation Assay (MTS) (Promega) following the manufacturer's instructions.

4.5.1 Synthesis of CyNE 2-DG and IRDye 800CW 2-DG

CyNE 2-DG:

3 (as described in earlier Chapter 3) and HATU (25 mg, 0.07 mmol) were dissolved in 5 mL of anhydrous DMF under N₂ atmosphere and stirred at r.t. for 10 min. 2-D-deoxyglucosamine•HCl (15 mg, 0.07 mmol) was treated with DIEA (14 µL, 0.10 mmol) and added to the reaction mixture. The reaction was stirred for another 2 h at r.t., then the solvent was evaporated under reduced pressure and the resulting green solid was purified by normal-phase column chromatography (elution with DCM-MeOH (9:1)) to obtain **CyNE 2-DG** as a green solid (41 mg, yield 68%).

IRDye 800CW 2-DG:

2-amino-2-deoxy-D-glucose hydrochloride (Glucosamine hydrogen chloride) 50 equivalents were solubilized in 20 mM Sodium bicarbonate buffer (pH 8.3) at ambient temperature¹⁵. Then, aqueous solution of **IRDye 800CW NHS** ester (1 equivalent, 5 mg) was added to the reaction mixture and stirred it for 2h at room temperature. The dye conjugate was purified by HPLC, monitored at 780 nm, using diode array detector. The column (150-mm, Luna C18 column) was equilibrated and eluted at 2 mL/min using a gradient with 5% acetonitrile: 100% Acetonitrile within 23 min. Sample was dried overnight under vacuum, with light protection.

tR: 7.94 min (RP-HPLC gradient from 5 to 100% B in 23 min)

ESI (HRMS) calc. for $C_{52}H_{63}N_3O_{19}S_4^{-3}$: 1161.3101, found ($z=2$): 580.6488.

Characterization of CyNE 2-DG:

NMR characterization of 2-D-deoxyglucosamine•HCl and CyNE 2-DG

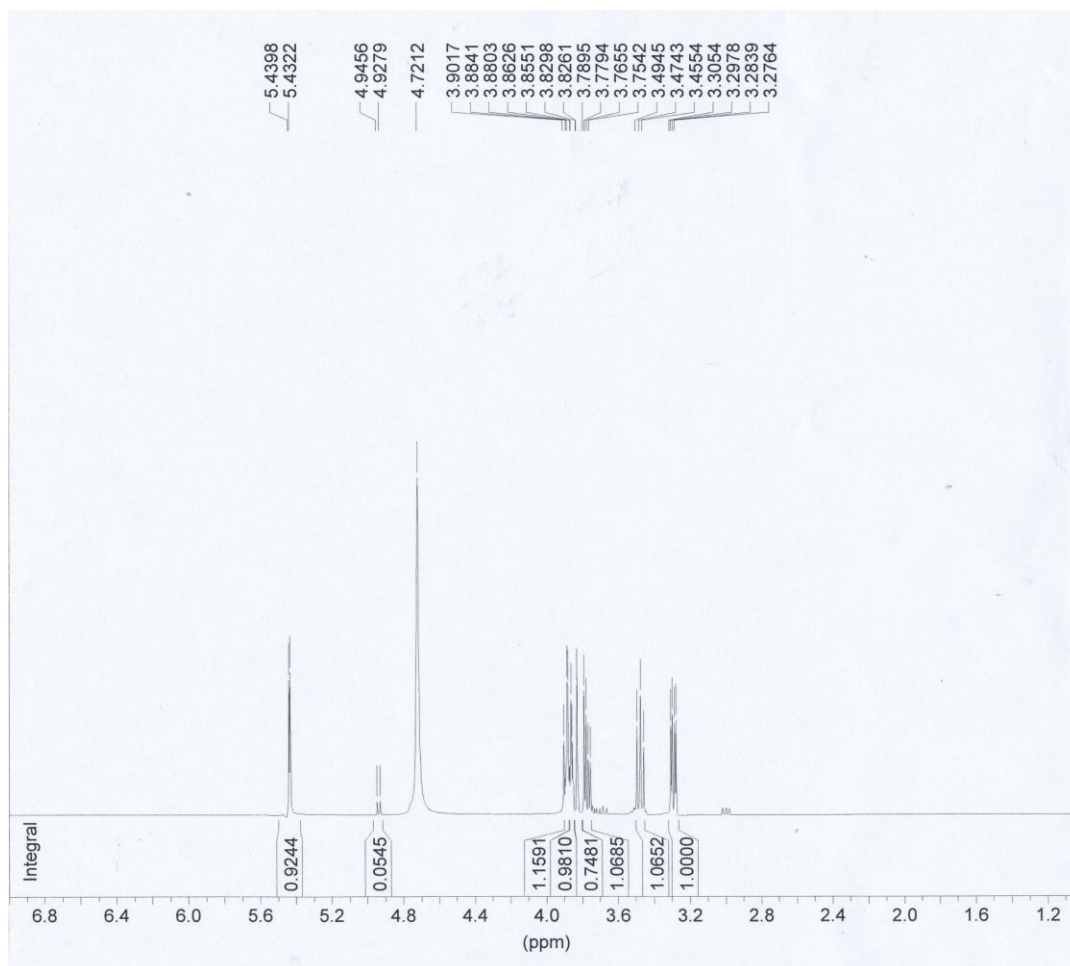


Figure 4.10. $^1\text{H-NMR}$ spectrum of 2-D-deoxyglucosamine•HCl in D_2O :

$\delta = 3.27$ (dd, 1H, $J_1 = 11$ Hz, $J_2 = 3.5$ Hz), 3.47 (t, $J = 9.5$ Hz), 3.75 - 3.78 (m, 1H), 3.82 - 3.90 (m, 3H), 4.94 (d, 0.05H_β , $J = 8.8$ Hz), 5.43 (d, 0.93H_α , $J = 3.5$ Hz).

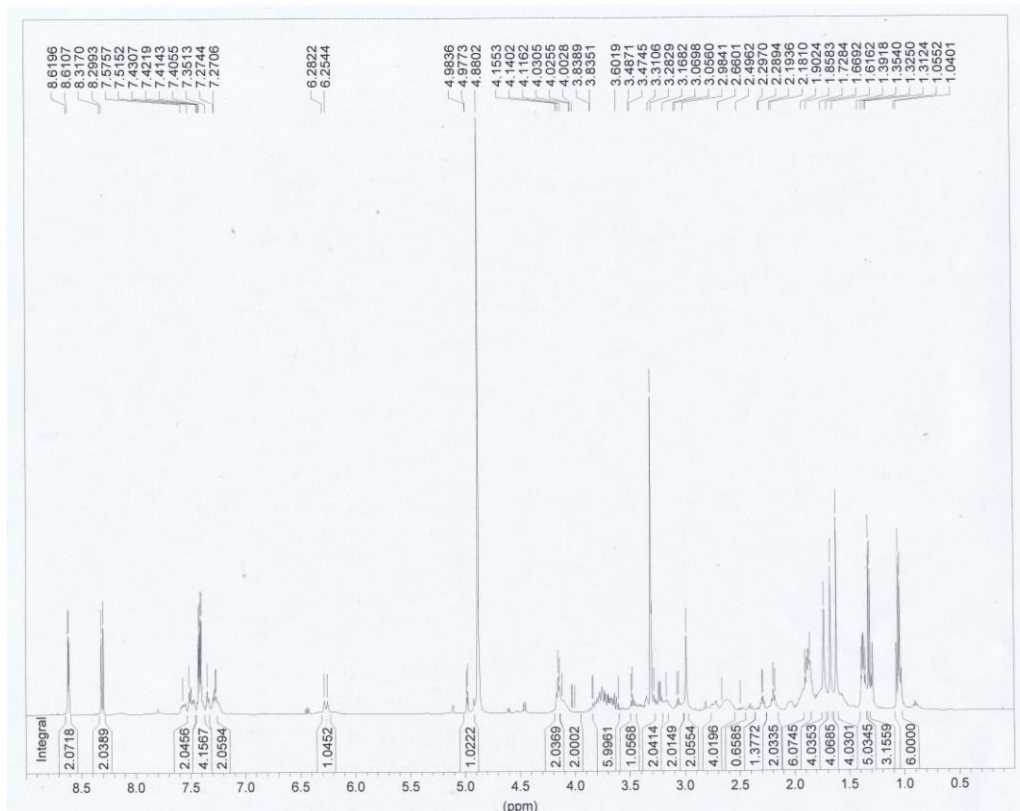


Figure 4.11. $^1\text{H-NMR}$ spectrum of **CyNE 2-DG** in MeOD: 1.04 (t, 6H, $J = 7.5\text{Hz}$), 1.32 (d, 3H, $J = 6.6\text{ Hz}$), 1.35-1.39 (m, 5H), 1.61 (s, 4H), 1.66 (s, 4H), 1.72 (s, 4H), 1.83-1.90 (m, 6H), 2.18 (t, 2H, $J = 8.0\text{ Hz}$), 2.28-2.39 (m, 2H), 2.52-2.62 (m, 4H), 2.98 (t, 2H, $J = 5.4\text{ Hz}$), 3.05 (t, 2H, $J = 5.4\text{ Hz}$), 3.06-3.26 (m, 4H), 3.47 (t, 4H), 3.60-3.83 (m, 6H), 4.06 (m, 2H), 4.15 (t, 2H, $J = 7.5\text{ Hz}$), 4.97 (d, 1H, $J = 3.2\text{ Hz}$), 6.25 (d, 1H, $J = 14.1\text{ Hz}$), 7.24-7.58 (m, aromatic 8H), 8.29 (d, 2H, $J = 10.5\text{ Hz}$), 8.61 (d, 2H, $J = 3.5\text{ Hz}$). tR: 6.15 min; ESI (HRMS) calc. for $\text{C}_{56}\text{H}_{80}\text{N}_5\text{O}_7^+$: 934.6052, found: 934.6070.

4.5.3 Cell culture and cellular imaging

MCF7 and MDA-MB-231 cells were purchased from American Type Culture Collection (ATCC) and maintained in DMEM containing 10% fetal bovine serum (FBS). Serum-starved cultures of different cell lines were incubated at $37\text{ }^\circ\text{C}$ for 20 min with $20\text{ }\mu\text{M}$ dyes (**CyNE 2-DG** or **IRDye 800CW 2-DG**) in low-glucose DMEM media, washed with PBS ($\times 1$) and treated with Hoechst for nuclear staining ($37\text{ }^\circ\text{C}$,

10 min). For competition experiments with D-glucose and L-glucose, cells were incubated at 37 °C for 3 h with low-glucose DMEM containing 0, 10 or 50 mM glucose. **CyNE 2-DG** was then added incubated at 37 °C for 20 min, washed with PBS (×1) and treated with Hoechst for nuclear staining (37 °C, 10 min). Cell images were taken in a Nikon Ti microscope at 10× magnification with 360±20/460±25 and 750/800 filter cubes for Hoechst and NIR fluorescence images respectively.

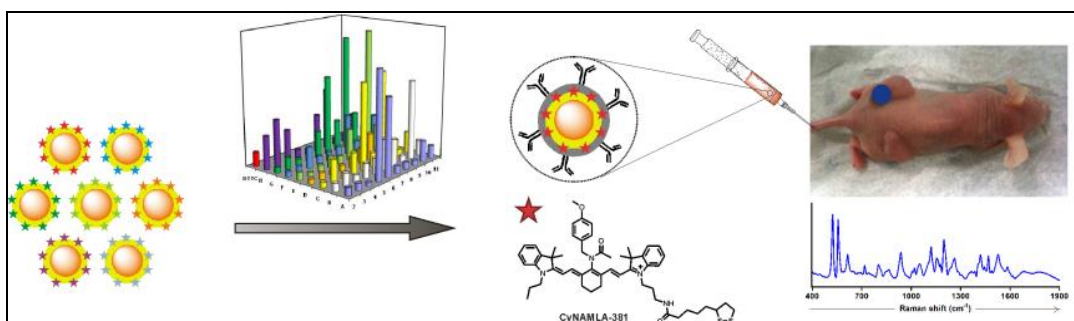
4.6 References

1. D. S. Miller, S. Letcher, D. M. Barnes, *Am. J. Physiol.* **1996**, *271*, F508.
2. G. Di Chiro, E. Oldfield, D. Bairamian, N. J. Patronas, R. A. Brooks, L. Mansi, B. H. Smith, P. L. Kornblith, R. Margolin, *J. Comput. Assist. Tomogr.* **1983**, *7*, 937.
3. J. N. Talbot, D. Grahek, K. Kerrou, N. Younsi, V. de Beco, C. Colombet-Lamau, Y. Petegnief, N. Cailleux, F. Montravers, *Gynecol. Obstet. Fertil.* **2001**, *29*, 775.
4. A. Nehlig, E. Wittendorp-Rechenmann, C. D. Lam, *J. Cereb. Blood. Flow. Metab.* **2004**, *24*, 1004.
5. (a) O. Warburg, *Science* **1956**, *125*, 309. (b) R. A. Medina, G. I. Owen, *Biol. Res.* **2002**, *35*, 9.
6. M. Zhang, Z. H. Zhang, D. Blessington, H. Li, T. M. Busch, V. Madrak, J. Miles, B. Chance, J. D. Glickson, G. Zheng, *Bioconjugate Chem.* **2003**, *14*, 709.
7. (a) T. Yamamoto, S. Tanaka, S. Suga, S. Watanabe, K. Nagatomo, A. Sasaki, Y. Nishiuchi, T. Teshima, K. Yamada, *Bioorg. Med. Chem. Lett.* **2011**, *21*, 4088.; (b) S. R. Millon, J. H. Ostrander, J. Q. Brown, A. Raheja, V. L. Seewaldt, N. Ramanujam, *Breast Cancer Res. Treat.* **2011**, *126*, 55.; (c) R. G. O'Neil, L. Wu, N. Mullani, *Mol. Imaging Biol.* **2005**, *7*, 388.; (d) C. Zou, Y. Wang, Z. Shen, *J. Biochem. Biophys. Methods* **2005**, *64*, 207.; (e) K. Yoshioka, M. Saito, K. B. Oh, Y. Nemoto, H. Matsuoka, M. Natsume, H. Abe, *Biosci. Biotechnol. Biochem.* **1996**, *60*, 1899.
8. (a) K. Yoshioka, H. Takahashi, T. Homma, M. Saito, K. B. Oh, Y. Nemoto, H. Matsuoka, *Biochim. Biophys. Acta* **1996**, *1289*, 5.; (b) K. Yoshioka, M. Saito, K. B. Oh, Y. Nemoto, H. Matsuoka, M. Natsume, H. Abe. *Biosci. Biotechnol. Biochem.* **1996**, *60*, 1899.; (c) K. B. Oh, H. Matsuoka, *Int. J. Food Microbiol.* **2002**, *76*, 47.; (d) R. G. O'Neil, L. Wu, N. Mullani, *Mol. Imaging Biol.* **2005**, *7*, 388.

9. K. Glunde, C. A. Foss, T. Takagi, F. Wildes, Z. M. Bhujwalla, *Bioconjugate Chem.* **2005**, *16*, 843.
10. S. J. Park, H. Y. Lee, M.-H. Cho, S. B. Park, *Angew. Chem. Int. Ed.* **2007**, *46*, 2018.
11. Y. S. Tian, H. Y. Lee, C. S. Lim, J. Park, H. M. Kim, Y. N. Shin, E. S. Kim, H. J. Jeon, S. B. Park, B. R. Cho, *Angew. Chem. Int. Ed.* **2009**, *48*, 8027.
12. Z. Cheng, J. Levi, Z. M. Xiong, O. Gheysens, S. Keren, X. Y. Chen, S. S. Gambhir, *Bioconjugate Chem.* **2006**, *17*, 662.
13. Z. Zhang, H. Li, Q. Liu, L. Zhou, M. Zhang, Q. Luoc, J. Glickson, B. Chance, G. Zheng, *Biosens. Bioelectron.* **2004**, *20*, 643.
14. E. R. Trivedi, A. S. Harney, M. B. Olive, I. Podgorski, K. Moin, B. F. Sloane, A. G.M. Barrett, T. J. Meade, B. M. Hoffman, *Proc. Nat. Acad. Sci. U. S. A.* **2010**, *107*, 1284.
15. J. L. Kovar, W. Volcheck, E. Sevick-Muraca, M. A. Simpson, D. M. Olive, *Anal. Biochem.* **2009**, *384*, 254.
16. H. Zhou, K. Luby-Phelps, B. E. Mickey, A. A. Habib, R. P. Mason, D. Zhao, *PLoS One* **2009**, *4*, e8051.
17. A. Samanta, M. Vendrell, R. Das, Y. T. Chang, *Chem. Commun.* **2010**, *46*, 7406.
18. A. Samanta, M. Vendrell, S. W. Yun, Z. Guan, Q. H. Xu, Y. T. Chang, *Chem. Asian J.* **2011**, *6*, 1353.
19. (a) T. K. Nayak, M. K. Dennis, C. Ramesh, R. Burai, R. W. Atcher, L. A. Sklar, J. P. Norenberg, H. J. Hathaway, J. B. Arterburn, E. R. Prossnitz, *ACS Chem. Biol.* **2010**, *5*, 681. (b) G. Sahagun, S. A. Moore, M. N. Hart, *Am. J. Physiol.* **1990**, *259*, H162.
20. S. R. Millon, J. H. Ostrander, J. Q. Brown, A. Raheja, V. L. Seewaldt, N. Ramanujam, *Breast Cancer Res. Treat.* **2011**, *126*, 55.
21. K. Yamada, M. Nakata, N. Horimoto, M. Saito, H. Matsuoka, N. Inagaki, *J. Biol. Chem.* **2000**, *275*, 22278.

CHAPTER 5

ULTRASENSITIVE NIR RAMAN REPORTERS FOR SERS BASED IN VIVO CANCER DETECTION



5.1 Introduction

Raman spectroscopy measures the changes in vibrational frequency due to polarization of the molecules under the electric field of the incident photon. It represents a powerful technique to obtain molecular fingerprints in liquid or gas states, mainly regarding information on intermolecular interactions, molecular structures and inherent dynamics of the molecules. However, the signal to noise ratio in Raman spectroscopy is usually a bottleneck for highly sensitive detection. Surface Enhanced Raman Spectroscopy (SERS) has recently emerged as an advanced spectroscopic method in which the magnitude of the Raman cross sections are highly influenced when Raman active molecules are placed on the surface of roughened noble metal surface. Eventually, this technique has become an alternative in bioimaging to fluorescence-based spectroscopy, as it can minimize photobleaching, peak overlapping, and low signal to noise ratio in complex biological systems.¹⁻³ SERS probes are based on the 10^{14} - 10^{16} fold scattering enhancement through the electrostatic adsorption caused by the proximity of Raman-active signature molecules to the surface of metal nanoparticles (NPs),⁴⁻⁷ which can be modulated with molecular recognition motifs to render diagnostic tools for optical imaging and therapeutic studies.⁸⁻¹² SERS probes have great potential for multiple functions, from cellular studies to *in vivo* tumor recognition. Gold nanoparticles (AuNPs), which exhibit unique electromagnetic properties, have been widely employed to prepare nanotags as contrast agents for diagnostic imaging applications. Furthermore, AuNPs are particularly used for *in vivo* imaging applications due to their low toxicity⁴ and reactive roughen surface. Although AuNP-based Raman reporters provide a robust platform, the preparation of ultrasensitive SERS probes is hampered by the limited availability, sensitivity and reproducibility of Raman intensity. Most of the commonly used Raman signature molecules are active in the UV-visible range (e.g. crystal violet, malachite green isothiocyanate, rhodamine-6G, Nile blue, 2-naphthalenethiol, DRITC and DXRITC), and thus have a restricted potential for *in vivo* imaging.¹³⁻¹⁶

This drawback is particularly important at the NIR region, where the availability of reporters is restricted to a few Raman-active molecules. The adequacy of the NIR region for *in vivo* studies has raised the interest in NIR SERRS (Surface Enhanced Resonance Raman Spectroscopy)-active molecules. NIR light can penetrate much deeper into tissue and pass through the skin compared to visible light, and enables the assessment of molecular and physiological events in tissue samples. In addition, many macromolecules, intrinsic tissue or organelles have low light absorption, less autofluorescence, and low light scattering which often come across in visible light. To date the cyanine derivative **DTTC** has been regarded as a standard in NIR SERRS studies,⁹ but it shows only a moderate Raman intensity that limits the preparation of highly sensitive probes for *in vivo* applications.^{17,18}

5.2 Objectives

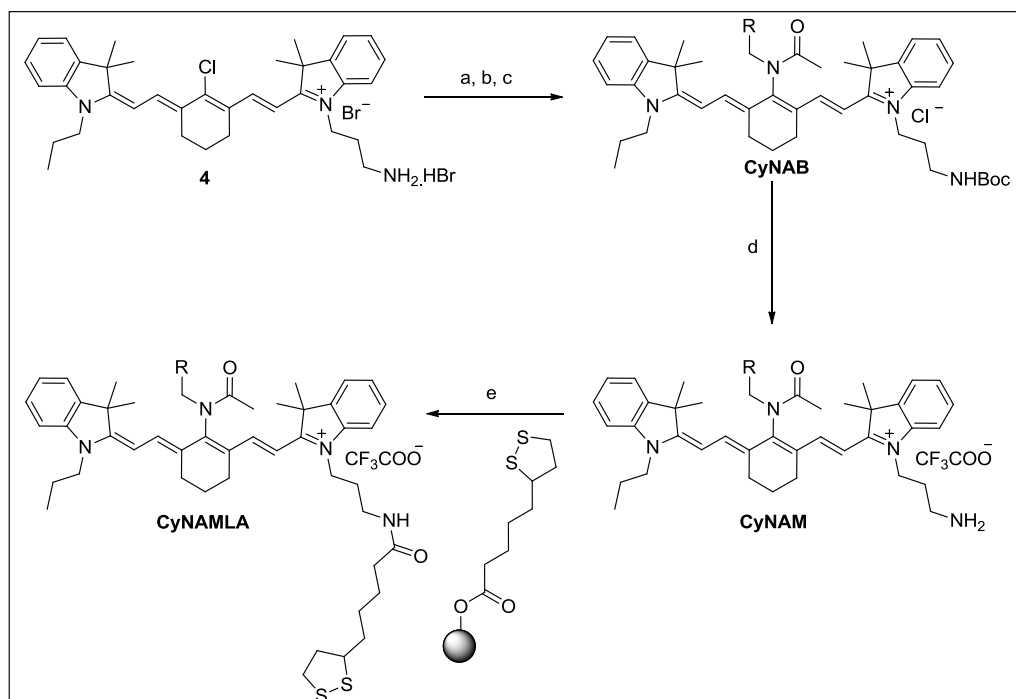
Since little is known about the correlation between the cyanine scaffold and its Raman intensity, I designed a library of structurally diverse tricarbocyanines with the aim to discover novel NIR SERRS-active compounds that surpassed the sensitivity of **DTTC**. Based on the several advantages of NIR Raman reporters and AuNPs, herein I report the first combinatorial approach to discover novel and highly sensitive NIR SERS reporters. The synthesis and screening of an 80-member tricarbocyanine library and chemisorbed on AuNPs led to the identification of **CyNAMLA-381** as an NIR SERS reporter with 12-fold higher sensitivity than the standard 3,3'-diethylthiatricarbocyanine (**DTTC**), and we (I. Dr. Kaustabh Kumar Maiti and Dr. Yun Seong Wook) validated its advantages for the construction of ultrasensitive *in vivo* SERS probes.

5.3 Result and discussion

5.3.1 Design and synthesis of library

The tricarbocyanine core is an accessible NIR structure whose central chlorine atom can be replaced with different nucleophiles.¹⁹ I designed the synthesis of tricarbocyanine derivatives by substitution with different amines, and acetylated the resulting alkyl- or benzyl amino groups to obtain compounds with NIR-absorption properties and good chemical stability in aqueous media (CyNA).²⁰ As in this structure does not have any linker for further modification, I designed a new amine linker on the side chain of tricarbocyanine scaffold by maintaining CyNA scaffold which is mainly responsible for good photophysical properties and diversity. The modification of CyNA scaffold to CyNAM has been successfully done according to Scheme 5.1.

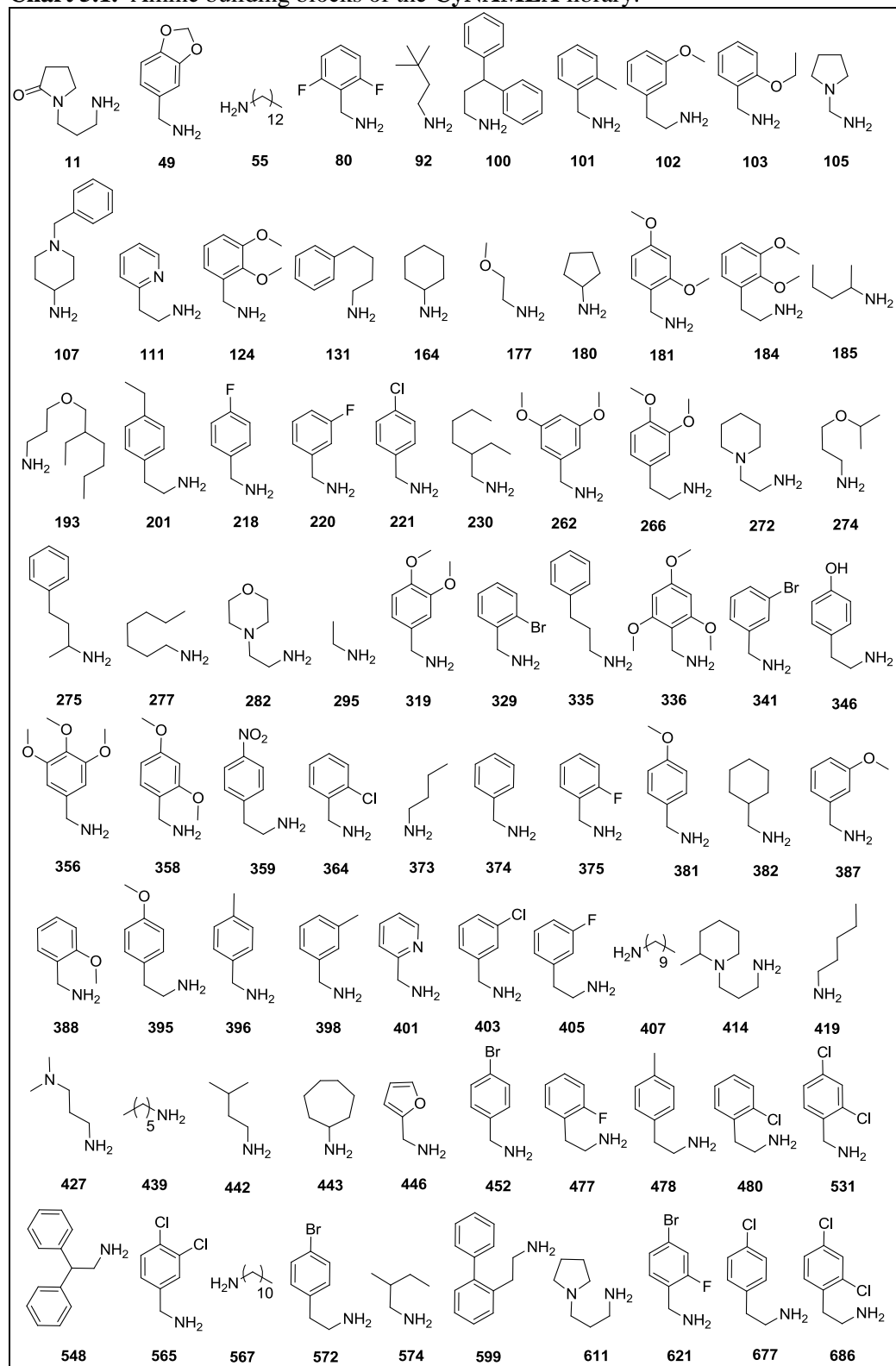
Scheme 5.1. Synthesis of lipoic acid-containing amine acetylated tricarbocyanines (CyNAMLA).



Reagents and conditions: a) Boc_2O , DIEA, CHCl_3 , 60 °C, 4-6 h; b) R-NH_2 , DIEA, CH_3CN , 60 °C, 20-90 min; c) CH_3COCl , DIEA, CH_2Cl_2 , 0 °C, 5-10 min; d) $\text{TFA-CH}_2\text{Cl}_2$ (1:9), r.t., 6 h; e) lipoic acid activated ester resin, $\text{CH}_2\text{Cl}_2:\text{CH}_3\text{CN}$ (9:1), r.t., 16 h.

The main concern in this synthetic route is the modification of central chlorine atom of **4** by amine nucleophiles, as the free amine in the side chain of tricyanopyridine may act as a nucleophile. However, I have successfully overcome the synthetic barricade by Boc (*tert*-butyl carbonate) protection of amine group on the side chain and modified the central chlorine atom by 80 different primary amines including heterocyclic, alkyl and aromatic from commercial source (Chart 5.1) in a combinatorial manner to make an intermediate **CyNAB** derivative. The **CyNAB** compounds were treated with an optimized TFA-DCM (1:9) solution that overcame the liability of the tricyanopyridine core in acidic conditions.²² In order to prepare compounds that could be chemisorbed on AuNPs,²¹ the final coupling of **CyNAM** to a lipoic acid activated ester resin yielded 80 derivatives (**CyNAMLA**).

Chart 5.1. Amine building blocks of the **CyNAMLA** library.



5.3.2 Characterization of CyNAMLA library

80-member CyNAMLA compounds were characterized by HPLC-MS analysis. The purities of the whole library were determined by integration of the UV absorbance signal at 365 nm. The absorbance spectra of 10 μ M in DMSO solution was recorded in SpectraMax M2 plate reader. Table 5.1 shows the purity, experimental mass analysis data and absorbance values of the whole CyNAMLA library.

Table 5.1. Characterization data of the CyNAMLA library

Plate code	Compound code	M ⁺ (exp.)* ^a	purity (%) ^{*b}	λ_{abs} (nm)	Raman intensity ^{*c}
A2	CyNAMLA-11	890.4	91	804	2374
A3	CyNAMLA-49	899.4	93	806	2271
A4	CyNAMLA-55	947.4	94	805	1125
A5	CyNAMLA-80	891.5	96	804	32082
A6	CyNAMLA-92	849.4	95	803	23452
A7	CyNAMLA-100	959.4	89	804	2312
A8	CyNAMLA-101	869.4	97	803	2102
A9	CyNAMLA-102	899.4	91	804	1602
A10	CyNAMLA-103	899.4	92	806	6424
A11	CyNAMLA-105	862.4	94	804	3878
B2	CyNAMLA-107	938.4	85	805	2397
B3	CyNAMLA-111	869.4	97	805	4021
B4	CyNAMLA-124	915.5	91	804	2201
B5	CyNAMLA-131	897.5	71	806	4419
B6	CyNAMLA-164	847.6	74	803	4777
B7	CyNAMLA-177	823.3	97	802	9396
B8	CyNAMLA-180	833.4	91	804	8236
B9	CyNAMLA-181	915.5	80	804	2109
B10	CyNAMLA-184	929.4	70	803	24133

B11	CyNAMLA-185	835.4	71	805	4603
C2	CyNAMLA-193	935.5	88	803	1610
C3	CyNAMLA-201	897.5	72	804	6915
C4	CyNAMLA-218	873.3	95	804	1922
C5	CyNAMLA-220	873.3	97	805	6604
C6	CyNAMLA-221	889.3	96	804	26102
C7	CyNAMLA-230	877.5	94	804	4341
C8	CyNAMLA-262	915.5	95	805	27810
C9	CyNAMLA-266	929.5	75	806	3013
C10	CyNAMLA-272	876.5	93	805	1986
C11	CyNAMLA-274	865.5	96	806	6417
D2	CyNAMLA-275	897.5	80	804	1408
D3	CyNAMLA-277	863.4	94	804	2046
D4	CyNAMLA-282	878.5	90	805	1296
D5	CyNAMLA-295	793.5	96	804	1888
D6	CyNAMLA-319	915.5	94	805	2850
D7	CyNAMLA-329	933.5	75	804	4790
D8	CyNAMLA-335	883.5	89	805	8158
D9	CyNAMLA-336	945.5	88	805	2548
D10	CyNAMLA-341	933.4	70	804	1071
D11	CyNAMLA-346	927.5	87	805	2940
E2	CyNAMLA-356	945.5	97	806	2333
E3	CyNAMLA-358	915.5	98	804	1121
E4	CyNAMLA-359	914.5	97	805	2068
E5	CyNAMLA-364	889.4	96	804	3561
E6	CyNAMLA-373	821.5	94	804	2487
E7	CyNAMLA-374	855.5	97	803	9636
E8	CyNAMLA-375	873.5	97	804	1976
E9	CyNAMLA-381	885.5	98	804	38210
E10	CyNAMLA-382	861.5	99	804	7947

E11	CyNAMLA-387	885.5	97	804	3910
F2	CyNAMLA-388	885.5	96	805	1620
F3	CyNAMLA-395	899.5	96	805	1876
F4	CyNAMLA-396	869.5	93	806	6521
F5	CyNAMLA-398	869.6	94	805	2629
F6	CyNAMLA-401	856.5	91	804	2920
F7	CyNAMLA-403	889.4	98	804	3417
F8	CyNAMLA-405	887.4	92	805	12149
F9	CyNAMLA-407	905.4	94	806	3000
F10	CyNAMLA-414	904.6	88	806	5267
F11	CyNAMLA-419	835.5	83	804	9354
G2	CyNAMLA-427	850.4	80	805	1735
G3	CyNAMLA-439	849.6	81	805	3589
G4	CyNAMLA-442	835.5	75	803	1989
G5	CyNAMLA-443	807.5	71	806	1833
G6	CyNAMLA-446	845.5	80	804	8301
G7	CyNAMLA-452	933.4	71	805	24271
G8	CyNAMLA-477	887.9	97	804	9679
G9	CyNAMLA-478	883.4	92	805	35116
G10	CyNAMLA-480	903.5	89	805	10253
G11	CyNAMLA-531	923.2	88	805	5272
H2	CyNAMLA-548	945.4	70	803	10165
H3	CyNAMLA-565	923.3	92	805	14019
H4	CyNAMLA-567	919.5	90	802	9879
H5	CyNAMLA-572	947.4	94	804	2718
H6	CyNAMLA-574	835.5	93	804	1763
H7	CyNAMLA-599	945.5	85	804	11616
H8	CyNAMLA-611	876.5	81	804	18833
H9	CyNAMLA-621	951.3	75	804	2050
H10	CyNAMLA-677	903.3	83	805	2455

H11	CyNAMLA-686	937.4	72	806	8146
-----	-------------	-------	----	-----	------

*(a) ESI-MS m/z corresponding to $[M^+]$ values.

*(b) Purities were determined by integration of the UV absorbance signal at 365 nm.

*(c) SERS spectra were obtained from excitation at 785 nm with a laser power of 60 mW.

*(d) The main product corresponded to the double acetylated derivative.

5.3.3 Measurement of SERS

I employed 60 nm diameter AuNPs as a noble nanoparticle with roughened metal surface, which is an important requirement for SERS studies. **CyNAMLA** compounds proved to be remarkably NIR-active with absorbance maximum wavelengths around 800 nm in DMSO (Figure 5.1). Hence, I conjugated the **CyNAMLA** library to AuNPs in order to study their SERS properties.

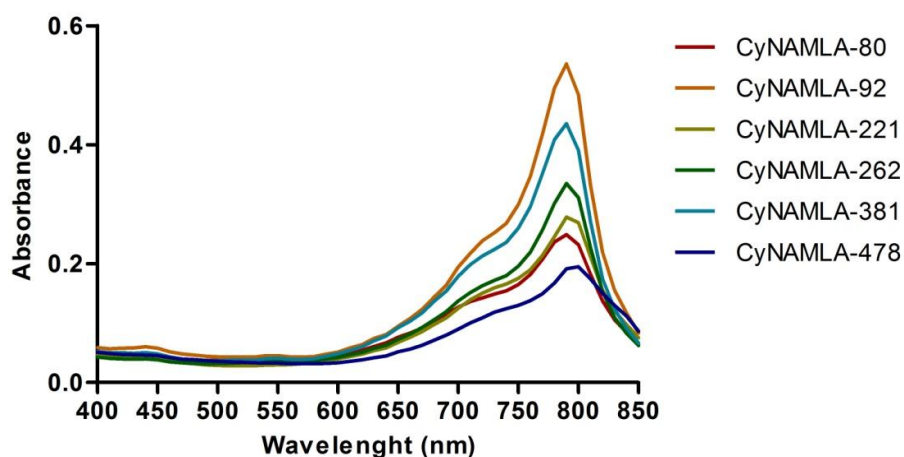


Figure 5.1. Absorbance spectra of the 6 selected **CyNAMLA** compounds (10 μ M concentration, pH=7.4, 20 mM PBS).

CyNAMLA excitation maxima are around 790 nm (Figure 5.1), and I applied 785 nm laser sources for the excitation of Au-nanotags. Practically, only 785 nm and 633 nm laser sources are available in SERS microscopes, and the 785 nm source can generate a higher SERS signal intensity due to the resonance with the excitation frequency and electronic transition of NIR reporter molecules. The SERS properties

of **CyNAMLA** compounds were examined under a compact Raman scanner upon incubation of every compound with citrate-stabilized gold nanoparticles. This primary screening revealed that the SERS intensities of **CyNAMLA** compounds varied significantly throughout the library (Table 5.1, Figure 5.3), indicating that the SERS properties depended on the amine structure.

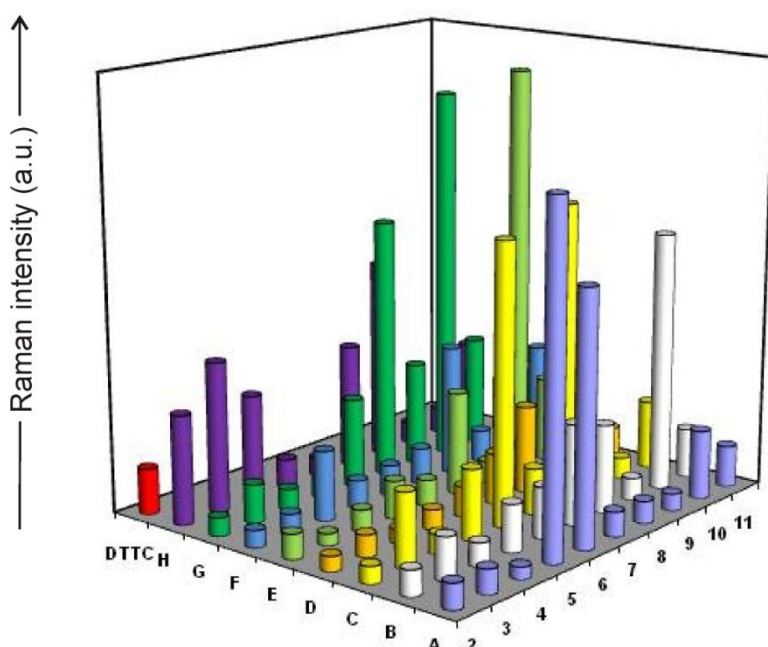


Figure 5.2. Comparative SERS intensities of the whole **CyNAMLA** library. SERS spectra were measured in a compact Raman scanner with excitation at 785 nm and 60 mW laser power. The intensity of the reference standard **DTTC** is plotted in a red bar.

Notably, six derivatives containing mostly aromatic amines (**CyNAMLA-80**, **92**, **221**, **262**, **381** and **478**, represented in Figure 5.2 as A5, A6, C6, C8, E9 and G9 respectively) exhibited very high SERS intensities that exceeded the signal intensity of **DTTC**, and were selected for further analysis. The selected SERS active reporter molecules were further carried out in a Renishaw InVia Raman microscope (Renishaw, UK, model: HPNIR785) using an excitation wavelength of 785 nm. Figure 5.4 clearly indicates that the SERS signal intensity of **CyNAMLA-381** displays around 12-fold higher sensitivity than the standard **DTTC**.

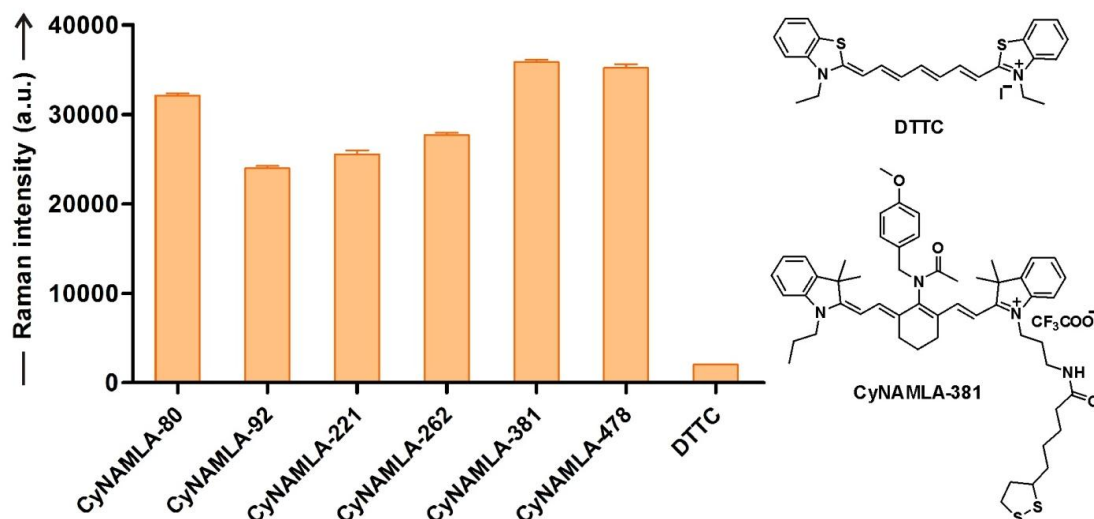


Figure 5.3. SERS intensities of the selected CyNAMLA-AuNPs. SERS spectra data were measured at 523 cm^{-1} for CyNAMLA and 495 cm^{-1} for DTTC in a Renishaw Raman microscope (excitation: 785 nm).

I have studied the SERS spectra ranging from 400 cm^{-1} to 2000 cm^{-1} of selected best six compounds among whole library. Interestingly, all the Raman active molecules having a number of bands that might be assigned as follows: 523 cm^{-1} as $\gamma(\text{S-S})$, 1059 cm^{-1} as $\gamma(\text{CH}_2\text{-S})$, 1124 cm^{-1} as $\gamma(\text{C-C})$, 1202 cm^{-1} as aromatic vibration of the polycyclic structure, and 1469 cm^{-1} as $\gamma(\text{CH}_3\text{-C})$ anti-symmetry stretching.^{24, 25} Figure 5.4 indicated that the SERS spectra of all the Raman active molecules are unique and all the selected compounds showed much higher intensity than standard DTTC.

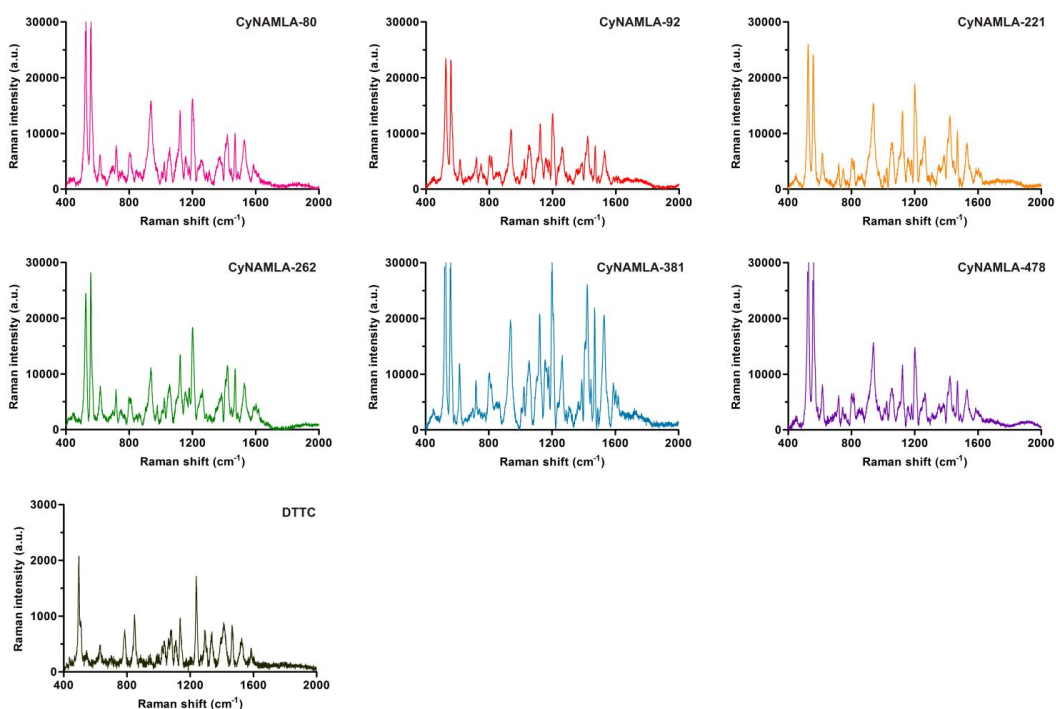
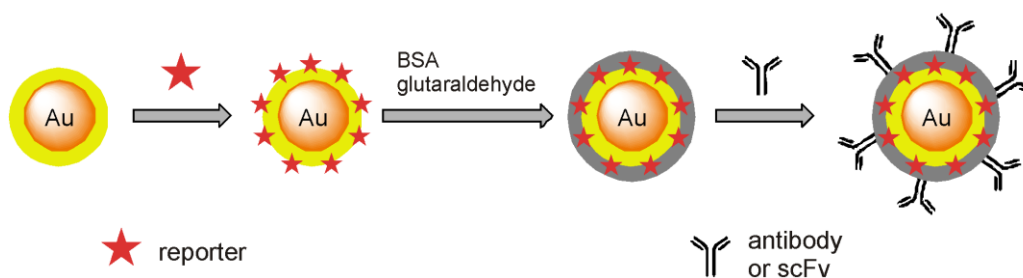


Figure 5.4. SERS spectra of BSA-encapsulated nanotags that were derivatized with **CyNAMLA-80**, **CyNAMLA-92**, **CyNAMLA-221**, **CyNAMLA-262**, **CyNAMLA-381**, **CyNAMLA-478** and **DTTC**, Raman spectral range: 400 to 2000 cm^{-1} , resolution: 1 cm^{-1} , acquisition time: 10 s.

5.3.4 Encapsulation of AuNPs and TEM characterization

The encapsulation of SERS-active nanoparticles is a crucial step because it can prevent their aggregation and the desorption of Raman signature molecules from the NPs, and it can be used to introduce functional groups on their surface for bioconjugation.²⁶⁻²⁹ To evaluate the long-term stability of the six selected **CyNAMLA-AuNPs**, we (I and Dr. Kaustabh Kumar Maiti) modified them with bovine serum albumin (BSA) and glutaraldehyde so that amine-containing molecules (i.e. antibodies, proteins or other macromolecules) could be attached to the resulting cross-linked organic layer on the surface (Scheme 5.2).³⁰

Scheme 5.2. Preparation of BSA-stabilized and antibody or scFv-conjugated SERS nanotags



Previously Qian et al. reported that the gold nanoparticles rapidly precipitate or aggregate under harsh conditions.⁹ AuNPs and their SERS spectra are quite stable after encapsulation with polyethylene glycol (PEG) due to the formation of protective layer on the gold colloid. Similarly, Huang et al. also reported the BSA encapsulation for the stability of the nanoparticles. In the present work we (I and Dr. Kaustabh Kumar Maiti) applied BSA encapsulation to increase the stability of SERS signal intensity and minimize the aggregation among the nanoparticles. In addition, the BSA coating layer allows efficient conjugation to tumor-targeting ligands. The increased size (65-70 nm) of the BSA-encapsulated **CyNAMLA**-AuNPs was confirmed by transmission electron microscopy (TEM). In addition, the plasmon spectra in Figure 5.5 showed a minor band around 600 nm, indicating that there is no major aggregation of the Au colloids.

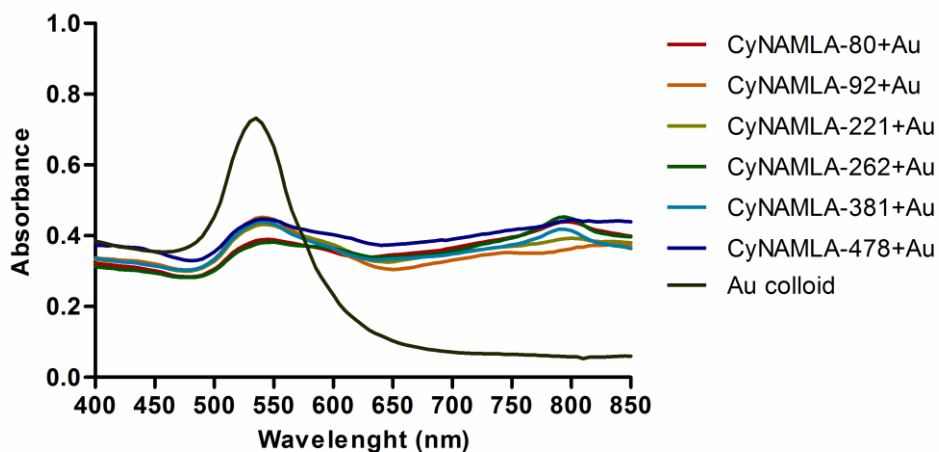


Figure 5.5. Surface plasmon absorption spectra of Au-colloids containing CyNAMLA reporters.

Similarly, dimers and trimers can be found in one of the TEM images (Figure 5.6a), but in all samples, I observed that the predominant form of our colloids are as monomers (Figure 5.6b) rather than as small aggregates.

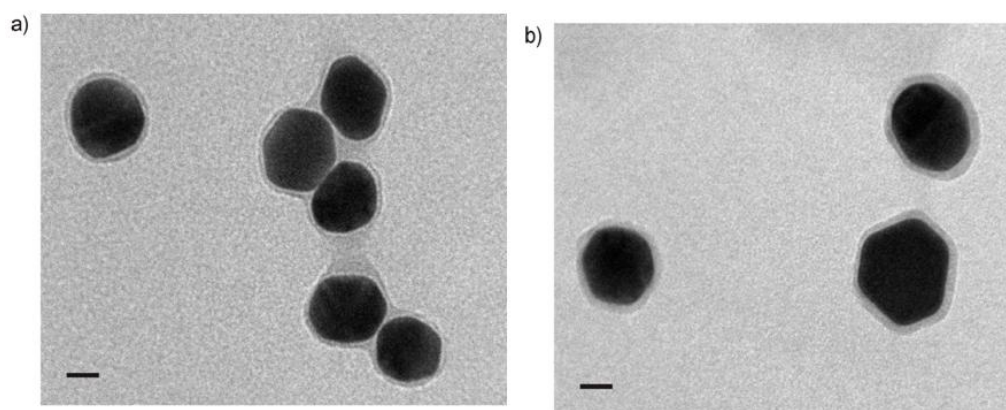


Figure 5.6. Transmission electron microscopy (TEM) images of: (a) BSA-encapsulated **CyNAMLA-381** nanotags, (b) antibody-conjugated BSA-encapsulated **CyNAMLA-381** nanotags. Scale bar: 20 μm .

5.3.5 Stability measurement of SERS nanotags

I analyzed the stability of the SERS intensities for 1 month at highest peaks 523 cm^{-1} and 495 cm^{-1} , for **CyNAMLA** and DTTC compounds respectively. For the SERS measurements of **CyNAMLA**-gold colloid mixtures, 20 μM solutions of **CyNAMLA** compounds in deionized water were mixed with Au colloid ($2.6 \times$

1010 particles/mL) in a 1:9 ratio (v/v). 20 μ L of the reporter-Au colloid mixture solutions were placed on a clean glass slide with a cover slip and measured under the Raman microscope. The results are plotted as average intensities of 5 independent measurements from one single sample preparation. Remarkably, the nanotags exhibited consistent stable SERS intensities over time, with a low relative standard deviation (2 to 3%) (Figures 5.7-5.13). From the above analysis of the SERS intensity and signal stability, **CyNAMLA-381** was chosen as the best Raman reporter in terms of both signal intensity and stability.

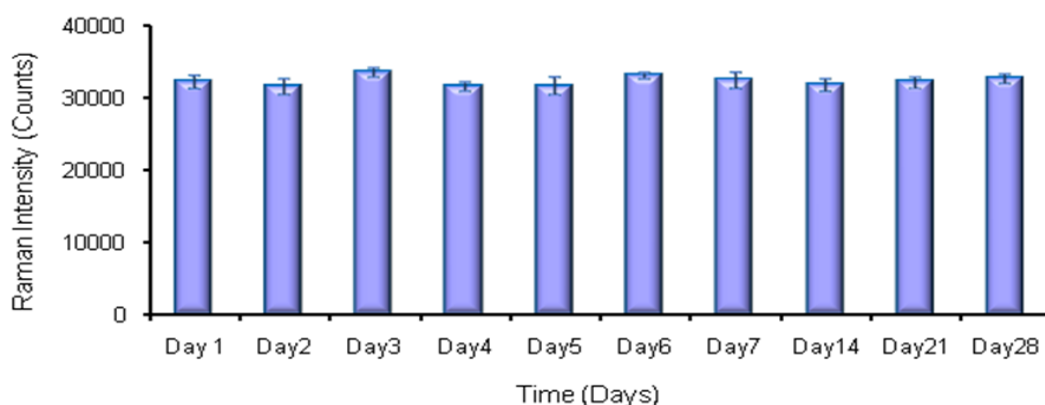


Figure 5.7. Time-course SERS measurements of **CyNAMLA-80** nanotags. 20 μ M solutions of CyNAMLA-80 compounds in deionized water were mixed with Au colloid (2.6×10^{10} particles/mL) in a 1:9 ratio (v/v).

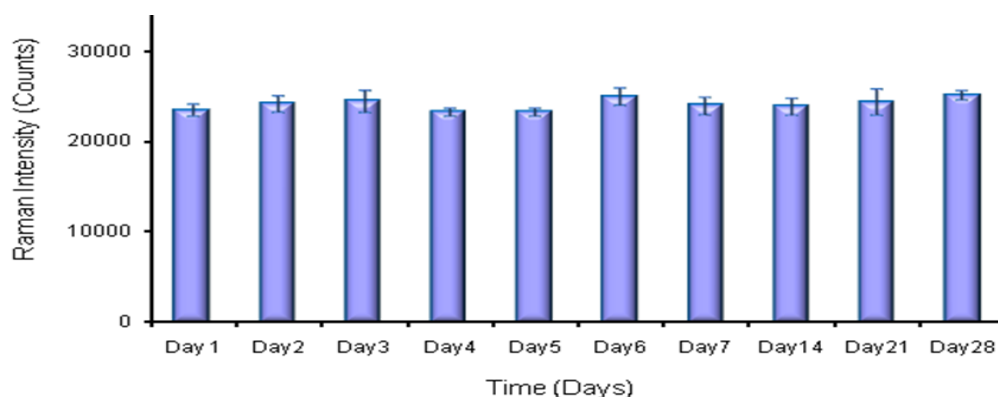


Figure 5.8. Time-course SERS measurements of **CyNAMLA-92** nanotags. 20 μ M solutions of CyNAMLA-92 compounds in deionized water were mixed with Au colloid (2.6×10^{10} particles/mL) in a 1:9 ratio (v/v).

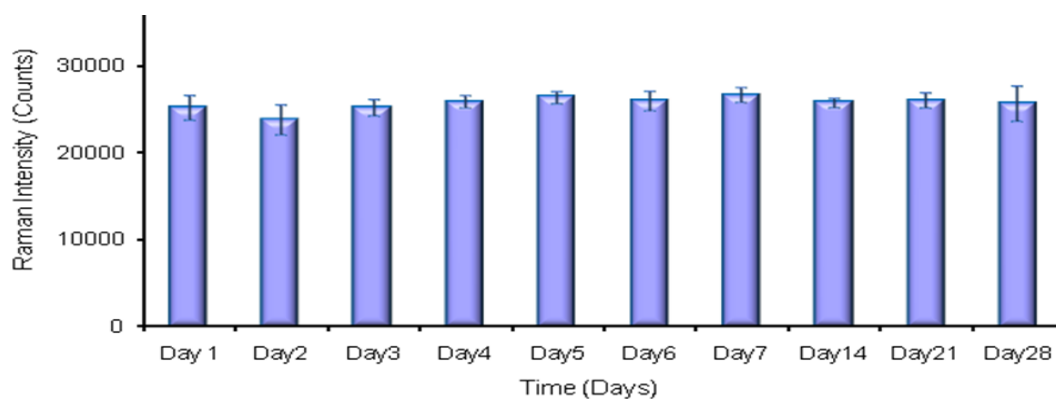


Figure 5.9. Time-course SERS measurements of **CyNAMLA-221** nanotags. 20 μM solutions of CyNAMLA-221 compounds in deionized water were mixed with Au colloid (2.6×10^{10} particles/mL) in a 1:9 ratio (v/v).

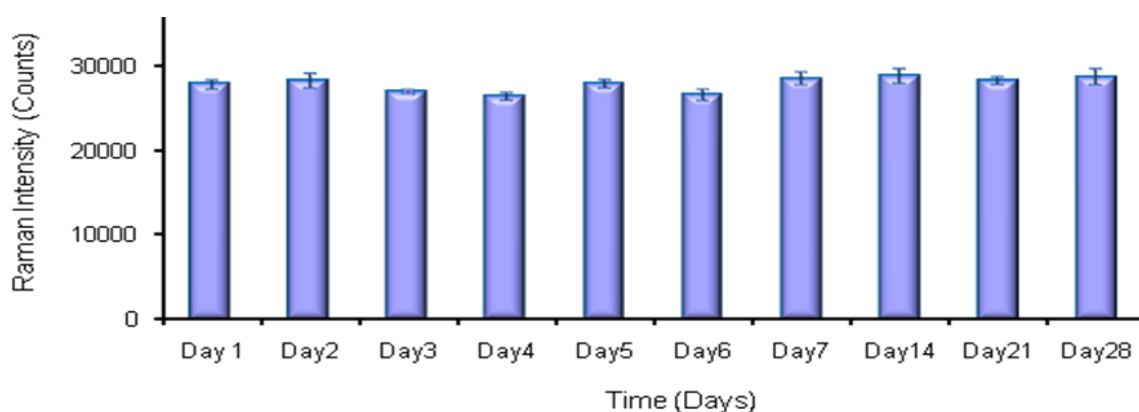


Figure 5.10. Time-course SERS measurements of **CyNAMLA-262** nanotags. 20 μM solutions of CyNAMLA-262 compounds in deionized water were mixed with Au colloid (2.6×10^{10} particles/mL) in a 1:9 ratio (v/v).

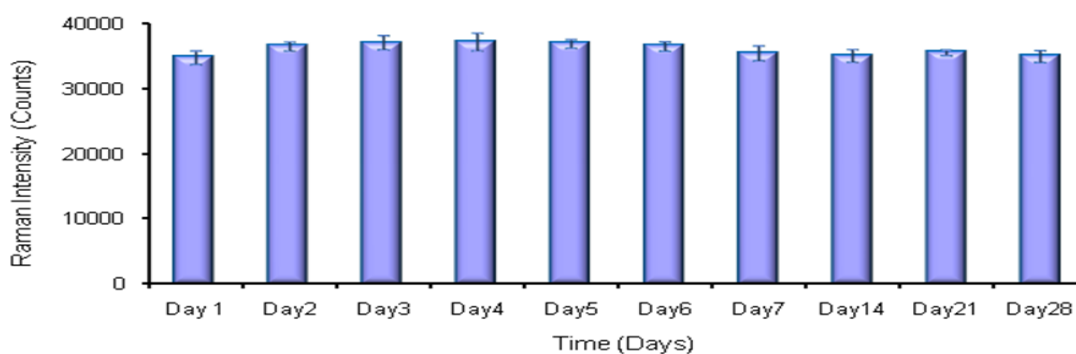


Figure 5.11. Time-course SERS measurements of **CyNAMLA-381** nanotags. 20 μM solutions of CyNAMLA-381 compounds in deionized water were mixed with Au colloid (2.6×10^{10} particles/mL) in a 1:9 ratio (v/v).

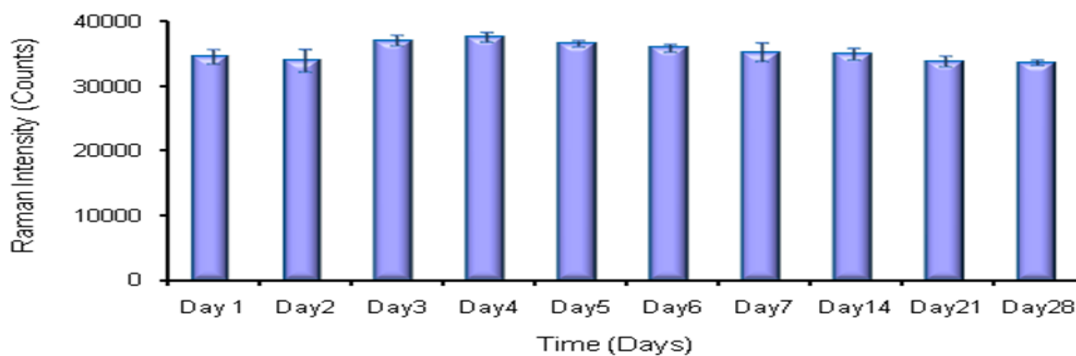


Figure 5.12. Time-course SERS measurements of **CyNAMLA-478** nanotags. 20 μ M solutions of CyNAMLA-478 compounds in deionized water were mixed with Au colloid (2.6×10^{10} particles/mL) in a 1:9 ratio (v/v).

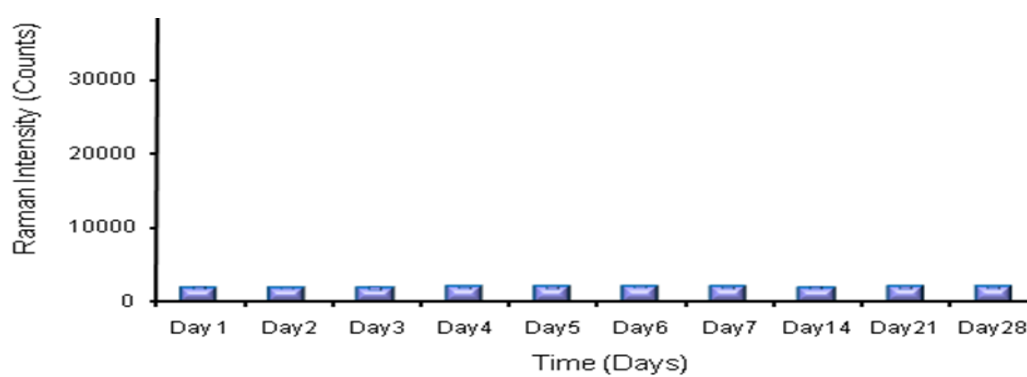


Figure 5.13. Time-course SERS measurements of **DTTC** nanotags. 20 μ M solutions of DTTC compounds in deionized water were mixed with Au colloid (2.6×10^{10} particles/mL) in a 1:9 ratio (v/v).

5.3.6 Antibody conjugation and SERS study

With the discovery of **CyNAMLA-381** as a NIR highly sensitive SERS reporter molecule, we (I and Dr. Kaustabh Kumar Maiti) applied it to the preparation of SERS probes for cancer cell detection and discrimination. To prepare SERS nanotags that could selectively detect cancer cells expressing HER2 receptors, we conjugated **CyNAMLA-381**-AuNPs to two HER2-recognition motifs: a full anti-HER2 monoclonal antibody (170 kDa) and a scFv anti-HER2 (26 kDa) antibody.³² Generally, HER2 signaling pathway plays an important role in cell proliferation, and is upregulated in most breast cancers.³¹ Specially, ScFv anti-HER2 (MW $\frac{1}{4}$ 25 kDa), a small antibody fragment recognizes the herceptin receptor (HER2) that is overexpressed in many types of human malignant tumors. Hence, Dr. Kaustabh

Kumar Maiti studied SDS-PAGE analysis to confirm the conjugation of ScFv anti-HER2 to the nanotags. Figure 5.14 clearly shows the SDS-PAGE analysis of ScFv-nanotag and the original scFv.

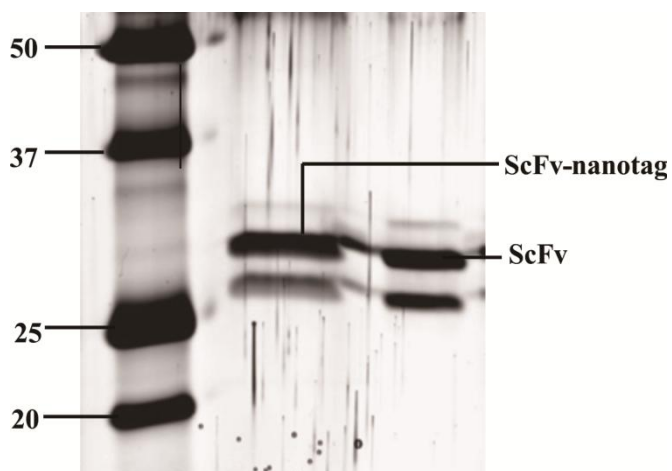


Figure 5.14. SDS-PAGE of scFv-anti-HER2 antibody upon conjugation to SERS nanotags.

After full characterization of the nanotags conjugated ScFv antibody, I examined firstly their *in vitro* specificity in SKBR-3 (HER2-positive) and MDA-MB231 (HER2-negative) cancer cells. Upon incubation of SKBR-3 cells with antibody-conjugated **CyNAMLA-381**-AuNPs, strong SERS signals were observed, while negligible signals were detected after incubating the same NPs with MDA-MB231 cells (Figure 5.15).

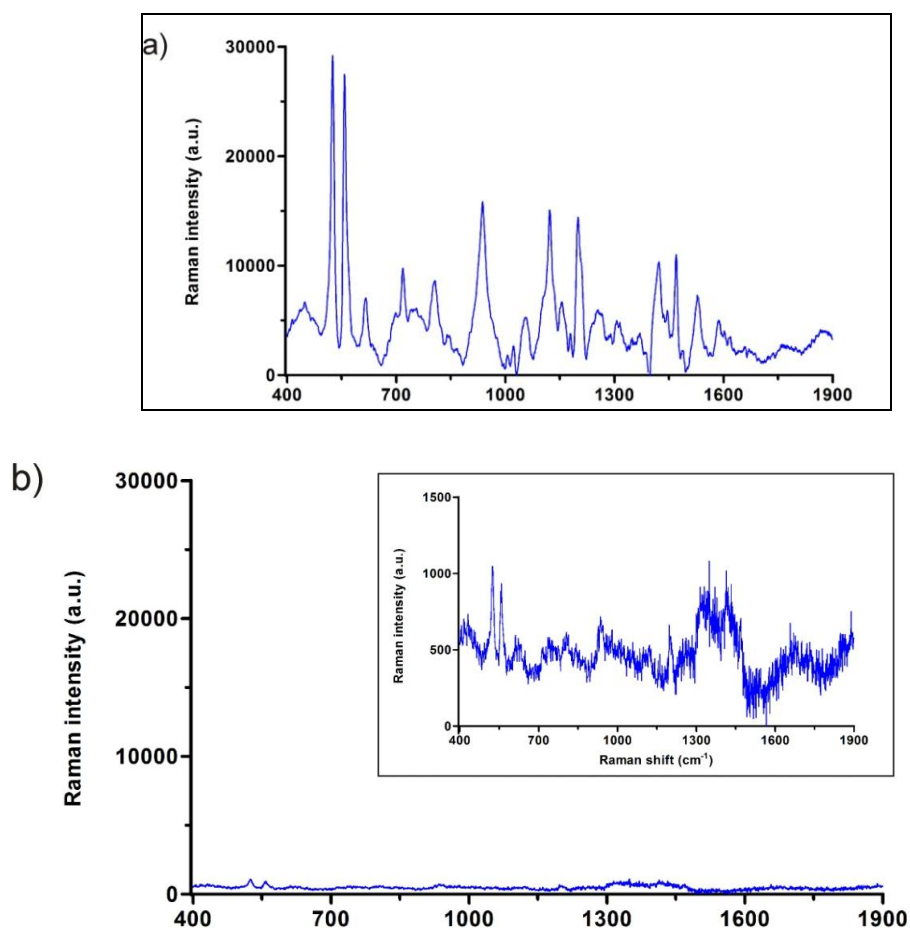


Figure 5.15. SERS spectra upon incubation with scFv-conjugated SERS nanotags in: a) HER-2 positive SKBR-3 cells, b) HER-2 negative MDA-MB231 cells. The measurements were performed with excitation at 785 nm and a laser power of 60 mW.

I also confirmed the target specificity of **CyNAMLA-381-AuNPs** in SKBR-3 cells by competition assays between antibody-conjugated nanotags and free HER2-recognition motifs: a 10 to 15-fold decrease of the SERS signals in the presence of the competing anti-HER2 antibodies was observed (Figure 5.16). Interestingly, the signal intensities obtained with scFv-conjugated nanotags were 1.5 times stronger than those with the full-HER2 antibody. This data suggests that scFv-conjugated nanotags can not only maintain the recognition properties but also improve the detection of full-size antibodies. Furthermore, the smaller size of scFv can significantly reduce the interstitial tumor pressure that impedes intratumoral distribution when using larger recognition motifs.⁹

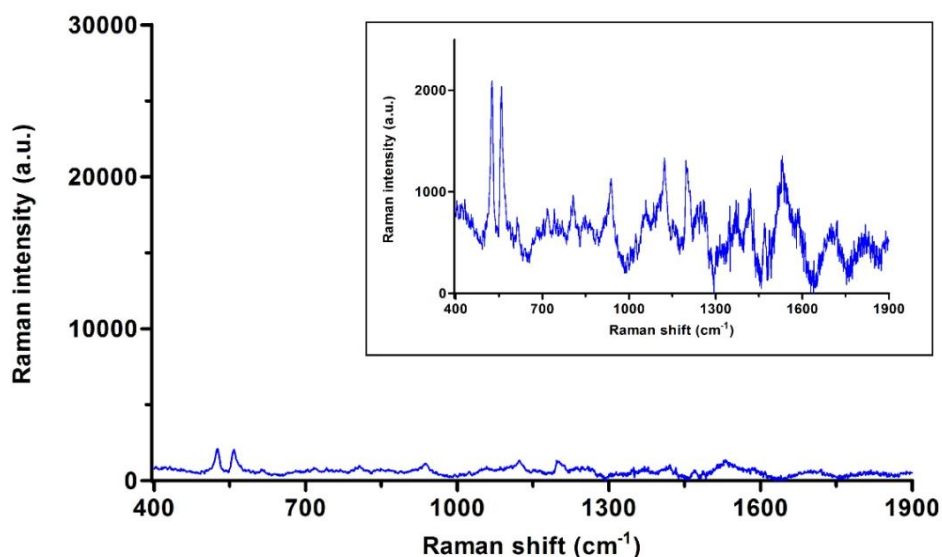


Figure 5.16. SERS spectra upon incubation with scFv-conjugated SERS nanotags in: SKBR-3 cells upon competition between scFv-conjugated SERS nanotags and free scFv (anti-HER2). For insets contain zoom spectra. The measurements were performed with excitation at 785 nm and a laser power of 60 mW.

5.3.7 Cell SERS mapping

We (I and Dr. Kaustabh Kumar Maiti) performed SERS mapping experiments in SKBR-3 and MDA-MB231 cells (Figure 5.17).³³ Mapping images of SKBR-3 cells after incubation with scFv-conjugated **CyNAMLA-381**-nanotags displayed high SERS intensities at representative frequencies of **CyNAMLA-381** (i.e. 523 cm⁻¹). On the other hand, no distinguishable signals were observed in MDA-MB231 cells under the same experimental conditions. The mapping pictures confirmed that the interaction between scFv anti-HER2-conjugated nanotags and SKBR-3 cells was mainly localized at the cell surface, which corresponds well with the high expression of HER2 receptors at the plasma membrane of cancer cells.³⁴ While the exact limits of the cell boundary may be difficult to determine due to the resolution of the bright field images, there is a good correlation in many points of the SERS maps and the bright field images, which confirms that the interaction between nanotags and SKBR-3 cells mainly takes place at the cell surface.

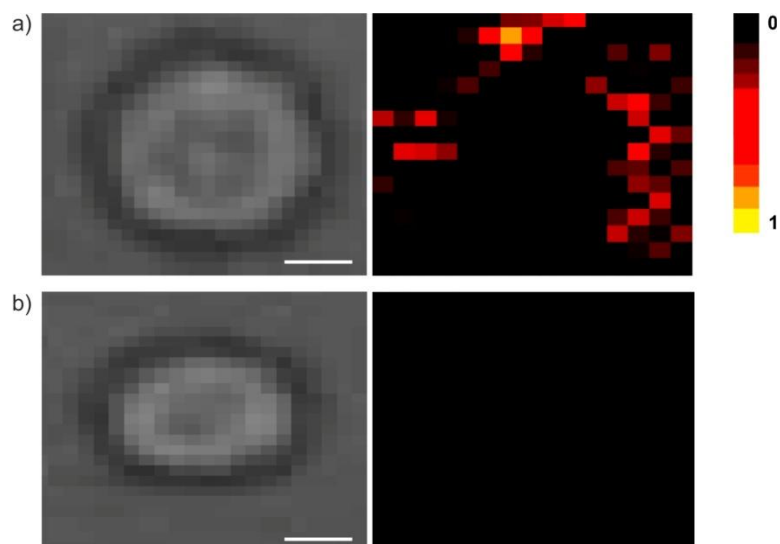


Figure 5.17. Bright field and SERS mapping images of cells treated with **CyNAMLA-381**-nanotags: a) SKBR-3, b) MDA-MB231 cells. All mapping images (523 cm^{-1}) were scanned at an interval of $2\text{ }\mu\text{m}$ (785 nm excitation) and the intensities were normalized between the lowest (0) and the highest color (1) values. Scale bar: $10\text{ }\mu\text{m}$.

Reflective mode dark-field images³⁵ of SKBR-3 cells that were incubated with scFv-conjugated **CyNAMLA-381**-SERS nanotags also displayed a number of bright spots on the cell surface due to the recognition of the receptor, while the same experimental conditions in MDA-MB231 cells showed a negligible scattering (Figure 5.18). The corresponding SERS spectra showed that only intense SERS signals were observed from the particles located on the cell surface of the HER2-positive cells (points 2 and 3), and no SERS signals were detected in other regions of the SKBR-3 cells (point 1) nor in MDA-MB231 cells (points 4 and 5).

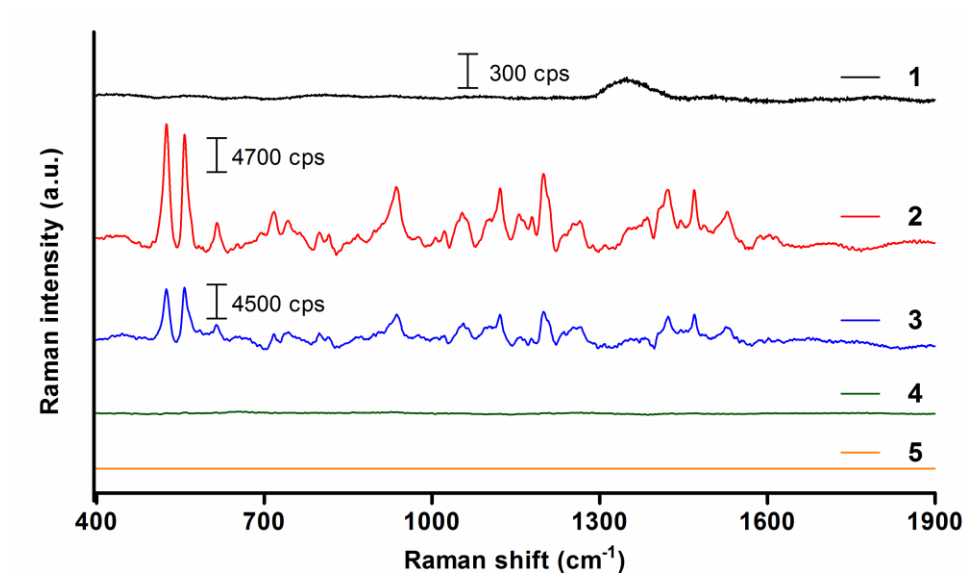
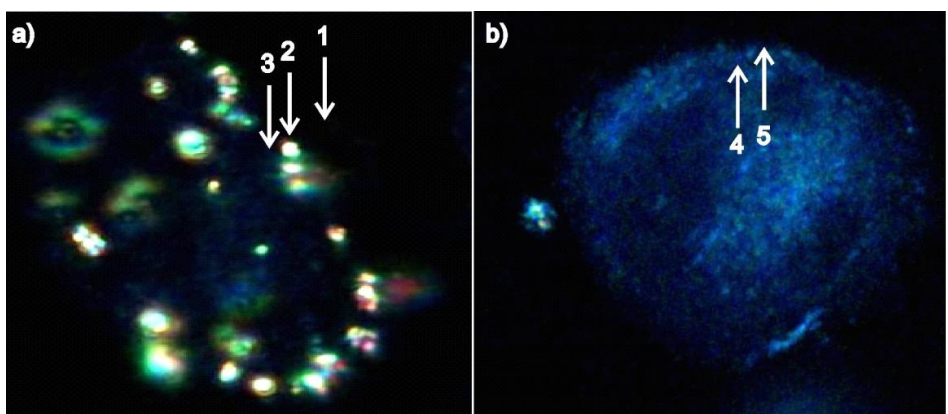


Figure 5.18. Dark-field reflective microscopy images (CytoViva) and SERS spectra from points 1-5 (indicated with arrows) in: a) SKBR-3 and b) MDA-MB231 cells.

The broad spectral bump in the region of $\sim 1300\text{-}1500\text{ cm}^{-1}$ may be characteristic of glass luminescence especially when very low Raman-active molecules are placed on the glass material and excited at 785 nm.

5.3.8 *In vivo* cancer detection in xenograft mice

Finally, in order to validate the optical detection by scFv-conjugated CyNAMLA-381-SERS nanotags *in vivo*, we (I, Dr. Kaustabh Kumar Maiti and Dr. Yun Seong Wook) injected them in nude mice bearing xenografts generated from SKBR-3 cells. After 5 h of the tail vein injection, we measured the SERS spectra of

the tumor site through the skin with a NIR laser beam. Whereas the signal of the tumor site perfectly resembled the SERS spectra of the pure nanotag, no SERS signal was detected from other anatomical locations (i.e. upper dorsal) (Figure 5.19).

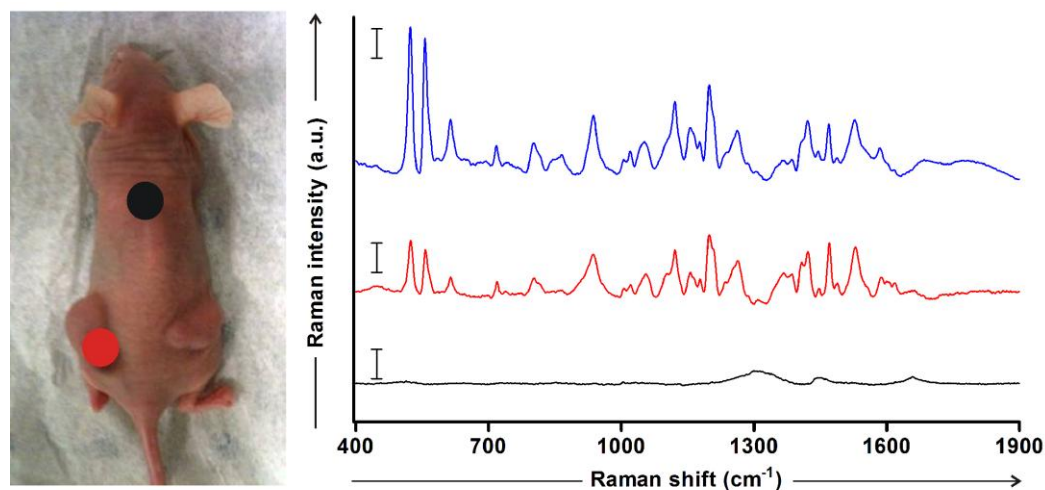


Figure 5.19. *In vivo* detection of HER2-positive tumors with scFv-conjugated CyNAMLA-381-SERS nanotags: SERS spectra of pure nanotags (blue), and SERS signals of the tumor location (red) and a non-tumorogenic area (black).

On the contrary, we (I. Dr. Kaustabh Kumar Maiti and Dr. Yun Seong Wook) observed that no significant SERS signal (Figure 5.20) was detected after injecting the nanotags in xenograft models prepared with HER2-negative cancer cells (MDA-MB231).

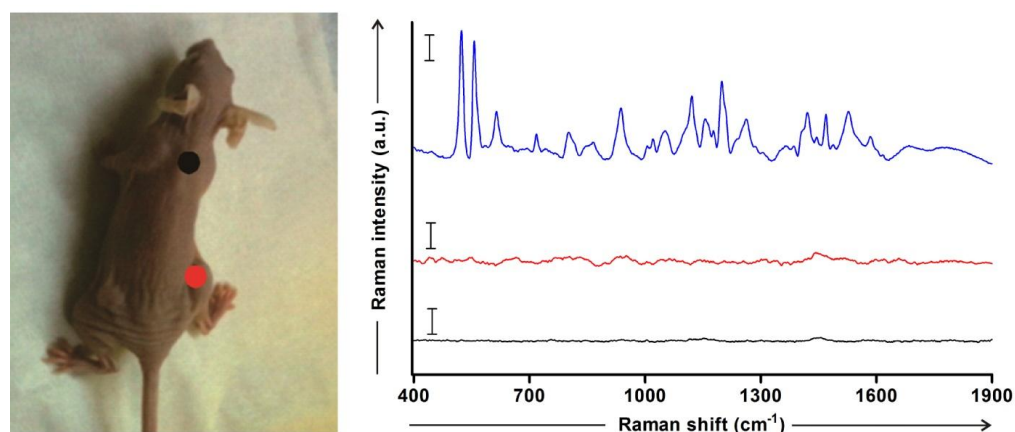


Figure 5.20. *In vivo* imaging of MDA-MB231 (HER2-negative) tumors with scFv-conjugated CyNAMLA-381-SERS nanotags: SERS spectra of pure nanotags (blue), and SERS signals of the tumor (red), and of a non-tumor area (i.e. upper dorsal) (black). Scale bar: 5000 cps.

5.3.10 *In vivo* SERS imaging

We (I, Dr. U.S. Dinish and Dr. Kaustabh Kumar Maiti) performed SERS mapping experiments in xenograft mice, by mapping tumor and non-tumor regions separately. As shown in Figure 5.21, distinctive SERS mapping images between two regions were distinguishable according to their SERS intensity. Mapping experiments in SKBR-3 xenograft models revealed much higher SERS intensities (523 cm^{-1}) in the tumor region when compared to non-tumor areas. These results clearly indicated that the scFv-conjugated **CyNAMLA-381**-SERS nanotags were able to specifically detect HER2-positive tumors *in vivo*. The differences between white light images from cancer and normal tissue may be due to the fact that the focus of the light for both tumor and non-tumor areas may be set at different depths, since it is practically difficult to maintain the exact same depth for both regions in the experimental set-up.

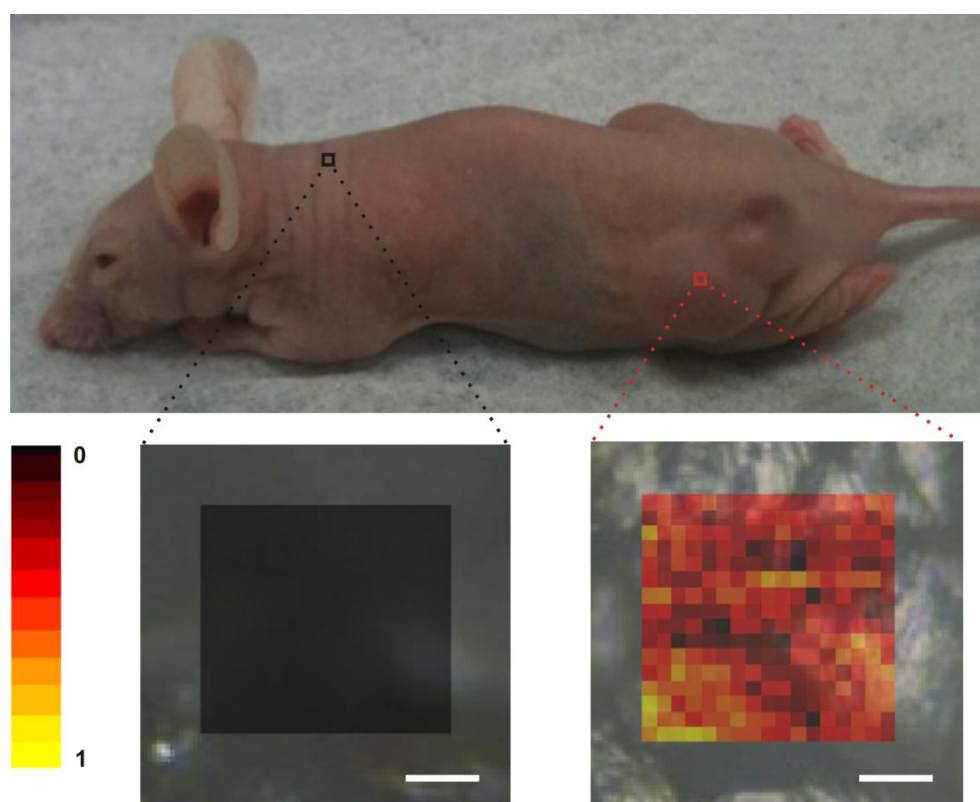


Figure 5.21. SERS mapping images (523 cm^{-1}) from tumor (red square) and non-tumor upper dorsal (black square) regions upon injection of **CyNAMLA381**-anti-HER2 nanotags. All mapping images (size: $30 \times 30\ \mu\text{m}^2$) were scanned at an interval of $2\ \mu\text{m}$ (785 nm excitation wavelength) and the intensities were normalized between the lowest (0) and the highest color (1) values. Scale bar: $10\ \mu\text{m}$.

5.4 Conclusion

In summary, I prepared a lipoic acid-containing NIR-active tricarbocyanine library (**CyNAMLA**), and screened the SERS properties after chemisorption in AuNPs. **CyNAMLA** compounds exhibited strong SERS intensities, and I identified **CyNAMLA-381** as a highly sensitive NIR SERS reporter molecule with excellent signal stability and 12-fold higher sensitivity than the current standard **DTTC**. We (I, Dr. Kaustabh Kumar Maiti and Dr. Yun Seong Wook) further applied **CyNAMLA-381** to the preparation of ultrasensitive SERS probes for *in vivo* cancer imaging by conjugating **CyNAMLA-381**-AuNPs to scFv anti-HER2 antibodies. These nanotags displayed very good SERS intensity and selectivity towards HER2-positive cancer cells under both Raman and dark-field microscopes. Furthermore, we confirmed their *in vivo* application in HER2-positive and negative xenograft models. The high sensitivity and tumor specificity of scFv-conjugated **CyNAMLA-381**-SERS nanotags proves their excellent potential as non-invasive diagnostic tools and opens up a new window for the development of SERS probes for cancer bioimaging.

5.5 Experimental details

Materials and methods:

DTTC was purchased from Sigma Aldrich. Anti-HER2 (sc-71667, Neu 0.N.211) was supplied by Santa Cruz Biotechnology, Inc. For the preparation of scFv (anti-HER2) antibody the V_H and V_L genes of anti-HER2 antibody were amplified and cloned into pComb3X vector containing HA tag. The recombinant plasmid was transformed into *E. coli* BL21 DE3. Transformed *E. coli* were grown in SB medium until the OD at 600 nm reached 1.0 on a shaker at 230 rpm, followed by induction with 1 mM isopropyl- β -D-thiogalactopyransoside (IPTG) followed by overnight incubation at 30 °C. Soluble scFv was purified via anti-HA antibody conjugated protein A column. Surface plasmon absorption spectra were measured on a SpectraMax M2 spectrophotometer (Molecular Devices), and the data analysis was performed using GraphPad Prism 5.0 and Origin 6. SERS measurements were carried out in a Renishaw InVia Raman (UK) microscope with a laser beam directed to the sample through 50 \times and 20 \times objective lens and a Peltier cooled CCD detector in Singapore Bioimaging Consortium, Agency for Science, Technology and Research (A*STAR), Singapore. Samples were excited with a 785 nm excitation wavelength laser and Stokes shifted Raman spectra were collected in the range of 400 to 2000 cm^{-1} with 1 cm^{-1} resolution. Prior to every measurement, a calibration with a silicon standard (Raman peak centered at 520 cm^{-1}) was performed. WiRE 3.0 software package was used for data acquisition.

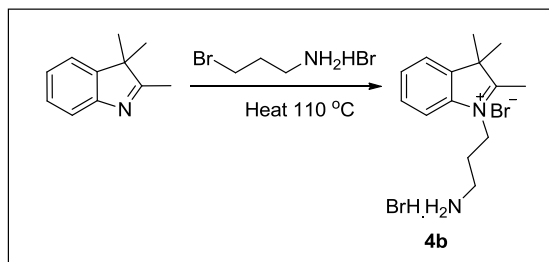
5.5.1 Synthesis and characterization of **4** and CyNAB

Synthesis of **1a** and **4b**:

In earlier Chapter 2, I have demonstrated the synthetic procedures and characterization of **1a** and **1b**.

Synthesis of 4b:

Scheme 5.3. Synthesis of 4b.



Reagents and conditions: 3-bromopropylamine hydrobromide, 110 °C, 10 h.

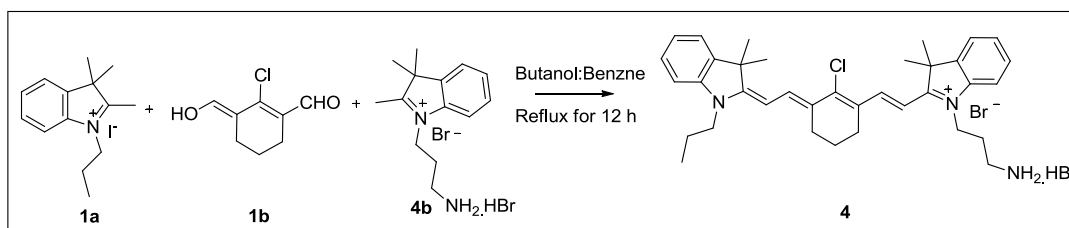
3-bromopropylamine hydrobromide (2.7 g, 12.5 mmol, 1 eq.) was added in a seal tube containing 2, 3, 3-trimethyl-3H-indole (2.0 mL, 12.5 mmol, 1 eq.) under N₂ atmosphere, and was gently heated up to 110 °C in an oil bath. The mixture was kept at 120 °C for 10 h with stirring. After the reaction was completed, the mixture was cooled down to r.t. to form a solid cake that was washed with Et₂O and a chloroform-Et₂O (1:1) solution. The resulting solid was then dried under high vacuum to obtain **4b** as a white solid (4.3 g, yield 85%).

¹H-NMR (300 MHz, DMSO-*d*₆): 1.55 (s, 6H), 2.16-2.21 (m, 2H), 2.50 (s, 3H), 3.05-3.07 (m, 2H), 4.60 (t, 2H, *J* = 7.5 Hz), 7.61-8.08 (m, 4H).

tR: 2.10 min, ESI-MS *m/z* (C₁₄H₂₂BrN₂⁺) calc: 217.2, found: 217.1.

Synthesis of 4:

Scheme 5.3. Synthesis of 4.



Reagents and conditions: Butanol: Benzene (7:3) refluxes for 12 h.

Under N₂ atmosphere, **1b** (1.0 g, 6 mmol, 1 eq.) and **4b** (2.3 g, 6 mmol, 1 eq.) were dissolved in 50 mL of butanol-benzene (7:3) and refluxed for 2 h in 110 °C oil bath. The mixture was then cooled down to r.t. followed by addition of **1a** (2.0 g, 6 mmol, 1 eq.) in butanol-benzene (7:3), and then refluxed for another 12 h at 120 °C in a Dean-Stark condenser. The solvent was then evaporated and the resulting green solid mixture was washed with Et₂O and purified by normal phase chromatography (elution with DCM-MeOH, 95:5) to obtain **4** as a green solid (3.0 g, yield 78%).

¹H-NMR (500 MHz, CDCl₃): 1.02 (t, 3H, *J* = 7.5 Hz), 1.67 (s, 6H), 1.69 (s, 6H), 1.82-1.86 (m, 2H), 1.97 (t, 2H, *J* = 6.6 Hz), 2.37 (t, 2H, *J* = 7.2 Hz), 2.55 (m, 2H), 2.99 (t, 2H, *J* = 7.2 Hz), 3.57 (t, 2H, *J* = 6.6 Hz), 3.92 (t, 2H, *J* = 6.6 Hz), 4.76 (t, 2H, *J* = 6.6 Hz), 5.92 (d, 1H, *J* = 13.5 Hz), 6.62 (d, 1H, *J* = 14.4 Hz), 7.00-7.72 (m, 8H), 7.33 (d, 1H, *J* = 13.5 Hz), 7.41 (d, 1H, *J* = 14.4 Hz).

tR: 5.37 min, ESI (HRMS) m/z (C₃₆H₄₆BrClN₃⁺) calc: 554.3297, found: 554.3316.

Synthesis of CyNAB:

4 (2.5 g, 4.5 mmol, 1 eq.) was dissolved in CHCl₃, DIEA (2.9 g, 22.5 mmol, 5 eq.) and Boc₂O (1.5 g, 6.8 mmol, 1.5 eq.) were added, and the reaction mixture was refluxed for 4 h. The mixture was washed with H₂O (2 x 100 mL) and diluted HCl (0.1 mL) and the combined organic layers were evaporated and purified by normal phase chromatography (elution with DCM-MeOH, 95:5) to obtain to obtain **CyNAB** as a green solid (3.0 g, 91%).

¹H-NMR (300 MHz, CDCl₃): 1.06 (t, 3H, *J* = 7.2Hz), 1.43 (s, 9H), 1.70 (s, 12H), 1.86-1.90 (m, 2H), 1.97 (t, 2H, *J* = 6.6 Hz), 2.66 (t, 2H, *J* = 7.2 Hz), 2.81 (t, 2H, *J* = 6.5 Hz), (2.76 (t, 2H, *J* = 7.2 Hz), 3.38 (t, 2H, *J* = 6.6 Hz), 4.00 (t, 2H, *J* = 6.5 Hz), 4.42 (t, 2H, *J* = 7.0 Hz), 6.01 (d, 1H, *J* = 13.5 Hz), 6.46 (d, 1H, *J* = 14.1 Hz), 6.46-7.35 (m, 8 H), 8.23 (d, 1H, *J* = 13.0 Hz), 8.39 (d, 1H, *J* = 15.0 Hz).

tR: 6.51 min, ESI (HRMS) m/z (C₄₁H₅₃ClN₃O₂⁺) calc: 654.3302, found: 654.3846.

5.5.2 Synthesis and characterization of CyNAMLA library

Synthesis of lipoic acid nitrophenol resin:

Aminomethyl nitrophenol polystyrene resin was prepared according to reported procedures.¹ The nitrophenol resin (2 g, 2.9 mmol, 1 eq.) was swollen in 10 mL of DMF, and lipoic acid (2 g, 10 mmol, 3.3 eq.), *N,N'*-diisopropylcarbodiimide (1.2 mL, 12 mmol, 4 eq.) and a catalytic amount of DMAP (20 mg) were added to the resin, which was continuously shaken for 24 h at r.t. Subsequently, the resin was washed with DCM (10 × 25 mL) and dried under vacuum until use.

General procedure for the synthesis of the CyNAMLA library:

For all 80 compounds, **CyNAB** (60 mg, 92 μmol, 1 eq.) and the primary amine building blocks (see Table 5.1) (368 μmol, 4 eq.) were dissolved in ACN, and DIEA (26.8 μL, 184 μmol, 2 eq.) was added. The reaction mixture was heated at 80 °C for 0.5 – 3 h, depending on the reactivity of the amine. The resulting blue color crude mixture was neutralized with 0.1 M HCl, and dried under vacuum. The crude then dissolved in DCM and treated with excess DIEA (268 μL, 1.84 mmol, 20 eq.) and acetyl chloride (460 μmol, 5 eq.) at 0 °C for 10 min. The final green mixture was washed with 0.1 M HCl to remove excess DIEA, concentrated under vacuum, and purified by normal phase chromatography (elution mixture: DCM-MeOH (ranging from 100:0 to 95:5)). Subsequently, the compounds were treated with TFA-DCM (1:9) at r.t overnight, washed with an aqueous NaHCO₃ and dried under vacuum. A 1 μmol aliquot of all 80 compounds were dissolved in 1 mL DCM: ACN (2:1) and treated with an excess of lipoic acid nitrophenol resin (30 mg, 10 μmol, 10 eq.) overnight at r.t. The resulting mixtures were purified with short silica-based columns to render 80 **CyNAMLA** compounds, which were characterized by HPLC-MS (Table 5.1).

General procedure for the synthesis of CyNAMLA-80, 92, 221, 262, 381 and 478:

For every compound, **CyNAB** (100 mg, 0.13 mmol) was mixed with the corresponding amine (Chart 5.1, 0.27 mmol, 2 eq.) and DIEA (38.6 μ L, 0.13 mmol, 1 eq.) in ACN. The reaction mixtures were heated at 65 °C for 40-60 min, quenched with 0.1 N HCl, concentrated under vacuum, and purified by normal-phase chromatography (elution with DCM-MeOH, 95:5). The resulting intermediates were treated with TFA-DCM (1:9) overnight at r.t., followed by washings with NaHCO₃ and dried under vacuum. Finally, compounds were dissolved in DCM: ACN (2:1) and treated with an excess of lipoic acid nitrophenol resin overnight at r.t. The resulting mixtures were purified with short silica-based columns (elution with DCM-MeOH, 93:7).

Characterization of CyNAMLA-80, 92, 221, 262, 381 and 478

CyNAMLA-80 (12 mg, yield 10%). ¹H-NMR (500 MHz, CDCl₃): 1.07 (t, 3H, *J* = 7.0 Hz), 1.25 (s, 6H), 1.56 (s, 6H), 1.71-1.75 (m, 4H), 1.83-1.92 (m, 2H), 1.94 (s, 3H), 2.05-2.08 (m, 2H), 2.44-2.49 (m, 3H), 2.61-2.64 (m, 4H), 3.08-3.11 (m, 4H), 3.15 (t, 2H, *J* = 6.5 Hz), 3.45 (t, 2H, *J* = 5.0Hz), 3.57-3.61 (m, 2H), 3.85 (t, 2H, *J* = 7.2 Hz), 4.51 (s, 2H), 4.59 (t, 2H, *J* = 6.2Hz), 5.26 (d, 1H, *J* = 13 Hz), 5.83 (d, 1H, *J* = 13.5 Hz), 6.54 (d, 1H, *J* = 7.5 Hz), 6.67 (d, 1H, *J* = 7.0 Hz), 7.13-7.98 (m, 11H).

tR: 6.48 min, ESI (HRMS) *m/z* (C₅₃H₆₅F₂N₄O₂S₂⁺), calc: 891.4512; found: 891.4525.

CyNAMLA-221 (15 mg, yield 11%). ¹H-NMR (500 MHz, CDCl₃): 1.06 (t, 3H, *J* = 7.0 Hz), 1.44 (s, 6H), 1.51 (s, 6H), 1.68-1.71 (m, 4H), 1.83-1.87 (m, 2H), 1.90 (s, 3H), 2.05-2.08 (m, 2H), 2.42-2.49 (m, 3H), 2.66-2.71 (m, 4H), 3.08-3.13 (m, 4H), 3.16 (t, 2H, *J* = 5.0Hz), 3.45 (t, 2H, *J* = 5.0Hz), 3.59-3.61 (m, 2H), 3.85 (t, 2H, *J* = 7.5Hz), 4.51 (t, 2H, *J* = 6.2Hz), 4.56 (s, 2H), 4.91 (d, 1H, *J* = 14.0 Hz), 5.85 (d, 1H, *J* = 13.0 Hz), 6.62 (d, 1H, *J* = 7.5 Hz), 6.94 (d, 1H, *J* = 7.0 Hz), 7.13-7.71 (m, 12H).

tR: 6.64 min, ESI (HRMS) *m/z* (C₅₃H₆₆ClN₄O₂S₂⁺), calc: 889.4310; found: 889.4334.

CyNAMLA-262 (14 mg, yield 11%). ¹H-NMR (500 MHz, CDCl₃): 1.06 (t, 3H, *J* = 7.0 Hz), 1.25 (s, 6H), 1.58 (s, 6H), 1.68-1.74 (m, 4H), 1.84-1.88 (m, 2H), 1.92 (s, 3H), 1.99-2.04 (m, 2H), 2.39-2.47 (m, 3H), 2.56-2.59 (m, 4H), 3.07-3.12 (m, 4H), 3.38 (t, 2H, *J* = 6.5 Hz), 3.47 (t, 2H, *J* = 5.0 Hz), 3.56-3.59 (m, 2H), 3.66 (s, 3H), 3.72 (s, 3H), 3.85 (t, 2H, *J* = 7.2 Hz), 4.36 (s, 2H), 4.55 (t, 2H, *J* = 6.2 Hz), 5.86 (d, 1H, *J* = 13.0 Hz), 5.97 (d, 1H, *J* = 13.5 Hz), 6.44 (d, 1H, *J* = 7.5 Hz), 6.58 (d, 1H, *J* = 7.0 Hz), 7.14-8.03 (m, 11H).

tR: 6.45 min, ESI (HRMS) m/z (C₅₅H₇₁N₄O₄S₂⁺), calc: 915.4911; found: 891.4901.

CyNAMLA-381 (20 mg, yield 15%). ¹H-NMR (500 MHz, CDCl₃): 1.05 (t, 3H, *J* = 7.5 Hz), 1.53 (s, 6H), 1.59 (s, 6H), 1.67-1.74 (m, 4H), 1.83-1.87 (m, 2H), 1.88 (s, 3H), 2.02-2.08 (m, 2H), 2.39-2.46 (m, 3H), 2.69-2.71 (m, 4H), 3.06-3.11 (m, 4H), 3.12 (t, 2H, *J* = 5.0 Hz), 3.46 (t, 2H, *J* = 5.0 Hz), 3.64 (s, 3H), 3.59-3.61 (m, 2H), 3.84 (t, 2H, *J* = 7.5 Hz), 4.59 (t, 2H, *J* = 6.2 Hz), 4.35 (s, 2H), 5.01 (d, 1H, *J* = 14.0 Hz), 5.87 (d, 1H, *J* = 14.5 Hz), 6.69 (d, 1H, *J* = 9.0 Hz), 6.78 (d, 1H, *J* = 9.0 Hz), 7.13-8.01 (m, 12H).

tR: 6.50 min, ESI (HRMS) m/z (C₅₄H₆₉N₄O₃S₂⁺), calc: 885.4806; found: 885.4796.

CyNAMLA-478 (18 mg, yield 13%). ¹H-NMR (500 MHz, CDCl₃): 1.07 (t, 3H, *J* = 7.5 Hz), 1.59 (s, 6H), 1.65 (s, 6H), 1.70-1.76 (m, 4H), 1.86-1.89 (m, 2H), 1.95 (s, 3H), 2.1-2.13 (m, 2H), 2.24 (s, 3H), 2.42-2.45 (m, 3H), 2.50-2.54 (m, 4H), 2.70 (t, 2H, *J* = 7.5 Hz), 3.08-3.11 (m, 4H), 3.11 (t, 2H, *J* = 6.5 Hz), 3.46 (t, 2H, *J* = 6.5 Hz), 3.57-3.59 (m, 2H), 3.89 (t, 2H, *J* = 7.5 Hz), 4.42 (t, 2H, *J* = 7.5 Hz), 4.57 (t, 2H, *J* = 6.5 Hz), 5.89 (d, 1H, *J* = 13.5 Hz), 5.94 (d, 1H, *J* = 13.5 Hz), 6.42 (d, 1H, *J* = 14.0 Hz), 6.66 (d, 1H, *J* = 15.0 Hz), 7.13-8.01 (m, 12H).

tR: 6.74 min, ESI (HRMS) m/z (C₅₅H₇₁N₄O₂S₂⁺), calc: 883.5013; found: 883.5028.

5.5.3 Procedures for SERS measurements

The spectral measurements were carried out in a Renishaw InVia Raman microscope (Renishaw, UK, model: HPNIR785) using an excitation wavelength of 785 nm. In brief, the laser system is coupled to a Leica microscope so that the laser beam is directed to the sample through a 50× or 20× objective lens and a Peltier cooled CCD detector is used to collect the Raman signals. The WiRE 3.0 software package provided with the Raman system was employed for instrument control and data acquisition. Stokes shifted Raman spectra were collected in the range of 400 to 2000 cm^{-1} with a resolution of about 1 cm^{-1} . The maximum laser power at the sample was measured to be 60 mW and the exposure time was set at 10 s throughout the measurements. The shutter of the laser was immediately closed after each measurement to minimize any possible photodamage on the sample under a prolonged illumination. Baseline correction of the measured spectra was performed to remove the broad background and fluorescence band. Prior to each measurement, the instrument was calibrated with a silicon standard whose Raman peak is centered at 520 cm^{-1} . For the SERS measurements of CyNAMLA-gold colloid mixtures, 20 μM solutions of CyNAMLA compounds in de-ionized water were mixed with Au colloid (2.6×10^{10} particles/mL) in a 1:9 ratio (v/v). 20 μL of the reporter-Au colloid mixture solutions were placed on a clean glass slide with a cover slip and measured under the Raman microscope. The results are plotted as average intensities of 5 independent measurements from one single sample preparation.

5.5.4 BSA encapsulation of CyNAMLA-AuNPs and stability studies

CyNAMLA compounds (20 μM solutions in deionized water) were mixed with Au colloid (2.6×10^{10} particles/mL) in a 1:9 ratio (v/v). After 10 min incubation, colloids were treated with BSA (0.5% in deionized water) mixed with 25% glutaraldehyde (15:1) and reacted at r.t. for 4 h followed by centrifugation (8000 rpm, 5 min). Glutaraldehyde was used to form a cross-linked organic encapsulation layer

around the gold and stabilize the particles, preventing the distortion of the reporter molecules. In order to remove the excess of glutaraldehyde, pellets were resuspended in 10 mM glycine with 10 mM sodium citrate (pH = 7.8) at r.t. Finally, the encapsulated Au colloids were washed 3 times by centrifugation (8000 rpm, 5 min), resuspended in 1 mM sodium citrate, and stored at 4 °C. For bioconjugation and long time storage we resuspended the encapsulated gold colloid in PBS.

The SERS signals of BSA-encapsulated nanotags that were derivatized with **CyNAMLA-80**, **CyNAMLA-92**, **CyNAMLA-221**, **CyNAMLA-262**, **CyNAMLA-381**, **CyNAMLA-478** and **DTTC** were measured for one month. SERS spectra were obtained upon excitation with a 785 nm laser (60 mW power), and the SERS intensities of the highest Raman peaks (i.e. 523 cm⁻¹ for **CyNAMLA** compounds and 495 cm⁻¹ for **DTTC**), are plotted as means ± standard deviation of 5 independent measurements taken from the same sample at different time points.

5.5.5 Procedures for Antibody conjugation and TEM characterization

Antibody conjugation:

The carboxylic acids groups of BSA were activated with *N*-(3-(dimethylamino)-propyl)-*N*'-ethylcarbodiimide (EDC) (125 nmol) and *N*-hydroxysuccinimide (NHS) (125 nmol). After 30 min incubation, excess of EDC and NHS was removed by 3 rounds of centrifugation (8000 rpm, 10 min), and resuspended in PBS using Amicon Ultra 3K centrifuge microcons (Milipore). The activated particles were then reacted with mouse monoclonal anti-HER2 or scFv anti-HER2 at 25 °C for 2 h and then overnight at 4 °C. Non-specific binding chemicals and antibodies were removed by centrifugation (8000 rpm, 10 min) and the final nanotags were resuspended in PBS and stored at 4 °C.

TEM characterization:

TEM images were taken in a Jeol JEM-1010 Transmission Electron Microscope. Acceleration voltage was 40 ~ 100KV and stability was 2 ppm min⁻¹. The magnification range of the instrument covers from 50 to 600,000× with a resolution of 0.3000 nm. Images of these BSA encapsulated nanotags were taken at a 250,000× magnification.

5.5.6 SERS experiments in cells

Human cancer cell lines (MDA-MB231 and SKBR-3) were grown in RPMI 1640 medium supplemented with 10% (v/v) fetal bovine serum (FBS) and antibiotics (100 U mL⁻¹ penicillin/100 µg mL⁻¹ streptomycin mixture) at 37 °C in a humidified atmosphere with 5% CO₂. HER2 positive (SKBR-3) and negative (MDA-MB231) cells were grown as indicated above in 12-well plates, incubated with scFv-conjugated SERS nanotags (450 pM) in the absence or presence of pre-incubated free scFv anti-HER2 (10-fold excess, approx. 4 nM) for 1 h at 37 °C, washed with cold PBS (× 3), gently scrapped and resuspended in PBS to a cell density of 1 × 10⁶ cells/mL for SERS measurements.

5.5.7 SERS mapping in SKBR-3 and MDA-MB231 cells

SERS mapping experiments were performed in a Renishaw InVia Raman microscope system with a laser beam directed to the sample through a 20× objective lens, and a Peltier cooled CCD detector. Cells were plated in a 8-well glass slide at a density of 10⁶ cells/mL, and after incubation with antibody-conjugated **CyNAMLA381**-nanotags (450 pM) for 4 h at 25 °C rinsed with PBS (×3) and media (×2, 15 min incubation per wash). Samples were excited with a 785 nm excitation wavelength with a laser focal spot of 2 µm and 30 mW power and mapping

measurements at 523 cm^{-1} were carried out as raster scans in $2\text{ }\mu\text{m}$ steps over the specified area (aprox. $30 \times 30\text{ }\mu\text{m}^2$) with 1 s as the integration time per step.

5.5.8 Dark-field microscopy experiments

Approximately 50,000 cells (SKBR-3 or MDA-MB231) were plated in a 8-well chamber slide (Lab-Tek II, Nunc, USA) and incubated overnight at $37\text{ }^\circ\text{C}$, 5% CO_2 . After 24 h, the medium was removed and scFv-conjugated SERS nanotags (450 pM) in serum-free medium were added to the cells. The cells were incubated for 1 h at $37\text{ }^\circ\text{C}$, and fixed with 4% paraformaldehyde for 15 min. The cells were then rinsed twice with PBS, and subsequently mounted with Vectasheild fluorescent mounting medium. Cells were visualized using an enhanced dark field (EDF) illumination system (CytoViva) attached to a Nikon Eclipse 80i microscope. The system consisted of a CytoViva 150 dark-field condenser that was in place of the original condenser of the microscope and attached via a fiber optic light guide to a Solarc 24 W metal halide light source. Images were taken under a $60\times$ oil objective lens with an iris. A drop of the NP-reacted cell suspension was added to poly-L-lysine-coated microscope slides, and samples were viewed as wet mounts, using type A immersion oil.

5.5.9 SERS experiments in xenograft mice

Balb/c nude mice from the Biological Resource Centre (Biomedical Sciences Institute) were anesthetized by intraperitoneal injection of ketamine (150 mg/kg)/xylazine (10 mg/kg) at the age of 4-6 weeks, and SKBR-3 or MDA-MB231 cells were injected subcutaneously into the rear flank (5×10^6 cells per site in a volume of $150\text{ }\mu\text{L}$). When the tumors grew to a size around 0.2 cm in diameter, scFv-conjugated SERS nanotags (450 pM, $100\text{ }\mu\text{L}$) were injected into the tail vein of the mice. After 5 h, mice were anesthetized by intraperitoneal injection of ketamine and xylazine mixture solution and *in vivo* SERS measurements were performed using a Renishaw InVia Raman microscope with 785 nm laser excitation and 60 mW laser

power. The integration time was set as 30 s and the laser was coupled to the sample through a 20× objective lens with a beam spot of aprox. 2 μm . The animal experiment procedures were performed in accordance with a protocol approved by the Institutional Animal Care and Use Committee (IACUC).

5.5.10 SERS mapping experiments in xenograft mice

SERS mapping experiments were performed in a Renishaw InVia Raman microscope system with a laser beam directed to the sample through 20× objective lens and a Peltier cooled CCD detector in SKBR-3 xenograft mice prepared as above mentioned. Specified skin areas (aprox. 30 x 30 μm^2) were excited with a 785 nm excitation wavelength with a laser focal spot of 2 μm and 30 mW power, and mapping measurements at 523 cm^{-1} were carried out as raster scans in 2 μm steps with 1 s as the integration time per step.

5.6 References

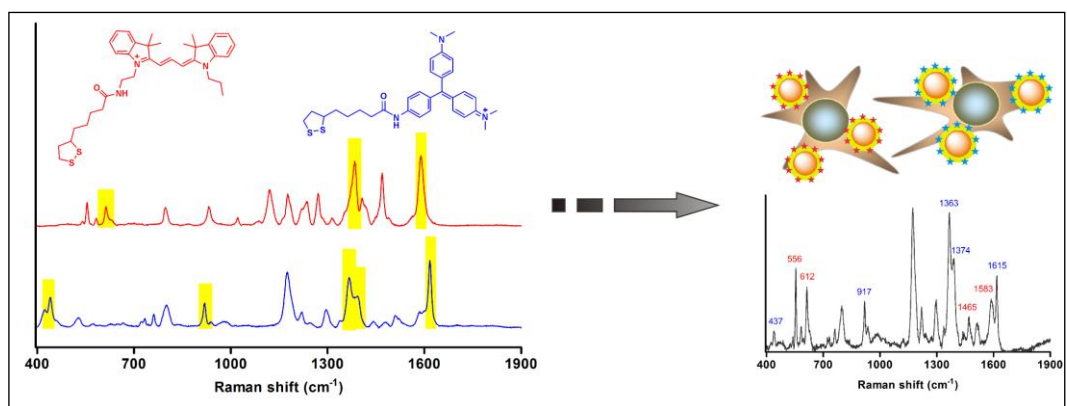
1. N. M. S. Sirimuthu, C. D. Syme, J. M. Cooper, *Anal. Chem.* **2010**, *82*, 7369.
2. M. Xiao, J. Nyagilo, V. Arora, P. Kulkarni, D. Xu, X. Sun, D. P. Dave, *Nanotechnology* **2010**, *21*, 035101.
3. G. Han, C. C. You, B. J. Kim, R. S. Turingan, N. S. Forbes, C. T. Martin, V. M. Rotello, *Angew. Chem. Int. Ed.* **2006**, *45*, 3165.
4. J. Yang, Z. Wang, X. Tan, J. Li, C. Song, R. Zhang, Y. Cui, *Nanotechnology* **2010**, *21*, 345101.
5. G. Goddard, L. O. Brown, R. Habbersett, C. I. Brady, J. C. Martin, S. W. Graves, J. P. Freyer, S. K. Doorn, *J. Am. Chem. Soc.* **2010**, *132*, 6081.
6. D. Graham, K. Faulds, *Chem. Soc. Rev.* **2008**, *37*, 1042.
7. Q. Hu, L. L. Tay, M. Noestheden, J. P. Pezacki, *J. Am. Chem. Soc.* **2007**, *129*, 14.
8. A. Ingram, L. Byers, K. Faulds, B. D. Moore, D. Graham, *J. Am. Chem. Soc.* **2008**, *130*, 11846.
9. X. Qian, X. H. Peng, D. O. Ansari, Q. Y. Goen, G. Z. Chen, D. M. Shin, L. Yang, A. N. Young, M. D. Wang, S. Nie, *Nat. Biotechnol.* **2008**, *26*, 83.
10. S. R. Emory, S. M. Nie, *Anal. Chem.* **1997**, *69*, 2631.
11. Y. L. Wang, J. L. Seebald, D. P. Szeto, J. Irudayaraj, *ACS Nano* **2010**, *4*, 4039.
12. R. S. Golightly, W. E. Doering, M. J. Natan, *ACS Nano* **2009**, *3*, 2859.
13. Y. Zhang, H. Hong, W. B. Cai, *Curr. Pharma. Biotechnol.* **2010**, *11*, 654.
14. Y. S. Huh, A. J. Chung, D. Erickson, *Microfluid. Nanofluid.* **2009**, *6*, 285.
15. J. M. Nam, C. S. Thaxton, C. A. Mirkin, *Science* **2003**, *301*, 1884.
16. W. J. Qin, L. Y. Yung, *Nucleic Acids Res.* **2007**, *35*, e111.
17. G. R. Souza, C. S. Levin, A. Hajitou, R. Pasqualini, W. Arap, J. H. Miller, *Anal. Chem.* **2006**, *78*, 6232.
18. P. J. Huang, L. K. Chau, T. S. Yang, L. L. Tay, T. T. Lin, *Adv. Funct. Mater.* **2009**, *19*, 242.

19. a) X. Peng, F. Song, E. Lu, Y. Wang, W. Zhou, J. Fan, Y. Gao, *J. Am. Chem. Soc.* **2005**, *127*, 4170.; b) A. Zaheer, R. E. Lenkinski, A. Mahmood, A. G. Jones, L. C. Cantley, J. V. Frangioni, *Nat. Biotechnol.* **2001**, *19*, 1148.
20. A. Samanta, M. Vendrell, R. Das, Y. T. Chang, *Chem Commun.* **2010**, *46*, 7406.
21. K. K. Maiti, U. S. Dinish, C. Y. Fu, J. J. Lee, K. S. Soh, S. W. Yun, R. Bhuvaneshwari, M. Olivo, Y. T. Chang, *Biosens. Bioelectron.* **2010**, *26*, 398.
22. C. Encinas, S. Miltsov, E. Otazo, L. Rivera, M. Puyol, J. Alonso, *Dyes Pigm.* **2006**, *71*, 28.
23. R. Shukla, V. Bansal, M. Chaudhary, A. Basu, R. R. Bhonde, M. Sastry, *Langmuir* **2005**, *21*, 10644.
24. K. G. Allum, J. A. Creighton, J. H. S. Green, G. J. Minkoff, L. J. S. Prince, *Spectrochimica Acta Part A: Molecular Spectroscopy* **1968**, *24*, 927.
25. J. D. Gelder, K. D. Gussem, P. Vandenabeele, L. Moens, *J. Raman Spectrosc.* **2007**, *38*, 1133.
26. H. Jang, Y. K. Kim, S. R. Ryoo, M. H. Kim, D. H. Min, *Chem. Commun.* **2010**, *46*, 583.
27. C. C. Lin, Y. M. Yang, Y. F. Chen, T. S. Yang, H. C. Chang, *Biosens. Bioelectron.* **2008**, *24*, 178.
28. S. Lee, H. Chon, M. Lee, J. Choo, S. Y. Shin, Y. H. Lee, I. J. Rhyu, S. W. Son, C. H. Oh, *Biosens. Bioelectron.* **2009**, *24*, 2260.
29. D. Graham, D. G. Thompson, W. E. Smith, K. Faulds, *Nat. Nanotechnol.* **2008**, *3*, 548.
30. L. Sun, K. B. Sung, C. Dentinger, B. Lutz, L. Nguyen, J. W. Zhang, H. Y. Qin, M. Yamakawa, M. Q. Cao, Y. Lu, A. J. Chmura, J. Zhu, X. Su, A. A. Berlin, S. Chan, B. Knudsen, *Nano Lett.* **2007**, *7*, 351.
31. C. Ma, X. Niu, J. Luo, Z. Shao, K. Shen, *Cancer. Sci.* **2010**, *101*, 2220.
32. H. Park, S. Lee, L. Chen, E. K. Lee, S. Y. Shin, Y. H. Lee, S. W. Son, C. H. Oh, J. M. Song, S. H. Kang, J. Choo, *Phys. Chem. Chem. Phys.* **2009**, *11*, 7444.

33. C. D. Syme, N. M. S. Sirimuthu, S. L. Faley, J. M. Cooper, *Chem. Commun.* **2010**, *46*, 7921.
34. W. Ueda, S. Wang, N. Dumont, J. Y. Yi, Y. Koh, C. L. Arteaga, *J. Biol. Chem.* **2004**, *279*, 24505.
35. H. Weinkauf, B. F. Brehm-Stecher, *Biotechnol. J.* **2009**, *4*, 871.
36. J. W. Lee, Y. Q. Louie, D. P. Walsh, Y. T. Chang, *J. Comb. Chem.* 2003, **5**, 330.

CHAPTER 6

MULTIPLEX CANCER CELL DETECTION BY SERS NANOTAGS WITH CYANINE AND TRIPHENYLMETHINE RAMAN REPORTERS



6.1 Introduction

In the last few years SERS spectroscopy has captured attention as a promising analytical tool due to the capacity to provide molecular information with high sensitivity. SERS employs Raman active signature molecules and noble metal nanoparticles (e.g AuNPs or AgNPs).¹⁻⁴ Generally, higher sensitivity can be achieved through an additional resonance enhancement, termed surface-enhanced resonant Raman scattering (SERRS) when the excitation occurs in resonance with electronic transitions in the signature molecules. The basic requirements for SERRS are that Raman active dyes must be adsorbed onto a roughened noble metal surface to provide the surface enhancement of the scattered light and also must absorb light in a suitable wavelength, in resonance with the applied excitation frequency of the light. As a result, sharp distinguishable fingerprints (e.g. vibrational spectrum of signature molecules) with enhanced signal intensities, narrow band widths and multiplexing properties can be detected.^{5,6} To date, single imaging agents (e.g fluorescent probes) are unlikely to provide enough information to accurately monitor a specific disease process. While challenging, the simultaneous detection of multiple targets may facilitate the development of more precise diagnostic tools. The multiplexing potential of SERS nanotags relies on the narrow spectrum band widths of the vibrational Raman spectra of the reporter molecules, and allows the simultaneous recognition of closely related targets. Although the concurrent detection of defined multiple targets can facilitate the development of accurate diagnostic probes, the identification of multiplex reporter pairs that are compatible under the same experimental conditions is difficult. Our group recently reported the excellent properties of triphenylmethines as Raman signature molecules,⁷ and demonstrated the improved stability of their SERS signal upon chemisorption on AuNPs using a lipoic acid (LA) linker. A triphenylmethine derivative (**B2LA**, Figure 6.3) was identified as an outstanding reporter in terms of both SERS signal intensity and long-term

stability.⁸ In order to study the multiplexing capabilities of **B2LA** SERS nanotags, we (Dr. Kaustabh Kumar Maiti and I) evaluated their compatibility with different Raman-active chemical compounds. As I discussed on the ultrasensitive NIR Raman reporters based on the cyanine structure (**CyNAMLA**) in Chapter 5, we (Dr. Kaustabh Kumar Maiti and I) aimed at finding multiplex partners of the **B2LA** Raman reporter. The main discrepancy between triphenylphosphine and NIR cyanine derivatives is their difference in the optimum laser source. Triphenylphosphine derivatives are highly active under the 633 nm laser, whereas NIR cyanine reporters are highly active under the 785 nm laser.

6.2 Objectives

Herein SERS nanotags have been prepared to accomplish the multiplex detection of different cancer cell lines. I evaluated the adequacy of lipoic acid-containing cyanine derivatives (**Cy3LA** and **Cy5LA**) to function as multiplex partners with a triphenylmethine Raman reporter (**B2LA**) under a single excitation wavelength (e.g. 633 nm laser). **B2LA** and cyanine SERS nanotags have been then applied for the detection of different cancer cells using different antibodies. Specifically, the multiplex antibody-conjugated SERS nanotags (e.g. anti-EGFR and anti-HER2) that recognize different types of cancer cells (i.e. OSCC and SKBR-3 respectively) have been applied to detect both cell lines using a single excitation wavelength. A few multiplex peaks have been identified from both pairs **Cy3LA/B2LA** and **Cy5LA/B2LA**.

6.3 Result and Discussion

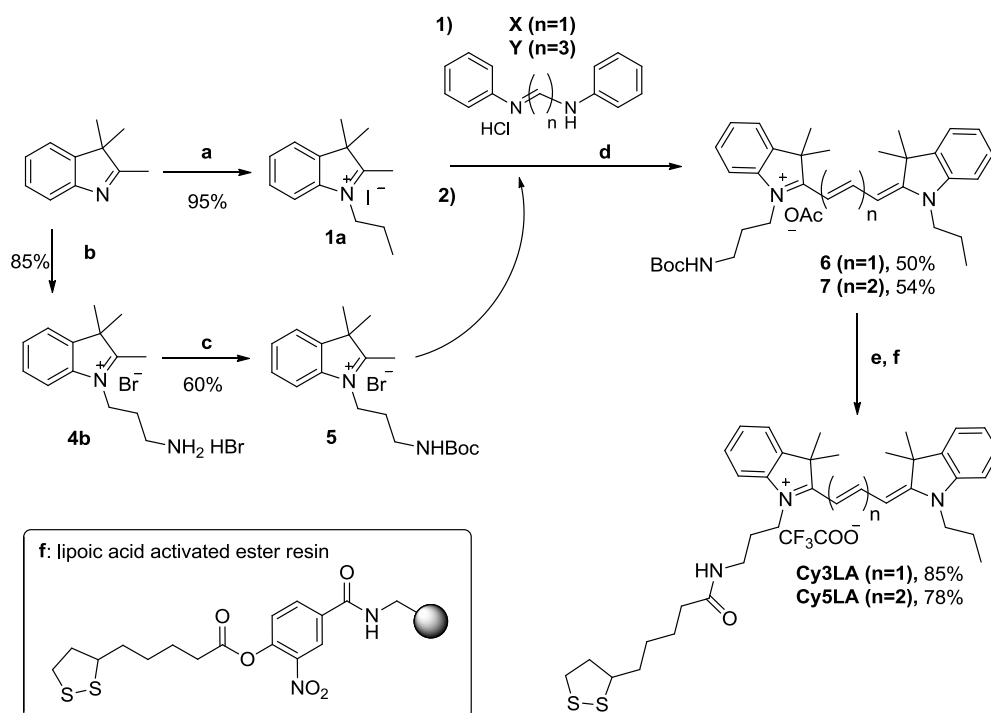
6.3.1 Design and Synthesis

I focused on the synthesis of cyanine dyes which are well-known dyes with absorption properties in the red/far-red region of the visible range.⁹⁻¹² It is obvious that positively charged Raman reporters are attracted to the surface of the negatively

charged citrate buffered nanoparticles. Therefore we demonstrated the synthesis of **Cy3LA** and **Cy5LA** SERS nanotags based on positive charge species. A range of positively charged species have been investigated including Cy3LA, Cy5LA, and B2LA motifs to examine their multiplex capabilities.

To adapt **Cy3** and **Cy5** structures to chemisorption, I designed the synthesis of lipoic acid linker (**Cy3LA** and **Cy5LA**, respectively) so that they could be attached on AuNPs using thiol-based chemistry (Scheme 6.1). Starting from 2,3,3-trimethylindoline, I prepared the intermediates **1a** and **4b** using reported procedures.¹⁴⁻¹⁶ Afterwards, **1a** was condensed to the commercially available bis-phenylimines **X** and **Y** in acidic conditions, followed by the subsequent addition of **5**, the Boc-protected derivative of **4b**. As a result, the Boc-derivatives of **Cy3** and **Cy5** (**6** and **7**, respectively) were obtained with overall yields slightly over 50%. Deprotection of **6** and **7** with an optimized TFA-DCM (1:9) solution afforded the corresponding free amine compounds, which were treated with a lipoic acid-containing activated ester resin¹⁷ to obtain **Cy3LA** and **Cy5LA** in good purities and yields.

Scheme 6.1. Synthesis of lipoic acid cyanine derivatives.



Reagents and conditions: (a) 1-iodopropane, CH₃CN, 80 °C, 15 h; (b) 3-bromopropylamine hydrobromide, 120 °C, 10 h; (c) di-tert-butyl dicarbonate, DIEA, CHCl₃, reflux, 4 h; (d) AcOH, acetic anhydride, pyridine, 110 °C; (e) TFA-DCM (1:9), r.t., 16 h; (f) lipoic acid activated ester resin, CH₂Cl₂, r.t., 16 h.

6.3.2 Preparation of SERS nanotags and encapsulation

We (Dr. Kaustabh Kumar Maiti and I) employed AuNPs as a roughened noble metal surface due to their low toxicity and adaptability to bioconjugation. **Cy3LA**, **Cy5LA** and **B2LA** were used as Raman reporters which proved to be suitable for SERRS due to their maximum absorbance wavelengths around 500-600 nm. Notably, their surface plasmon absorbance spectra remained similar (i.e. maxima around 534 nm) in the presence of Au-colloids (Figure 6.1).

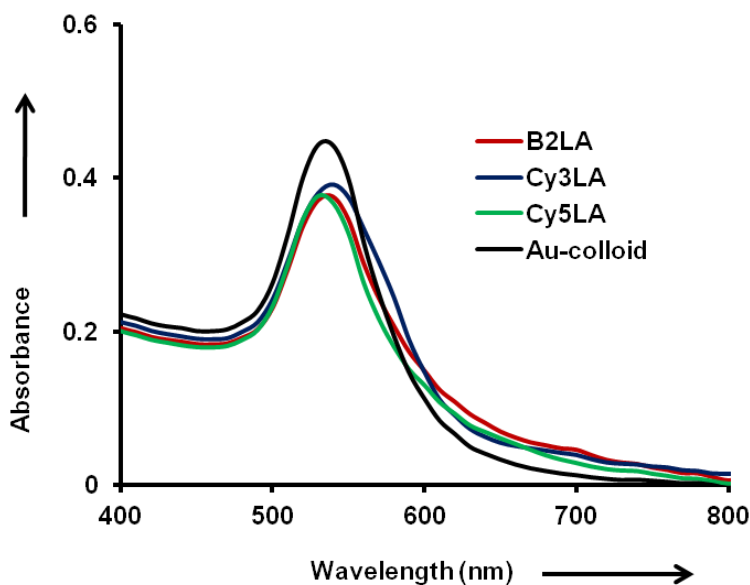
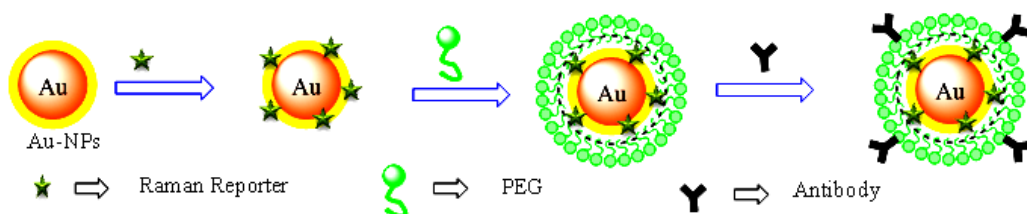


Figure 6.1. Surface plasmon absorption spectra of Au-colloids and **B2LA**, **Cy3LA** and **Cy5LA**-nanotags.

The chemisorption of Raman reporters is a critical step to ensure the stability and reproducibility of SERS nanotags over time.⁸⁻¹³ To date different research groups have developed different methods to stabilize the SERS signal intensity. I described the BSA encapsulation in Chapter 5 to stabilize the SERS signal intensity. I followed different strategy which was described by Qian et al. in which AuNPs are stabilized by encapsulation with polyethyleneglycol (PEG) due to the formation of a protective layer on the gold colloid (Scheme 6.2).

Scheme 6.2. Synthesis of stable SERS nanotags encapsulated with PEG-SH and conjugated to antibodies.



Nanotags derivatized with **B2LA** and **Cy3LA** were encapsulated with a mixture of thiol polyethyleneglycol (PEG-SH) and carboxylic acid-containing PEG-

SH that allowed the covalent linkage to the free amine groups of antibodies.³ Furthermore, we (I and Dr. Kaustabh Kumar Maiti) confirmed that the SERS signal intensities of both nanotags were stable for several days (Figure 6.2).

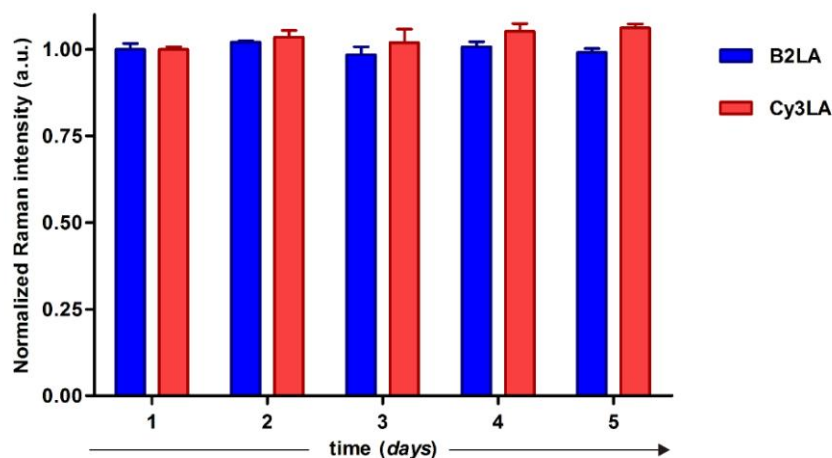


Figure 6.2. Evaluation of the stability of the SERS signals for **B2LA** anti-EGFR and **Cy3LA** anti-HER2 nanotags. Values are represented as means \pm SD ($n=3$).

6.3.3 Measurement of SERS

After chemisorbing **B2LA**, **Cy3LA** and **Cy5LA** on AuNPs, we (I and Dr. Kaustabh Kumar Maiti) analyzed their SERS spectra under the 633 nm laser and evaluated their multiplexing compatibility. Notably, a number of peaks could be used to uniquely identify the three different nanotags: 1617, 1374, 1366, 918 and 440 cm^{-1} for **B2LA**-AuNPs, 1589, 1383 and 613 cm^{-1} for **Cy3LA**-AuNPs and 1596, 1501, 1404 and 1353 cm^{-1} for **Cy5LA**-AuNPs (Figure 6.3). Whereas the discrimination between **Cy3LA** and **Cy5LA**-derivatized nanotags may require further optimization, it was apparent that the combination of triphenylmethine and cyanine Raman reporters could be used as a basis for the construction of multiplex SERS nanotags, and we (Dr. Kaustabh Kumar Maiti and I) explored their application for the detection of related cancer cells.

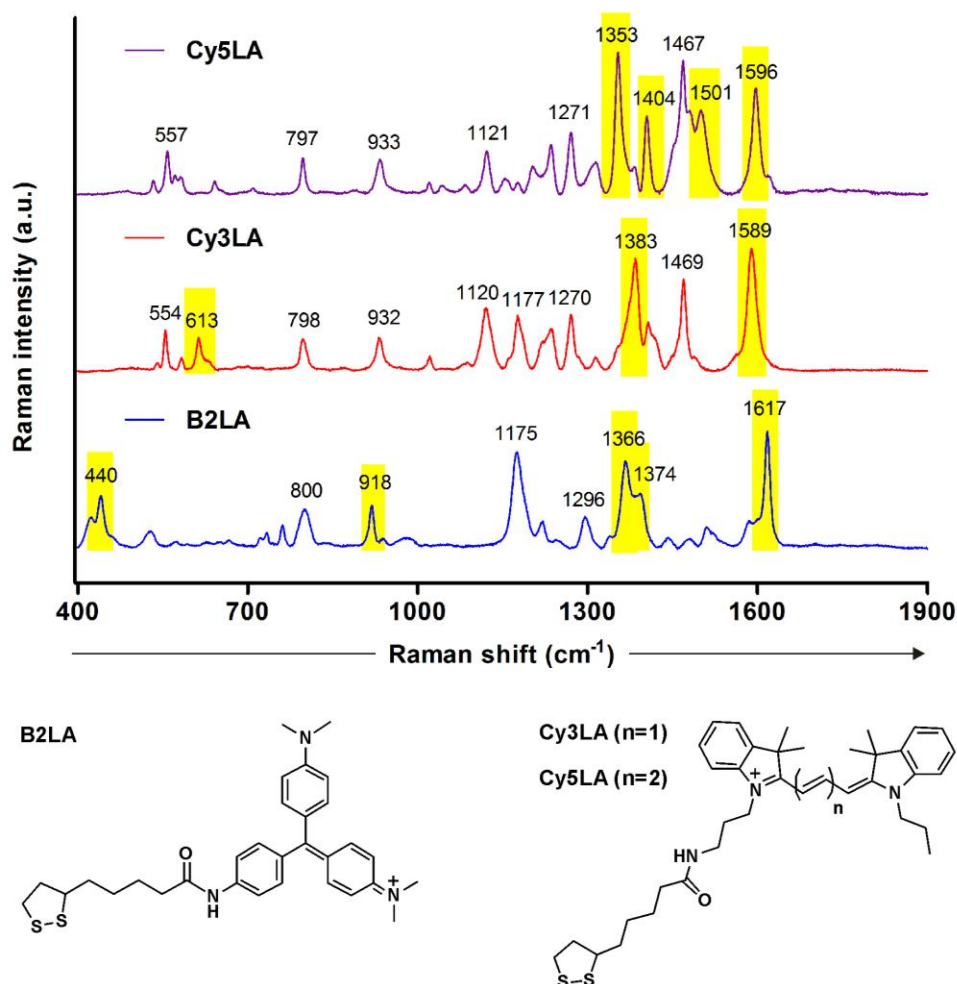


Figure 6.3. Normalized SERS spectra of **B2LA**, **Cy3LA** and **Cy5LA** after chemisorption on AuNPs. Spectra were measured in a Raman microscope (633 nm laser excitation, 6.2 mW laser power, acquisition time: 10s) and plotted as average intensities ($n=3$). The most distinctive peaks from every reporter are highlighted in yellow.

6.3.4 Antibody conjugation and Characterization

After encapsulation, we (Dr. Kaustabh Kumar Maiti and I) conjugated monoclonal antibodies against two different epidermal growth factor receptors (EGFR (Erb-B1) and HER2 (Erb-B2)) to render **B2LA** anti-EGFR and **Cy3LA** anti-HER2 nanotags. EGFR is over-expressed in diverse cancer cells (e.g. OSCC), and HER2 is a well-known breast cancer marker with a high expression in SKBR-3 cells.¹⁸ The antibody conjugation was verified by the appearance of protein

absorption peaks at 280 nm, and the size of the fully functionalized nanotags was determined by transmission electron microscopy (TEM) (Figure 6.4).

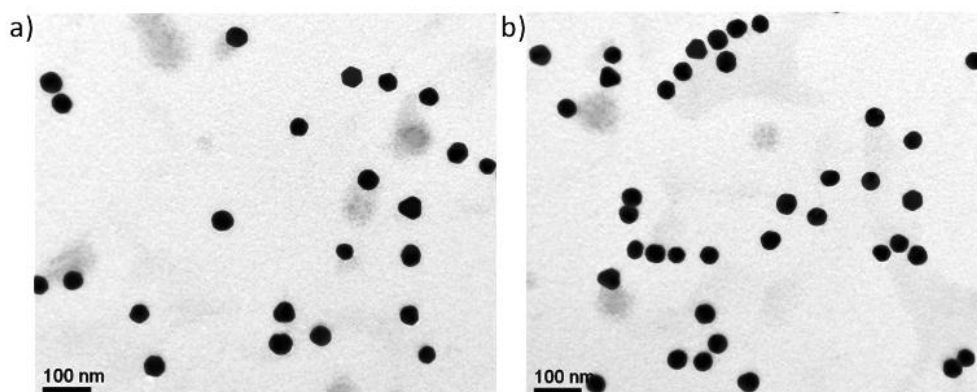


Figure 6.4. Transmission Electron Microscopy (TEM) images of nanotags derivatized with: (a) **B2LA**, (b) **Cy3LA**

6.3.5 Cell SERS studies

In order to examine the multiplex differential recognition of **B2LA** anti-EGFR and **Cy3LA** anti-HER2 nanotags in cells, we (Dr. Kaustabh Kumar Maiti and I) incubated an equal amount of both nanotags in OSCC cells (EGFR-positive and HER2-negative) and SKBR-3 cells (HER2-positive and EGFR-negative). After washings with PBS, the SERS measurement in OSCC cells fully resembled the SERS spectra of **B2LA** (Figure 6.5a) whereas the SERS signal of SKBR-3 cells coincided with the spectra of **Cy3LA** (Figure 6.5b). Moreover, as negative controls, we did not observe significant SERS signals in OSCC or SKBR-3 cells after incubation with antibody-free **B2LA** and **Cy3LA**-nanotags.

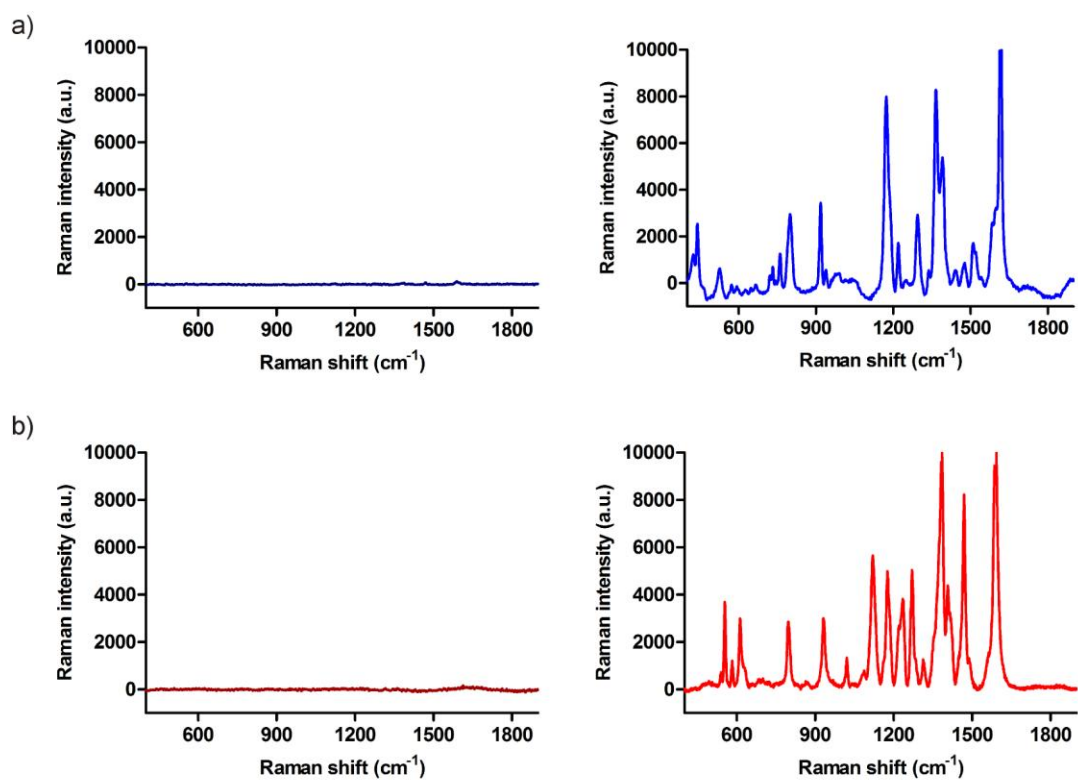


Figure 6.5. (a) SERS spectra of OSCC cells after incubation with antibody-free **B2LA**-nanotags (left) or anti-EGFR **B2LA**-nanotags (right); (b) SERS spectra of SKBR-3 cells after incubation with antibody-free **Cy3LA**-nanotags (left) or anti-HER2 **Cy3LA**-nanotags (right).

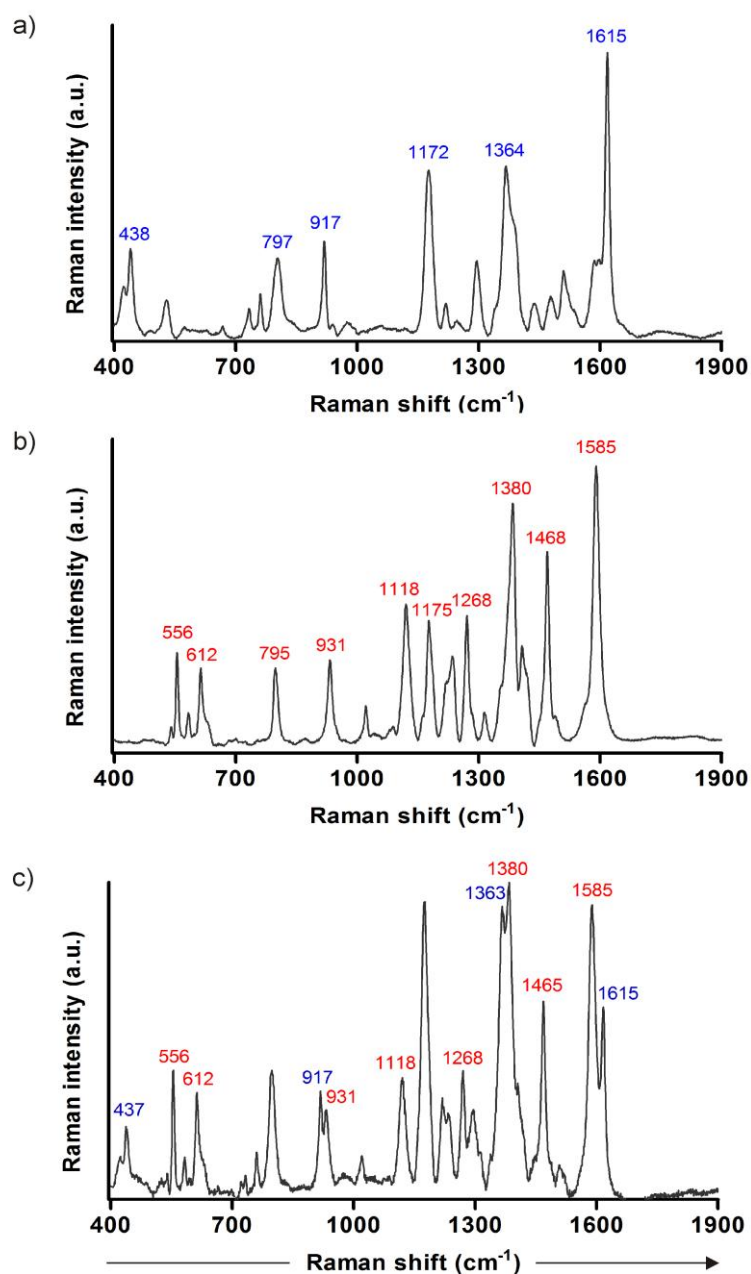


Figure 6.6. Multiplex SERS spectra upon incubation of both **B2LA** anti-EGFR and **Cy3LA** anti-HER2 nanotags with: (a) OSCC cells, (b) SKBR-3 cells, (c) co-cultured cells. Spectra were measured with a Raman microscope (633 nm excitation wavelength, 6.2 mW laser power, acquisition time: 10s) and plotted as average intensities ($n=3$).

Altogether, these results clearly indicated that: 1) **B2LA** anti-EGFR and **Cy3LA** anti-HER2 nanotags specifically recognized OSCC and SKBR-3 cells with non-overlapping SERS peaks, 2) the SERS signals derived from any possible non-specific binding of the two nanotags were negligible. Finally, we demonstrated that

B2LA and **Cy3LA**-nanotags could be used as a multiplex platform by recognizing both OSCC and SKBR-3 cells after they were co-cultured in the same wells. Upon incubation with an equal proportion of both **B2LA** and **Cy3LA**-nanotags, the SERS signals of the co-cultured cells showed clearly separable peaks from the two reporter molecules: 1615, 1363, 917 and 437 cm^{-1} for **B2LA** anti-EGFR, and 1585, 1465, 1380, 1268, 1118, 931, 612 and 556 cm^{-1} for **Cy3LA**- anti-HER2 (Figure 6.6). With this data, we (Dr. Kaustabh Kumar Maiti and I) attested that **B2LA** and **Cy3LA** are fully compatible Raman reporters for the preparation of multiplex SERS nanotags.

6.3.6 Cell SERS mapping

To confirm the recognition properties of **B2LA** anti-EGFR and **Cy3LA** anti-HER2 nanotags and analyze their localization in OSCC and SKBR-3 cells, we performed SERS mapping experiments in both cell lines.

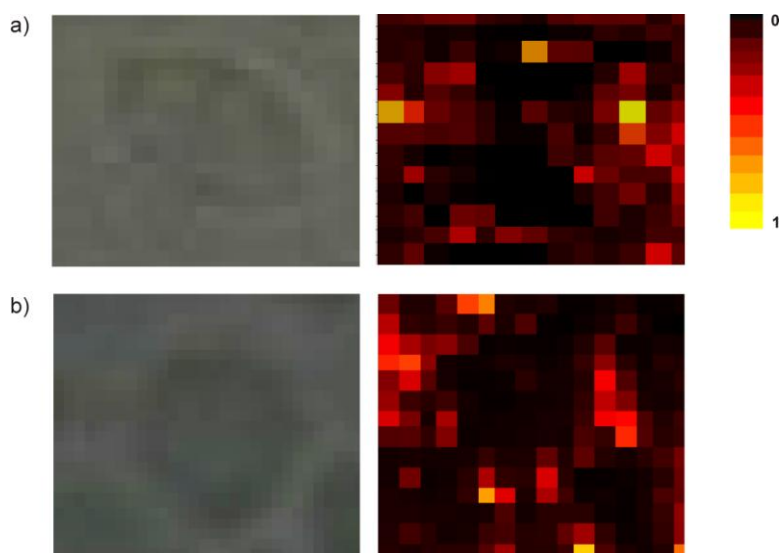


Figure 6.7. Bright field and SERS mapping images of: (a) **B2LA** anti-EGFR nanotag-treated OSCC cells (1615 cm^{-1}), (b) **Cy3LA** anti-HER2 nanotag-treated SKBR-3 cells (1468 cm^{-1}). All mapping images (size: $30 \times 30 \mu\text{m}^2$) were scanned at an interval of $2 \mu\text{m}$ (633 nm excitation wavelength).

As shown in Figure 6.7, images of nanotag-treated OSCC cells and SKBR-3 cells displayed intense SERS signals at two distinguishable frequencies (e.g. 1615

and 1468 cm^{-1} respectively) in the cell surface region. Non-treated OSCC and SKBR-3 cells showed negligible SERS signals at both frequencies (Figure 6.8). These mapping pictures confirmed that the interaction between **B2LA** anti-EGFR and **Cy3LA** anti-HER2 nanotags and their respective receptors was mainly localized at the cell surface, which corresponds well with the high expression of EGFR and HER2 at the plasma membrane of cancer cells.^{19, 20}

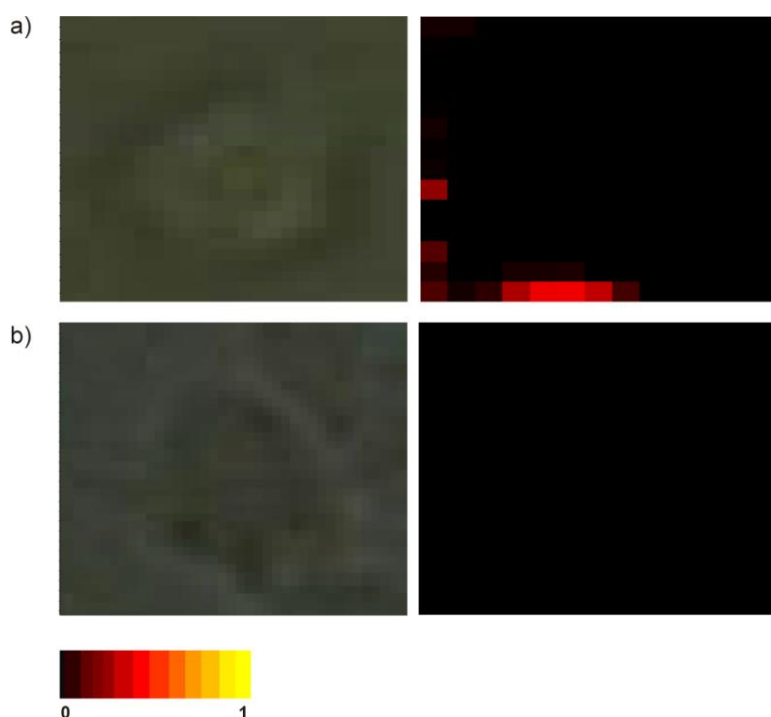


Figure 6.8. Bright field and SERS mapping images of: (a) non-treated OSCC cells (1615 cm^{-1}), (b) non-treated SKBR-3 cells (1468 cm^{-1}). All mapping images (size: $30 \times 30\ \mu\text{m}^2$) were scanned at an interval of $2\ \mu\text{m}$ (633 nm excitation wavelength) and the intensities were normalized between the lowest (0) and the highest color (1).

6.4 Conclusions

In summary, I developed a novel multiplex SERS platform for cancer cell detection based on the combination of triphenylmethine and cyanine Raman reporters. The SERS compatibility under a single excitation wavelength between a selected triphenylmethine and different lipoic acid-containing cyanine reporters was examined. Nanotags derivatized with a selected pair (**B2LA** and **Cy3LA**) were

derivatized with anti-EGFR and anti-HER2 antibodies, and proved to specifically recognize the respective cancer cells (e.g. OSCC and SKBR-3) with non-overlapping SERS peaks. After confirming the performance of these nanotags in co-culture conditions and determining their localization by SERS mapping experiments, we (Dr. Kaustabh Kumar Maiti and I) demonstrated that **B2LA** and **Cy3LA** are fully compatible Raman reporters for the preparation of multiplex SERS nanotags and can be used for the concurrent detection of related cancer cells.

6.5 Experimental details

Materials and Methods: As described earlier Chapter 2 and 5.

6.5.1 Synthesis and characterization of Cy3LA and Cy5LA

Intermediate **1a**, **4b** have been synthesized according previously described in Chapter 2 and Chapter 5.

Synthesis of **5**:

4b (0.38 g, 1 mmol, 1 eq.) and di-tert-butyl dicarbonate (0.55 g, 2.5 mmol, 2.5 eq.) were added to a mixture of dry CHCl_3 (30 mL) and DIEA (0.88 mL, 5 mmol, 5 eq.). The reaction mixture was gently heated to reflux temperature and stirred for 4 h. After that, the organic layer was extracted with Et_2O , dried over anhydrous Na_2SO_4 , and concentrated under reduced pressure. Purification of the crude residue on a silica gel column (elution with CH_2Cl_2 -MeOH 50:1) rendered **5** as a light brown liquid (1.26 g, yield 60%).

$^1\text{H-NMR}$ (300 MHz, CDCl_3): 1.33 (s, 9H), 1.44 (s, 6H), 1.84-1.87 (m, 2H), 2.27(s, 3H), 3.42 (t, 2H, $J = 6.5$ Hz), 3.55 (t, 2H, $J = 7.0$ Hz), 6.52-7.12 (m, 4H). tR: 5.21 min, ESI-MS m/z ($\text{C}_{19}\text{H}_{29}\text{N}_2\text{O}_2^+$) calc: 317.2, found: 317.1.

Synthesis of **6**:

N,N-diphenylformamidin hydrochloride **X**, (0.39 g, 2 mmol, 1 eq.) was condensed with **1a** (0.66 g, 2 mmol, 1 eq.) in a solution of $\text{ACOH}:\text{Ac}_2\text{O}$ (1:1) at 110 °C for 20 min, and cooled down to r.t. Then **5** (1.2 g, 3 mmol, 1.5 eq.) and pyridine were added to the mixture and stirred under reflux. After 1 h, the reaction mixture was poured into water and NaHCO_3 was slowly added with stirring until complete neutralization was reached. After diluting with CH_2Cl_2 the organic layer was washed, dried over anhydrous Na_2SO_4 and concentrated under reduced pressure. Purification of the crude residue on a silica gel column (elution with CH_2Cl_2 -MeOH 50:2) rendered **6** as a blue solid (0.57 g, yield 50%).

ESI-MS m/z ($\text{C}_{33}\text{H}_{44}\text{N}_3\text{O}_2^+$) calc: 528.35, found: 528.2.

Synthesis of 7:

Malonaldehyde bis(phenylimine) hydrochloride **Y**, (0.52 g, 2 mmol, 1 eq.) was condensed with **1a** (0.66 g, 2 mmol, 1 eq.) in a solution of AcOH:Ac₂O (1:1) at 110 °C for 20 min, and cooled down to r.t. Then **5** (1.2 g, 3 mmol, 1.5 eq.) and pyridine were added to the mixture and stirred under reflux. After 1 h, the reaction mixture was poured into water and NaHCO₃ was slowly added with stirring until complete neutralization was reached. After diluting with CH₂Cl₂ the organic layer was washed, dried over anhydrous Na₂SO₄ and concentrated under reduced pressure. Purification of the crude residue on a silica gel column (elution with CH₂Cl₂-MeOH 50:2) rendered **7** as a blue solid (0.66 g, yield 54%).

ESI-MS m/z (C₃₆H₄₈N₃O₂⁺) calc: 554.4, found: 554.2.

Synthesis of Cy3LA and Cy5LA:

For the preparation of **Cy3LA**, **6** (0.10 g, 0.19 mmol) was treated with a solution of TFA-DCM (1:9) at r.t. overnight, washed with a solution of NaHCO₃, and the organic layer was dried over anhydrous Na₂SO₄ and concentrated under reduced pressure. The resulting solid was dissolved in a solution of CH₂Cl₂-CH₃CN (9:1), added to the lipoic acid nitrophenol resin and shaken for 16 h at r.t. After the reaction, the resulting filtrates were combined and dried under pressure to render **Cy3LA** as a blue solid (92 mg, yield 85%). The same procedure was used starting from **7** to obtain **Cy5LA** (95 mg, yield 78%).

Cy3LA: ¹H-NMR (500 MHz, CDCl₃): 1.08 (t, 3H, *J* = 7.0 Hz), 1.69-1.72 (m, 4H), 1.84 (s, 6H), 1.85 (s, 6H), 1.87-1.91 (m, 4H), 2.40-2.44 (m, 2H), 3.08-3.10 (m, 2H), 3.14-3.17 (m, 2H), 3.48-3.52 (m, 2H), 3.58-3.62 (m, 2H), 4.17 (t, 2H, *J* = 7.5 Hz), 4.25 (t, 2H, *J* = 7.5 Hz), 5.29 (s, 3H), 7.06-8.42 (m, 8H), 8.39 (bs, 1H).

¹³C-NMR (126 MHz, CDCl₃): 11.25, 20.97, 25.59, 26.45, 28.08, 28.12 (2C), 28.87(2C), 29.62, 30.85, 34.58, 35.83, 36.45, 40.08, 42.91, 45.89, 53.34, 56.53, 104.43, 110.98, 121.92, 121.99, 125.14, 125.26, 128.75, 128.96, 140.49, 140.55,

141.77, 150.89, 173.62, 173.80, 174.43. tR: 3.98 min, ESI-HRMS m/z ($C_{37}H_{50}N_3O$ S_2^+) calc: 616.3390, found: 616.3388

Cy5LA: 1H -NMR (500 MHz, $CDCl_3$): 1.09 (t, 3H, $J = 7.0$ Hz), 1.59-1.62 (m, 4H), 1.69 (s, 6H), 1.72 (s, 6H), 1.84-1.95 (m, 4H), 2.45-2.49 (m, 3H), 3.08-3.10 (m, 2H), 3.14-3.17 (m, 2H), 3.48-3.52 (m, 2H), 3.58-3.62 (m, 2H), 3.94 (t, 2H, $J = 7.5$ Hz), 4.40 (t, 2H, $J = 7.5$ Hz), 6.17 (d, 2H, $J = 7.2$ Hz), 6.98 (d, 1H, $J = 8.0$ Hz), 7.06-8.42 (m, 8H), 8.61 (bs, 1H).

^{13}C -NMR (126 MHz, $CDCl_3$): 11.43, 20.69, 25.67, 26.78, 28.04, 28.28, 28.89(2C), 28.92 (2C), 30.37, 34.63, 36.12, 36.59, 38.40, 38.76, 43.58, 45.49, 48.83, 49.40, 56.62, 102.74, 106.02, 110.11, 111.44, 122.02, 122.94, 124.55, 125.59, 127.84, 128.97, 140.67, 141.61, 141.82, 142.43, 151.90, 153.85, 171.22, 173.68, 174.47. tR: 4.07 min, ESI-HRMS m/z ($C_{39}H_{52}N_3O$ S_2^+) calc: 642.3546, found: 642.3555.

6.5.2 Nanotags labeling and antibody conjugation

The reporter molecules (**B2LA** and **Cy3LA**, 10 μ M) were incubated with citrate-stabilized Au-colloid for 10 min before the heterofunctional linker HS-PEG- CO_2H (10 μ M) was added to both solutions (volume: 2.6 mL). After shaking for 15 min, the Au-colloid was exposed to excess PEG-SH (1.8 mL, 10 μ M) to maximize the surface coverage and stabilize the PEG and the chemisorbed reporter molecule. After 4 h, free PEG-SH was removed incubation by 3 rounds of centrifugation (4000 rpm, 15 min), and the colloid was re-suspended in PBS for bioconjugation. The carboxylic acids groups were activated with *N*-(3-(dimethylamino)-propyl)-*N'*-ethylcarbodiimide (EDC) (125 nmol) and *N*-hydroxysuccinimide (NHS) (125 nmol). After 30 min incubation, excess of EDC and NHS was removed by 3 rounds of centrifugation (8000 rpm, 10 min), and re-suspended in PBS using Amicon Ultra 3K centrifuge filters (Milipore). The activated particles were then reacted with two different antibodies at 25 $^{\circ}C$ for 2 h and then overnight at 4 $^{\circ}C$: for B2LA nanotags, a

mouse monoclonal anti-EGFR IgG_{2a} (12 nM); for Cy3LA nanotags, a mouse monoclonal anti-HER2. Further non-specific binding chemicals and antibodies were removed by centrifugation (8000 rpm, 10 min) and the final nanotags were re-suspended in PBS and stored at 4 °C.

6.5.3 Thiolated PEG encapsulation

Freshly prepared reporter solutions at different concentrations (e.g. 5 to 30 μM) were mixed with Au colloid in a 1:9 ratio (v/v) to optimize the reporter concentration. Maximum SERS intensities and minimum colloidal aggregation were obtained at 10 μM concentration of reporter. After 10 min incubation, a 100 μM solution of thiolated PEG (PEG-SH, M.W, PEG: 5 kDa) was added in 10 to 20-fold excess and incubated overnight incubation. Excess of PEG-SH was removed by 3 rounds of centrifugation (5000 rpm for 6 min) and re-suspension in water.

6.5.4 SERS measurements of B2LA, Cy3LA and Cy5LA-gold colloid

20 μM solutions of **B2LA**, **Cy3LA** and **Cy5LA** in deionized water were mixed with Au colloid (2.6×10^{10} particles/mL) in a 1:9 ratio (v/v). 20 μL of the reporter-Au colloid mixture solutions were placed on a glass slide with cover slip, and their Raman spectra (range: 400 to 2000 cm^{-1} , resolution: 1 cm^{-1} , acquisition time: 10 s) were measured in a Renishaw InVia Raman microscope under excitation with a 633 nm excitation wavelength laser (6.2 mW power). The results are plotted as average intensities of three independent experiments.

6.5.5 Measurement of SERS spectra and SERS mapping in OSCC, SKBR-3 cells and co-cultured cells

Cell culture:

OSCC and SKBR-3 cells were grown in RPMI1640 medium supplemented with 10% (v/v) fetal bovine serum (FBS) and antibiotics (100 U mL⁻¹ penicillin/100 µg mL⁻¹ streptomycin) in a humidified atmosphere at 37 °C with 5% (v/v) CO₂. Approximately 5 × 10⁵ cells per well were seeded on 12-well culture plates the day before SERS measurements.

Measurement of SERS spectra:

OSCC, SKBR-3 and co-cultures cells were grown as mentioned above in 12-well culture plates. For co-culture experiments, an equal amount (aprox. 5×10⁵ cells) of OSCC and SKBR-3 cells were plated in the same well 24 h before the measurements. Antibody-conjugated **B2LA** and **Cy3LA**-nanotags (450 pM) were incubated with OSCC, SKBR-3 or co-cultured cells for 1 h at 25 °C. Afterwards, the cells were washed with cold PBS (×3), gently scrapped and re-suspended in PBS (every well of a 12 well-plate containing approximately 5×10⁵ cells was re-suspended in 100 µL PBS). Raman experiments were performed in a Renishaw InVia Raman microscope with a laser beam directed to the sample through 20× objective lens and a Peltier cooled CCD detector. Samples were excited with a 633 nm excitation wavelength laser, and Raman spectra were collected in the range of 400 to 2000 cm⁻¹ with 1 cm⁻¹ resolution. Acquisition time for all spectra was 10 s.

SERS mapping Experiments:

For SERS mapping experiments, cells were plated in a 8-well glass slide at a density of 10⁶ cells/mL, and after incubation with antibody-conjugated **B2LA** and **Cy3LA**-nanotags (450 pM) for 1 h at 25 °C, cells were rinsed with cold PBS (×3) and subsequently placed on a cover slip with mounting media. Raman experiments were

performed in a Renishaw InVia Raman microscope with a laser beam directed to the sample through 20× objective lens and a Peltier cooled CCD detector. Samples were excited with a 633 nm excitation wavelength and a laser power of 6.2 mW, and measurements were carried out as raster scans in 2 μm steps over OSCC and SKBR-3 cells with a computer-controlled *xy*-stage.

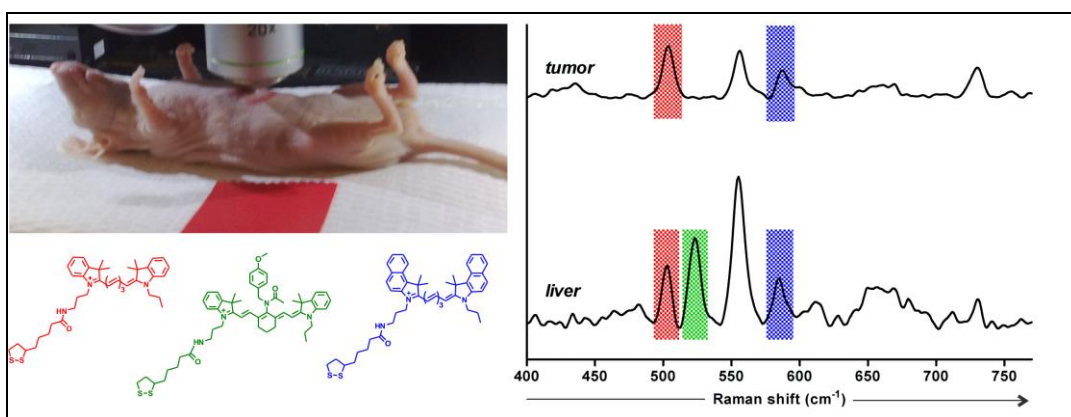
6.6 References

1. C. L. Zavaleta, B. R. Smith, I. Walton, W. Doering, G. Davis, G. B. Shojaei, M. J. Natan and S. S. Gambhir, *Proc. Natl. Acad. Sci. U. S. A.* **2009**, *106*, 13511.
2. X. M. Qian, X. Zhou and S. Nie, *J. Am. Chem. Soc.* **2008**, *130*, 14934.
3. X. Quin, X-H. Peng, D. O. Ansari, Q. Yin-Geon, G. Z. Chen, D. M. Shin, L. Yang, A. N. Young, M. D. Wang, S. Nie, *Nat. Biotechnol.* **2008**, *26*, 83.
4. S. Keren, C. Zavaleta, Z. Cheng, A. de la Zerda, O. Gheysens, S. S. Gambhir, *Proc. Natl. Acad. Sci. U. S. A.* **2008**, *105*, 5844.
5. J. Kneipp, H. Kneipp, B. Wittig, K. Kneipp, *Nanomedicine* **2010**, *6*, 214-226.
6. A. Matschulat, D. Drescher, J. Kneipp, *ACS Nano* **2010**, *6*, 3259.
7. S. J. Cho, Y. H. Ahn, K. K. Maiti, U. S. Dinish, C.Y. Fu, P. Thoniyot, M. Olivo, Y. T. Chang, *Chem. Commun.* **2010**, *46*, 722.
8. K.K. Maiti, U.S. Dinish, C. Y. Fu, J. J. Lee, K. S. Soh, S. W. Yun, R. Bhuvaneswari, M. Olivo, Y. T. Chang, *Biosens. Bioelectron.* **2010**, *26*, 398.
9. K. Jia, Y. Wan, A. D. Xia, S. Y. Li, F. B. Gong, G. Q. Yang, *J. Phys. Chem. A.* **2007**, *111*, 1593.
10. A. Toutchkine, P. Nalbant, K. M. Hahn, *Bioconjugate Chem.* **2002**, *13*, 387.
11. H. J. Gruber, G. Kada, B. Pragl, C. Riener, C. D. Hahn, G. S. Harms, W. Ahrer, T. G. Dax, K. Hohenthanner, H. G. Knaus, *Bioconjugate. Chem.* **2000**, *11*, 161.
12. A. Iqbal, L. Wang, K. C. Thompson, D. M. J. Lilley and D. G. Norman, *Biochemistry* **2008**, *47*, 7857.
13. M. Gellner, K. Kompe, S. Schlucker, *Anal. Bioanal. Chem.* **2009**, *394*, 1839.
14. B. Chipon, G. Clave, C. Bouteiller, M. Massonneau, P. Y. Renard, A. Romieu, *Tetrahedron Lett.* **2006**, *47*, 8279.
15. C. Bouteiller, G. Clave, A. Bernardin, B. Chipon, M. Massonneau, P. Y. Renard, A. Romieu, *Bioconjugate Chem.* **2007**, *18*, 1303.
16. A. Toutchkine, D. V. Nguyen, K. M. Hahn, *Bioconjugate Chem.* **2007**, *18*, 1344.

17. J. W. Lee, Y. Q. Louie, D. P. Walsh, Y. T. Chang, *J. Comb. Chem.* **2003**, *5*, 330.
18. H. Zhang, A. Berezov, Q. Wang, G. Zhang, J. Drebin, R. Murali, M. I. Greene, *J. Clin. Invest.* **2007**, *117*, 2051.
19. P. Monaghan, M. G. Ormerod, M. J. O'Hare, *Int. J. Cancer* **1990**, *46*, 935.
20. W. Ueda, S. Wang, N. Dumont, J. Y. Yi, Y. Koh, C. L. Arteaga, *J. Biol. Chem.* **2004**, *279*, 24505.
21. J. W. Lee, Y. Q. Louie, D. P. Walsh, Y. T. Chang, *J. Comb. Chem.* **2003**, *5*, 330.

CHAPTER 7

MULTIPLEX TARGETED IN VIVO CANCER DETECTION USING SENSITIVE NIR SERS NANOTAGS



7.1 Introduction

SERS offers high spectral sensitivity as well as a multiplexing capability that makes it a promising tool for many bio-analytical applications. The multiplexing capability of SERS nanotags exists due to narrow bandwidths of the Raman spectra of the reporter molecules and provides the opportunity for the simultaneous recognition of closely related targets.¹⁻³ The recent high demand for a sensitive and simultaneous detection of multiple targets *in vivo* has led the researchers to use nanoparticle (NPs) based on SERS technique.⁴⁻¹⁰ In most cases, such sensing modality is realized by anchoring strong Raman active molecule (reporter molecule, RM) on to the surface of metal NPs, which can be further conjugated with molecular recognition motifs to render specific targeting.¹¹⁻²⁰ Such nanoprobe are termed as SERS nanotags and its sensitivity inherently depends on the Raman reporter molecules. SERS nanotags have shown significant advantages over conventional fluorescence-based NPs such as quantum dots.^{12, 21-22} Quantum dots have shown great potential as *ex vivo* multiplex imaging probes but they possess several limitations such as i) limited availability at NIR region,^{1,22} ii) stability and photobleaching^{22,23}, iii) spectral overlapping^{1,22} and iv) cytotoxicity.^{1,12,22,24} The use of gold NPs (AuNP) in SERS nanotags provides the advantage of low toxicity among others.

Previously, highly Raman active molecules such as crystal violet (CV) and malachite green isothiocyanate (MGITC), rhodamine-6G, Nile blue, 2-naphthalenethiol, TRITC (tetramethylrhodamine-5-isothiocyanate) and polymethine cyanine core molecules such as Cy3, Cy5 and DTTC (3,3'-diethyl-thiatricarbocyanine) have been used as reporters for the development of SERS nanotags.^{12,25-28} However, one of the limitations of the SERS nanotags for *in vivo* applications is the limited availability of sensitive reporter molecules, that are strongly active at NIR regions. To address this problem, previously in Chapter 5 I demonstrated that **CyNAMLA-381** among 80-member tricarboyanine library

showed a 12-fold higher sensitive compared to the standard DTTC.²⁹ SERS-nanotags constructed with **CyNAMLA-381** have been successfully demonstrated for ultrasensitive detection of tumors *in vivo*.

One of the key advantages of SERS is its multiplexing potential, which is yet to be fully explored mainly due to the limited number of available ultrasensitive RMs. *In vitro* multiplexing in cell lines using SERS nanotags constructed with commercial RMs has been also recently studied.³⁰ Based on this approach, I also proved in Chapter 6 that the polymethine cyanine dyes (**Cy3LA**, **Cy5LA**) can be a multiplex partner to the triphenylmethine core (**B2LA**). In addition, the applicability of polymethine cyanine dyes as a multiplex partner in cancerous cells clearly indicates the potential to identify the various tumors *in vivo*.

7.2 Objectives

In this chapter, I synthesized a highly Raman active NIR Raman reporter-set (**Cy7LA** and **Cy7.5LA**) as a Raman multiplex partner compatible with **CyNAMLA-381** which was selected as a most sensitive RMs in Chapter 5. For the demonstration of the *in vivo* multiplexing capability, we (Dr. Kaustabh Kumar Maiti, Dr. U.S. Dinish and I) injected an equal amount of bio conjugated nanotags (**CyNAMLA-381**, **Cy7LA** and **Cy7.5LA**) through the tail vein of a mouse bearing tumor xenograft for the demonstration of targeted multiplex sensing of cancer in mouse model. Moreover, we also reported the kinetic of the SERS probes over several days, demonstrating the possibility of *in vivo* pharmacokinetic study.

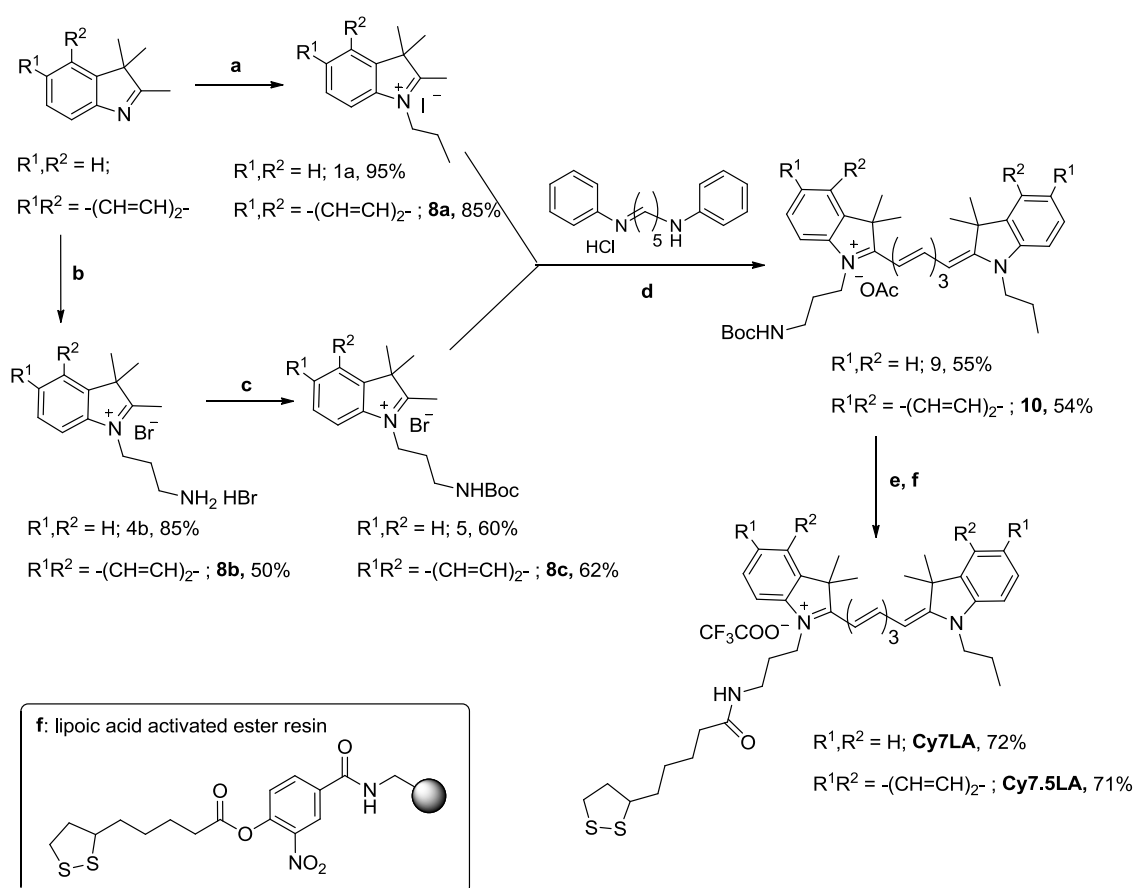
7.3 Results and Discussion

7.3.1 Design and synthesis of NIR Raman reporters

I applied a lipoic acid (LA) linker strategy to NIR dyes **Cy7** and **Cy7.5** to form two new RMs (**Cy7LA** and **Cy7.5LA**) that could be chemisorbed onto Au-NPs for SERS studies.³¹⁻³² I first prepared the scaffold **9** and **10** with an aminopropyl

linker (Scheme 7.1). The Boc-protected aminopropyl group of **9** and **10** was synthesized by established synthetic protocol followed by treatment with an optimized trifluoroacetic acid (TFA)-dichloromethane (DCM) (1:9) solution.³³ The amine intermediates then reacted with activated ester resin of lipoic acid to yield target compounds **Cy7LA** and **Cy7.5LA** with an average purity of 90%.

Scheme 7.1. Synthesis of lipoic acid-containing amine acetylated tricarbocyanines (**Cy7LA** and **Cy7.5LA**).



Reagents and conditions: (a) 1-iodopropane, CH₃CN, 80 °C, 12 h; (b) 3-Bromopropylamine hydrobromide, 120 °C, 12 h; (c) Di-tert-butyl dicarbonate, DIEA, CHCl₃, reflux, 4 h; (d) AcOH, Acetic anhydride, pyridine, 110 °C; (e) TFA-DCM (1:9), r.t., 15 h; (f) lipoic acid activated ester resin, CH₂Cl₂, r.t., 15 h.

7.3.2 SERS measurement of NIR Raman reporters

UV-Vis absorption studies (Figure 7.1) confirms that these compounds are ideally suitable for NIR excitation. The maximum absorption wavelengths of these compounds are found to be at 795, 745 and 780 nm cm^{-1} for **CyNAMLA-381**, **Cy7LA** and **Cy7.5LA** respectively.

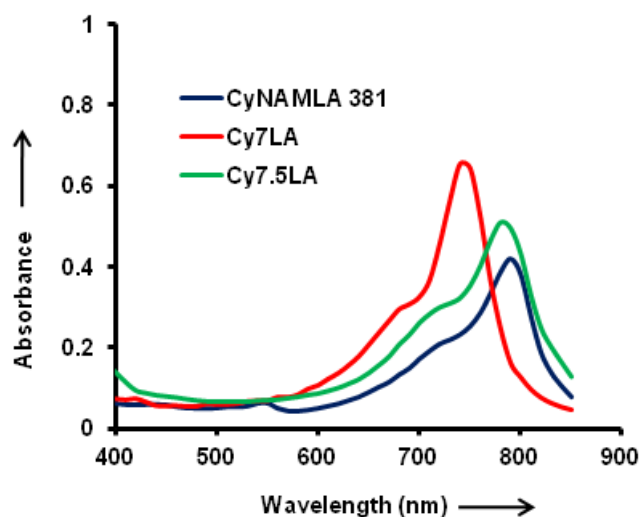


Figure 7.1. UV-Vis absorption of **Cy 7LA**, **Cy 7.5LA** and **CyNAMLA-381**(10 μM) in PBS buffer (pH 7.3) with 1% DMSO.

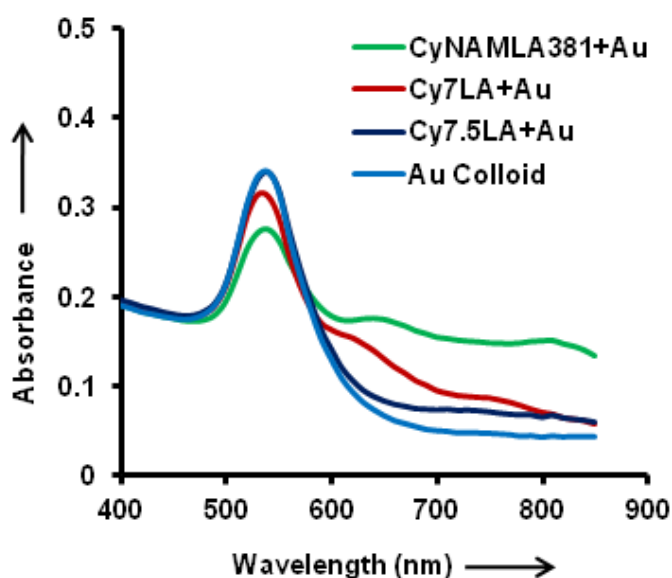


Figure 7.2. Surface plasmon absorption spectra of **Cy 7LA**, **Cy 7.5LA** and **CyNAMLA-381**(10 μM) in Au colloid (citrate buffer) with 1% DMSO.

SERS properties of RMs were studied with 785 nm laser excitation after anchoring them onto citrate-stabilized 60 nm AuNPs. The plasmon resonance spectra of Au colloid and Au-Cy7LA, Au-Cy7.5LA and Au-CyNAMLA-381 conjugate are shown in Figure 7.2. The clean spectra confirm that no aggregation occurred in the colloidal nanotags. Among the tested candidate dyes, Cy7LA and Cy7.5LA showed strong SERS signal in NIR range comparable to CyNAMLA-381 (Figure 7.3). SERS spectra of other two compounds are in the Figure 7.4

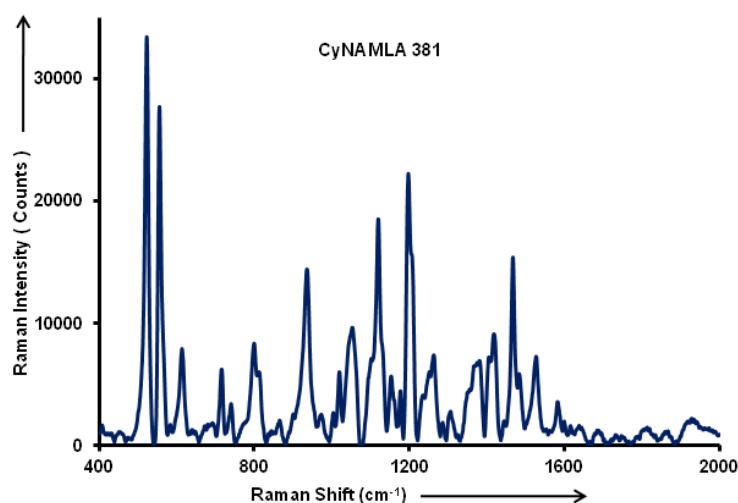


Figure 7.3. Normalized SERS spectra of **CyNAMLA 381** after chemisorption on AuNPs. Spectra were measured in a Raman microscope (785 nm laser excitation, acquisition time: 10s) and plotted as average intensities ($n=3$).

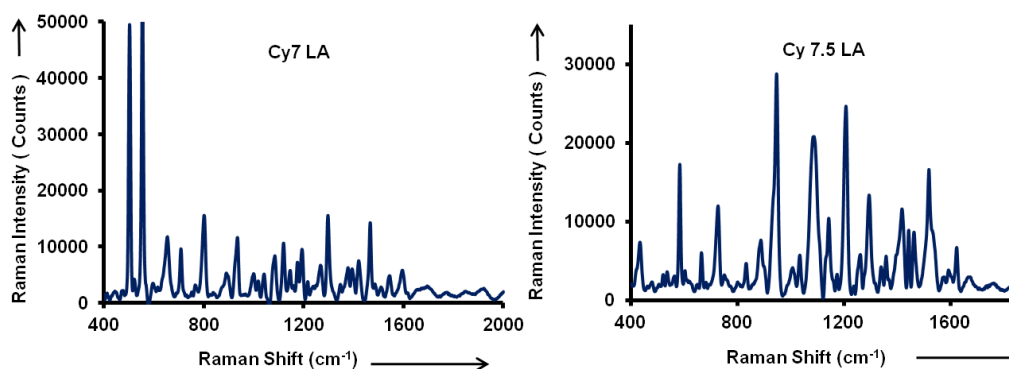


Figure 7.4. Normalized SERS spectra of **Cy7 LA** and **Cy7.5LA** after chemisorption on AuNPs. Spectra were measured in a Raman microscope (785 nm laser excitation, acquisition time: 10s) and plotted as average intensities ($n=3$).

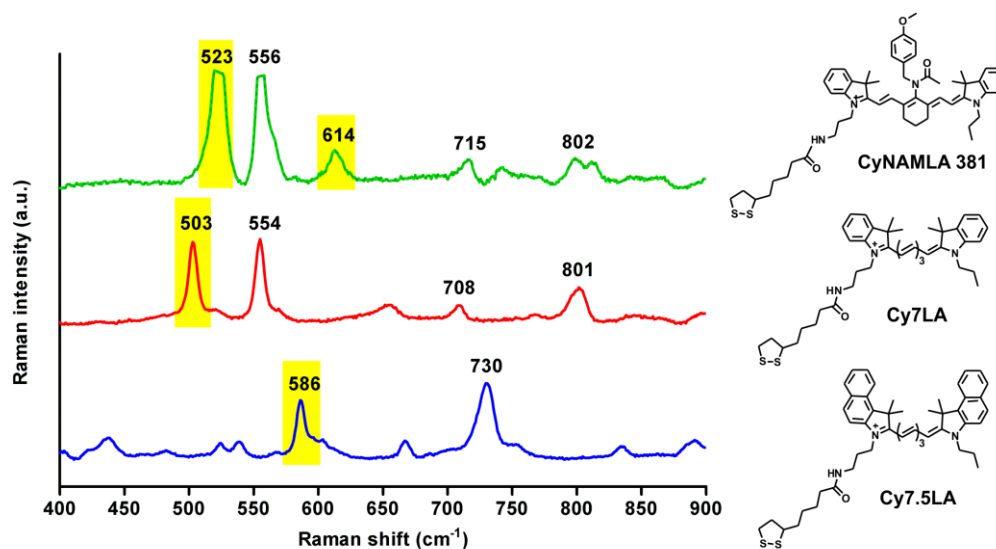


Figure 7.5. Normalized SERS spectra of **CyNAMLA-381**, **Cy7LA** and **Cy7.5LA** after chemisorption on AuNPs. Spectra were measured using a Raman microscope (785 nm laser excitation, 30 mW laser power, acquisition time: 10s) and plotted as average intensities ($n=3$). The most distinctive peaks from each reporter are highlighted in yellow.

As shown in Figure 7.5, the SERS signals exhibited characteristic Raman peaks for every RM that that could be monitored in a multiplex mode (503 cm^{-1} for **Cy7LA**; 586 cm^{-1} for **Cy7.5LA** and $523, 614\text{ cm}^{-1}$ for **CyNAMLA-381**). The relative SERS enhancement of the three nanotags was calculated from the highest intensity Raman peak for each nanotags, 523 cm^{-1} for **CyNAMLA-381**, 556 cm^{-1} for **Cy7LA** and 949 cm^{-1} for **Cy7.5LA**. It was found that **Cy7LA**-nanotag showed about 1.5 times higher intensity than **CyNAMLA-381** nanotag while intensity of **Cy7.5LA** nanotag was about 0.76 times lower than **CyNAMLA-381** nanotag (Figure 7.3 & Figure 7.4).

7.3.2 Signal stability of SERS nanotags

These NPs-RM complexes were further encapsulated using bovine serum albumin (BSA) and glutaraldehyde as a cross-linking agent. Such encapsulation can help in preventing the aggregation and desorption of RMs from the NPs, and provided

the functional groups on their surface for further bioconjugation.^{26, 34-37} The excess glutaraldehyde was removed by treatment with glycine treatment. The long-term stability of SERS-signals of **CyNAMLA-381**, **Cy7LA** and **Cy7.5LA**-AuNPs was studied for a period of one month. SERS intensities of the highest Raman peaks (i.e. 523 cm^{-1} for **CyNAMLA-381**, 503 cm^{-1} for **Cy7LA** and 949 cm^{-1} for **Cy7.5LA**) obtained from 5 independent measurements taken from the same sample at different time and used to monitor the stability of these nanotags. Remarkably, these nanotags did not show any significant aggregation and exhibited stable SERS intensities over time, with a very low relative standard deviation of ~5% as shown in Figure 7.6. As evident from Figure 7.7, transmission electron microscopy (TEM) revealed that the size of these nanotags was around 65 nm. The observed 5 nm increment in size is attributed to the BSA layer encapsulation.

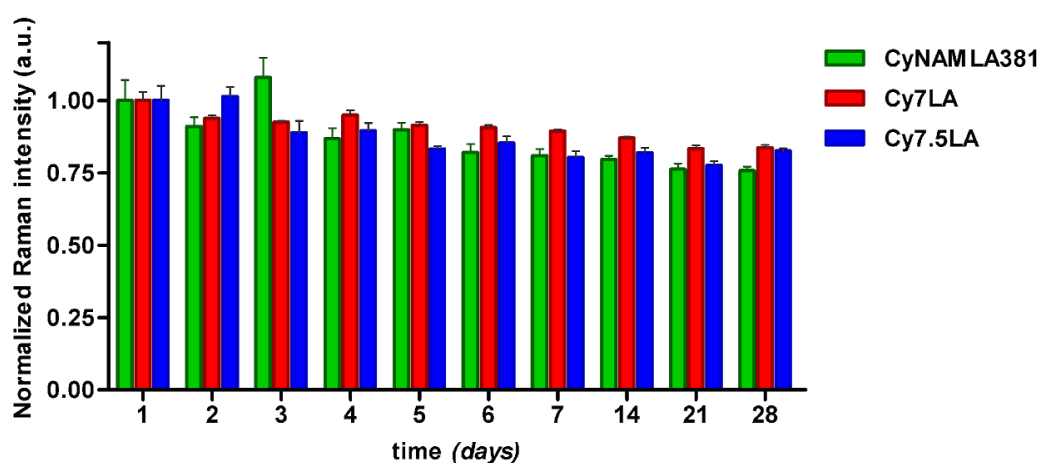


Figure 7.6. Time course SERS measurement of three nanotags. SERS intensities of the highest Raman peaks (i.e. 523 cm^{-1} for **CyNAMLA-381**, 503 cm^{-1} for **Cy7LA** and 949 cm^{-1} for **Cy7.5LA**), are plotted as means \pm standard deviation of 5 independent measurements taken from the same sample at different time points.

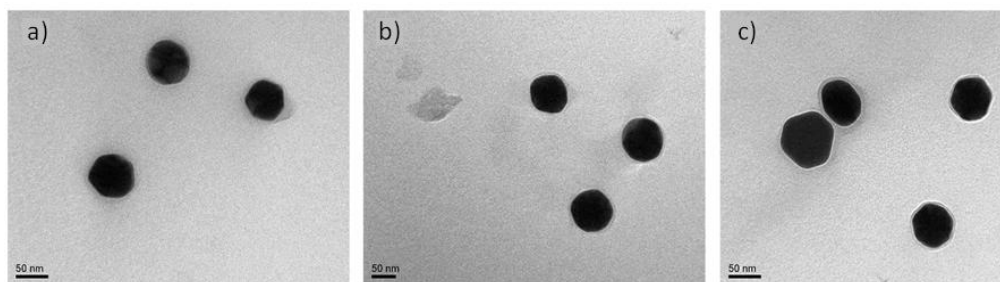


Figure 7.7. Transmission electron microscopy (TEM) images of: a) BSA-encapsulated **CyNAMLA-381** nanotag, b) BSA-encapsulated **Cy7LA** nanotag, c) BSA-encapsulated **Cy7.5LA** nanotag; Scale bar: 50 nm.

7.3.4 SERS multiplex detection in liver and tumor site

To demonstration of the multiplexing capability *in vivo*, we (Dr. Kaustabh Kumar Maiti and Dr. U.S. Dinish and I) injected three BSA encapsulated nanotags (**CyNAMLA-381**, **Cy7LA** and **Cy7.5LA**) in equal amount through the tail vein of xenografts mouse model. SERS measurements were performed 5 h after the injection by focusing the laser beam on the desired anatomical region (e.g. liver) through the skin. The measured spectra displayed a combination of the three individual spectrums from three nanotags and clearly revealed the distinct Raman shift corresponding to each RMs as shown in Figure 7.8. The Raman shift at 503 cm^{-1} was originated from **Cy7LA** while 523 cm^{-1} and 586 cm^{-1} were contribution of **CyNAMLA-381** and **Cy7.5LA** respectively.

After the successful demonstration of the multiplex detection in liver, we focused on targeted sensing using a xenograft tumor model from OSCC cells (oral squamous cell carcinoma) with a high expression of EGFR and low expression of Her 2 receptor. We (Dr. Kaustabh Kumar Maiti and I) prepared two SERS nanotag probes using **Cy7LA** and **Cy7.5LA** as reporter and conjugated with monoclonal anti-EGFR antibody while a third nanotag used **CyNAMLA-381** as a reporter and was conjugated to an anti-Her 2 antibody as negative control. We (Dr. Kaustabh Kumar Maiti and Dr. U.S. Dinish and I) measured the SERS spectra from the tumor site 5 h after injection of equal amount of all three nanotags. The measured SERS spectra

resembled a clear combination of **Cy7LA** and **Cy7.5LA** peaks, with no observation of the characteristic peak at 523 cm^{-1} from **CyNAMLA-381** (Figure 7.9). This data clearly indicated the selective accumulation of the two anti-EGFR antibody conjugated SERS nanotags (**Cy7LA** and **Cy7.5LA**) in the tumor. Furthermore, we measured the SERS signal from the liver site and found that the spectra contained the characteristic peaks from all three nanotags. Moreover, no SERS signal was detected from other anatomical regions (e.g. upper dorsal region).

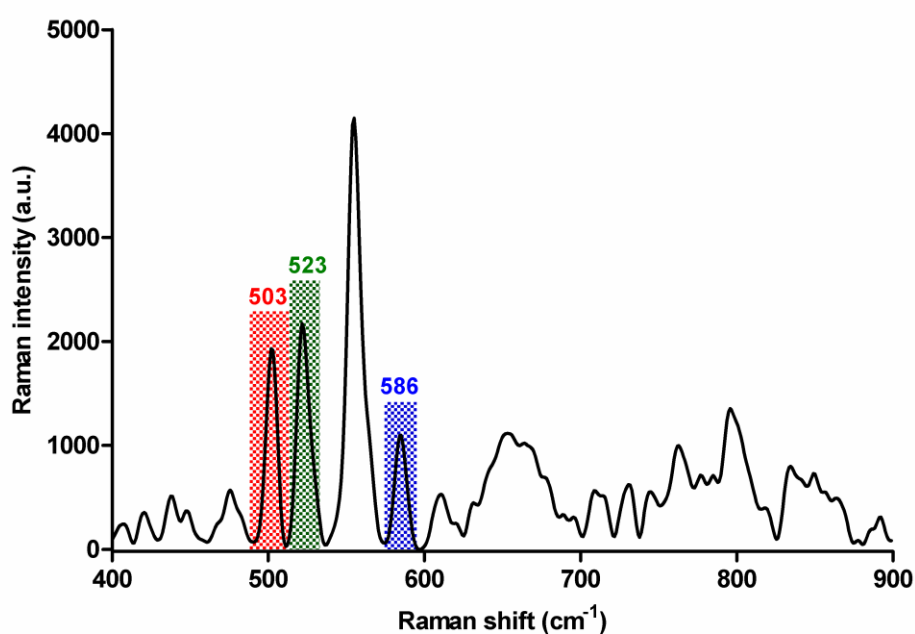


Figure 7.8. Multiplex SERS detection from liver site. Peaks at 503 cm^{-1} corresponds to **Cy7LA** (red shade); 523 cm^{-1} corresponds to **CyNAMLA-381** (green shade); 586 cm^{-1} corresponds to **Cy7.5LA** (blue shade). SERS spectra obtained with 785 nm laser excitation at 30 mW power and integration time 20s.

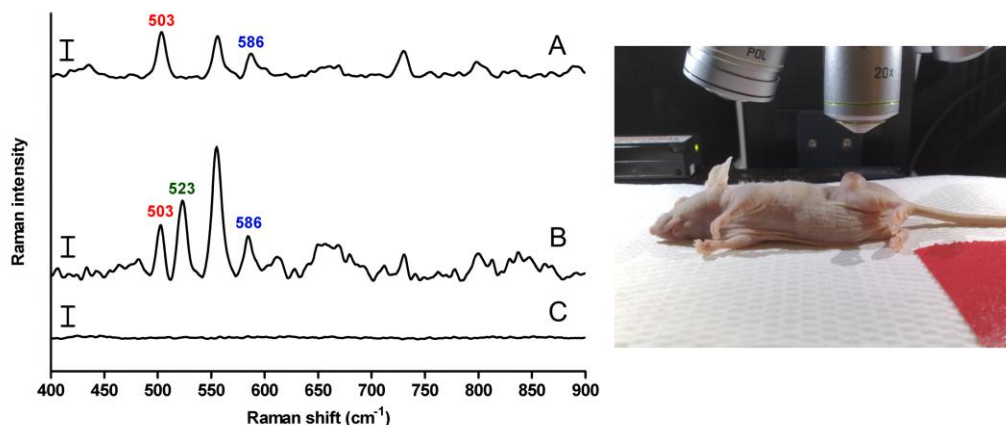


Figure 7.9. *In vivo* multiplex detection in xenograft tumor: A:- SERS spectra from tumor site (peaks obtained at 503 and 586 cm^{-1} from two EGFR positive nanotags, **Cy7LA** and **Cy7.5LA**); B:- SERS spectra from liver site (peaks obtained at 503, 523 and 586 cm^{-1} from two EGFR nanotag **Cy7LA**, **Cy7.5LA** and anti-HER2 nanotag **CyNAMLA-381**); C:- SERS spectra from dorsal region. SERS spectra were obtained at 785 nm laser excitation at 30 mW power and integration time 20 s. Scale bar: 2000 cps.

We also repeated the experiment with another combination of antibodies with **Cy7LA** and **CyNAMLA-381** nanotags conjugated to anti-EGFR antibody and **Cy7.5LA** nanotag conjugated to anti-Her2 antibody. The SERS measurements from tumor site revealed the presence of **Cy7LA** and **CyNAMLA-381** nanotags only and again all three nanotags were identified at the liver site (Figure 7.10).

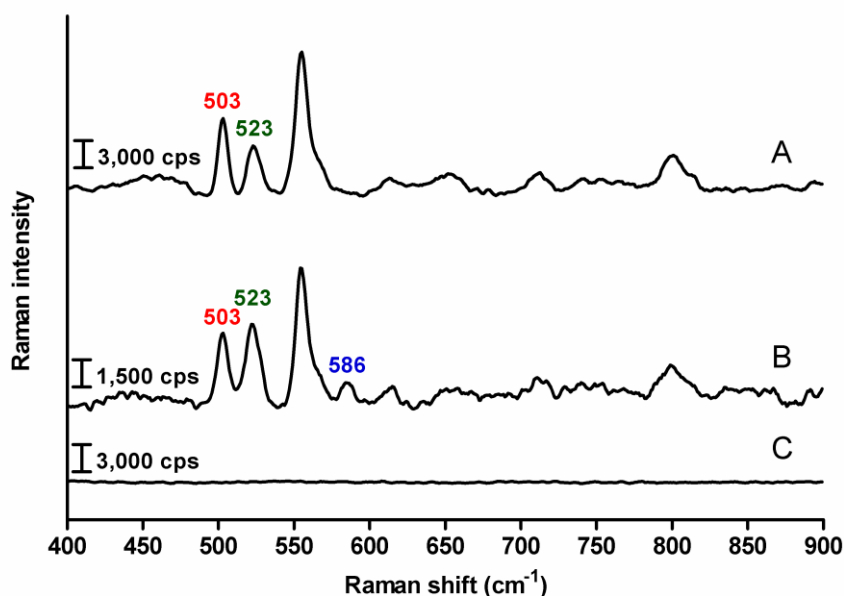


Figure 7.10. *In vivo* multiplex detection of xenograft tumor: A:- SERS spectra from tumor site (peaks obtained at 503 and 523 cm^{-1} from two EGFR positive nanotag **Cy7LA** and **CyNAMLA-381**); B:- SERS spectra from liver site (peaks obtained at 503, 523 and 586 cm^{-1} from two anti-EGFR nanotag **Cy7LA**, **CyNAMLA-381** and anti-HER2 nanotag **Cy7.5LA**); C. SERS spectra from dorsal region. SERS spectra were obtained at 785 nm laser excitation at 30 mW power and integration time 20 s. Scale bar: 2000 cps.

7.3.5 *In vivo* SERS mapping experiment

The previous experiments confirmed that the specificity of the prepared nanotags. The selective targeting was totally independent of the RMs, and simply relied on the recognition of receptors by the antibodies conjugated to the nanotags. SERS mapping can reveal the localization and distribution of every functionalized nanotag.^{30, 38-39} Hence, we performed mapping experiment at tumor and liver sites (area: $600 \times 400 \mu\text{m}^2$) using the above combination of nanotags (**CyNAMLA-381** & **Cy7LA** as anti-EGFR and **Cy7.5LA** as anti-HER2). We confirmed the selective targeting of anti-EGFR nanotags in the tumor (Figure 7.11a and 7.11b, right column) and concurrent passive localization of all three nanotags in liver (Figure 7.11a, b, c, left column). The SERS mapping results confirms that the two anti-EGFR nanotags were distributed more or less uniformly throughout the tumor area and confirmed the

absence of any non-specific binding of the anti-HER2 nanotags in the tumor location (Figure 7.11c right column).

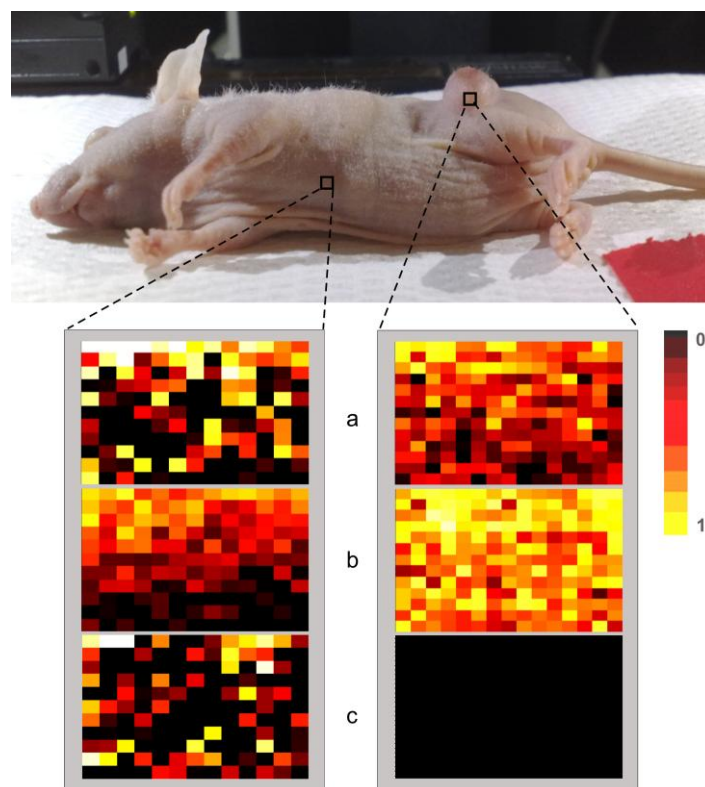


Figure 7.11. Multiplex SERS mapping images: Left column from liver site and right column from tumor site. (a:- mapping corresponding to peak 523 cm^{-1} for **CyNAML-381**; b:- mapping corresponding to peak 503 cm^{-1} for **Cy7LA** and c:- mapping for the peak at 586 cm^{-1} for **Cy7.5LA**). Intensities were normalized.

7.3.6 Determination of detection limit

The determination of limit of detection (LOD) provides an understanding about the sensitivity of the constructed nanotag.⁴⁰ To measure the LOD, we chose **Cy7LA**-nanotag as a representative candidate and we examined its concentration dependent *in vitro* SERS measurement of anti-EGFR conjugated nanotag in a suspension OSCC cells. We observed that the intensity of the Raman peaks increased in a dose dependent manner with an estimated LOD around 54 pM (Figure 7.12).

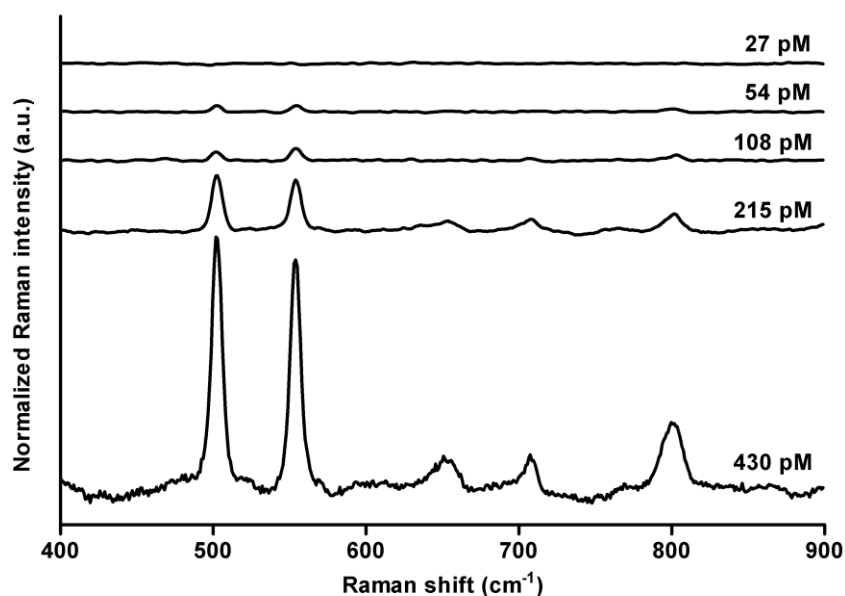


Figure 7.12. Normalized SERS spectra of EFGR-labeled **Cy7LA**-nanotag at different concentrations, 430, 215, 108, 54 and 27 pM.

7.3.7 Time-course distribution of SERS nanotags

We also studied the time-course distribution of these SERS nanotags in tumor and liver, taking advantage of the long-term stability and multiplexing capabilities. We monitored the SERS intensity for a period of 8 days at tumor sites after injection of **CyNAMLA-381** and **Cy7LA** anti-EGFR nanotags as and anti-HER2 **Cy7.5LA** nanotags. We could observe that SERS intensity from 503 and 523 cm^{-1} peaks in tumor site increased up to 24 h and then remained more or less stable for 8 days, which indicates that the nanotags are highly specific and stable over a period of time (Figure 7.13). On the other hand, SERS intensities from all three nanotags showed a gradual decrease after 48 h in liver site and then sharp fall to marginal level in 8 days. Our observation suggests that these nanoparticles might have been excreted through the fecal pathway, which agrees with the report on the excretion of BSA encapsulated Au-NPs.⁴¹⁻⁴² Also, RES (reticuloendothelial system) of the body can also function to phagocytose these nanoparticles types of nanoparticles, which is later moved into liver and generally excreted as feces with bile.⁴² The relatively easy clearance of our

nanotags from the liver and their excellent sensitivity, stability and tumor specificity validates their potential as a promising *in vivo* theragnostic probes.

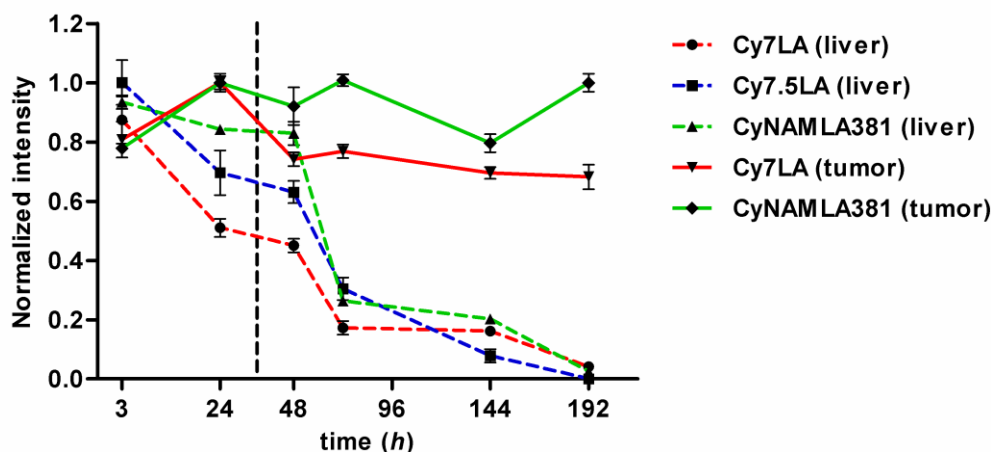


Figure 7.13. Kinetics study of nanotags in tumor and liver site with normalized intensity of 503 cm^{-1} for Cy7LA, 523 cm^{-1} for CyNAMLA-381 and 586 cm^{-1} for Cy7.5LA nanotags. Spectra were measured and plotted as average intensities ($n=3$) with error bar denoting relative standard deviation.

7.4 Conclusions

In summary, we report two new lipoic acid-containing NIR active tricyanocyanine Raman reporters (Cy7LA and Cy7.5LA) as multiplex partner of our previously discovered CyNAMLA-381 for *in vivo* multiplex targeted imaging. We have successfully demonstrated the selective *in vivo* multiplex targeted detection and this study may help to design sensitive nanoprobe for the simultaneous detection of multiple diseases. Furthermore, we studied the time-course distribution and localization of these nanotags in tumor and liver over a period of 8 days. The SERS intensity from targeted nanotags in tumor was stable for relatively long-term while their intensity in the liver decrease steadily after 2 days, which indicates the possible excretion via fecal pathway. This study will accelerate the design of biocompatible SERS nanoprobe for *in vivo* imaging application in the near future.

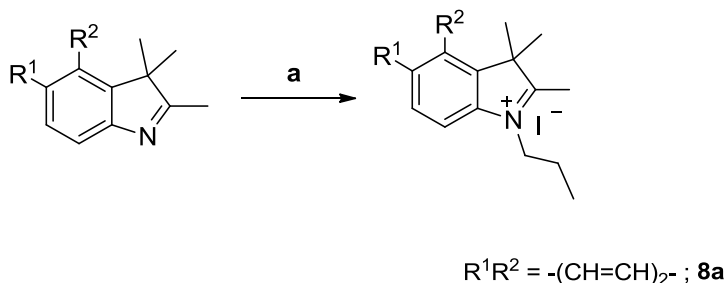
7.5 Experimental details

Materials and methods: As described earlier Chapter 2 and 5.

7.5.1 Synthesis of Cy7LA and Cy 7.5LA

Synthesis of 8a.

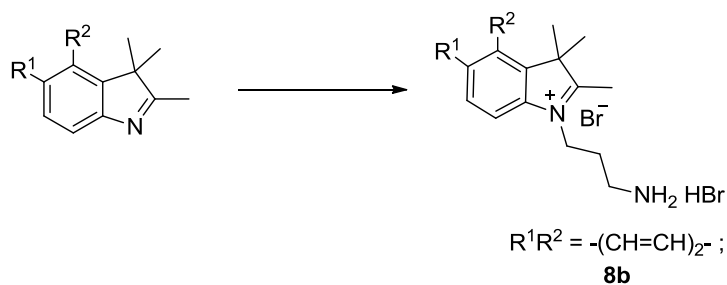
Scheme 7.2 Synthesis of 8a.



1-Iodopropane (4 g, 24 mmol, 5 eq) was added to the solution of 1,1,2-trimethyl-1H-benz[e]indole (1 g, 4.8 mmol, 1 eq) in ACN and refluxed for 15 hour. The reaction mixture was cooled down to r.t and concentrated under reduced pressure to get solid residue which was washed by ether for several time and recrystallized from methanol solution. tR: 2.62 min, ESI m/z ($C_{18}H_{22}N^+$) calc: 252.2; found: 252.1. 1H -NMR (300 MHz, DMSO- d_6): 1.02 (t, 3H, J= 7.2 Hz), 1.76 (s, 6H), 1.90-1.97 (m, 2H), 2.95 (s, 3H), 4.57 (t, 2H, J=7.8 Hz), 7.70-8.20 (m, 6H). (6.1 g, yield 85%)

Synthesis of 8b:

Scheme 7.3. Synthesis of 8b

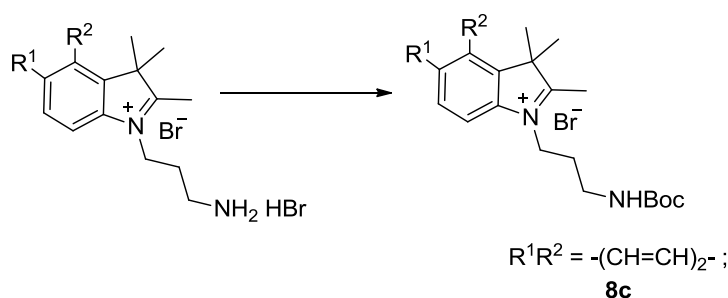


Reagents and conditions: 3-Bromopropylaminehydrogenbromide, 1,2-dichlorobenzene, 110 °C, 12 h.

3-Bromopropylaminehydrogenbromide (1.1 g, 4.7 mmol) was added slowly to a stirred solution of 1,1,2-trimethyl-1H-benz[e]indole (1 g, 4.7 mmol) in 1,2-dichlorobenzene at 110 °C. The reaction mixture was stirred for overnight at 110 °C after complete addition. The solution was decanted and washed with ether solution to obtain a solid compound. The solid was recrystallized in methanol to give 1 g (53%) as a white solid. tR: 2.34 min ESI m/z (C₁₈H₂₄BrN₂⁺) calc: 267.2; found: 267.1. ¹H-NMR (300 MHz, DMSO-d₆): 1.34 (s, 6H), 1.74-1.77 (m, 2H), 2.92 (s, 3H), 4.47 (t, 2H, J=7.8 Hz), 7.70-8.20 (m, 6H). (1 g, yield 50%).

Synthesis of 8c:

Scheme 7.4. Synthesis of 8c

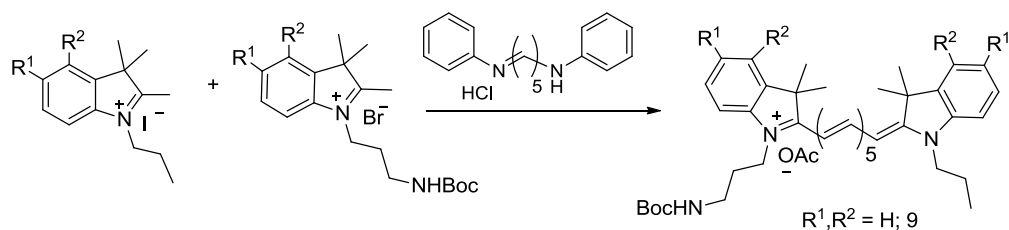


Reagents and conditions: Boc₂O, DIEA, CHCl₃, 60 °C, 4 h.

The solid crude **8b** (0.5 g, 1.1 mmol) was dissolved in CHCl₃ in presence of *N,N'*-Diethylisopropylamine (0.8 ml, 4.5 mmol) and the reaction mixture was refluxed for 4 h after addition of Di-*tert*-butyl dicarbonate (0.36 g, 1.65 mmol). After that the reaction mixture was washed with 0.1 N HCl (5 x 100mL), water (5 x 100 mL) and dried over Na₂SO₄. The organic solution was removed under reduced pressure to obtain an oily reddish color compound. Purification of the crude residue on a silica gel column (elution with CH₂Cl₂-MeOH 50:3) rendered **8c** as a light brown liquid (0.25 g, yield 48%) tR: 4.25 min ESI m/z (C₂₃H₃₁N₂O₂⁺) calc: 367.3; found: 367.4. ¹H-NMR (300 MHz, CDCl₃): 1.43 (s, 9H), 1.64 (s, 6H), 1.86-1.96 (m, 2H), 3.20 (s, 3H), 3.45 (t, 2H, J = 6 Hz), 4.36 (t, 2H, J = 5.4 Hz), 6.94-7.51 (m, 6H). (350 mg, yield 62%)

Synthesis of 9:

Scheme 7.5. Synthesis of 9.

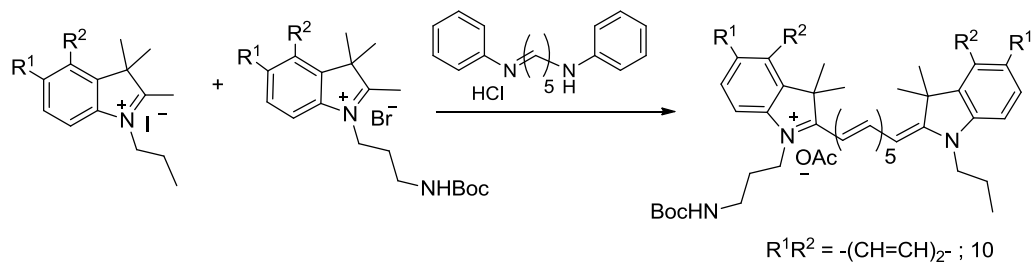


Reagent and conditions: a) AcOH, Ac₂O, 110 °C, 25 min. b) pyridine, 110 °C, 1 h.

N-[5-(phenylamino)-2,4-pentadienylidene]anilinemono hydrochloride (0.28 g, 1 mmol, 1 eq.) was condensed with **1a** (0.32 g, 2 mmol, 1 eq.) in a solution of AcOH:Ac₂O (1:1) at 100 °C for 25 min, and cooled down to r.t. Then **5** (0.39 g, 1 mmol, 1.0 eq.) and pyridine were added to the mixture and stirred under reflux. After 1 h, the reaction mixture was cooled down to r. t. and neutralized by NaHCO₃ saturated solution and washed with 0.1 (N) HCl solutions (3 × 100 mL), followed by aqueous solution (5 × 100 mL) and dried over anhydrous Na₂SO₄ and concentrated under reduced pressure. Purification of the crude residue on a silica gel column (elution with CH₂Cl₂-MeOH 50:2) rendered **9** as a green solid (0.35 g, yield 55%).
tR: 6.24 min ESI m/z (C₃₈H₅₀N₃O₂⁺) calc: 580.4; found: 580.5.

Synthesis of 10:

Scheme 7.6. Synthesis of 10.



Reagent and conditions: a) AcOH, Ac₂O, 110 °C, 20 min. b) pyridine, 110 °C, 1 h.

N-[5-(phenylamino)-2,4-pentadienylidene]anilinemonohydrochloride (0.2 g, 0.7 mmol, 1 eq.) was condensed with **8a** (0.27 g, 0.7 mmol, 1 eq) in a solution of ACOH:Ac₂O (1:1) at 110 °C for 20 min, and cooled down to r.t. Then **8c** (0.35 g, 0.7 mmol, 1 eq) and pyridine were added to the mixture and stirred under reflux. After 1 h, the reaction mixture was poured into water and NaHCO₃ was slowly added with stirring until complete neutralization was reached. After diluting with CH₂Cl₂ the organic layer was washed, dried over anhydrous Na₂SO₄ and concentrated under reduced pressure. Purification of the crude residue on a silica gel column (elution with CH₂Cl₂-MeOH 50:2) rendered **10** as a green solid (0.4 g, yield 54%). tR: 6.72 min ESI m/z (C₄₆H₅₄N₃O₂⁺) calc: 680.4; found: 680.4.

Synthesis of **Cy7LA**:

9 (0.1 g, 0.15 mmol) was treated with a solution of TFA-DCM (1:9) at r.t. overnight, neutralized with a solution of NaHCO₃, and the organic layer was dried over anhydrous Na₂SO₄ and concentrated under reduced pressure. The resulting solid that was dissolved in a solution of CH₂Cl₂-CH₃CN (9:1) added to the lipoic acid activated nitrophenol resin and shaken for 24 h at r.t. After the reaction, the resulting filtrates were combined and dried under pressure, followed the purification by DCM: MeOH (50:2) as eluting solvent to render **Cy7LA** as a slight green solid (82 mg, yield 72%).

¹H-NMR (500 MHz, CDCl₃): 1.05 (t, 3H, J = 7.5Hz), 1.25-1.34 (m, 4H), 1.37-1.47 (m, 2H), 1.63 (s, 6H), 1.65 (s, 6H), 1.80-1.85 (m, 4H), 2.09-2.14 (m, 2H), 2.42 (t, 2H, J = 8 Hz), 3.05-3.17 (m, 2H), 3.45 (d, 2H, J = 4.5 Hz), 3.57 (t, 1H, J = 7 Hz), 3.83 (t, 2H, J = 7 Hz), 4.35 (t, 2H, J = 7.3 Hz), 5.92 (d, 1H, J = 13.5 Hz), 6.50 (t, 1H, J = 12.5 Hz), 6.82 (d, 1H, J = 7.2 Hz), 6.93 (d, 2H, J = 7.5 Hz), 7.13 (t, 2H, J = 7.5 Hz), 7.30-7.33 (m, 4H), 7.40 (t, 1H, J = 7.5 Hz), 7.52 (t, 1H, J = 4.5 Hz), 7.71 (d, 2H, J = 3.5 Hz)

tR: 6.42 min, ESI (HRMS) m/z (C₄₁H₅₄N₃OS₂⁺) calc: 668.3703, found: 668.3707

Synthesis of Cy7.5LA:

The same procedure was followed starting from **10** to obtain Cy7.5LA (75 mg, yield 71%).

¹H-NMR (500 MHz, CDCl₃): 1.08 (t, 3H, J = 7.5Hz), 1.43-1.47 (m, 3H), 1.63-1.78 (m, 5H), 1.91 (s, 6H), 1.97 (s, 6H), 2.18-2.19 (m, 2H), 2.37-2.45 (m, 2H), 2.51 (t, 2H, J = 7.5 Hz), 3.06-3.14 (m, 2H), 3.51 (d, 2H, J = 4.5 Hz), 3.56 (t, 1H, J = 7 Hz), 3.95 (t, 2H, J = 7.5 Hz), 4.15-4.21 (m, 1H), 4.52 (t, 1H, J = 7.5 Hz), 5.93 (d, 1H, J = 13.5 Hz), 6.53 (t, 1H, J = 12 Hz), 6.92 (d, 2H, J = 7.5 Hz), 7.25 (m, 1H), 7.40-7.59 (m, 6H), 7.86-7.95 (m, 6H), 8.05 (d, 2H, J = 8.5 Hz). tR: 6.81 min, ESI (HRMS) m/z (C₄₉H₅₈N₃OS₂⁺) calc: 768.4016, found: 768.4049

7.5.2 *In vivo* SERS multiplexing

Balb/c nude mice from the Biological Resource Centre (Biomedical Sciences Institute, A*STAR) were anesthetized by intraperitoneal injection of ketamine (150 mg/kg)/xylazine (10 mg/kg) at the age of 4-6 weeks, and OSCC cells (5 x 10⁶ cells per site in a volume of 150 μL) were injected subcutaneously into the rear flank. When the tumors grew to a size around ~ 0.2 cm in diameter, anti-EGFR antibody-conjugated SERS nanotags for targeted (positive control) and anti-HER2 antibody-conjugated nanotag for non-targeted (negative control) (430 pM, 100 μL) were injected into the tail vein of the mice. After 5 h, mice were anesthetized by intraperitoneal injection of ketamine and xylazine mixture solution and *in vivo* SERS measurements were performed from tumor site and non-tumorigenic area i.e. liver and dorsal region using Raman microscope with specified area using 30mW, 785 nm laser excitation. The integration time was set as 20 s and the laser was coupled to the sample through a 20X objective lens with a beam spot of approx. 3 μm. The animal experiment procedures were performed in accordance with a protocol approved by the Institutional Animal Care and Use Committee (IACUC).

7.5.3 SERS mapping

SERS mapping experiments were performed in a Renishaw InVia Raman microscope system with a laser beam directed to the sample through a 20X objective lens. Antibody conjugated nanotag (**CyNAMLA-381**-nanotag, **Cy7LA**-nanotag and **Cy7.5LA**-nanotag) with equal concentration (450 pM) were injected through tail-vein. SERS-mapping in tumor and non-tumor area was conducted by selecting small area. Laser excitation at 785 nm wavelength (focal spot of 3 μm) and 30 mW power was used. Mapping measurements at 523 cm^{-1} for **CyNAMLA-381**, 503 cm^{-1} for **Cy7LA** and 586 cm^{-1} for **Cy7.5LA** were carried out as raster scans in 40 μm steps over the specified area (aprox. 600 x 400 μm^2) with 1 s integration time.

7.5.4 Limit of detection (LOD) study

To find out the limit of detection (LOD) of the best SERS-nanotag **Cy7LA**, a variable concentration dependent SERS study of the gold NPs has been carried. Anti-EGFR antibody-conjugated nanotag (**Cy7LA**-reporter) with NPs concentration 430 pM, 215 pM, 108 pM, 54 pM and 27 pM were incubated with OSCC cells for 2 hours at 37 $^{\circ}\text{C}$, and then washed with cold PBS ($\times 3$), gently scrapped and resuspended in PBS to a cell density of 1×10^6 cells/mL for SERS measurements. As shown in Figure 7.13, the normalized SERS spectra for the EGFR-labelled **Cy7LA**-nanotag with five different concentrations were obtained. Raman peak 503 cm^{-1} for **Cy7LA** was used for quantitative evaluation. The expected intensity of Raman peak increases continuously with increasing concentration of the targeted NPs. Based on these results the we observed the detection limit of the naotag is around 54 pM.

7.6 References

1. S. Keren, C. Zavaleta, Z. Cheng, A. de la Zerda, O. Gheysens, S. S. Gambhir, *Proc. Natl. Acad. Sci. U. S. A.* **2008**, *105*, 5844.
2. M. Gellner, K. Kompe, S. Schlucker, *Anal. Bioanal. Chem.* **2009**, *394*, 1839.
3. K. C. Bantz, A. F. Meyer, N. J. Wittenberg, H. Im, O. Kurtulus, S. H. Lee, N. C. Lindquist, S. H. Oh, C. L. Haynes, *Phys. Chem. Chem. Phys.* **2011**, *13*, 11551.
4. S. Schlucker, *Chemphyschem* **2009**, *10*, 1344.
5. N. M. Sirimuthu, C. D. Syme, J. M. Cooper, *Anal. Chem.* **2010**, *82*, 7369.
6. J. Yang, Z. Wang, X. Tan, J. Li, C. Song, R. Zhang, Y. Cui, *Nanotechnology* **2010**, *21*, 345101.
7. G. Goddard, L. O. Brown, R. Habbersett, C. I. Brady, J. C. Martin, S. W. Graves, J. P. Freyer, S. K. Doorn, *J. Am. Chem. Soc.* **2010**, *132*, 6081.
8. D. Graham, K. Faulds, *Chem. Soc. Rev.* **2008**, *37*, 1042.
9. Q. Hu, L. L. Tay, M. Noestheden, J. P. Pezacki, *J. Am. Chem. Soc.* **2007**, *129*, 14.
10. K. K. Strelau, R. Kretschmer, R. Moller, W. Fritzsche, J. Popp, *Anal. Bioanal. Chem.* **2010**, *396*, 1381.
11. A. Ingram, L. Byers, K. Faulds, B. D. Moore, D. Graham, *J. Am. Chem. Soc.* **2008**, *130*, 11846.
12. X. Qian, X. H. Peng, D. O. Ansari, Q. Yin-Goen, G. Z. Chen, D. M. Shin, L. Yang, A. N. Young, M. D. Wang, S. Nie, *Nat. Biotechnol.* **2008**, *26*, 83.
13. S. R. Emroy, S. M. Nie, *Anal. Chem.* **1997**, *69*, 2631.
14. Y. Wang, J. L. Seebald, D. P. Szeto, J. Irudayaraj, *ACS Nano* **2010**, *4*, 4039.
15. R. S. Golightly, W. E. Doering, M. J. Natan, *ACS Nano* **2009**, *3*, 2859.
16. M. K. Gregas, F. Yan, J. Scaffidi, H. N. Wang, T. Vo-Dinh, *Nanomedicine* **2011**, *7*, 115.
17. J. Kneipp, H. Kneipp, B. Wittig, K. Kneipp, *Nanomedicine*, **2010**, *6*, 214.
18. X. Wang, X. Qian, J. J. Beitler, Z. G. Chen, F. R. Khuri, M. M. Lewis, H. J. Shin, S. Nie, D. M. Shin, *Cancer Res.* **2011**, *71*, 1526.

19. Y. H. Kim, J. Jeon, H. S. Hong, K. W. Rhim, S. Y. Lee, H. Youn, K. J. Chung, C. M. Lee, S. D. Lee, W. K. Kang, M. J. Nam, *Small* **2011**, *7*, 2052.
20. M. Y. Sha, H. Xu, M. J. Natan, R. Cromer, *J. Am. Chem. Soc.* **2008**, *130*, 17214.
21. M. Han, X. Gao, J. Z. Su, S. Nie, *Nat Biotechnol.* **2001**, *19*, 631.
22. C. L. Zavaleta, B. R. Smith, I. Walton, W. Doering, G. Davis, B. Shojaei, M. J. Natan, S. S. Gambhir, *Proc. Natl. Acad. Sci. U. S. A.* **2009**, *106*, 13511.
23. M. H. J. G. W. Sark van, M. T. L. P. Frederix, J. D. H. Vanden, C. H. Gerriten, *J. Phys. Chem. B* **2001**, *105*, 8281.
24. I. L. Medintz, H. Mattoussi, A. R. Clapp, *Int. J. Nanomedicine* **2008**, *3*, 151.
25. G. V. Maltzahn, A. Centrone, J. H. Park, R. Ramanathan, J. M. Sailor, A. T. Hatton, N. S. Bhatia, *Adv. Mater.* **2009**, *21*, 3175.
26. S. Lee, H. Chon, M. Lee, J. Choo, S. Y. Shin, Y. H. Lee, I. J. Rhyu, S. W. Son, C. H. Oh, *Biosens. Bioelectron.* **2009**, *24*, 2260.
27. P. J. Huang, L. K. Chau, T. S. Yang, L. L. Tay, T. T. Lin, *Adv. Funct. Mater.* **2009**, *19*, 242-248.
28. S. Mahajan, J. Richardson, T. Brown, P. N. Bartlett, *J. Am. Chem. Soc.* **2008**, *130*, 15589.
29. A. Samanta, K. K. Maiti, K. S. Soh, X. Liao, M. Vendrell, U. S. Dinish, S. W. Yun, R. Bhuvaneshwari, H. Kim, S. Rautela, J. Chung, M. Olivo, Y. T. Chang, *Angew Chem. Int. Ed. Engl.* **2011**, *50*, 6089.
30. A. Matschulat, D. Drescher, J. Kneipp, *ACS Nano* **2010**, *4*, 3259.
31. K. K. Maiti, U. S. Dinish, C. Y. Fu, J. J. Lee, K. S. Soh, S. W. Yun, R. Bhuvaneshwari, M. Olivo, Y. T. Chang, *Biosens. Bioelectron.* **2010**, *26*, 398.
32. K. K. Maiti, A. Samanta, M. Vendrell, K. S. Soh, M. Olivo, Y. T. Chang, *Chem. Commun.* **2011**, *47*, 3514.
33. J. Alonso, C. Encinas, S. Miltsov, E. Otazo, L. Rivera, M. Puyol, *Dyes Pigments* **2006**, *71*, 28.

34. H. Jang, Y. K. Kim, S. R. Ryoo, M. H. Kim, D. H. Min, *Chem. Commun.* **2010**, *46*, 583.
35. C. C. Lin, Y. M. Yang, Y. F. Chen, T. S. Yang, H. C. Chang, *Biosens. Bioelectron.* **2008**, *24*, 178.
36. D. Graham, D. G. Thompson, W. E. Smith, K. Faulds, *Nat. Nanotechnol.* **2008**, *3*, 548.
37. L. Sun, B-K. Sung, C. Dentinger, B. Lutz, L. Nguyen, J. Zhang, H. Qin, M. Yamakawa, M. Cao, Y. Lu, A. Chmura, J. Zhu, X. Su, A. A. Berlin, S. Chan, B. Knudsen, *Nano Lett.* **2007**, *7*, 351.
38. A. Pallaoro, G. B. Braun, N. O. Reich, M. Moskovits, *Small* **2010**, *6*, 618.
39. C. D. Syme, N. M. Sirimuthu, S. L. Faley, J. M. Cooper, *Chem. Commun.* **2010**, *46*, 7921.
40. S. Y. Huh, J. A. Chung, B. Cordovez, D. Erickson, *Lab Chip* **2009**, *9*, 433.
41. G. Renand, R. L. Hamilton, J. R. Havel, *Hepatology* **1989**, *9*, 380.
42. K. T. Yong, I. Roy, H. Ding, E. J. Bergey, P. N. Prasad, *Small* **2009**, *5*, 1997.

CHAPTER 8

8.1 Conclusion

NIR fluorescence (λ_{max} : 700-1000 nm) has received substantial attention in various chemical and biological studies. Despite the several advantages of NIR tricyanocyanine dyes, the photodegradation is a serious problem for the NIR cyanine dyes having absorbance λ_{max} longer than 700 nm. First, we examined the mechanism of photodecomposition for the amine derivative of tricyanocyanine dye in aqueous media. We hypothesized that the lone pair electron of nitrogen atom cloud enriched the π electron system which eventually reacts with singlet oxygen in presence of light. As a result, derivatives of tricyanocyanine are not suitable for long time imaging study. To overcome this limitation, we developed a photostable NIR cyanine dye in which amine group of **CyN** was acetylated and thus the photoactivating lone pair electron was removed. Since the photostability depended on different amine structures, we designed a **CyNA** library composed of 80 structurally different amines and screened them to identify the best photostable dye. We found **CyNA-414** as the most photostable dye with moderate quantum yield and good emission properties (820 nm), and compared to a commercially available standard NIR dye (e.g. Indocyanine green (**ICG**)).

Although the new photostable **CyNA-414** exhibited good properties as a NIR dye it lacked a reactive functional group to enable its use in protein labeling or small molecules. Hence, we adapted this molecule for bioconjugation processes by introducing a suitable spacer. The replacement of this spacer not only maintained good photophysical properties but also enabled bioconjugation. NIR protein-labeling dyes must ideally retain highly fluorescent emission and good photostability profiles once conjugated to the protein of interest, and must maintain the specific recognition and functional abilities of the protein. Therefore, we synthesized succinimidyl ester (**CyNE 790**) and compared its photophysical properties to the standard ICG-sulpho-

OSu. A detailed evaluation of their photobleaching in buffer showed a 15-fold higher photostability of **CyNE 790** compared to ICG-sulfo-OSu. Furthermore, the injection of **CyNE 790**-anti-EGFR treated SCC-15 and MCF-7 cells allowed the visualization of SCC-15 cells in mice and confirmed that the conjugation of **CyNE 790** did not affect the recognition properties of the monoclonal anti-EGFR antibody.

Due to the excellent photophysical properties of **CyNE 790** we prepared glucose derivatives of **CyNE 790** for cancer cell imaging in NIR region. It is known that malignant cancer cells show an increased glycolysis rate when compared to normal cells due to the over expression of glucose transporters (GLUTs) and the higher activity of hexokinases. These differences in metabolism have been applied to the identification of cancer cells and tumors by optical imaging methods that rely on the preparation of reporter-containing glucose analogues. Hence, we synthesized a new probe **CyNE-2DG** which is a novel NIR fluorescent deoxyglucose analogue. We validated the staining of cancer cells by this fluorescent deoxyglucose analogue and proved its superior cell-permeability of **CyNE 2-DG** over the NIR standard **IRDye 800CW 2-DG**, which supports its application for cancer cell imaging in the NIR region.

In addition to the application of NIR fluorophores to fluorescent imaging, we also explored an alternative imaging techniques such as Surface-enhanced Raman Scattering (SERS) that can minimize the limitations of fluorescence imaging. SERS probes are based on the 10^{14} – 10^{16} fold scattering enhancement caused by the proximity of Raman-active signature molecules to the surface of metal NPs which can be modulated with molecular recognition motifs to render diagnostic tools for optical imaging and therapeutic studies. However, the preparation of ultrasensitive SERS probes is hampered by the limited availability, sensitivity, and reproducibility of Raman-active compounds at NIR region. Thus, we aimed to develop novel signature molecules that are active in NIR region. For such purpose, we designed the first

combinatorial approach to discover novel and highly sensitive NIR SERS reporters. The synthesis of a lipoic acid-containing 80-member NIR-SERS active tricyanocyanine library (**CyNAMLA**) and the screening of this library led to the identification of best NIR SERS reporter. To prepare SERS nanotags that could selectively detect cancer cells expressing HER2 receptors *in vivo*, we conjugated **CyNAMLA-381-AuNPs** to a scFv anti-HER2 antibody. We injected the scFv-conjugated **CyNAMLA-381-SERS** nanotags in nude mice bearing xenografts generated from SKBR-3 cells. Whereas the signal of the tumor site perfectly resembled the SERS spectra of the pure nanotags, no SERS signal was detected from other anatomical locations. These results clearly indicate that the scFv-conjugated **CyNAMLA-381-SERS** nanotags were able to specifically detect HER2-positive tumors *in vivo*.

In addition to the applicability of SERS nanotags for *in vivo* cancer, we aimed to apply multiplexing Raman reporters for the cancer *in vitro* cellular assay. The concurrent detection of defined multiple targets can facilitate the development of accurate diagnostic probes. We designed derivative of cyanine dye such as **Cy3LA** and **Cy5LA** as good multiplexing of the previously reported **B2LA** compound. In order to examine the multiplex differential recognition of **B2LA** anti-EGFR and **Cy3LA** anti-HER2 nanotags in cells, we incubated an equal amount of both nanotags in OSCC cells (EGFR-positive and HER2-negative) and SKBR-3 cells (HER2-positive and EGFR-negative). After washings with PBS, the SERS measurement in OSCC cells fully resembled the SERS spectrum of **B2LA** whereas the SERS signal of SKBR-3 cells matched with the spectrum of **Cy3LA**. Thus, we demonstrated here that **B2LA** and **Cy3LA**-nanotags could be used as a multiplex platform by recognizing both OSCC and SKBR-3 cells after they were co-cultured.

Finally, we have synthesized of NIR-active Raman reporters which can be applicable for the multiple detection of cancer cell *in vivo*. We demonstrated the

multiplexing capability of three different Raman reporters (i.e. **CyNAMLA-381** and newly synthesized highly sensitive **Cy7 LA** and **Cy7.5 LA**), and their high sensitivity and tumor specificity of antibody-conjugated SERS nanotags showed their excellent potential as non-invasive diagnostic tools. For the first time, we successfully demonstrated the selective *in vivo* multiplex targeted detection with full multiplexing capability and this study may help to design novel SERS nanoprobe for the simultaneous detection of multiple disorders.

8.2 Future prospective

8.2.1 Design of a cell tracker NIR fluorescence imaging agent

We have discussed about the application of NIR cyanine dyes in fluorescent. **CyNE 790** dye can be further modified for the development of NIR cell-tracker dyes. According to Scheme 8.1, **CyNE 790** can be functionalized by means of an amine linker that can be further modified depending on the biological application. For instance, a chlorobenzyl functional group could be introduced to covalently bind macromolecules under physiological conditions. There are some examples based of this strategy in other fluorescent scaffolds¹⁻³. Maleimide derivative may also have a good potential to attach covalently to thiol motifs. Figure 8.1 shows that the covalent attachment to thiols derivatives can be used to label the cells, which could be monitored for trafficking and biodistribution studies.

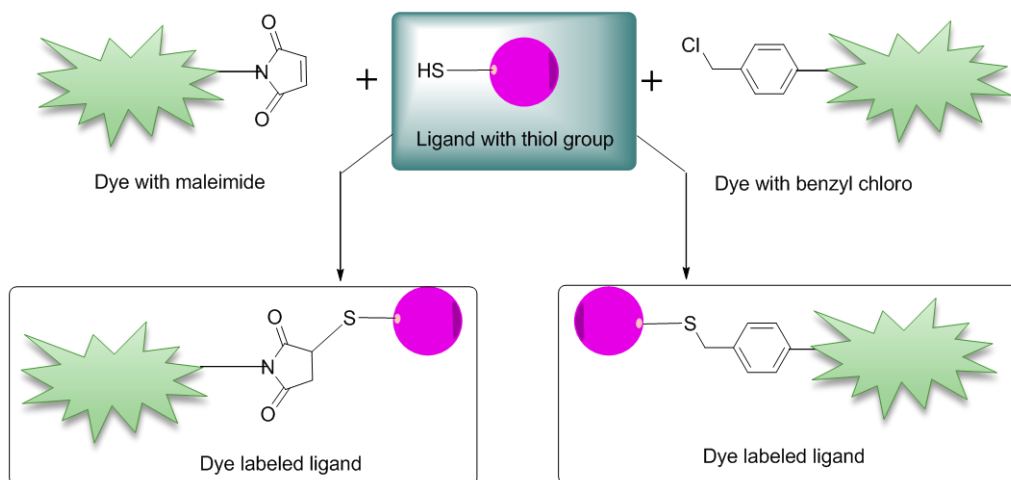
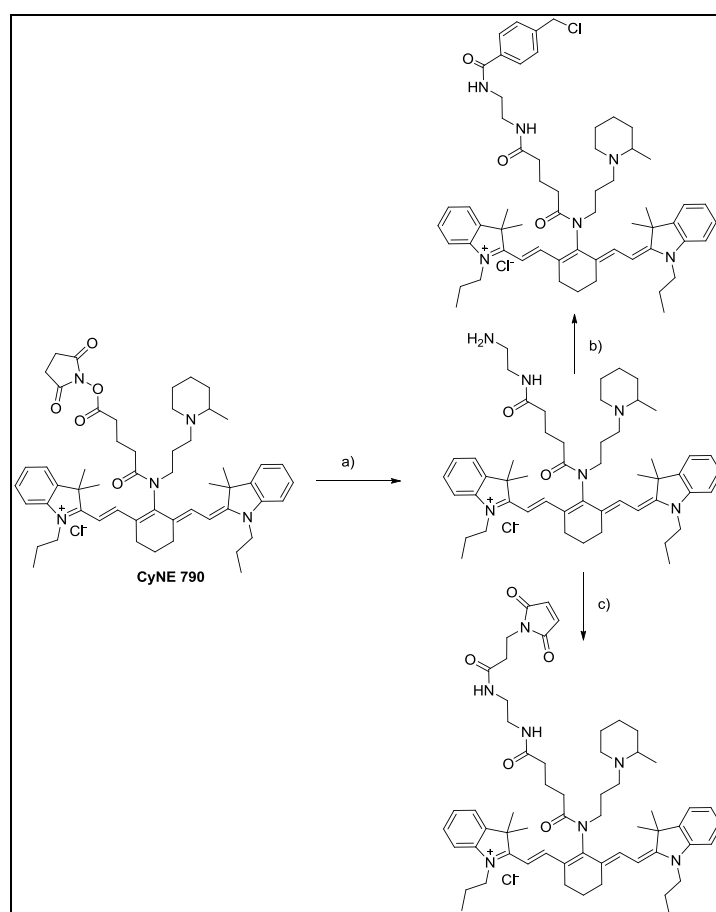


Figure 8.1. Design of NIR cell-tracker NIR fluorescent dyes.

Scheme 8.1. Synthesis of NIR cell-tracker dye



Reagents and conditions: a) CyNE 790 dissolved in Sodium bicarbonate buffer (pH 8.3) with cosolvent (2% DMSO) and ethylenediamine; b) 4-(chloromethyl)benzoyl chloride, DIEA, 0 °C; c) 3-Maleimidopropionic acid, HATU, DMF, r.t.

8.2.2 SERRS for ultrasensitive detection of multiple targets

Surface-enhanced Raman scattering (SERS) is an ultrasensitive technique that can detect chemicals at a trace level. In fact, SERS has been reported for the detection of single molecules, macromolecules. Another attractive feature of SERS is its ability to accurately detect multiple analytes in parallel way due to the multiplexing capability. Generally, NPs of the noble metals Ag and Au are employed as SERS substrates. A variety of factors such as size, aggregation and geometry of the NPs affect the maximum absorbance wavelength of the roughened metal surface. Most often, 20 to 80 nm NPs (Au or Ag) are described as SERS substrate but the size and the nature of these NPs determines their plasmon spectra. For example, the absorbance maxima of Au and Ag full spheres in water are 430 nm and 525 nm respectively. Their plasmon bands can be red shifted to NIR region when Au/Ag nanoshells with an outer diameter of 55 nm. In Au/Ag nanoshells, the shell thickness can be decreased with an increasing gold content, and as a result the plasmon band exhibits red shifted to NIR region when Au/Ag nanoshells with an outer diameter of 55 nm are used. In Au/Ag nanoshells, the shell thickness can be decreased with an increasing gold content, and as a result the Plasmon band exhibits a red shift to reach λ_{\max} around 600–700 nm (Figure 8.2). In addition, recently Halas and co-workers reported that the absorption peak of spherical gold nanoshells can be modified within the spectral range from 600 to 1200 nm whereas it is not easy to tune the plasmon spectra of spherical Au (or Ag) NPs.

NIR light absorbing nanoshells would be very attractive for the surface-enhanced resonance Raman scattering (SERRS). The basic requirements for SERRS are that either Raman-active dyes or SERS substrate (noble metals) must absorb light in a suitable wavelength, in resonance with the applied excitation frequency of the light. The resulting outcome is a signal of higher intensity than conventional SERS. Previously, we proved the applicability of SERRS effect using NIR Raman-active dyes, which are electronically excited under a 785 nm laser. However, we employed

gold colloid (60 nm, with 534 nm plasmon band) for SERS substrate which did not match with the excited light at 785 nm. We may consider Au/Ag nanoshells absorbing light at around 700 nm as SERS substrate in order to obtain a stronger SERRS effect by combining both NIR-active Raman reporters and NIR-active SERS substrates. As a result, sharp distinguishable fingerprints with enhanced signal intensities, narrow bandwidths and multiplexing properties could be used to prepare novel highly sensitive multiple detection probes.

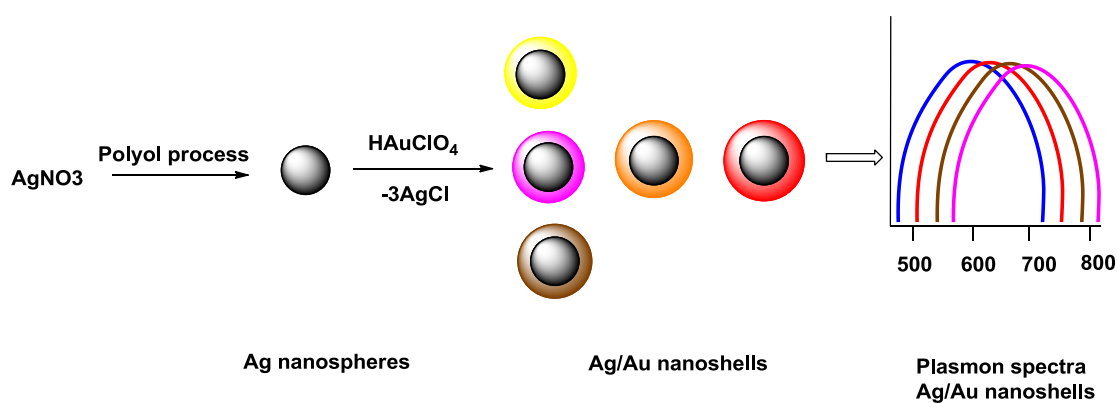


Figure 8.2. Schematic diagram for the preparation of Au/Ag nanoshells from Ag nanospheres. The plasmon spectra show a clear dependence on the size of the gold sphere and can reach the values in the NIR region.

8.3 References

1. F. K. Swirski, C. R. Berger, J. L. Figueiredo, T. R. Mempel, U. H. von Andrian, M. J. Pittet, R. Weissleder, *PLoS One* **2007**, 2, e1075.
2. C. Ionescu-Zanetti, L. P. Wang, D. Di Carlo, P. Hung, A. Di Blas, R. Hughey, L. P. Lee, *Cytometry A* **2005**, 65, 116.
3. C. Y. Fang, V. Vaijayanthimala, C. A. Cheng, S. H. Yeh, C. F. Chang, C. L. Li, H. C. Chang, *Small* **2011**, 7, 3363.
4. Y. Wang, H. Chen, S. Dong, E. Wang, *J. Chem. Phys.* **2006**, 125, 44710.
5. Y. Sun, B. T. Mayers, Y. Xia, *Nano Lett.* **2002**, 5, 481.
6. M. Gellner, B. Kustner, S. Schlucker, *Vibra. Spectrosc.* **2009**, 50, 43.